Republic of Iraq
Ministry of Higher Education and Scientific Research
University of Babylon
College of Engineering
Civil Engineering Department

Behavior of High Strength Light Weight Reinforced Concrete One-Way Ribbed Slabs

A Dissertation

Submitted to the College of Engineering at the University of Babylon in Partial Fulfillment of The Requirements for the Degree of Doctor of Philosophy in Engineering/ Civil Engineering/Structures

By

Tamara Amer Mohammed Abdulameer

Supervised by

Prof. Dr. Hayder Mohammed Kadhim Khudhair

2022 A.D **1443 A.H**

بِسْمِ اللَّهِ الرَّحْمَنِ الرَّحِيمِ ﴿١﴾الْحَمْدُ لِلَّهِ رَبِّ الْعَالَمِينَ ﴿٢﴾الرَّحْمَنِ الرَّحِيمِ﴿٣﴾مَالِكِ يَوْمِ الدِّينِ﴿٤﴾إِيَّاكَ نَعْبُدُ وَإِيَّاكَ نَسْتَعِينُ ﴿٥﴾اهْدِنَا الصِّرَاطَ الْمُسْتَقِيمَ ﴿٦﴾صِرَاطَ الَّذِينَ أَنْعَمْتَ عَلَيْهِمْ غَيْرِ الْمَغْضُوبِ عَلَيْهِمْ وَلَا الضَّالِّينَ﴿٧﴾

صدق الله العليُ العظيم

سورة الفاتحة

TO MY FAMILY

WITH MY

LOVE AND

RESPECT

Tamara Amer Mohammed

2022

CERTIFICATION

I certify that the preparation of this dissertation titled **"Behavior of High Strength Light Weight Reinforced Concrete One-Way Ribbed Slabs"** presented by **"Tamara Amer Mohammed"** was made under my supervision at the Department of Civil Engineering / College of Engineering / University of Babylon, as partial fulfillment of the requirements for the degree of Doctor of Philosophy in Civil Engineering (Structural Engineering).

Signature: 

Name: Prof. Dr. Hayder Mohammed Kadhim

Date: /7 / 2022

COMMITTEE CERTIFICATION

We certify as an examining committee that we have read this dissertation entitled **" Behavior of High Strength Light Weight Reinforced Concrete One-Way Ribbed Slabs "** and examined the student " Tamara Amer Mohammed Abdulameer" in its content and what related to it, and found it meets the standard of dissertation for the degree of Doctor of Philosophy in the Civil Engineering (Structural Engineering).

Signature:
Name: **Prof. Dr. Hayder M. Kadhem**
(Member and Supervisor)
Date: / /2022

Signature:
Name: **Asst. Prof. Dr. Khalid K. Shadhan**
(Member)
Date: / /2022

Signature:
Name: **Asst. Prof. Dr. Ali G. Abbas**
(Member)
Date: / /2022

Signature:
Name: **Prof. Dr. Mohammed J. Hamood**
(Member)
Date: / /2022

Signature:
Name: **Prof. Dr. Amer M. Ibrahim**
(Member)
Date: / /2022

Signature:
Name: **Prof. Dr. Mustafa B. Dawood**
(Chairman)
Date: / /2022

Approved by the Head of the Civil Engineering Department

Signature:
Name: **Prof. Dr. Thair J. Mizhir Alfatlawi**
(Head of the Civil Engineering Department)
Date: / / 2022

Approved by the Dean of the College of Engineering

Signature:
Name: **Prof. Dr. Hatem Hadi Obeid**
(Dean of the College of Engineering)
Date: / / 2022

ACKNOWLEDGMENTS

"In the Name of Allah, the Most Gracious, the Most Merciful"

At first, thank **Allah**, who gave me the willingness and strength to complete this research.

I would like to express sincere appreciation and deepest gratitude to my supervisor **Prof. Dr. Hayder Mohammed Kadhim Al-Mutairee**, for his advice, guidance, and encouragement throughout this work.

Thanks to the staff of the Civil Engineering Department /College of the Engineering /University of Babylon for their appreciable support.

A special thank and gratitude are due to **my dear father** and **my lovely mother** for their care, patience, and encouragement throughout the research period. I also wish to thank **my brother** and **my sister** for their encouragement and assistance.

Finally, thanks to all who participated in providing help and assistance to complete this work.

Tamara Amer Mohammed

2022

ABSTRACT

The present study includes an experimental and numerical investigation of high strength-lightweight reinforced concrete one-way ribbed slabs behavior.

The experimental program consists of testing twenty-one of one-way reinforced concrete slab specimens. These specimens were split into two groups according to the type of loading. Fifteen were tested under static load (two-point load), and others were tested under dynamic load (harmonic load). The slabs in the first group that were tested under static load were divided into six subgroups according to the type of concrete; high strength-lightweight concrete (HSLWC), high strength-normal weight concrete (HSNWC), normal strength-lightweight concrete (NSLWC), or normal strength-normal weight concrete (NSNWC); steel fibers volume fraction ratios, steel reinforcement ratios of ribs, the geometry of section (number of ribs) at same HSLWC volume, ribs spacing, slab type; ribbed or solid slab with approximately same HSLWC volume and different steel ratios. Meanwhile, the second group that was tested under dynamic load was divided into four subgroups according to the type of concrete; steel fibers ratios, the geometry of section, and slab type. Also, cubes, cylinders, and prisms for each batch mix were tested to determine the concrete's physical and mechanical characteristics.

Based on the findings of experimental testing, it is concluded that the HSLWC with an average cylinder compressive strength of about 42.2 MPa, the average oven-dry density of 1943 kg/m^3, and the thermal conductivity of about 0.81W/ (m.K) can be produced by using pumice stone with additive materials (sugar molasses, superplasticizer, and micro silica fume). The average cylinder compressive strength, oven-dry density, and thermal conductivity in comparable HSNWC are 58 MPa, 2408 kg/m^3, and 1.435 W/ (m.K), respectively.

It was found that the HSLWC ribbed slab specimen has a lower; total weight, ultimate load capacity, and deflection by the amount of 19%, 17.70%, and 17.33%, respectively, in comparison with the HSNWC slab specimen that was tested under static load. Consequently, the structural efficiency of HSLWC slab specimens had superiority over HSNWC, NSLWC, and NSNWC slabs by about 1.04%, 5.80%, and 19.16%, respectively.

Moreover, reducing the spacing between the ribs from 200mm to 180mm and 150mm increased the ultimate load by 8.33% and 17.97%, respectively. Furthermore, using HSLWC ribbed slab instead of HSLWC solid slab increased the ultimate load and structural efficiency by 130.37% and 125.72%, respectively, while the deflection decreased by 3.99%.

On the other hand, changing the number of ribs at the same HSLWC volume did not give a significant difference in strength capacity but gave economic benefit by reducing the fabrication cost of shear reinforcement.

However, it was found that the addition of steel fibers with the ratio of 0.5% and using a ribs reinforcement ratio of 0.44% in HSLWC ribbed slabs led to overcome on the strength reduction due to using HSLWC instead of HSNWC.

The experimental results of slab specimens under the effect of dynamic load showed that using HSLWC ribbed slab with 3-ribs decreased the average displacement amplitude at frequencies ranging from 5 to 50 Hz by 13.44% and 35.10% compared with HSNWC and solid slabs, respectively. Contrarily, using 1-rib and 0.25% steel fibers of HSLWC ribbed slabs decreased the average displacement amplitude by 54.03% and 15.54%, respectively, compared to the 3-ribs HSLWC slab.

Finally, the results of the comparison between the finite element analysis conducted using ABAQUS/2019 and the results of the experimental work presented reasonable validity where a maximum variation of the ultimate load and deflection was about 21.01% and 14.52%, respectively, for specimens under the effect of static load. Meanwhile, the maximum variation of the displacement amplitude of about 30% for specimens under the effect of the dynamic load. The parametric study of the present work involved numerical analysis to find the natural frequency and vibration modes. The effects of increasing operation frequency, support conditions, and spacing between the ribs on the behavior of one-way slabs under dynamic load.

LIST OF CONTENTS

DEDICATION II
CERTIFICATION III
COMMITTEE CERTIFICATION IV
ACKNOWLEDGMENTS V
ABSTRACT VI
LIST OF CONTENTS VIII
LIST OF FIGURES XII
LIST OF PLATES XVI
LIST OF TABLES XVI
NOTATION XVIII
ABBREVIATION XX
Chapter One: Introduction 1
1.1 Introduction 1
1.2 High Strength Concrete 2
1.3 Lightweight Concrete (LWC) 3
1.3.1 Lightweight Aggregate Concrete (LWAC) 3
1.3.2 Aerated Concrete and Foamed Concrete 4
1.3.3 No Fines Concrete (NFC) 5
1.4 Advantages and Disadvantages of LWC 5
1.4.1 Advantages of LWC 5
1.4.2 Disadvantages of LWC 5
1.5 Structural Lightweight Concrete (SLWC) 6
1.6 Sustainability of LWC 7
1.7 Reinforced Concrete Ribbed Slab 7
1.7.1 Design Limitations of Reinforced Concrete Ribbed Slab 8
1.7.2 Advantages and Disadvantages of Reinforced Concrete Ribbed Slab 9
1.8 Dynamic Load 10
1.9 Objectives and Scope of the Current Work 11
1.10 Layout of Thesis 12

Chapter Two: Literature Review 13
2.1 Introduction 13
2.2 Previous Studies on LWC 13
2.3 Previous Studies on HSC 18
2.4 Previous Studies of HSLWC 21
2.5 Behavior of High Strength–Lightweight Reinforced Concrete Members 25
2.6 Previous Studies on Behavior of Reinforced Concrete One–Way Slabs . 29
2.6.1 Behavior of Reinforced Concrete One–Way Solid Slabs 29
2.6.2 Behavior of Reinforced Concrete One–Way Ribbed Slabs 31
2.7 Behavior of Reinforced Concrete Members Under Harmonic Loads 38
2.8 Summary 40
Chapter Three: Experimental Work 42
3.1 General 42
3.2 Specimens Preparation 42
3.2.1 Materials Properties 42
3.2.2 Description of Specimens 45
3.2.3 Steel Reinforcement Details of Specimens 52
3.2.4 Formworks of Slab Specimens 53
3.2.5 Mix Proportions 54
3.2.6 Mixing Procedure 55
3.2.7 Casting and Curing 56
3.3 Tests of Fresh and Hardened Concrete 57
3.3.1 Tests of Fresh Concrete 57
3.3.2 Tests of Hardened Concrete 58
3.4 Testing Instrumentations and Software 62
3.4.1 Instrumentations of Static Test 62
3.4.2 Instrumentations of Dynamic Test 64
3.5 Testing Procedure 67
Chapter Four: Experimental Results and Discussion 69
4.1 Introduction 69
4.2 Mechanical and Physical Properties of Concrete Mixes 69

4.2.1 Compressive Strength 69
4.2.2 Splitting Tensile Strength..... 70
4.2.3 Flexural Tensile Strength (Modulus of Rupture)..... 71
4.2.4 Ultrasonic Pulse Velocity (UPV)..... 72
4.2.5 Density 73
4.2.6 Thermal Conductivity (λ)..... 74
4.2.7 Sound Insulation and Acoustic Impedance..... 75
4.2.8 Slump Test Results..... 77
4.3 Results of the Experimental Work of Slabs Specimens Under Static Loading 77
4.3.1 Cracking Behavior 78
4.3.2 Deflection Behavior 92
4.3.3 Strain Behavior..... 108
4.3.4 Comparison between Experimental and Theoretical Results 113
4.3.5 Structural Efficiency Analysis of One–Way Slabs..... 114
4.3.6 Sustainability Analysis of One–Way Slabs 116
4.4 Results of the Experimental Work of Slab Specimens Under Dynamic Loading..... 120
4.4.1 Harmonic Load -Time History..... 120
4.4.2 Behavior of Displacement Amplitude 122
4.4.3 Sound level-Time History..... 127
Chapter Five: Finite Element Analysis 129
5.1 General 129
5.2 Modeling of Reinforced Concrete Slabs..... 129
5.2.1Parts and Assembly..... 129
5.2.2 Convergence Study 132
5.2.3 Modeling of Materials..... 134
5.2.4 Interaction 141
5.2.5 Boundary Condition..... 142
5.2.6 Loading..... 143
5.2.7 Type of Analysis 144

5.3 Comparison Study Between the Results of the Experimental and FEM Analysis Under Static Load 144
5.3.1 Ultimate Load and Deflection Under Static Load 145
5.3.2 Load-Deflection Curves 146
5.3.3 Distribution of Von Mises stress at reinforcement bars 157
5.3.4 Crack Patterns 161
5.4 Comparison Study between the Results of the Experimental and FEM Analysis Under Dynamic Load 162
5.5 Parametric Studies 164
5.5.1 Natural Frequency and Vibration Modes 164
5.5.2 Increasing the Operating Frequency 167
5.5.3 Changing the Boundary Condition of the Supports 167
5.5.4 Changing the Ribs Spacing 168
Chapter Six: Conclusions and Recommendations for Future Studies .. 169
6.1 Conclusions 169
6.2 Recommendations for Future Studies 172
References 174
Appendix A: Summary of Materials Properties A-1
A.1 Cement Properties A-1
A.2 Aggregate Properties A-2
A.3 Sugar Molasses A-3
A.4 Steel Fiber A-3
A.5 Silica Fume A-4
A.6 Sika ®ViscoCrete ®– 5930L IQ A-6
Appendix B: Theoretical Calculations B-1
Appendix C: Device Specifications C-1

LIST OF FIGURES

Figure (1-1) Lightweight concrete types 3
Figure (1-2) Types of ribbed slab [16] 8
Figure (1-3) Different types of dynamic loads 11
Figure (2-1) Specimen's details for lightweight beams with NSC and HSC [49] 27
Figure (2-2) Beam and test setup details [51] 28
Figure (2-3) Parameters Arrangement [59] 32
Figure (2-4) Variation of slab samples [61] 33
Figure (2-5) Variation of slab samples [65] 36
Figure (2-6) Variation of slab samples [67] 37
Figure (3-1) Specimens of sub-group (G11) 46
Figure (3-2) Specimens of sub-group (G12) 47
Figure (3-3) Specimens of sub-group (G13) 47
Figure (3-4) Specimens of sub-group (G14) 48
Figure (3-5) Specimens of sub-group (G15) 48
Figure (3-6) Specimens of sub-group (G16) 49
Figure (3-7) Specimens of sub-group (G21) 50
Figure (3-8) Specimens of sub-group (G22) 50
Figure (3-9) Specimens of sub-group (G23) 51
Figure (3-10) Specimens of sub-group (G24) 51
Figure (3-11) Steel reinforcement and geometric sections details of specimens 52
Figure (3-12) Distribution of strain gauges across width of the slab 63
Figure (3-13) A schematic diagram of slab specimen under static test 67
Figure (4-1) Load-crack width curves of G11 85
Figure (4-2) Load-crack width curves of G12 85
Figure (4-3) Load-crack width curves of G13 86
Figure (4-4) Load-crack width curves of G14 86
Figure (4-5) Load-crack width curves of G15 87
Figure (4-6) Load-crack width curves of G16 87
Figure (4-7) First crack load of G11 88
Figure (4-8) First crack load of G12 89
Figure (4-9) First crack load of G13 90

Figure (4-10) First crack load of G14 91
Figure (4-11) First crack load of G15 91
Figure (4-12) First crack load of G16 92
Figure (4-13) Load-deflection curves of G11 94
Figure (4-14) Load-deflection curves of G12 95
Figure (4-15) Load-deflection curves of G13 96
Figure (4-16) Load-deflection curves of G14 97
Figure (4-17) Load-deflection curves of G15 98
Figure (4-18) Load-deflection curves of G16 99
Figure (4-19) Stiffness of all tested slabs specimens 99
Figure (4-20) Ductility of G11 102
Figure (4-21) Absorbed energy of G11 102
Figure (4-22) Ductility of G12 103
Figure (4-23) Absorbed energy of G12 104
Figure (4-24) Ductility of G13 104
Figure (4-25) Absorbed energy of G13 105
Figure (4-26) Ductility of G14 105
Figure (4-27) Absorbed energy of G14 106
Figure (4-28) Ductility of G15 106
Figure (4-29) Absorbed energy of G15 107
Figure (4-30) Ductility of G16 108
Figure (4-31) Absorbed energy of G16 108
Figure (4-32) Effective width for all slab specimens 109
Figure (4-33) Strain distribution across width of slab for G11 111
Figure (4-34) Strain distribution across width of slab for G12 111
Figure (4-35) Strain distribution across width of slab for G13 112
Figure (4-36) Strain distribution across width of slab for G14 112
Figure (4-37) Strain distribution across width of slab for G15 112
Figure (4-38) Strain distribution across width of slab for G16 113
Figure (4-39) Comparison between experimental and theoretical load 114
Figure (4-40) Structural efficiency for tested specimens 115
Figure (4-41) Embodied carbon emission for all slabs 118

Figure (4-42) Eco-strength efficiency of all slab specimens 119
Figure (4-43) Noise removing from recorded dynamic data 120
Figure (4-44) Harmonic load- time history 121
Figure (4-45) Amplitude displacement of tested slabs 123
Figure (4-46) Displacement-time history for tested slabs under dynamic load 125
Figure (4-47) Sound level behavior for tested slab specimens 128
Figure (4-48) Sound level -time history for tested slab specimens 128
Figure (5-1) Modeling of slabs under two-point loading 130
Figure (5-2) Details of modeling steel reinforcement 131
Figure (5-3) The convergence study 132
Figure (5-4) Finite element mesh density 133
Figure (5-5) Concrete response to uniaxial loading based on manual of the ABAQUS theory [119] 135
Figure (5-6) Compressive stress-inelastic strain curves 137
Figure (5-7) Compressive damage parameter-strain relationship for all concrete types 137
Figure (5-8) Tension stress-inelastic strain curves 139
Figure (5-9) Tension damage parameter-strain relationship for all concrete types 139
Figure (5-10) Constraints types adopted in this study 141
Figure (5-11) Details of boundary conditions of supports 143
Figure (5-12) The applied load on the specimens 143
Figure (5-13) Experimental vs. FEM deflection behavior for S1 147
Figure (5-14) Experimental vs. FEM deflection behavior for S2 147
Figure (5-15) Experimental vs. FEM deflection behavior for S3 148
Figure (5-16) Experimental vs. FEM deflection behavior for S4 149
Figure (5-17) Experimental vs. FEM deflection behavior for S5 149
Figure (5-18) Experimental vs. FEM deflection behavior for S6 150
Figure (5-19) Experimental vs. FEM deflection behavior for S7 151
Figure (5-20) Experimental vs. FEM deflection behavior for S8 151
Figure (5-21) Experimental vs. FEM deflection behavior for S9 152
Figure (5-22) Experimental vs. FEM deflection behavior for S10 153
Figure (5-23) Experimental vs. FEM deflection behavior for S11 153
Figure (5-24) Experimental vs. FEM deflection behavior for S12 154

Figure (5-25) Experimental vs. FEM deflection behavior for S13 155
Figure (5-26) Experimental vs. FEM deflection behavior for S14 155
Figure (5-27) Experimental vs. FEM deflection behavior for S15 156
Figure (5-28) Reinforcement bars stresses of slab S1 157
Figure (5-29) Reinforcement bars stresses of slab S2 157
Figure (5-30) Reinforcement bars stresses of slab S3 157
Figure (5-31) Reinforcement bars stresses of slab S4 158
Figure (5-32) Reinforcement bars stresses of slab S5 158
Figure (5-33) Reinforcement bars stresses of slab S6 158
Figure (5-34) Reinforcement bars stresses of slab S7 159
Figure (5-35) Reinforcement bars stresses of slab S8 159
Figure (5-36) Reinforcement bars stresses of slab S9 159
Figure (5-37) Reinforcement bars stresses of slab S10 159
Figure (5-38) Reinforcement bars stresses of slab S11 160
Figure (5-39) Reinforcement bars stresses of slab S12 160
Figure (5-40) Reinforcement bars stresses of slab S13 160
Figure (5-41) Reinforcement bars stresses of slab S14 161
Figure (5-42) Reinforcement bars stresses of slab S15 161
Figure (5-43) Crack patterns at failure for S1 162
Figure (5-44) Experimental vs. numerical displacement-time history for tested slabs at 50Hz 163
Figure (5-45) Mode shapes of one-way ribbed slab 166
Figure (5-46) Displacement amplitude of one-way slabs at frequencies 60 Hz to 80 Hz 167
Figure (5-47) Effect of support boundary condition on displacement amplitude of one-way Slabs 168
Figure (5-48) Effect of ribs spacing on vibration amplitude of one-way HSLWC ribbed slab 168

LIST OF PLATES

Plate (3-1) Hooked end steel fiber 44
Plate (3-2)Tensile test of a steel bar 45
Plate (3-3) Plywood and steel formworks 54
Plate (3-4) Concrete mixer 55
Plate (3-5) Casting and curing of concrete specimens 57
Plate (3-6) Slump test 58
Plate (3-7) Fresh density test 58
Plate (3-8) Compressive strength test 59
Plate (3-9) Splitting tensile strength test 59
Plate (3-10) Flexural tensile strength test 60
Plate (3-11) Ultrasonic pulse velocity test 60
Plate (3-12) Thermal conductivity test 61
Plate (3-13) pH meter test 62
Plate (3-14) Instrumentations of static test 64
Plate (3-15) Experimental dynamic test setup 66
Plate (3-16) Instrumentations of dynamic test 66
Plate (4-1) Cracks pattern for slabs under two-point loading 81
Plate (4-2) Cracks pattern for slabs under harmonic loading 126

LIST OF TABLES

Table (3-1): Properties of steel reinforcement 45
Table (3-2): Mix proportions of concrete mixes 55
Table (4-1): Results of compressive strength tests 70
Table (4-2): Results of splitting tensile strength test 71
Table (4-3): Results of modulus of rupture test 72
Table (4-4): Results of ultrasonic velocity test 73
Table (4-5): Results of density test 74
Table (4-6): Results of thermal properties 75
Table (4-7): Results of acoustic properties 76
Table (4-8): Results of workability properties 77
Table (4-9): Cracking and deflection details for slabs tested under static loading. 78
Table (4-10): Embodied carbon of material 117
Table (5-1): Calculated values of **Ec** 137
Table (5-2): Experimental and numerical results for tested slabs 145
Table (5-3): Comparison between experimental and numerical results for tested slabs 163
Table (5-4): Natural frequencies of all tested slabs under dynamic loading 165
Table (5-5): Theoretical and numerical results of natural frequency 166
Table (A-1): Cement's chemical and physical test results A-1
Table (A-2): Grading and properties of fine aggregate A-2
Table (A-3): Grading and properties of coarse aggregate (gravel) A-2
Table (A-4): Grading and properties of coarse aggregate (Pumice Stone) A-3
Table (A-5): Chemical analysis of Sugar Molasses [37] A-3
Table (A-6): Physical characteristics of steel fibers A-3

NOTATION

The following are the major symbols used in this dissertation:

Symbol	Description
A	Heat transfer area, m^2
AE	Absorbed energy, kN.mm
AI	Acoustic impedance, Rayl
b_o	Effective width of slab, mm
d_f	Diameter of fiber, mm
d_t	Temperature difference across the material
e	The eccentric distance between the center of mass and the center of rotation, m
E_c	Modulus of elasticity of concrete, MPa
E_s	Modulus of elasticity of steel, GPa
f	Frequency, kHz
f_c'	Concrete cylinder compressive strength, MPa
f_{cu}	Concrete cube compressive strength, MPa
f_r	Modulus of rupture, MPa
f_t	Splitting tensile strength, MPa
G_f	Fracture energy
K_s	Stiffness at service load level, kN/mm
l_f	Length of fiber, mm
m	Mass per area unit, kg/m^2
m_e	Eccentric mass weight, kg
P_{cr}	First cracking load, kN
P_d	Dynamic force, N
$P_{u\,Exp}$	Experimental ultimate load, kN
$P_{u\,FEM}$	Numerical ultimate load, kN
P_y	Yield load, kN
q	Heat transferred per unit time, W/ h
r	Heat resistivity, m^2.K/W
t	Material thickness, m
TR	Transmission losses, dB
V_f	Fiber volume fraction, %
w_c	Density of concrete, kg/m^3
W_{cr}	Crack width at service load level, mm
$\delta_{u\,Exp}$	Experimental deflection, mm
$\delta_{u\,FEM}$	Numerical deflection, mm
δ_y	Deflection at yield load, mm
ε_x	Longitudinal strain

λ	Thermal conductivity, W/ (m.K)
μ	Ductility
ρ	Steel reinforcement ratio
ρ_b	Balance steel reinforcement ratio
σ_{co}	Yield stress of concrete, MPa
υ	Poisson ratio
φ	Diameter of the reinforced bar, mm
Ω	Resistance, ohm
ω_o	Operating frequency, rad/sec

ABBREVIATION

Abbreviation	Description
a/d	Shear-span to depth ratio
ANSYS	Analysis system software
AP	Aluminum powder
BFS	Blast furnace slag
BR	Brittleness ratio
C3D8	Three-dimensional eight-node solid element
CA	Coarse aggregate
CC	Conventional concrete
cm	Centimeter
CDP	Concrete damaged plasticity
CS	Coconut shell
CSF	Condensed silica fume
d_c	Compressive damage parameter
d_t	Tensile damage parameter
3D	Three dimensions
et al.	And others
etc.	To the end
Exp.	Experimental
F0.25 HSLWC	High strength lightweight concrete with 0.25% steel fibers
F0.50 HSLWC	High strength lightweight concrete with 0.50% steel fibers
FA	Fly ash
FEA	Finite element analysis
FEM	Finite element method
g	Gram
h	Hour
HBS	Hollow block slab
HP	Horsepower
HPC	High-performance concrete
HPFRC	High-performance fiber reinforced concrete
HPLWAC	High performance lightweight aggregate concrete
HRWRA	High range water-reducing admixture
HSC	High strength concrete
HSLWC	High-strength lightweight concrete
HSNWC	High strength normal weight concrete
Hz	Hertz
i.e.	With other meaning
K	Kelvin
kg	kilogram
LECA	Light exfoliated clay aggregate

l_f/d_f	Aspect ratio of steel fibers
LVDT	Linear variable differential transducer
LWA	Lightweight aggregate
LWAC	Lightweight aggregate concrete
LWC	Lightweight concrete
m	Meter
MAS	Maximum aggregate size
MK	Metakaolin
ml	Milliliter
MPa	Mega Pascal (MN/m^2)
n	Weakness ratio
NFC	No fines concrete
NSC	Normal strength concrete
NSNWC	Normal strength normal weight concrete
Num.	Numerical
NWA	Normal-weight aggregate
NWAC	Normal-weight aggregate concrete
NWC	Normal-weight concrete
O.D	Oven dry
OPC	Ordinary Portland cement
P	Plastic fiber
PC	Portland cement
PP	Polypropylene fiber
SBS	Styropor block slabs
SCC	Self-compacting concrete
SCMs	Supplementary cementitious materials
sec	Second
SF	Silica fume
SFSCC	Steel fiber self-compacting concrete
SLWC	Structural lightweight concrete
SM	Sugar molasses
SP	Superplasticizer
t	Ton
T3D	Three-dimension two-nodes truss element
TDMS	Technical data management streaming
UPV	Ultrasonic pulse velocity
W	Watt
w/b	Water/binder ratio
w/c	Water to cement ratio
w/cm	Water-cementitious materials ratio

Chapter One

Introduction

Chapter One: Introduction

1.1 Introduction

A concrete slab is one of the main structural members in buildings, which is considered as the largest member consuming of concrete.

The main limitation of slab design in the construction of a reinforced concrete structure is the span between columns; a greater span between columns necessitates more supported beams and/or increased slab thickness; these requirements lead to an increase in the structure weight due to additional concrete and steel which make the structure more costly.

On the other hand, any increase in the structure's self-weight limits the horizontal slab's span, increases the structure's stress, and raises the inertia forces that must be resisted according to seismic considerations [1].

For a long time, lightweight aggregate concrete (LWAC) has been effectively utilized for structural applications. The density of lightweight concrete (LWC) is sometimes more essential than its strength in structural applications. For structural design and foundations, the dead load is reduced when the density is lower for the same strength level. There is a trend toward using higher strength for light-weight concrete (LWC) than for normal-weight concrete (NWC).

Several types of research and experimental studies were conducted to investigate other types of lightweight slabs by considering the above-mentioned conditions. One of these types was a ribbed slab.

The reinforced concrete ribbed slabs have become increasingly popular in the construction of industry as an alternative to solid slabs in building structures.

The ribbed slab was designed to reduce building costs, and in the last few years, these ribbed slabs have grown in popularity due to their cost savings [2]. The most important benefit of the ribbed slab is that it contributes to more sustainable construction by reducing the amount of concrete used.

1.2 High Strength Concrete

High-strength concrete (HSC) is known as concrete with a compressive design strength of 55 MN/m^2 or more [3].

Despite the fact that HSC is frequently seen as a new material, it has gradually developed over many years. The minimum strength range of HSC changes with time and geographic area and is determined mainly by the availability of raw materials, technical know-how, and industry demand. Concrete strength had gradually increased since the 1950s when it was 34 MPa; in the 1960s, (41-52) MPa, in the early 1970s, 62 MPa concrete was the product. In recent years, the rapid development in concrete technology that made HSC has higher compressive strength [3]. HSC has a number of advantages over conventional concrete (CC). The HSC is suitable for compression members such as piles and columns. Concrete having a greater compressive strength reduces the size of the column and increases existing floor space. In the structures like folded plates, domes, arches, and shells, where significant in-plane compressive stresses exist, HSC can also be used effectively. The considerably higher compressive strength of a structure with HSC will help lessen the total dead load on the foundation. Furthermore, the fundamental procedures of HSC provide a dense microstructure, making ingress of harmful

chemicals from the environment impossible to enter the core of the concrete, hence improving the structure's performance as well as long-term durability [4].

1.3 Lightweight Concrete (LWC)

LWC is a special concrete that has weights lighter than CC. It may be made with an oven-dry (O.D.) density range of about 0.3 t/m^3 to 2 t/m^3 [5]. There are three types of LWC; Figure (1-1) shows the principal methods to produce types of LWC.

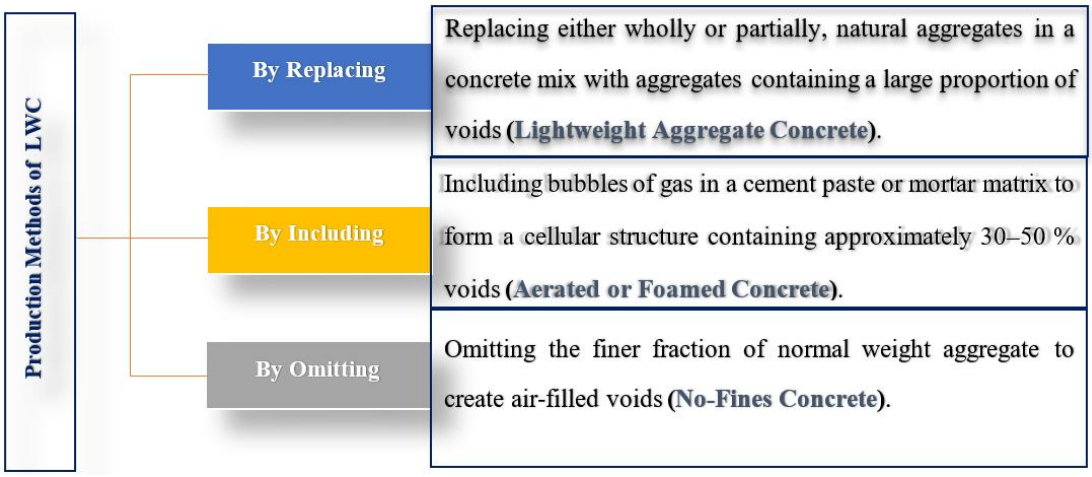

Figure (1-1) Lightweight concrete types

1.3.1 Lightweight Aggregate Concrete (LWAC)

The important characteristic of lightweight aggregate (LWA) is distinguished by its high porosity, which leads in a low specific gravity, big water absorption, and low strength.

LWA can be either natural or artificial materials. Natural LWA can be found in several regions of the world. Only mechanical treatment is required to make this aggregate ready for usage (crushing and sieving). Diatomite, pumice, scoria, volcanic cinders, and tuff are the primary aggregates categorized in this group [6], [7].

Thermal treatment of naturally occurring materials or waste materials from industrial processes results in artificial LWA production [7].

The natural resources utilized to manufacture LWA in the second category are as follows: vermiculite, perlite, slate, clay, shale, etc. On the other side, the industrial by-products used to produce LWA are Lytag (commercial name of sintered pulverized fuel ash), blast furnace slag (BFS), industrial waste, sludge, etc. [7].

1.3.2 Aerated Concrete and Foamed Concrete

Aerated, cellular, gas, or foamed concrete contain voids intentionally incorporated into the cement paste at the hardened state or mortar matrix, resulting in a cellular structure that has less density. These concretes will be split into two varieties, namely aerated and foamed [5].

1.3.2.1 Aerated Concrete

Aluminum powder (AP) is usually used to make gas (hydrogen) bubbles in cement paste or mortar matrix that is crafted from Portland cement of the right consistency. The amount of AP used is about 0.2 percent of the weight of the cement. AP reacts with alkalis and calcium hydroxide ($Ca(OH)_2$), which are dissolved in the solvent to make hydrogen bubbles [5]. This type of concrete is designed for factory production.

1.3.2.2 Foamed Concrete

It is categorized as having a higher than 25% air content. There are two main ways to add air in a mortar or concrete mixture [5]:

The first method, Foam, is a making machine that may be used in a conventional mixer or ready-mix concrete truck.

The second method, in a high-shear mixer, a foam-producing synthetic or protein-based admixture can be added to the other mix ingredients.

1.3.3 No Fines Concrete (NFC)

It is a form of LWC made without fine aggregate from CC. This concrete has only cement, water, and CA. Each CA particle is coated with a thin cement paste coating (up to 1.3 mm) which forces it into point-to-point contact with surrounding particles, resulting in interstitial gaps. The interconnections between the spaces result in porous open-textured concrete with lower shrinkage, density, and strength [5].

1.4 Advantages and Disadvantages of LWC

LWC is going to be one of the important construction materials due to its many advantages compared with its few disadvantages as described below [8]:

1.4.1 Advantages of LWC

- Rapid and simple construction.
- Both efficient in terms of transportation and lowers the need for labor.
- Lower thermal expansion coefficient.
- Superior resistance to earthquakes.

1.4.2 Disadvantages of LWC

- Extremely sensitive to the amount of water in the mixture.

-Difficultly to lay and finish because of the aggregate's angularity and porosity. The cement mortar may separate and float to the surface in some mixtures.

- To ensure proper mixing, the mixing period is longer than for NWC.

1.5 Structural Lightweight Concrete (SLWC)

Compressive strength and density are two essential parameters of SLWC. The following definitions of lightweight structural concrete are used in international codes and standards:

BS EN1992-1-1, 2004 (British) [9] SLWC has a density of not more than 2.20 t/m^3.

ENV 1992-1-4 (Unified Standard of European) [10] Concrete has a closed structure and an O.D. density of less than 2.0 t/m^3 if it is made up of or contains a proportion of natural or manufactured LWA.

UNI 7548.1 (Italy) [11] LWAC is made with LWA, which is characterized by its density being not more than 1.850 t/m^3.

PN-91/B-06263 (Poland) [12] Concrete with a dry density of less than 2.0 t/m^3 composed of cement, LWA of mineral origin, water, possible mineral additives, and chemical admixtures.

NS 3473, 1992 (Norway) [13] Concrete has an O.D. density of around (1.20-2.20) t/m^3 based on LWA.

DIN 1045-1 (German) [14] SLWC has an O.D. density of around (0.8-2.0) t/m^3 and compressive strength of more than16 MPa.

ACI 213-14 (USA) [15] SLWAC which has at 28 days, the cylinder compressive strength must be at least 17 MPa. And an equilibrium density ranges between (1.12 and 1.92) t/m^3.

SLWC comprises all LWA or a combination of LWA and normal-weight aggregate. While high-strength lightweight concrete (HSLWC), according to ACI 213-14 [15], can be defined as a SLWC with 28-day compressive strength of 40 MN/m^2 or greater.

1.6 Sustainability of LWC

Sustainability, when used in the concrete industry, generally indicates the following conditions [15]:

- Saving on materials being utilized in the project.
- Extended lifecycle through enhanced durability in the environment for which it was designed.
- Overall environmental impact of manufacturing, transporting, and placing the concrete product in the final structure.

1.7 Reinforced Concrete Ribbed Slab

Concrete in the tension zone can be collected in regularly spaced ribs cast monolithically and capped with a slab since its resistance in tension is very low compared to its resistance in compression.

Ribbed slabs, sometimes called one-way joist slabs, concrete ribs, or joists spaced uniformly and only spanning in one direction. The ribs integrated into the concrete slab may span perpendicular to the ribs between the columns.

A ribbed slab leads to a lighter slab compared to an equivalent solid slab, which helps reduce the weight. Reducing the amount of concrete beneath the usual neutral axis of a solid slab allows for a reduction in concrete consumption. This adds much more to environmental sustainability, as less cement and carbon footprint manufacturing is achieved by reducing concrete volume. Because of this, ribbed slabs contribute to a lower self-weight, thus bringing a low self-weight of the structure itself.

Ribbed slabs are most economical in hotels, schools, hospitals, and residential construction when long spans and loads are small.

Ribbed slabs are divided into two categories: hollow block slabs (HBSs) and moulded slabs, as shown in Figure (1-2) below.

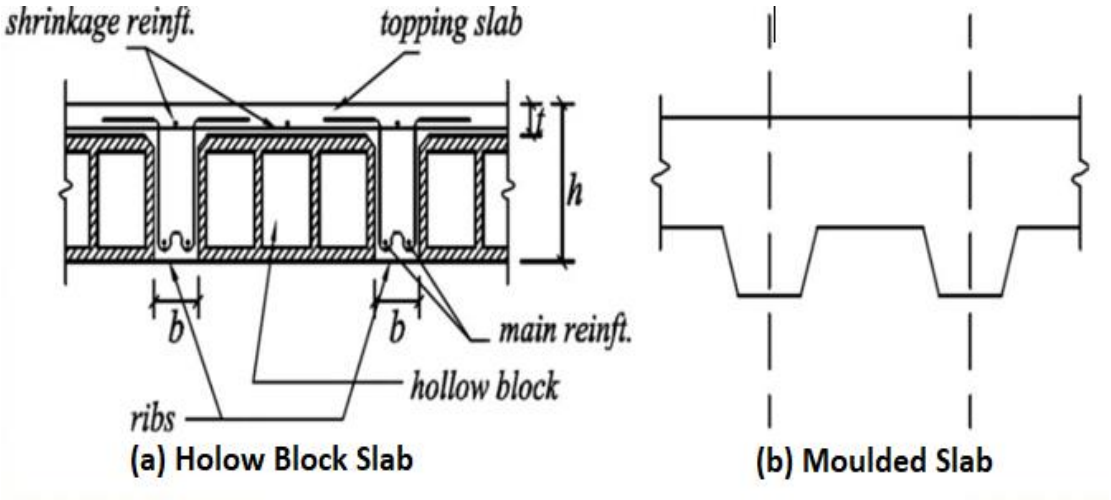

Figure (1-2) Types of ribbed slab [16]

Each slab form is made up of a series of reinforced concrete ribs that span in short directions and support a thin topping slab above. The HBS is ideally suited for small, irregularly shaped floors as the hollow blocks can be simply fitted into forms that are not regular. In contrast, the moulded slab is most economical and suitable for vast symmetrically supported floors. Moulds made of steel or fiberglass can be utilized to create temporary formwork. Ribbed slabs can be utilized in one-way and two-way slabs (waffle slabs). Depending on the span, either hidden beams or drops may be utilized to support these slabs. Slabs are considered one-way; if the ribs are only in one direction, regardless of panel length ratio [16].

1.7.1 Design Limitations of Reinforced Concrete Ribbed Slab

British Standard (BS 8110) [17] and ACI 318-19 Code [18] put some limits for design ribbed slab as illustrated below:

According to BS 8110 [17]:

1- The width of a rib will be determined by the spacing of the bars, cover, and fire resistance.

2- The thickness of the concrete flange or topping should not be less than 5 cm or 1/10 of the clear distance between ribs for slabs without permanent blocks, whichever is greater.

3- Clear spacing between ribs must not be more than 150 cm.

While the limitations of ACI 318-19 Code [18] are:

1- Ribs must be at least 10 cm wide in all places along with the deep.

2- The overall depth of the ribs must be less than (3.5 × minimum widths).

3- Clear spacing between ribs must not be more than 75 cm.

4- Slab thickness shall be at least the greater of ((0.0833 the clear spacing between ribs) and 5 cm).

Any one-way ribbed slab that does not meet the requirements of 1 through 4 must be designed as beams and slab.

1.7.2 Advantages and Disadvantages of Reinforced Concrete Ribbed Slab

The advantages of ribbed slabs are [19]:

- Weight and material savings.
- Design to long spans.
- Offering an attractive appearance that is appropriate for architectural design.
- Formwork pans that can be reused might save money on the ribbed slab.
- Easy to penetrate vertically between ribs.

Ribbed slabs have the following drawbacks:

- The fire rating may be influenced by the slab's thickness of the slab between the ribs.
- Requiring unique or proprietary formwork.
- Requiring greater floor-to-floor height.

1.8 Dynamic Load

A load is said to be dynamic if its magnitude, direction, and position all change over the course of a certain period of time. During the course of their existence, structures are often subjected to at least one different kind of dynamic load.

Deterministic and non-deterministic dynamic loads can be categorized according to their nature. A deterministic load is one in which the magnitude, location, and time variation of the load are all known. This type of analysis is known as deterministic analysis. The analysis is called non-deterministic if the fluctuation in load over time is unknown, in which case the loading is referred to as random or stochastic.

Periodic and non-periodic dynamic loads are other terms for dynamic loads. The term "periodic loading" refers to a loading that occurs at regular periods. Figure (1-3a) shows a sine or cosine function as a single type of periodic loading. There is a periodic motion in a vibration caused by spinning mass. Simple harmonic motion, as depicted in Figure (1-3a), is a form of periodic loading. A non-harmonic periodic loading is depicted in Figure (1-3b). The sum of a significant number of harmonic terms in a Fourier series can reflect the majority of periodic loads. 'Non-periodic' refers to any loading that does not fall into the periodic category. Nonperiodic loads include those seen in Figures (1-3c) and (1-3d), which depict blast loading and earthquake ground motion, respectively [20].

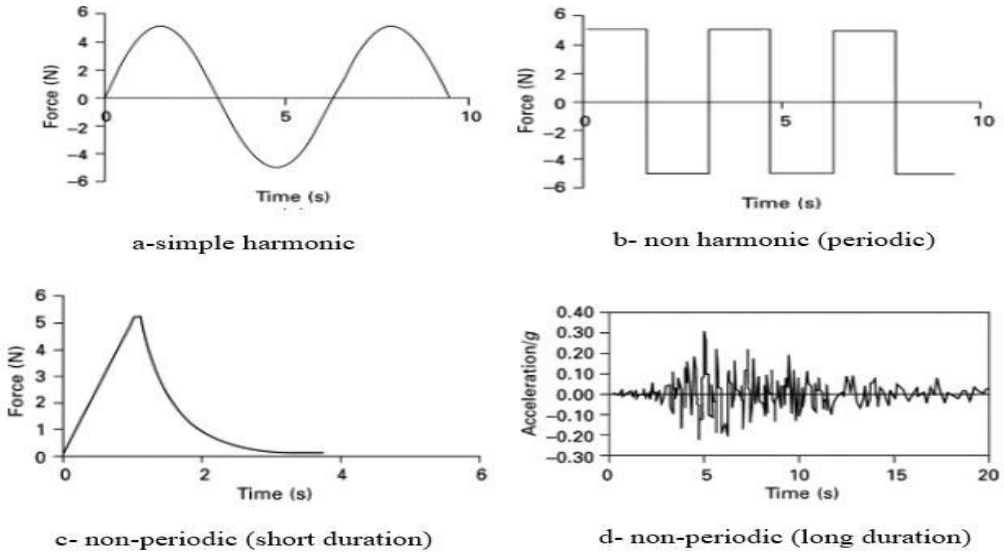

Figure (1-3) Different types of dynamic loads

1.9 Objectives and Scope of the Current Work

1- Experimental investigation to develop a concrete mix that meets strength, density, and workability requirements of high strength-lightweight concrete (HSLWC) using pumice stone and by-product materials such as sugar molasses.

2- Experimental investigation of the physical and mechanical characteristics of HSC and normal-strength concrete (NSC) with and without LWA.

3- Comparing the observed static behavior of HSC and NSC with and without LWA of one–way reinforced ribbed slabs.

4- Investigating the effect of steel fiber inclusion, steel reinforcement ratio, geometry of section, ribs spacing on the static behavior of HSLWC one-way ribbed slab.

5- Investigating the effect of different types of concrete, inclusion of steel fiber, geometry of section on the dynamic behavior of one–way reinforced ribbed slabs.

6- Comparing the observed structural static and dynamic behavior of HSLWC one-way ribbed slab and solid slab at the same concrete volume.

7- Investigating the efficiency of using HSLWC in producing a one-way ribbed slab.

8- Comparing experimental results and predicated values using ACI 318-19 code.

9- Performing numerical analysis by non-linear finite element method using the ABAQUS program, including the parametric studies.

1.10 Layout of Thesis

The study is divided into six chapters:

Chapter One provides a general introduction and general information about HSC, LWC, one-way ribbed slab units, and dynamic load.

Chapter Two covers all previous researches relevant to the topic of this study, which includes experimental, numerical, and theoretical studies. **Chapter Three** covers the experimental program, including the materials utilized, the slab models' features and manufacturing method, and testing. **Chapter Four** presents the findings of the experiments and a discussion of them.

Chapter Five contains the numerical analysis of slab specimens using the finite element method carried by the ABAQUS computer program and comparing results with those experimental results.

Chapter Six presents conclusions and recommendations for future work.

Chapter Two

Literature Review

Chapter Two: Literature Review

2.1 Introduction

A review of the previous investigations related to the subject of this thesis is presented in this chapter, providing a general overview on different previous studies on high strength-lightweight concrete (HSLWC) that may help in developing the behavior of one–way ribbed slab.

This chapter is organized as follows: previous studies on lightweight concrete (LWC), high strength concrete (HSC), HSLWC and behavior of HSLWC members, behavior of one-way slabs, and behavior of reinforced concrete members under harmonic load.

2.2 Previous Studies on LWC

In the past, attempts were made to lower the self–weight of concrete to enhance the efficiency of concrete as a structural material. Replacing partially or totally the normal-weight aggregate concrete (NWAC) with lower weight aggregates generates LWC, was intended in this investigation.

AL-Rubayie (2007) [21] produced structural-lightweight concrete (SLWC) by including crushed bricks as both coarse aggregate (CA) and fine aggregate, as well as CA solely with the use of normal-weight fine aggregate. The density of the resulting concrete has been investigated. Results of cube compressive strength ranged from 22.5 MPa to 39.5 MPa for broken bricks concrete, while dry density was (1160-2110) kg/m^3. The modulus of rupture was (3.7-7.3) MPa, whereas the splitting tensile strength ranged from 1.66 MPa to 4.81 MPa.

Abdeen and Hodhod (2010) [22] utilized fired crushed brick, vermiculite, as well as light exfoliated clay aggregate (LECA). The brick

industry's byproducts made it possible to get the first kind. The other types were created locally for a wide range of functions. Nine mixes of concrete were produced using the exact proportions of cement and water 400 kg/m^{3}and 200 kg/m^3, respectively, and different types of aggregate. They found a 45 percent reduction in the unit weight of SLWC compared to NWC and a 50 percent decrease in the compressive strength of SLWC. Also, the tensile strength gives a lower value than NWC.

Al-Bayati et al. (2013) [23] casted five series of different concrete mixes, the type of concrete mixes depended on the volumetric replacement ratio (0, 25, 50, 75, and 100) % of the LWA, which was made from natural local material (porcelanite stone). The experimental test results showed that cylinder compressive strength and density was (30.8, 27.1, 22.1, 18.8, and 17.5) MPa and (2401, 2245, 2121,1972, and 1841) kg/m^3 for (0, 25, 50, 75, and 100) % of graded porcelanite replacement, respectively. They further represented new empirical predicted formulas for cube compressive strength, cylinder compressive strength, and their relationship.

Al-Aridee (2014) [24] investigated the ability to use local clays (Attapulgite), from the southwest of Iraq, as a CA. The experimental work involved manufacturing the LWA and investigating the mechanical characteristics of the attapulgite aggregate concrete, and comparing the results with porcelanite aggregate concrete. The tests result of dry specific gravity was (1.45) and the bulk density was (808 kg/m^3) for the Attapulgite LWA at a temperature of treatment burning (1100°C) for a duration of (half-hour), and the result of a density of 1824 kg/m^3 for a cylinder compressive strength was (27.7 MPa) with the ratio of (w/c = 0.4) and percentages of increase for (compressive strength, splitting strength, rupture modulus, and elasticity modulus) were about 58.85

percent, 41 percent, 183 percent, and 81 percent), respectively, relative to the corresponding porcelanite aggregate concrete with the same mix proportions.

Abbas and Abdulzahra (2015) [25] presented different types of LWA in their study to produce LWC. These types were (white thermostone, red ceramic, and red block) aggregate, all of these aggregates have been brought from construction waste. They carried out a test on both fresh and hardened concrete. They observed that the increase in the proportion of CA reduced the compressive strength, modulus of elasticity, tensile strength, and slump flow. Also, the red ceramic concrete can be classified as the best type of LWC. However, the final results were within the limits of standards.

Jomaa'h and Algubory (2017) [26] highlighted on a specialized study to replacing (0,25, 50, 75, and 100) % as volumetric ratios of normal CA by lightweight CA (claystone (bonza) and thermostone), in this study (compressive strength, indirect tensile strength (splitting tensile strength and rupture modulus), and elastic modulus) as well as the unit weight, thermal conductivity, and absorption have been evaluated. The experimental results showed that a drop in compressive strength was between (4.85-63.31) %, indirect tensile strength was between (5.66-72.75) % for splitting tensile strength and (3-40) % for modulus of rupture). Also, elastic modulus, oven-dry (O.D.) density, absorption, and thermal conductivity were between (3.85-40.93) %, (9.11-40.04) %, (4.58-11.8) %, and (23.16-68.87) %, respectively, compared to concrete with normal CA.

Khalil et al. (2017) [27] investigated the use of recycled brick from the waste of construction as lightweight CA in high-performance lightweight aggregate concrete (HPLWAC). This HPLWAC is strengthened with

one-type fiber (mono) and with mixed fibers of more than one type (hybrid) at (volume fraction (V_f) = 0.75%) of macro hooked steel fiber (S1), straight steel fiber (S), macro crimped plastic fiber (P), and micro polypropylene fiber (PP). The cube compressive strength and dry density of HPLWAC without fibers were 41.2MPa, and 1930 kg/m^3, respectively. One HPLWAC mixture (without fiber), two mono fiber concrete mixtures ((0.75% S1) and (0.75% P)), two double hybrid fiber concrete mixtures ((0.5 % S1 + 0.25% PP) and (0.5% P + 0.25 S)), and one concrete mixture with triple hybrid fibers (0.25%S+ 0.25% S1+ 0.25% PP) were produced to study both fresh and hardened characteristics of concrete (workability, fresh density, O.D. density, compressive strength, splitting tensile strength, rupture modulus, and absorption). The experimental results showed that the HPLWAC specimens with double and triple fibers had much higher splitting tensile strength and rupture modulus in comparison to HPLWAC specimens without fiber. The increase in splitting tensile strength for specimens with mono S1 and mono were 65.9% and 45.5%, respectively, at 28 days of age relative to the HPLWAC without fibers. The increase in splitting tensile strength for triple hybrid fiber-reinforced specimens was 68.6%, while the increase in modulus of rupture was 59.6% at 28 days of age relative to the HPLWAC without fibers specimens. Furthermore, the percentage of the increase in the compressive strength for specimens with mono S1 and triple hybrid fiber was 5.78 and 31.6, respectively. In comparison, mono P reduced compressive strength by about 8.3% at 28 days of age relative to HPLWAC without fibers.

Al-Mamoori et al. (2018) [28] conducted an experimental study to produce lightweight aggregate concrete (LWAC) from locally available natural and waste materials. The light CA which was devoted in this

study were (gravel, porcelinite, pumice, and hybrid (brick + thermestone)). The destructive and non-destructive tests were conducted in this study. They got that from waste, recycled, and natural local resources that can be used to manufacture SLWAC with a density of no more than 2000 kg/m^3 with (150 × 300) mm cylinder compressive strength ranging from (25.3-36.1) MPa at 28 days. The reduction in the mechanical properties (densities, cylinder compressive strength, ultrasonic pulse velocity (UPV), splitting tensile strength, modulus of rupture, and elasticity modulus for different aggregate types and volumetric ratio replacement as compared with natural gravel aggregate were:

- 100 % porcelinite: (19.99, 27.66, 22, 38.65, 41.22, and 27.17) %.

- 100 % pumice: (20.71, 8.38, 28.31, 15.95, 19.39, and 12.32) %.

- 75 % brick + 25 % thermestone: (21.50, 35.79, 32.59, 43.78, 51.22, and 28.26) %, respectively.

Hama et al. (2018) [29] presented a study to improve the tensile strength of porcelanite LWAC by using chopped carbon fibers. The results displayed that strength of (compressive and splitting tensile) and elastic modulus of carbon fibers porcelanite LWAC improved with increasing carbon fiber percentage of mix volume up to 2 % (by volume) compared to reference LWAC (i.e., no fibers inclusion). The percentage of improvement was (14.40, 68.00, and 10.66) for compressive strength, splitting tensile strength, and elastic modulus, respectively. The LWC density decreased with the increase in carbon fibers because chopped carbon has a low density. Also, the chopped carbon improved the ductility of porcelanite LWA.

Jomaa'h et al. (2019) [30] focused on changing the normal-weight CA with lightweight CA (rubber, claystone (bonza), polystyrene, and thermostone) at different volumetric ratios of (25, 50, and 75) % additionally to the preparation of a control mixture to assess mechanical characteristics of concrete. The test results showed that a drop in the mechanical characteristics of concrete with an increase in the lightweight CA, the ranges of the reduction in the compressive strength, density, splitting tensile strength, and modulus of rupture were (24.58–72.27) %, (5.72–31.36) %, (15.09–71.73) %, and (34.75-65.55) % compared with control mixture, respectively.

2.3 Previous Studies on HSC

Many authors investigated the HSC such as, **Jin and Li (2003)** [31] reported the improvements in mechanical characteristics of concrete through the inclusion of the different mineral admixtures like silica fume (SF), slag, fly ash (FA), and metakaolin (MK), and the stress-deformation response. They observed that the various mineral admixtures have varying effects on the characteristics of young concrete. MK typically exhibited the most remarkable improvement in the mechanical properties of young concrete.

Mazloom et al. (2004) [32] studied the short and long-term mechanical characteristics of HSC, which were included (compressive strength, elasticity modulus, creep, and shrinkage). The cement was replaced partially with SF at ratios of replacement (0, 6, 10, and 15) % with a fixed w/b ratio of 0.35. Various superplasticizer (SP) dosages were used to achieve the desired slump in each mixture. The outcomes of the tests revealed that the development of concrete mixtures with SF was negligible after 90 days. However, after one year, the control concrete increased by 26 % and 14 % compared to its strength at 28 and 90 days,

respectively. At 28-day, the compressive strength with 15 % SF was approximately 21% higher than that of control concrete. Therefore, the incorporation of SF into the concrete mixture mainly affects the short–term concrete strength. The 6%, 10 %, and 15 % SF inclusion did not affect the total shrinkage but increased the autogenous concrete shrinkage and reduced drying concrete shrinkage by (16.67 %, 33 %, and 50 %) and (11 %, 22.5 %, and 35.6%), respectively. Furthermore, the creep decreased as the level of SF replacement increased.

Justice et al. (2005) [33] investigated the behavior of two different types of MK (11.1 and 25.4) m^2/g as supplementary cementitious materials (SCMs) in concrete mixtures. Mechanical properties such as (compressive and tensile) strength, as well as elastic modulus, were investigated when MK and SF were used to replace 8% of the cement weight in control mixtures (without SCM) at different water-to-cementitious materials ratios (w/cm) (0.40 to 0.60), respectively. Tensile strength and elastic modulus rose while setting time decreased in pastes containing both MKs. Both MKs inhibited the fast chloride ion permeability and expansion compared to SF and control mixtures due to the alkali-silica reaction. Both MKs outperformed SF, but the finer MK produced higher outcomes.

Hariharan et al. (2011) [34] conducted an experimental study to test the compressive strength of HSC, which was produced by partially substituting SF for cement at a ratio of (0, 6, and 10) percent and FA class C used in various proportions (0 %,30 %, 40%, and 50%), the concrete mixes proportions had a w/b ratio of 0.4 and different dosages of SP. The content of the binder was 450 kilograms per cubic meter. Early gains in strength were evident from the addition of SF, whereas long-term gains were evident from the addition of FA. The compressive strength of

concrete was discovered to be increased by the PC-FA-SF concrete's ternary system over the binary system constructed with only FA and SF.

Ahmed and Abd (2016) [35] highlighted the effect of different types of SCMs in binary blends on the mechanical properties of HSC. The works experimental included three stages. The first stage involved locally preparing cementitious materials as cement replacement (pumice and MK) at levels of 10%, 15%, and 20% and exported SF at replacement ratios of (8 percent, 10 percent, and 15 percent). The second stage involved casting several trail mixes to choose the optimum SP and w/cm ratio to obtain slump (60–80) mm. The last stage involved tests finding the compressive strength, splitting tensile strength, and modulus of rupture. These properties were evaluated for various days (ranging from 7 to 180). The results indicated that SF outperformed other SCMs (pumice or MK) in aspects like compressive strength, splitting tensile strength, and rupture modulus development at ages ranging from 7 to 180 days, with an average percentage increase of approximately 19 percent, 23 percent, and 18.7 percent, respectively, when using (8 percent, 10 percent, and 15 percent) of SF.

Al-Mamoori F. and Al-Mamoori A. (2018) [36] investigated the influence of using sugar molasses (SM) supplies from Iraqi factories on HSC and cement paste in hot Iraqi weather, at percentages of (0, 0.05, 0.1, 0.2, and 0.3) percent from the weight of cement as a retarder agent. It was got the optimum dosage of SM was 0.2 % which gave an increase in the compressive strength at 28-day by about 11.2 % and delayed the time of the initial setting by about 277 minutes.

2.4 Previous Studies of HSLWC

Slate et al. (1986) [37] summarized the outcomes of an experimental study of the mechanical characteristics of HSLWC under the effect of short–term loads. Concretes had compressive strengths up to 59 MPa, and densities ranged from (1440 to 1650) kg/m^3. Information was found about compressive strength, strength development with time, specimen size, elastic modulus, Poisson ratio (υ), rupture modulus, splitting tensile strength, and drying effect. The deformation characteristics under load also were investigated. Depending on the experimental outcomes presented, they found that:

- At early ages, moist–cured HSLWC showed a faster rate of strength development than corresponding low-strength LWC, and this disparity became insignificant at later ages.
- For high-strength LWC, the uniaxial compression stress-strain relationship was steeper and more linear with increasing stress–strength ratio than for low-strength LWC.

The υ for LWC was approximately 0.2, without depending on the test's concrete strength, age, and curing condition.

Zhang and Gjorv (1991) [38] presented data on the HSLWC compressive strength characteristics up to 100 MPa with a density of around 1.865 t/m^3 and compared it with other types of concrete (high-strength normal-weight concrete (HSNWC), LWC, and NWC). Five different LWAs (one type of sintered FA and four various types of expanded clay) were studied. The results indicated that the tensile/compressive strength ratio of HSLWC appears to be lower than that of HSNWC. The elasticity modulus was significantly lower than that of NWC. The ultimate strain at peak load was more significant than

NWC. The stress-strain curve with low to medium strength was more linear than LWC in the ascending part.

Mor (1992) [39] investigated the influence of condensed silica fume (CSF) on the mechanical characteristics of HSC produced from LWA and compared these properties with the same strength properties of NWC. For four concrete mixes with the same compressive strength (69 MPa), the rupture modulus, elasticity modulus, stress-strain curve properties, and bond-slip of steel reinforcing bars were tested with different contents of CSF (0 %, and 13% to 15 %) by cement weight and low water-cement ratios (0.25 to 0.34). The author found that the addition of CSF reduced the modulus of rupture. In contrast, this addition did not significantly change the modulus of elasticity to compressive strength ratio for both LWAC and NWAC. However, it doubled the steel-concrete bond strength for LWAC without a significant effect on NWAC. The lower modulus of elasticity of LWAC, when used in conjunction with an appropriate aggregate and cement paste matrix, the bond adhesion is better used, allowing for higher levels of stress and strain.

Al- Khaiat and Haque (1998) [40] investigated the physical properties and initial curing effect on the early strength of LWC. They produced a LWC with a cube compressive strength of 50 MPa and a fresh density of 1.80 t/m^3 by utilizing Lytag CA and fine aggregate. They found that the drying shrinkage of the SLWC up to three months was more than (600) macro strain. On another side, For the first month of exposure, the compressive strength of SLWC appears to be less susceptible than that of NWC to a lack of cure. In contrast, the lack of curing appears to have a comparable effect on the long-term strength growth of SLWC as it does on the NWC.

Rossignolo et al. (2003) [41] presented the outcomes of SLWC produced from Brazilian LWAs (expanded clay). In their investigation, the cement quantity ranged from 0.440 to 0.710 t/m^3, and SF was used in a dosage of 10% by weight of cement replacement. The compressive strength and dry concrete density at 28-day were found to vary between 39.5 and 53.6 MPa and 1.460 and 1.605 t/m^3, respectively

Katkhuda et al. (2009) [42] studied the influence of adding SF on the compressive and tensile strengths of HSLWC was tested at 28 days. SF was substituted with 0 percent, 5 percent, 10 percent, 15 percent, 20 percent, and 25 percent for w/cm ratios ranging from 0.26 to 0.42. The results showed that the best SF replacement percentages for getting the best results were:

- Compressive strength ranges from 15 percent to 25 percent depending on the w/cm ratio of the mix.

- Splitting tensile strength was almost unique where it was noted 15 percent for w/cm (0.26 and 0.30) and 20 percent for w/cm (0.34, 0.38, and 0.42).

- Flexural tensile strength depended on the w/c ratio. The optimum percentage was 15 percent for w/cm (0.26), 20 percent for w/cm (0.3 and 0.34), and 25 percent for w/cm (0.38 and 0.42). The optimal percentage of SF replacement increased with the w/cm ratio as the case for compressive strength. They found that the compressive and indirect tensile strengths improved with SF inclusion. However, the percentage of optimum replacement was not constant because it depended on the w/cm ratio of the mixture.

Al-Baghdadi (2011) [43] highlighted the development of HSLWC utilizing a local clay brick waste as a lightweight CA, hydrated lime as

(mineral admixtures), and SP. Based on the results of this work, it has been concluded that HSC with a density of no more than 2.0 t/m^3 can be produced using mineral admixtures (hydrated lime) and SP and local bricks as CA (i.e., LWA). The archived compressive strength of cube (150 mm) at 28 days ranged from 27.2 MPa to 53.7 MPa, with O.D. density ranging between (1.9-1.96) t /m^3; the strength of splitting tensile varied (from 3.1 MPa to 4.0 MPa), and modulus of rupture ranged from 4.5 MPa to 7.1 MPa, and the modulus of elasticity results ranged between (22800-26000) MPa. According to **Sajedi and Shafigh (2012)** [44], the use of LECA aggregates, with mineral admixtures and chemical admixtures, coupled with limestone, a mix of high-strength structural lightweight concrete was developed. When combined with LWAs, limestone enhanced the mechanical qualities of concrete. From 1.610 t/m^3 to 1.965 t/m^3 (dry density) and 34 MPa to 67 MPa (cube compressive strength) of SLWC was achieved.

Fawzi et al. (2013) [45] conducted an experimental study to look for the effect of MK as a ratio of cement replacement on the physical and mechanical characteristics of porcelinate LWC. The test outcomes indicated that using MK improves the mechanical properties of porcelinate LWC. The optimum MK replacement percentage for obtaining maximum 28-day improvement was 15%, and the improvement in compressive strength, splitting tensile strength, flexural strength, elastic modulus, and unit weight was (135.5 %, 80.5 %, 97.4 %, 49.8 %, and 15.25), respectively with reference mix which had compressive strength 20 MPa and unit weight 1.567 t/m^3.

Wei et al. (2020) [46] investigated the influence of the LWA size on the compressive strength, flexural strength, splitting tensile strength, and dry density of high strength-lightweight aggregate concrete. In this

investigation, four sizes of the expanded shale aggregate were adopted. The test results showed that the absence of medium-size particles declined the dry density and compaction of HSLWC. Meanwhile, the specimens having medium-size of LWA showed the highest cube compressive strength up to 72 MPa at 28-day. Furthermore, specimens having a single size of LWA displayed lower flexural and splitting tensile strengths than those having three sizes of LWA.

2.5 Behavior of High Strength–Lightweight Reinforced Concrete Members

Ahmad and Baker (1991) [47] focused on the flexure behavior of high strength-lightweight reinforced concrete beams throughout testing six singly reinforced concrete beams. All beams were (360 cm length × 15.24 cm wide × 30.48 cm deep). The variables in this research were the cylinder compressive strength of concrete ($35.9 < f_c' < 75.9$) MPa and the tensile steel reinforcement to the balance steel reinforcement ratio ($0.18 < \rho/\rho_b < 0.54$). The results were presented; the load-deformation behaviors, crack patterns, and ductility (μ) index. They reported that to achieve a μ equal to 3, ρ/ρ_b should not be more than 0.4 for beams with f_c' equal to 55 MPa and ρ/ρ_b should not be more than 0.2 for beams with f_c' equal to 75.9MPa. Furthermore, they compared their experimental results with the ACI 318 code. They found that the flexural design provisions of the ACI 318 Code are found to be adequate for predicting the strength of singly reinforced HSLWC beams.

Ahmad and Batts (1991) [48] emphasized the flexure behavior of high strength-lightweight doubly reinforced concrete beams throughout testing six reinforced concrete beams. All beams were (360 cm length × 15.24 cm wide × 30.48 cm deep), the tension steel reinforcement to compression reinforcement ratio was kept as 2, and stirrups reinforcement

placed at space of the half depth of the section. The variables in this study were the compressive strength of concrete (46.2 < f_c' < 76.3) MPa and the tensile steel reinforcement to the balance steel reinforcement ratio (0.16 < ρ/ρ_b < 0.47). The results were presented as the load-deformation behaviors, crack patterns, and μ. They reported that to achieve a μ equal to 3, ρ/ρ_b should not be more than 0.4 for beams with f_c' equal to 55 MPa and ρ/ρ_b should not be more than 0.2 for beams with f_c' equal to 75.9MPa, furthermore, they noted that ACI 318 rectangular stress block underestimated the flexural capacity for doubly reinforced HSLWC beams and the strain value of 0.003 recommended by the ACI 318 code appeared to be suitable for doubly reinforced HSLWC with f_c' less than 75.9 MPa.

Ahmad et al. (1995) [49] investigated the experimental behavior of shear capacity of lightweight reinforced concrete beams with normal and high compressive strength concrete. In this investigation, the compressive strength, shear reinforcement ratio, and shear span to depth ratio (a/d) were ranged from (30.5-89.5) MPa, (0-0.784) %, and (1-4), respectively. The specimen's details as shown in Figure (2-1). The results indicated that for the range of factors examined, μ decreased with an increase in the compressive strength. When shear reinforcement was applied at about five times the minimal amount needed by ACI 318-89 [50] code, normal compressive strength concrete beams with a/d of three demonstrated a near plastic post-peak behavior. Using a higher amount of shear reinforcement up to 0.0051 had a minor influence on the shear μ of beams with a/d equal to one. Though, for beams with a/d equal to two and three, the shear μ increased. For beams with a/d equal to three, changing the amount of reinforcement of shear from 0.0051 to 0.0065 increased the

shear μ by 25 %. An additional increase in the reinforcement of shear ratio did not result in an increase in the μ of the shear.

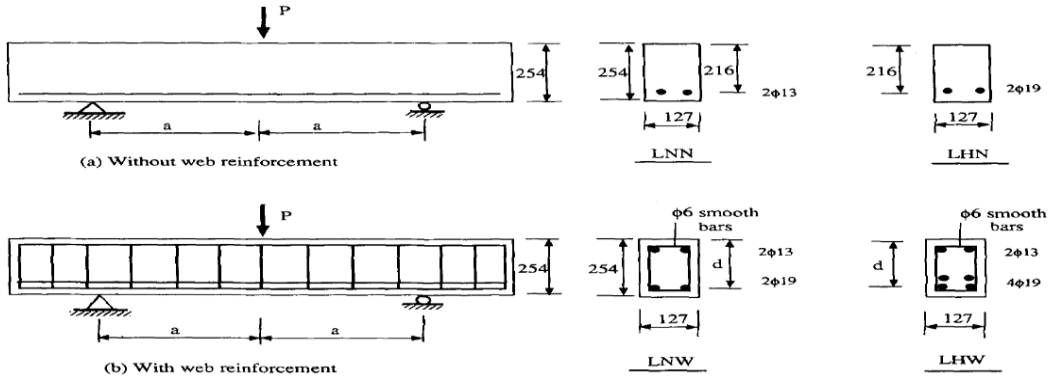

Figure (2-1) Specimen's details for lightweight beams with NSC and HSC [49]

Sin et al. (2011) [51] tested 18 simply supported LWAC beams and 3 NWC beams; the beam details are shown in Figure (2-2). Compressive strength (20–80) MPa based on 100 mm cube, longitudinal reinforcement ratio in tension zone (0.67 %, 1.02 %, 1.45 %, 1.61 %, and 2.22 %), longitudinal reinforcement ratio in compression (0 %, 0.43 %, 0.73 %, and 1.11 %), the spacing between the stirrups in the flexural zone (0 mm, 50 mm, 90 mm, 130 mm, and 180 mm), and steel bar diameter (ϕ13 mm, ϕ16 mm, and ϕ 20 mm) were used to investigate the structural behavior of HSC beams and to compare with reference beams. The authors found that:

- At assumed service load (the ultimate load multiplied approximately by 0.625), the cracking behavior of an LWAC beam concerning maximum crack width and the number of cracks was slightly better than the equivalent NWC beam.

- Although LWAC beams exhibit greater deflections than their NWC counterparts under an estimated service load, LWAC beams are less ductile.

- The ultimate strengths of LWAC beams were as same as the NWC beams.

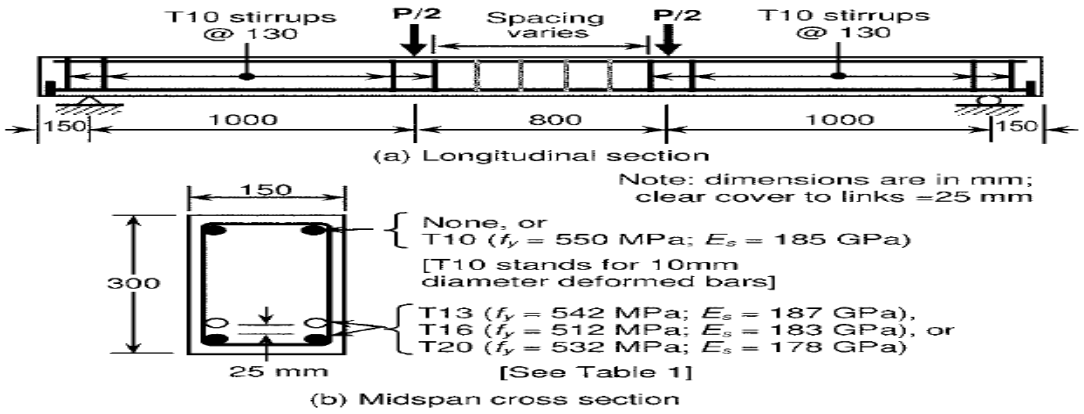

Figure (2-2) Beam and test setup details [51]

Carmo et al. (2013) [52] focused on the effect of LWAC on the structural behavior (bending and ductility) of reinforced concrete rectangular beams. The experimental work was divided into three series to assess the influence of the difference between each series' parameters. The first series was created to look into the effects of changing the ratio of tensile steel reinforcement, which was varied between (0.54% and 2.96%). The second series was to investigate the effect of varying transverse steel reinforcement ratios at the flexural zone, which was (0 %, 0.6%, and 1.68%), and the last series utilized to investigate the influence of compressive strength, which was ranged from 35 MPa to 70 MPa. It was stated that the capacity of LWAC beams to sustain deformation depends on the ratio of tensile steel reinforcement. When the reinforcement ratio is increased, the deformation capacity decreases. In addition, the increase in compressive strength of concrete produces an increase in the vertical deformation and curvature, especially when the steel ratio is low. Within the flexural zone and when no transverse steel reinforcement was present, the beams exhibited brittle failure compared to beams with transverse steel reinforcement, particularly those with a

more longitudinal tensile steel reinforcement ratio. Additionally, they said that increasing compressive strength regulated the failure mode and changed it to tension failure in some circumstances involving over-reinforced beams. The stiffness ratio was measured and generally lower than two and different from that predicted by EC2-04 [9].

2.6 Previous Studies on Behavior of Reinforced Concrete One–Way Slabs

2.6.1 Behavior of Reinforced Concrete One–Way Solid Slabs

Altun and Haktanir (2001) [53] proposed that structural members be made from composite reinforced concrete. Two layers are used to construct composite reinforced concrete: a lower layer of NWC, and an upper layer of SLWC, both of which are laid in the fresh phase. A structural behavior of composite reinforced concrete slab elements was equivalent to that of normal reinforced concrete slab elements with superiority in a reduction of the dead weight.

Adil and Abdul Razzaq (2017) [54] casted and tested five simply supported reinforced concrete slabs under point load to study the structural response of two-layer reinforced concrete slabs. LWC with a compressive strength of (25 MPa, 18 MPa, and 15 MPa) was used in the first layer. The second layer was NWC with compressive strength of 25 MPa. The test results showed that using LECA in concrete reduced the composite concrete slab's weight by approximately (11.4%-17.5%). Also, the same response for tested slabs was observed under the influence of loading for both NWC and composite concrete slabs.

Jomaa'h et al. (2018) [55] conducted experimental research to investigate the structural behavior of one–way solid lightweight reinforced concrete slab. The experimental program consisted of cast nine

simply supported one–way solid slabs with two types of lightweight coarse aggregates (claystone and thermostone) in different volumetric aggregate replacement ratios (0, 25, 50, 75, and 100) %. The compressive strength and density were (38.44-12.38) MPa and (2426.41-1502.37) kg/m^3, respectively. The authors found that the mixtures with claystone aggregates gave higher compressive strength and unit weight than thromestone aggregate. The first crack load and ultimate load for slabs decrease with the increase of LWA content. It was further found that the low μ and stiffness for the slabs by increasing the light weight coarse aggregates. In the same year, the numerical analysis was conducted by **Adheem et al. (2018)** [56] to investigate the structural behavior of one–way solid lightweight reinforced concrete slab under static loading. The main variables investigated in this study were types of lightweight aggregates (crushed brick and porcelenite), the thickness of slabs, and the applied loads. It was found that when compared to normal-weight concrete, crushed brick concrete's ultimate load raised by 17.33 percent, and porcelenite concrete dropped by 27.33 percent. Crushed brick is tougher than porcelenite aggregate when used as LWA.

Babu and Rex (2019) [57] presented a study on the structural behavior of LWC slabs. Slab specimens of size (1300 × 500 × 70) mm were designed and poured for different ratios of volumetric replacement (0%, 25%, 50%, 75% and 100%) of coconut shell (CS). A two-point loading test was applied on slabs, and variables such as ultimate moment capacity, absorbed energy, stiffness, ductility index, and cracking pattern were discovered. It was found that:

- The first crack load of CS concrete slab was (14.28 to 64.29) % less than normal particulate slabs.

- The ultimate load of CS concrete slab was 6.89 % to 31.03% less than normal particulate slabs.

- The ductility factor of the CS concrete slab was 29.47% to 75.37% higher than normal particulate slabs.

- The absorbed energy of CS concrete slab increased from (8.77 to 26.84) % higher than normal particulate slabs.

- when the normal-weight CA was replaced up to 50% with CS, the resulting CS concrete represented the same flexural behavior as the normal-weight CA concrete.

2.6.2 Behavior of Reinforced Concrete One–Way Ribbed Slabs

Souza et al. (2014) [58] conducted an experimental study on eight solid and one-way ribbed slabs to find the slab portion's contribution to the shear stress resistance. The panels were split into two groups. Four slabs make up the first group with dimensions (1300 mm × 2000 mm), and the others consist of four slabs (2000 mm × 2000 mm), respectively. The total thickness of the panels was 300 mm with the various flange thicknesses of (30, 50, 80, and 100) mm; the rib's width was 80 mm and spaced 610 mm in the first group (L= 1300 mm), and 960 mm in the second group (L= 2000 mm). All tested slabs have the same longitudinal reinforcement of 245 mm^2 with a yielding strain of 0.023, and compressive strength was 30 MPa at 28 days. Two-line loads were applied on the slabs with (a/d) of 2.15. The experimental investigation outcomes of one-way ribbed slabs revealed that all tested slabs were dominated by shear failure and that the flange's effective contribution in resisting shear stresses was significant. Flexural reinforcement strains increased proportionally to flange depth, resulting in greater ductility. A minor increase in ultimate load by increasing the panel's width.

Al-Azzwi and Al-Asdi (2017) [59] investigated one-way reinforced hollow block slab nonlinear behavior. Eleven of simply supported one-way slabs, three slabs comprised as reference (solid slabs), and others as hollow block slabs (HBSs), the cross-sectional area was reduced by (23.3 % and 29.1 %). The holes were created using a styropor to counteract the tensile loads in the inefficient concrete zones. All slabs have dimensions (1100 mm × 600 mm × 120 mm) with an effective span of 100 cm, except one has a depth of 85 mm. The slab specimens were coordinated as depicted in the flow chart in Figure (2-3). They observed that there were better effects with a rise in HBS cross-sectional area than an increase in rib count at the same percentage reduction in HBS cross-sectional area. Moreover, when the cross-sectional area of a hollow block and solid slabs were reduced to the same level, the HBS with the minimum shear reinforcement had a higher strength capacity. During loading, the cracks in HBSs formed more slowly than in solid slabs.

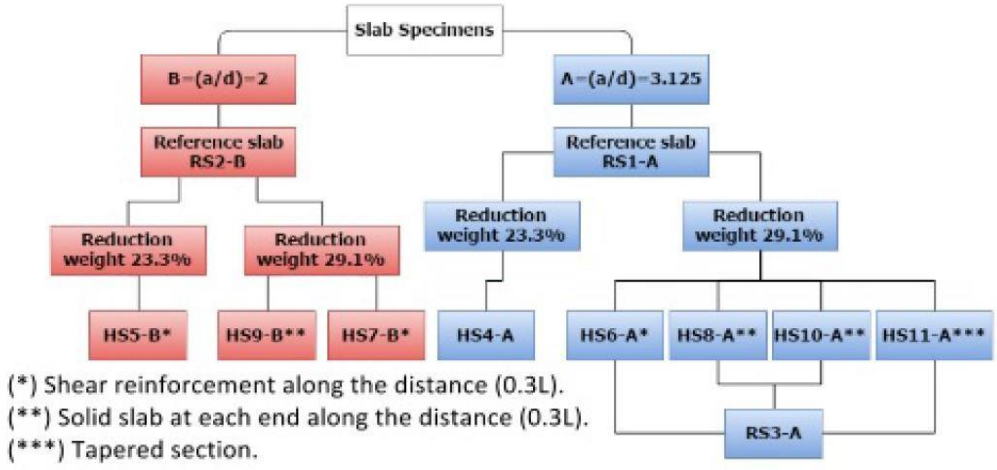

Figure (2-3) Parameters Arrangement [59]

Abdul Rahman et al. (2017) [60] studied the structural behavior of reinforced concrete ribbed slabs with fiber inclusion. The primary material in this study was steel fibers, with no conventional reinforcements used. Three equivalent specimens of ribbed slabs with

variations in the topping thickness of 10.0 cm, 7.5 cm, and 5.0 cm were tested under one-point loading. The test results of these specimens revealed that the ultimate loading of the ribbed slab with 10.0 cm topping was comparable to the loading carrying capacity of the 7.5 cm topping, while 5.0 cm gave the lowest strength. A combination of steel fibers helped to give a long deflection softening than a sudden brittle failure, thus proving its ability to increase the capacity of absorbed energy and improve cracking behavior. While the study of the ultimate strength and behavior of self–compacting ribbed concrete slab with fiber inclusion under two-point loading was carried out by **Ahmad et al. (2017)** [61], they prepared three slabs with dimensions (2800 mm ×1200 mm × 200 mm) as shown in Figure (2-4), the volume fraction of hooked ends steel fiber was 1 % with an aspect ratio equal to 65, the results of all reinforced steel fiber self-compacting concrete (SFSCC) ribbed slabs compared with the conventionally reinforced ribbed slab. Depending on these outcomes. They deduced that the performance of the steel fiber reinforced slabs was almost equivalent to the ordinary reinforced concrete ribbed slab without fibers.

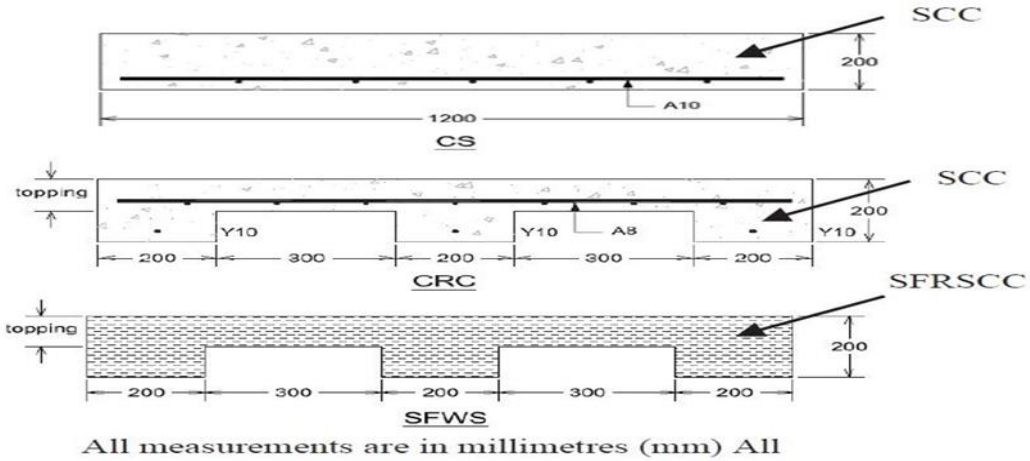

Figure (2-4) Variation of slab samples [61]

Four one-way LWC panels (1150 mm × 450 mm), three ribbed and one flat slabs, were poured and tested under a two-point loading by **Abdulkareem and Alfeehan (2018)** [62]; two parts were included in this study, the first part included the experimental work and the second part included the numerical work. The main variable in this study was the ratio of the depth of the ribs to the overall depth of the beam (d/h), which was equal to (0, 0.319, 0.477, and 0.625). All tested specimens have the same concrete amount and steel reinforcement ratio. The reinforcing steel was made up of many layers of bidirectional micro-reinforcement that each layer had a diameter of (1.55 mm) and clear spacing of (10 mm) in each direction. Furthermore, the rib width was the same as the thickness of the slab as a fixed condition in all the tested specimens. At each stage of the loading process, the load capacity and deflection data were collected. The numerical side was completed with the help of the ANSYS program, which was used to analyze the specimens and validate the outcomes. The results exhibited that increasing the (d/h) ratio enhanced structural behavior by increasing the load-carrying capacity and reducing deflection to a specific limit. A demonstration of compatibility between the numerical and experimental results has been accomplished.

In the same year, **Farouk (2018)** [63] analyzed continuous one-way normal reinforced ribbed slabs using finite element theory (ANSYS software). The variables in this study included the influence of the rigidity of the middle supports and cross-ribs on the behavior of a one-way ribbed slab. Seven one-way slabs with two bays were evaluated. Each bay had a dimension of (6 m × 6 m) on the reference slab. The ribs were cross-sectioned (0.1 m × 0.25 m), and the top slab was 5 cm thick. Between the ribs, the net space was (0.4 m). The solid central part had a width of (1.8 m), while the solid edge parts on each side had a width of

0.3 m. The cross-section of the supported beams is (0.3 m × 1.05 m). The studied parameters illustrated that the cross-ribs reduce the slab's buckling, the produced stresses, and deformations in the primary rib and solid parts. Also, the ultimate load on slabs increases, delaying yielding the solid middle part's major reinforcement. The slabs with the middle beam give better results than the slabs with the solid middle part.

Khaleel (2018) [64] conducted an experimental and numerical study on the lightweight aggregate reinforced concrete slabs with compressive strength equal to 36.4 MPa, and crushed brick as CA. These slabs have a styropor block in different sizes (percent of the weight reduction) and two ratios of a/d. The experimental work included testing eleven simply supported LWC one-way slabs, three solid slabs as reference slabs, and eight styropor block slabs (SBS). Test results showed that utilizing SBS with a smaller cross-sectional area and less shear reinforcement caused an increase in strength capacity compared to lightweight reference slabs. The higher ratio of a/d for LWA solid slab lowered ultimate strength and deflection, whereas, at the same cross-sectional area, broad ribs in SBS resulted in better results than narrow ribs. The numerical analysis outcomes which were carried out by ANSYS software, showed acceptable agreement with the experimental test results.

Another study looked into the behavior of SFSCC of the ribbed slab but under the effect of punching shear. In this study, the various parameter (topping thickness variation and material distribution) has been observed for each square slab sample which cast with dimensions 1200 mm × 1200 mm × 200 mm with the thickness of topping was (100 and 120) mm, as shown in Figure (2-5). They found that adding steel fibers to ribbed slabs enhanced punched shear resistance and had a similar load capacity to slabs reinforced by about (7-18) %. This behavior has proven that SFSCC

can slow down its cracking under concentrated load **(Fodzi et al. (2019))** [65].

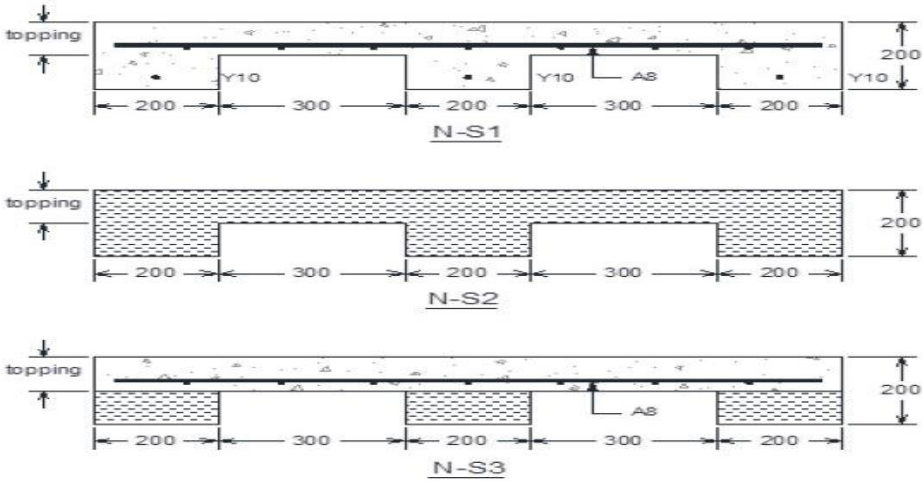

Figure (2-5) Variation of slab samples [65]

Depending on the results of this experimental study, a numerical analysis of the finite element method by a software program (ABAQUS) was carried out by the same researchers (**Fodzi and Hashim (2019)**) [66], it was observed that the type of slab with optimum performance was the one that was entirely reinforced with steel fibers.

In 2019, **(Al-Nasra et al.)** [67] highlighted how ribs spacing affected the performance of LWC of the one-way reinforced concrete ribbed slabs. The overall thickness, the concrete mix design, and the embedded steel reinforcement were kept constant. Five slabs were prepared and tested by flexural bending stress. Polystyrene foam blocks of variable width were used to fill the space between ribs while their height was kept constant, as shown in Figure (2-6) below. The special fiber was added to the concrete mix to enhance the performance of the concrete. The test outcomes revealed that the increase in the ribs spacing led to a decrease in the strength of the slab and a slight decrease in the strength to weight ratio. The material cost was also considered in this study.

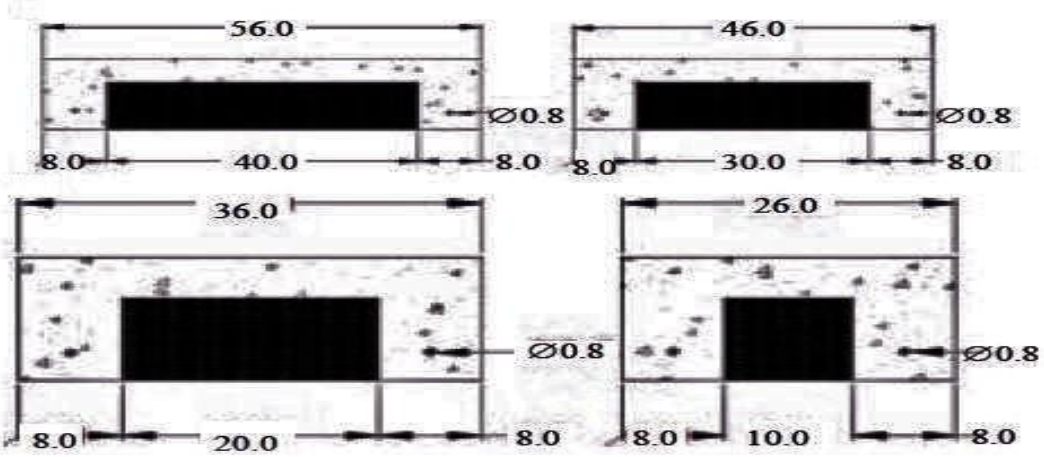

Figure (2-6) Variation of slab samples [67]

Vaivade et al. (2019) [68] conducted a numerical study with the ultimate as well as the serviceability limit states for high-performance concrete (HPC) ribbed slabs and high-performance fiber reinforced concrete (HPFRC). The effective use of these materials was analyzed using a nonlinear finite element model. The authors concluded that the utilization of HPFRC for ribbed slabs is successful compared to HPC slabs with identical cross-sections for slabs with spans ranging between (6-12) m. Also, utilizing HPFRC in place of HPC allows for a 42–46 percent increase in the uniformly distributed load intensity for ribbed slabs with identical cross-sections and permitted deflections.

Abdulhussein and Alfeehan (2020) [69] casted four flanged one-way ribbed lightweight reinforced concrete slabs and tested them under two-point loading. The variable in this study was the ratio of the depth of the rib to the overall depth of the beam, which was equal to (0.5, 0.701, 0.835, and 0.92). On the other hand, all slabs have the same amount of steel reinforcement ratio and concrete volume. The rib width was also equal to the thickness of slabs as a limitation in all slabs. The findings indicated that increasing the ratio of the depth of the rib to the overall depth of the beam improved the structural behavior by increasing the

ultimate load capacity and lowering the deflection up to a specific limit. It was found that the optimum ratio was (0.835).

2.7 Behavior of Reinforced Concrete Members Under Harmonic Loads

The problem of harmonic loads and heavyweight generated by the machines' engines is well-known in industrial buildings; therefore, the critical challenge in industrial facilities subject to harmonic loads is how to obtain a lightweight structure that resists these vibrations with a small reduction in strength; this is the most important load for the slab due to these reasons several authors studied the effect of harmonic load on the different structural members such as **Yanling et al. (2017)** [70] tested three steel-concrete composite beams with different degree of the shear connection under the effect of static and harmonic loads. The mid-span acceleration and deflection and the mean slip amplitude and slip amplitude at differing frequencies were measured. The results revealed that under the sine harmonic load, the mean slip value and slip amplitude at the steel girder and concrete slab, the mid-span acceleration, and dynamic deflection all show a sine wave shape and increase with the shear connection degree's reduction. For the slip's mean value and mid-span dynamic deflection, the static load components are most influential, whereas the slip amplitude is most affected by its load amplitude, and its acceleration is most dependent on its amplitude.

The dynamic resistance to loading of reinforced concrete slabs employing self-compact reactive powder concrete, as well as static loading, was investigated by **Bilal and Mohammed (2019)**. The eigenvalues and eigenvectors of the slab were calculated using the finite element approach, and the frequency response of the slab was analyzed using this method. According to the findings, self-compacted reactive

powder concrete exhibited less deflection than conventional concrete, and the magnitude of deflection varied depending on the slab boundary condition supports used.

Mahdi and Mohammed (2021) [71] presented an experimental and numerical study on the effect of harmonic load with different frequencies on the structural behavior of two-way bubble deck (BD) reinforced concrete slabs. The dimensions of the slabs were (2500mm×2500mm×200mm) with a bubble diameter of 12cm, and the distributions of the bubble were uniform with 14cm, 15cm, and 16cm spacing. The results demonstrated that the distribution of bubbles had a substantial impact on the structural behavior under harmonic load, and the numerical model was in excellent agreement with the experimental data.

Dakhela and Mohammed (2022) [72] investigated the behavior of fixed ends supported composite cellular beams with reinforced concrete deck slabs under harmonic loads. The experimental program involved three types of concrete (NWC, LWAC, and fiber LWAC) and different applied frequencies (5, 10, 15, 20, 25, and 30) Hz. The results of this study showed that LWAC response was significantly influenced by harmonic load (64 percent larger than NWC), and lattice cracks were discovered, particularly at 30 Hz, while fiber LWAC the harmonic load had a negligible influence on the vibration amplitude, and no cracks formed. Moreover, achieving NWC's amplitude limit of 11.11 percent was made possible by adding fiber to LWAC.

2.8 Summary

Based on the previous reviews that are presented in this chapter, several remarks are summarized:

1- It is worth noting that a lot of studies have been done on the mechanical features of LWAC for different resources of aggregate, such as aggregate made from (natural resources, industrial by-products, and recycled aggregate) but that are rarely studies dealt with the natural source of LWA (volcanic source) with by-product materials such as sugar molasses to product HSLWC.

2- Most previous researches were focused on investigating the behavior of one-way ribbed slabs with NWAC and LWAC with normal-strength concrete (NSC). This research focuses on studying the structural behavior of one-way ribbed slabs produced from HSC with and without LWA.

3- Most of the previous research concentrated on producing and studying the behavior of self-compacting concrete (SCC) and NSNWC one-way ribbed slabs with steel fibers addition. This study focuses on adding steel fiber with two-volume fraction ratios into HSLWC to produce and study the behavior of one-way ribbed slabs.

4- The majority of previous studies focused on U-shaped ends in produced one-way ribbed slabs, in this study focuses on the T-shaped ends.

5- Studies cited in the literature showed that different types of NSNWC were used in producing one-way solid slabs depending on the use of those slabs. In this study, HSLWC was used to produce a one-way solid slab with the same concrete volume as the one-way ribbed slab.

6- It was obvious from the literature reviewed in this chapter that earlier investigations focused mostly on the effect of a/d, depth of rib to a

total depth of ribbed slab on the behavior of one-way ribbed slab and did not cover the effects of changing the main tension steel reinforcement ratio of ribs, changing the geometry of section so that these parameters will be deepened in this study. Furthermore, the strength-to-weight ratio is very important in design criteria, transportation, and construction costs, so the effect of changing the ribs spacing on the behavior of HSLWC also be investigated in this study.

7- Most of the previous researches were interested in studying the behavior of one-way ribbed slabs under the effect of static loads. Therefore, this study aims to bridge the gap regarding the behavior of these slabs under two types of loading. The first is a two-point static load, and the other is a dynamic load (harmonic load). Harmonic load with different frequencies has been considered.

Chapter Three

Experimental Work

Chapter Three: Experimental Work

3.1 General

The behavior of reinforced concrete one-way slabs under static and dynamic loading was studied through testing twenty-one slab specimens with the effect of different concrete types, steel reinforcement ratios, the geometry of sections, spacings between ribs, and slab types.

A variety of tests are carried out, including testing on raw materials, fresh and hardened concrete, as well as tests of slab specimens subjected to two different kinds of loads.

3.2 Specimens Preparation

This section represents the different activities of producing one-way reinforced concrete slabs, including material properties, description of slab specimens, details of reinforcement, formwork, mixing proportions, mixing procedure, pouring of concrete, and curing.

3.2.1 Materials Properties

Standard tests according to Iraqi Specifications (IQS), American Society for Testing and Material (ASTM), and British Standard Institute (BSI) were used to characterize the physical and chemical properties of the materials that were used in this study. Concrete batches that were used in this work incorporated the following materials:

3.2.1.1 Cement

Iraqi manufactured Portland limestone cement (Karasta) produced by the “Lafarge” company was used in this study. The chemical and physical characteristics of the cement are existing in Appendix A, Table (A-1). These characteristics conformed with EN 197-1[73] and IQS No.5/2019 specifications of Portland cement [74].

3.2.1.2 Fine Aggregate (Sand)

Locally natural fine aggregate (from the Alukhidher region) was used in this study. In zone 2, this sand was graded in accordance with the limits of IQS No.45/1984 [75]. The physical and chemical characteristics of this sand are listed in Appendix A, Table (A-2).

3.2.1.3 Coarse Aggregate (CA)

Two types of natural CA were used in this study, the first type was normal-weight CA, and the other type was lightweight aggregate (LWA).

- **Normal-Weight Coarse Aggregate (Gravel)**

Locally natural CA (from Al-Nebai quarry) of maximum aggregate size (MAS) of 10 mm was used. The chemical and physical characteristics of gravel are listed in Appendix A, Table (A-3). Gravel characteristics conform to IQS No.45/1984 [75].

- **Light Weight Coarse Aggregate (Pumice Stone)**

Natural pumice stone is a volcanic rock (from the quarry on the border strip between Iraq, Iran, and Turkey) of MAS 10 mm, was used for LWC in this study. In addition to its black color, pumice stone is porous, low in density, has high permeability, and has high silicon oxide content (SiO_2). The pumice stone grading which conforms to the ASTM C330 [76], as shown in Table (A-4). The physical properties of pumice stone also are listed in Appendix A, Table (A-4).

3.2.1.4 Mixing Water

All concrete mixtures were mixed and cured with tap water.

3.2.1.5 Silica Fume (SF)

Micro SF is commercially known as MegaAdd MS(D) from CONMIX LTD. Company in UAE was used as a mineral admixture in producing high strength concrete mixtures. It is complying with ASTM C1240-15 [77]. The manufacturer's datasheet of this product is presented in Appendix A.

3.2.1.6 Superplasticizer (SP)

Sika ViscoCrete® 5930-L was utilized in this study as high range water-reducing admixture (HRWRA). It meets the requirement for SP according to ASTM C494/C494M-15a [78]. The manufacturer's datasheet of this product is presented in Appendix A.

3.2.1.7 Sugar Molasses (SM)

Molasses (SM) was used in this study which is a by-product liquid material of a sugar factory. It was obtained from Etihad Food Industries Co. LTD. at the Medhatya region in the province of Babylon. The chemical properties of SM are listed in Appendix A, Table (A-5).

3.2.1.8 Steel Fiber

Macro hooked end steel fiber was used in this study, at 35mm long and 70 aspect ratio, as shown in Plate (3-1). Table (A-6) (Appendix A) summarizes the fiber's physical properties.

Plate (3-1) Hooked end steel fiber

3.2.1.9 Steel Reinforcing Bars

Deformed steel bars of diameters (6 mm, 8 mm, and 10 mm) and deformed hot rolled mild steel bars (BRC) of 6 mm were used in this study. The characteristics of these deformed steel bars are described in Table (3-1). Plate (3-2) displays the tensile steel testing mechanical machine. The tensile test was done at the mineral laboratory of the Engineering of Minerals Science College at the University of Babylon following the ASTM A 496 [79] and ASTM A615 [80] standards.

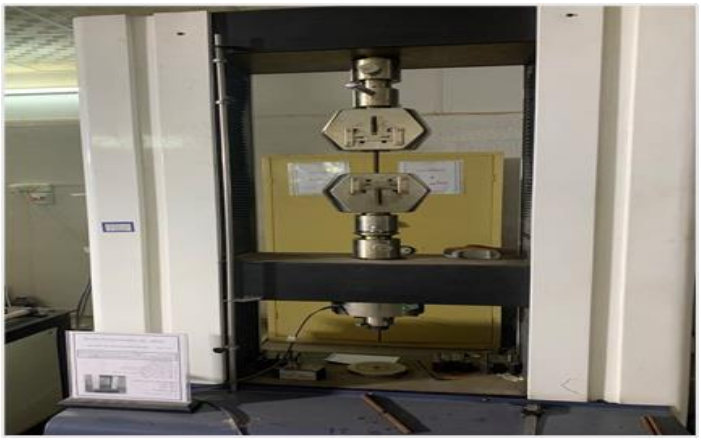

Plate (3-2)Tensile test of a steel bar

Table (3-1): Properties of steel reinforcement

Bar Size	Measured Bar Diameter (mm)	Bar Area (mm^2)	f_y (MPa)	f_u (MPa)	Grade	Specification No.
ϕ 6 mm	5.96	27.90	495	541	---	ASTM A 496
ϕ 8 mm	8.04	50.70	509	656	---	
ϕ10 mm	9.89	76.80	555	636	60	ASTM A 615

3.2.2 Description of Specimens

The experimental program in this study was divided into two groups depending on the loading type (static or dynamic). **First Group (G1)** consists of fifteen one–way slabs tested under static load (two-point loading). Also, this group is divided into six subgroups depending on the considered parameters:

- Using different concrete types (HSLWC, HSNWC, NSLWC, and NSNWC).
- Using hooked end steel fibers in HSLWC with different fiber volumetric ratios.
- Using different steel reinforcement ratios in HSLWC one–way ribbed slabs.
- Using different geometry of the sections by changing the number of ribs in HSLWC one–way ribbed slabs with the same concrete amount.
- Using different spacings between ribs in HSLWC one–way ribbed slabs by changing the width of the rib (b_w).
- Changing the type of HSLWC one–way slabs by using solid type with different steel reinforcement ratios.

Sub-Group (G11): this subgroup consists of four slab specimens devoted to study the effect of concrete type on the behavior of one–way ribbed slabs under static load. These slabs have the same geometry properties as shown in Figure (3-1). S1 is considered as the reference slab in this subgroup made with HSLWC, S2 made with HSNWC, S3 made with NSLWC, and S4 made with NSNWC.

Sub - Group (G 11)	The Variable: Concrete Type			
				
Slab Symbol	S 1	S 2	S 3	S 4
Concrete Type	HSLWC	HSNWC	NSLWC	NSNWC
Slab Type	Total Depth	Rib Width	Bar Dia. ϕ	Load Type
Ribbed	150 mm	100 mm	8 *mm*	Static

Figure (3-1) Specimens of sub-group (G11)

Sub-Group (G12): the influence of macro steel fiber inclusion with two fiber volume fraction ratios (0.25 and 0.50) % on the behavior of HSLWC one–way ribbed slabs under static load is studied. These slabs have the same geometry properties as shown in Figure (3-2). S1 is considered as the reference slab in this subgroup without steel fiber, S5 with the inclusion of 0.25 % of steel fiber, and S6 with the inclusion of 0.50 % of steel fiber.

Sub - Group (G 12)	The Variable: Steel Fiber Inclusion				
			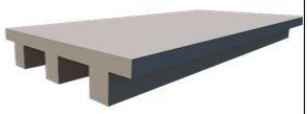		
Slab Symbol	S 1		S 5	S 6	
Steel Fiber Ratio	0.00 %		0.25 %	0.50 %	
Slab Type	Concrete Type	Total Depth	Rib Width	Bar Dia. ϕ	Load Type
Ribbed	HSLWC	150 mm	100 mm	8 *mm*	Static

Figure (3-2) Specimens of sub-group (G12)

Sub-Group (G13): the impact of using main ribs steel reinforcement of different diameters (8mm, 6mm, and 10mm) using the same geometry properties as shown in Figure (3-3), which is investigated to evaluate the structural performance of HSLWC one–way ribbed slab under static loading. S1 is considered as the reference slab in this subgroup with 6ϕ 8 mm (steel reinforcement ratio (ρ) = 0.28%), S7 with 6ϕ 6 mm (ρ = 0.16%), and S8 with 6ϕ10 mm (ρ = 0.44%).

Sub - Group (G 13)	The Variable: Steel Reinforcement Ratio			
				
Slab Symbol	S 1	S 7	S 8	
Bar Diameter (ϕ)	8 mm	6 mm	10 mm	
Slab Type	Concrete Type	Total Depth	Rib Width	Load Type
Ribbed	HSLWC	150 mm	100 mm	Static

Figure (3-3) Specimens of sub-group (G13)

Sub-Group (G14): different configurations of the sections, which was conducted by changing the number of ribs, is adopted to evaluate the effect of changing the section geometry on the behavior of HSLWC one–way ribbed slabs under static load, these slabs have a same concrete amount as shown in Figure (3-4). S1 is considered as the reference slab in this subgroup with three ribs, S9 consists of two ribs, and S10 consists of one rib.

Sub - Group (G 14)	The Variable: Geometry of Section				
					
Slab Symbol	S 1		S 9	S 10	
Number of Ribs	3		2	1	
Slab Type	Concrete Type	Total Depth	Summation of Ribs Width	Bar Dia. ϕ	Load Type
Ribbed	HSLWC	150 mm	300 mm	8 *mm*	Static

Figure (3-4) Specimens of sub-group (G14)

Sub-Group (G15): the changing of ribs spacing, which is achieved by changing the width of ribs, is adopted to study the effect of spacing between ribs on the behavior of HSLWC one–way ribbed slabs under static load. These slabs have the same number of ribs as shown in Figure (3-5). S1 is considered as the reference slab in this subgroup with ribs spacing of 200 mm, the ribs spacing of 180 mm and 150 mm in slabs S11 and S12, respectively.

Sub - Group (G 15)	The Variable: Ribs Spacing			
				
Slab Symbol	S 1	S 11	S 12	
Ribs Spacing	200 mm	180 mm	150 mm	
Rib Width	100 mm	120 mm	150 mm	
Slab Type	Concrete Type	Total Depth	Bar Dia. ϕ	Load Type
Ribbed	HSLWC	150 mm	8 *mm*	Static

Figure (3-5) Specimens of sub-group (G15)

Sub-Group (G16): this subgroup consists of four slab specimens devoted to study the behavior of two types of HSLWC one–way (ribbed and solid) slabs with different bar diameters of main reinforcement (6, 8, and 10) mm of solid slabs under static load. Ribbed slab S1 is considered a reference slab. S13, S14, and S15, these specimens have the same amount of concrete as shown in Figure (3-6), with different bar diameters of main reinforcement (8, 6, and 10) mm. Steel reinforcement ratio was (0.57, 0.31, and 0.9) % respectively.

Sub - Group (G 16)	The Variable: Slab Type					
						
Slab Type	Ribbed			Solid		
Slab Symbol	S 1			S 13	S 14	S 15
Bar Diameter (ϕ)	8 mm			8 mm	6 mm	10 mm
Concrete Type	Total Depth	Rib Width	Load Type	Concrete Type	Total Depth	Load Type
HSLWC	150 mm	100 mm	Static	HSLWC	83 mm	Static

Figure (3-6) Specimens of sub-group (G16)

Second Group (G2) consists of six one–way slabs tested under dynamic load (harmonic load). This group is also divided into four subgroups depending on:

- Using different concrete types (HSLWC, HSNWC, and NSNWC).
- Using hooked end steel fibers in HSLWC with a volume fraction of 0.25%
- Using different sections geometry by changing the number of ribs in HSLWC one–way ribbed slabs with the same concrete amount.
- Changing the type of HSLWC slab.

Sub-Group (G21): this subgroup consists of three slab specimens devoted to study the influence of changing concrete type on the behavior of one–way ribbed slabs under dynamic load. These slabs have the same geometry properties as shown in Figure (3-7). HS1 is considered as the reference slab in this subgroup made with HSLWC, HS2 made with HSNWC, and HS3 made with NSNWC.

Sub - Group (G21)	The Variable: Concrete Type			
				
Slab Symbol	HS 1	HS 2	HS 3	
Concrete Type	HSLWC	HSNWC	NSNWC	
Slab Type	Total Depth	Rib Width	Bar Dia. ϕ	Load Type
Ribbed	150 mm	100 mm	8 *mm*	Dynamic

Figure (3-7) Specimens of sub-group (G21)

Sub-Group (G22): the influence of macro steel fiber inclusion with fiber volume fraction ratio (0.25) % on the behavior of HSLWC one–way ribbed slabs under dynamic load is studied. These slabs have the same geometry properties as shown in Figure (3-8). HS1 is considered as the reference slab in this subgroup without steel fiber and HS4 with the inclusion of 0.25 % of steel fiber.

Sub - Group (G22)	The Variable: Steel Fiber Inclusion					
				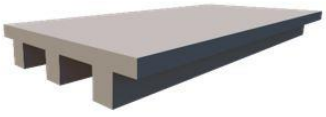		
Slab Symbol	HS 1			HS 4		
Steel Fiber Ratio	0.00 %			0.25 %		
Slab Type	Concrete Type	Total Depth	Rib Width	Bar Dia. ϕ	Load Type	
Ribbed	HSLWC	150 mm	100 mm	8 *mm*	Dynamic	

Figure (3-8) Specimens of sub-group (G22)

Sub-Group (G23): different configurations of sections, which was conducted by changing the number of ribs, is adopted to evaluate the effect of changing the geometry of section on the behavior of HSLWC one–way ribbed slabs under dynamic load, these slabs have the same concrete amount, as shown in Figure (3-9). HS1 is considered as the reference slab in this subgroup with three ribs and HS5 consists of one rib.

Sub - Group (G23)	The Variable: Geometry of Section					
						
Slab Symbol	HS 1		HS 5			
Number of Ribs	3		1			
Slab Type	Concrete Type	Total Depth	Summation of Ribs Width	Bar Dia. ϕ	Load Type	
Ribbed	HSLWC	150 mm	300 mm	8 *mm*	Dynamic	

Figure (3-9) Specimens of sub-group (G23)

Sub-Group (G24): this subgroup consists of two slab specimens dedicated to study the behavior of two types of HSLWC one–way (ribbed and solid) slabs under dynamic load. These slabs have the same amount of concrete. HS1 is considered as the reference slab in this subgroup and HS6 solid slab, as shown in Figure (3-10).

Sub - Group (G24)	The Variable: Slab Type							
								
Slab Type	Ribbed				Solid			
Slab Symbol	HS 1				HS 6			
Concrete Type	Total Depth	Rib Width	Bar Dia. ϕ	Load Type	Concrete Type	Total Depth	Bar Dia. ϕ	Load Type
HSLWC	150 mm	100 mm	8 mm	Dynamic	HSLWC	83 mm	8 mm	Dynamic

Figure (3-10) Specimens of sub-group (G24)

3.2.3 Steel Reinforcement Details of Specimens

The slab specimens were designed by the ultimate method to fail by tension mode under the applied loads. The steel reinforcement and geometry section details of the one-way slabs are shown in Figure (3-11).

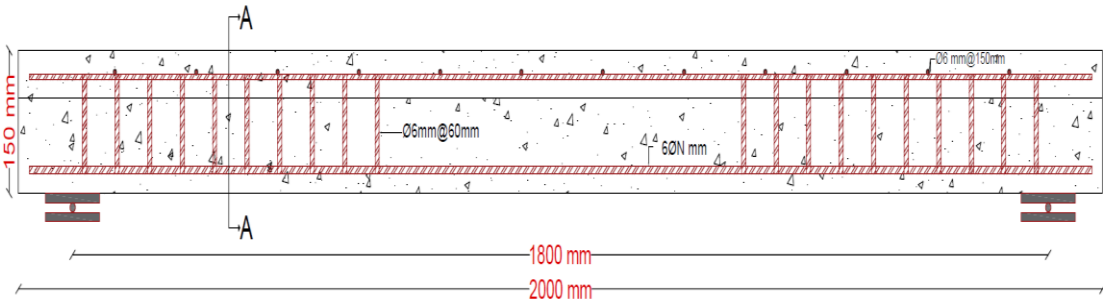

(a) Longitudinal section for steel reinforcement details of ribbed slabs

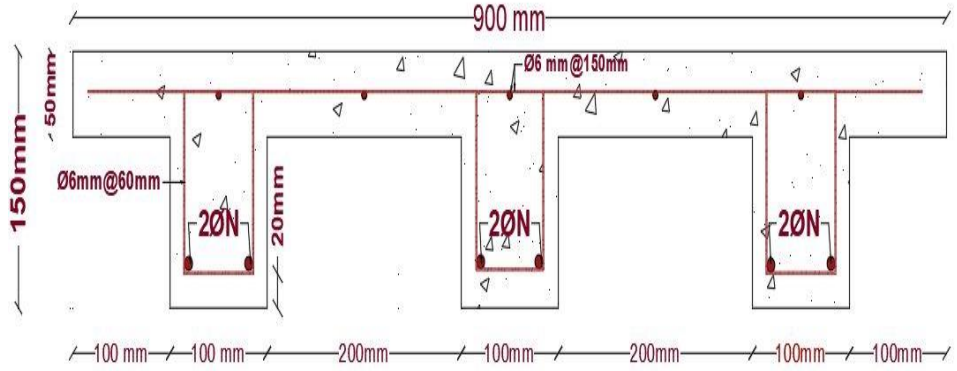

- N= 8mm for S1, S2, S3, S4, S5, S6, HS1, HS2, HS3, and HS4, N= 6 mm for S7, and N= 10 mm for S8.

(b) Section A-A of specimens (S1, S2, S3, S4, S5, S6, S7, S8, HS1, HS2, HS3, and HS4)

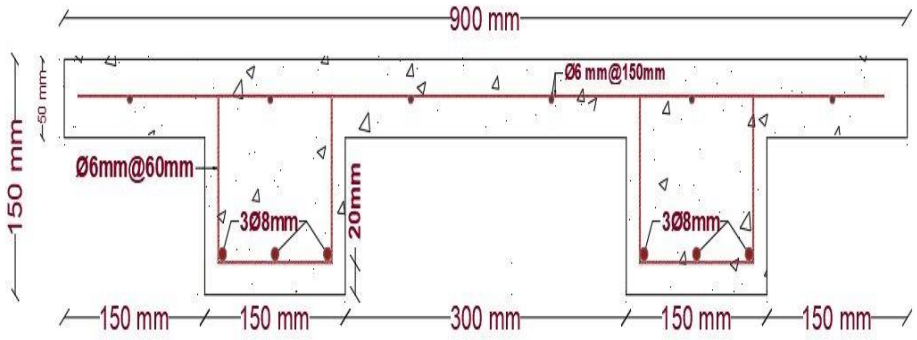

(c) Section A-A of the specimen (S9)

Figure (3-11) Steel reinforcement and geometric sections details of specimens

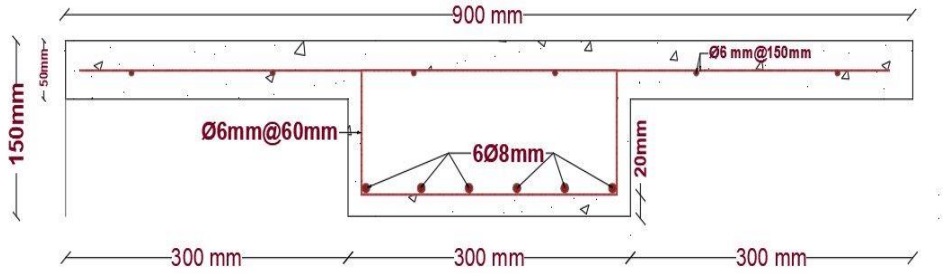

(d) Section A-A of specimens (S10, HS5)

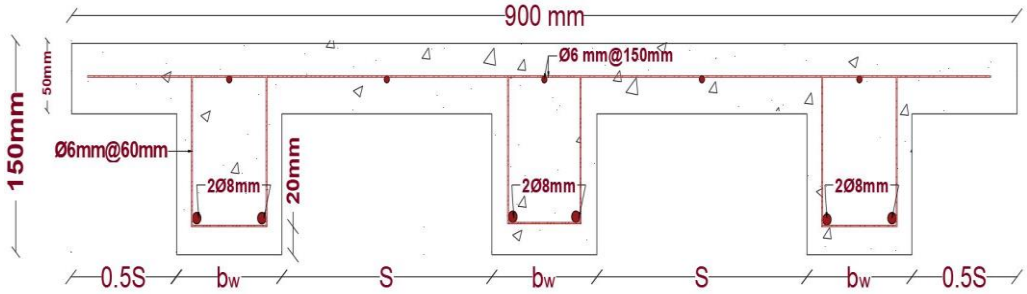

- b_w= 120 mm and S= 180 mm for S11 - b_w= 150 mm and S= 150 mm for S12

(e) Section A-A of Specimen (S11 and S12)

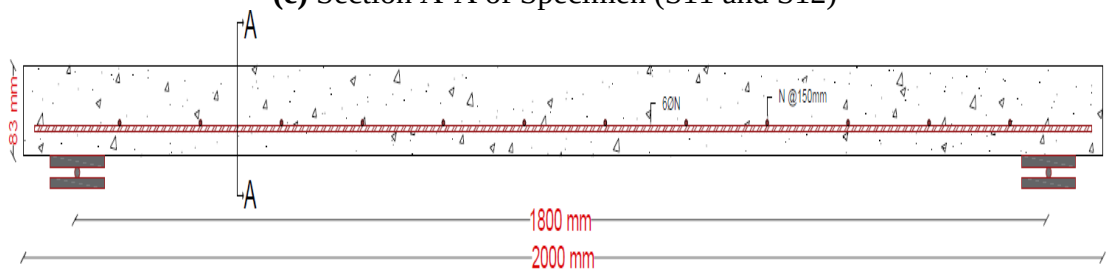

(f) Longitudinal section for steel reinforcement details of solid slabs

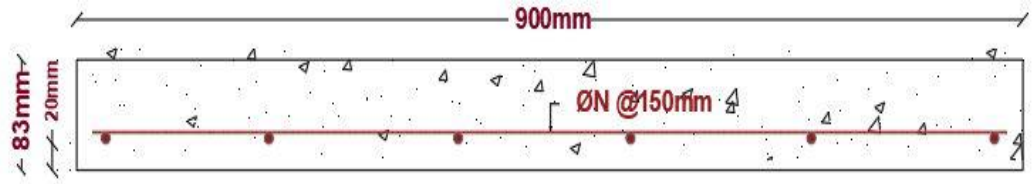

- N=8mm for S13 - N=6 mm for S14 - N=10 mm for S15

(g) Section A-A of specimens (S13, S14, S15, and HS6)

Figure (3-11) Continued

3.2.4 Formworks of Slab Specimens

Six wooden molds and one steel mold with different geometries are fabricated for casting the slab specimens, as shown in Plate (3-3). Both of the steel and wooden forms were supported by stiffeners and fixed on each side of the forms with bolts. The thickness of the steel plate was (2 mm), while the thickness of the plywood was (18 mm).

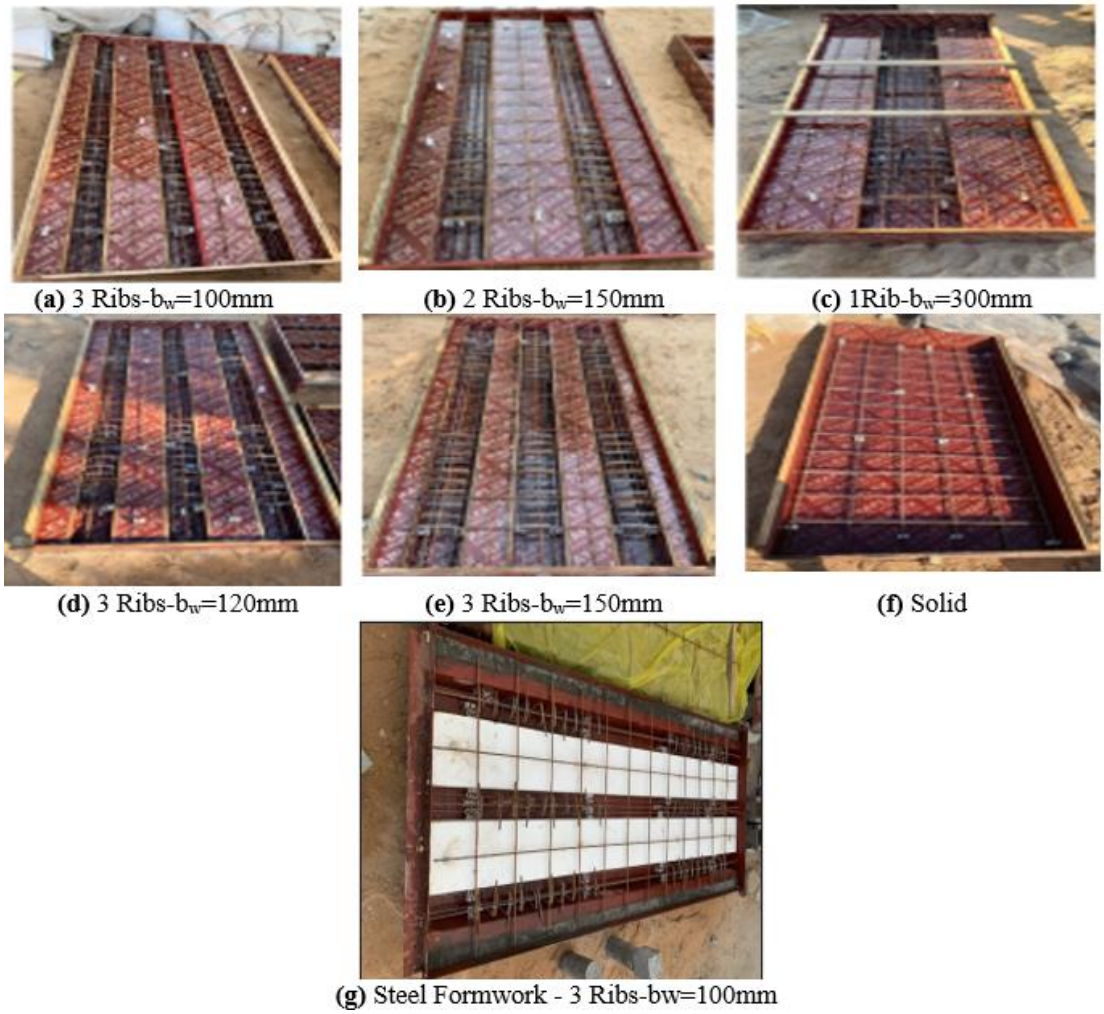

Plate (3-3) Plywood and steel formworks

3.2.5 Mix Proportions

Many trail mixes were performed to satisfy the required density and strength of HSLWC. The mixed design of NSLWC was performed according to ACI committee 211.2-98 [81]. The LWC mix is directly affected by the water absorption of pumice aggregate, so the pre-soaking method for pumice aggregate was used for 24 hours to keep the high absorption of pumice aggregate under control. HSNWC mix proportions were the same as HSLWC except for replacing the pumice with gravel at the same volumetric ratio and according to ACI committee 363R-10 [3]. Also, NSNWC mix proportions were the same as NSLWC except for

replacing the pumice with gravel at the same volumetric ratio. The mix proportions adopted in this study as tabularized in Table (3-2).

Table (3-2): Mix proportions of concrete mixes

Concrete Type	Materials (kg/m^3)								
	Cement	Sand	Gravel	Pumice Stone	Water	Silica Fume	Superpl-asticizer	Sugar Molasses	Steel Fiber
									
NSNWC	496	700	950	----	210	---	----	----	----
NSLWC	496	700	----	428	210	----	----	----	----
HSNWC	525	590	1100	----	142	75	7.85	1.05	----
HSLWC	525	590	----	495	142	75	7.85	1.05	----
F0.25HSLWC	525	590	----	495	142	75	7.85	1.05	19.5
F0.50HSLWC	525	590	----	495	142	75	7.85	1.05	39.0

3.2.6 Mixing Procedure

All material quantities were weighted and packed into the clean containers prior to the mixing operation. Also, it is vital to maintain a clean mixer. The drum mixer with a 375 liter capacity, as shown in Plate (3-4), was used for mixing HSLWC, HSNWC, NSLWC, NSNWC, F0.25HSLWC, and F0.5HSLWC. The mixing procedure for each type of concrete was based on previous studies.

Plate (3-4) Concrete mixer

- **The mixing procedure for HSLWC and HSNWC was as follows:**

  - The fine aggregate and CA (pumice stone for HSLWC and gravel for HSNWC) were added to a mixer and mixed for 120 seconds.

- The cementitious (cement + SF) were added to a mixer and blended for 120 seconds.

- Adding 50 % of water to a mixer and being mixed for 120 seconds.

- Adding the 25% of water, which was mixed with SP, gradually and mixed for 120 seconds.

- Adding the remaining water, which was mixed with SM, gradually and mixed for 180 seconds.

- **The mixing procedure for F0.25HSLWC and F0.5HSLWC was as follows:**

  For steel fibers HSLWC mixes, the same steps were adopted in HSLWC mixing procedure with adding in the final step of mixing the steel fibers slowly with the required quantity and being blended for 240 seconds.

- **The mixing procedure for NSLWC and NSNWC was as follows:**

  - The fine aggregate and coarse aggregate (pumice stone for NSLWC and gravel for NSNWC) were added to a mixer and mixed for 120 seconds.

  - The cement was added to a mixer and mixed for 120 seconds.

  - The water was added to a mixer and mixed for 180 seconds.

3.2.7 Casting and Curing

After completing the mixing of concrete, forms were treated with oil before putting steel reinforcement inside the form. The slab specimens are cast using the electric vibrator to ensure the concrete fills the molds.

After casting was completed, the top surface of the concrete was leveled and smoothed with a hand trowel. Then, the slab molds are covered with nylon sheets. After 48 hours, the slabs of high-strength concrete and after 24 hours, the slabs of normal-strength concrete and their control specimens (cubes, cylinders, and prisms) are removed from their molds and cured by covering the specimens with burlap sacks after being moistened. A nylon sheet was draped over the moist burlap sacks to keep the water from evaporating. While, the curing of the control specimens was by immersion in a water tank until 28 days, as shown in Plate (3-5).

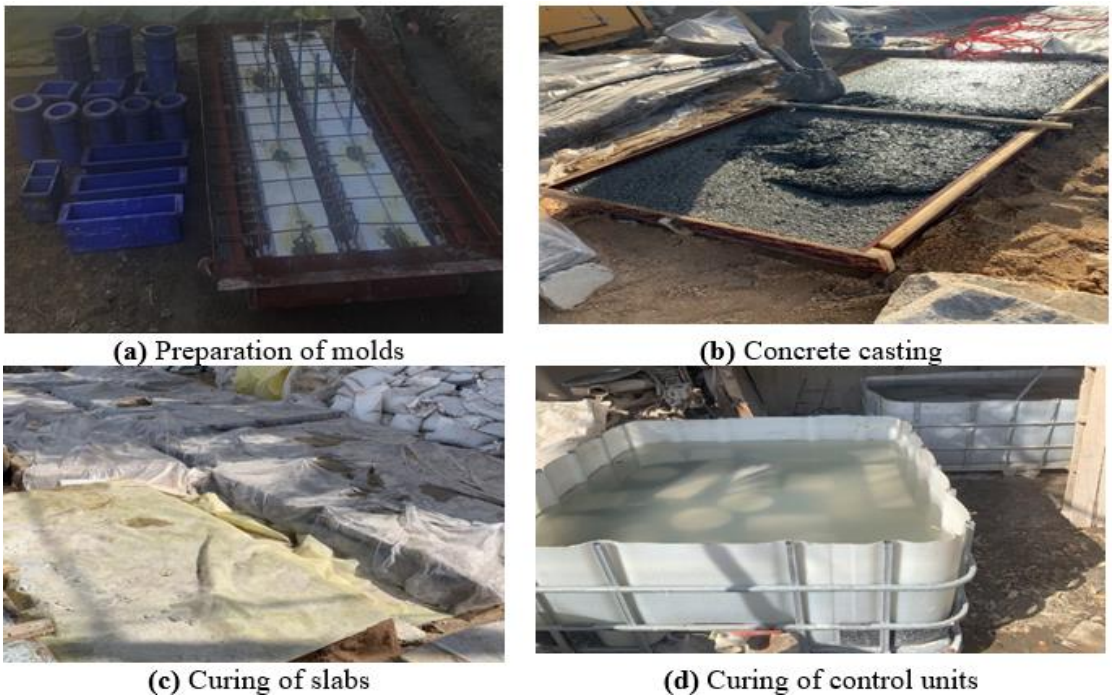

(a) Preparation of molds **(b)** Concrete casting

(c) Curing of slabs **(d)** Curing of control units

Plate (3-5) Casting and curing of concrete specimens

3.3 Tests of Fresh and Hardened Concrete

3.3.1 Tests of Fresh Concrete

3.3.1.1 Slump Test

The test of the slump for all mixes was conducted following ASTM C143/C143M–15 [82], as shown in Plate (3-6).

Plate (3-6) Slump test

3.3.1.2 Fresh Density Test

The test of the fresh density for all mixes was conducted following ASTM C567/C567M–19 [83]. An average of three cylinders of (150 mm×300 mm) for each mix batch after compacting was used to achieve this test, as shown in Plate (3-7).

Plate (3-7) Fresh density test

3.3.2 Tests of Hardened Concrete

3.3.2.1 Hardened Density Test

The hardened density test was conducted for all LWC according to ASTM C567/C567M–19 [83], and for all NWC according to ASTM C642/C642-13 [84], an average of three cylinders (100×200) mm were used to determine the oven-dry (O.D.) density for each mix batch.

3.3.2.2 Compressive Strength Test

The compressive strength tests were conducted on cylinders (300 ×150 mm) according to ASTM C39/C39M−15a [85] and cubes size (150 mm) according to BS 1881:part 116 [86]. A hydraulic universal compression testing machine at the Department of Civil Engineering / Babylon University laboratory was used for this test, as revealed in Plate (3-8).

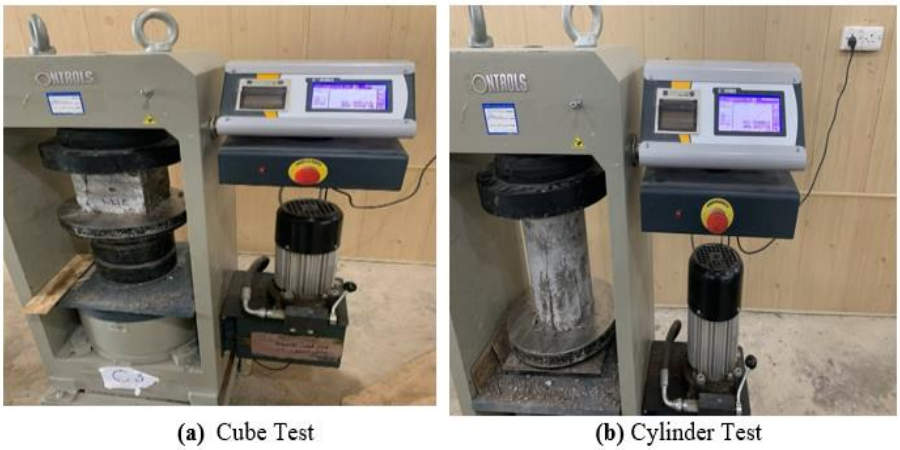

(a) Cube Test (b) Cylinder Test

Plate (3-8) Compressive strength test

3.3.2.3 Splitting Tensile Strength Test

The test of the splitting tensile was conducted for all mixes according to the ASTM C496/C496M–17 [87]. An average of three cylinders (100×200) mm were used to find the splitting tensile strength of each mix batch, as shown in Plate (3-9).

Plate (3-9) Splitting tensile strength test

3.3.2.4 Flexural Tensile Strength Test (Modulus of Rupture)

The flexural tensile test was conducted for all mixes according to the ASTM C78/C78M–18 [88]. An average of three prisms of dimensions (100×100×400) mm were used to find the modulus of rupture of each mix batch, as shown in Plate (3-10).

Plate (3-10) Flexural tensile strength test

3.3.2.5 Ultrasonic Pulse Velocity Test

The ultrasonic pulse velocity (UPV) test, as shown in Plate (3-11), was conducted for all mixes according to the ASTM C597–16 [89]. An average of three cubies (150) mm were used to determine the UPV for each mix.

Plate (3-11) Ultrasonic pulse velocity test

3.3.2.6 Thermal Conductivity

This test was carried out according to ASTM C1113-09 [90] at the national center for construction laboratories –Laboratory Baghdad, using "Quick Thermal Conductivity Meter" [91], as revealed in Plate (3-12). The cube specimens with dimensions (100×100×100) mm were used in the test. Three times the test was repeated for each specimen, and three thermal conductivity values were recorded with a standard deviation of less than 2%.

Plate (3-12) Thermal conductivity test

3.3.2.7 PH-Meter Test

The pH-meter test was conducted according to the ASTM F710-19 [92]. The method adopted in the pH test was to calibrate the pH electrode, then prepare the specimen (powdering), after that prepare the suspension (10 g of powdered and 10 ml of distilled water) stirring continuously, and finally, just after stirring, the measurement is taken when the pH value becomes stable and the value obtained for each of the mixtures is recorded, as shown in Plate (3-13). The outcomes from this test gave pH values in the ranges of (12.6-13.0) for all concrete mixes. In an alkaline concrete environment, a thin coating of adhering passive oxide forms on bars steel reinforcing used in concrete constructions to protect them from corrosion. During cement hydration, calcium hydroxide is formed,

resulting in a high pH, usually between 12.5 and 13.5. This high basic level is sufficient to maintain and protect the oxide film for an extended period of time [93]. So, these pH readings allow safe usage of SM together with (SF and SP) in producing HSLWC, HSNWC, F0.25HSLWC, and F0.5HSLWC mixes.

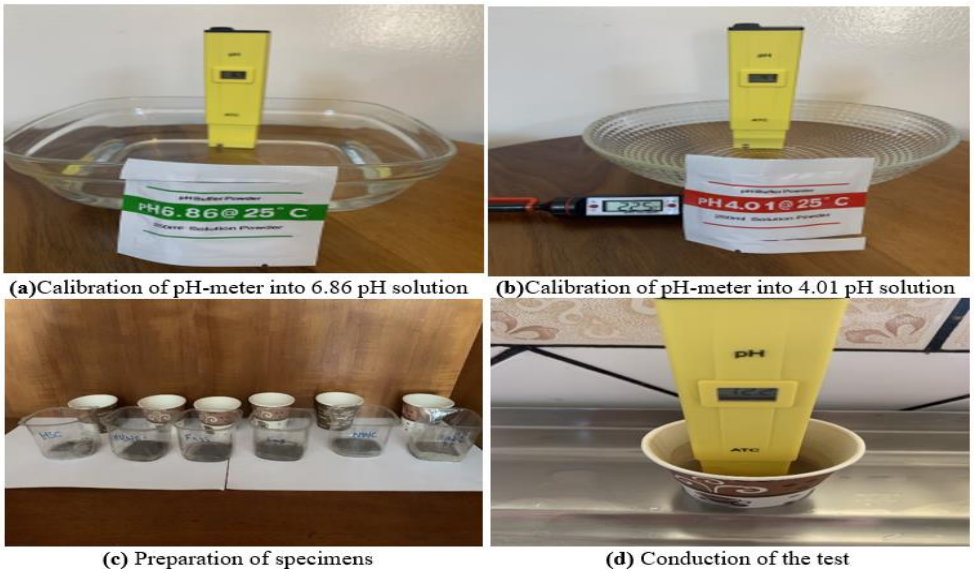

(a)Calibration of pH-meter into 6.86 pH solution (b)Calibration of pH-meter into 4.01 pH solution

(c) Preparation of specimens (d) Conduction of the test

Plate (3-13) pH meter test

3.4 Testing Instrumentations and Software

Different instruments were used to carry out the experimental part of this study for both static and dynamic loading. Load, deflection, crack width, and strain have been measured. The following is a brief illustration for each one of them.

3.4.1 Instrumentations of Static Test

- **Testing Machine:** A manufactured hydraulic jack testing machine with a capacity of about 60 t was used to test slab specimens under static load using the load control technique, as shown in Plate (3-14a).
- **Load Cell:** A sensor 24-bit analog to digital converter with 200 t capacity was used to measure the applied two-point load.

- **Deflection:** the linear variable differential transducer (LVDT) (10 cm), as shown in Plate (3-14b) indicators were used to measure the deflection (the location of the LVDT was at mid-span length).

- **Strain Gauge:** Four concrete strain gauges with 120 Ω resistance (Plate (3-14c)) were used to measure the strain distribution. These gauges were distributed on the slab surface at compression face across the width of the slab. Due to the symmetry, the concrete strain gauges are mounted only on the half-width of the slab by glued after the preparation of the concrete surface. The distribution locations of the strain gauges are shown in Figure (3-12).

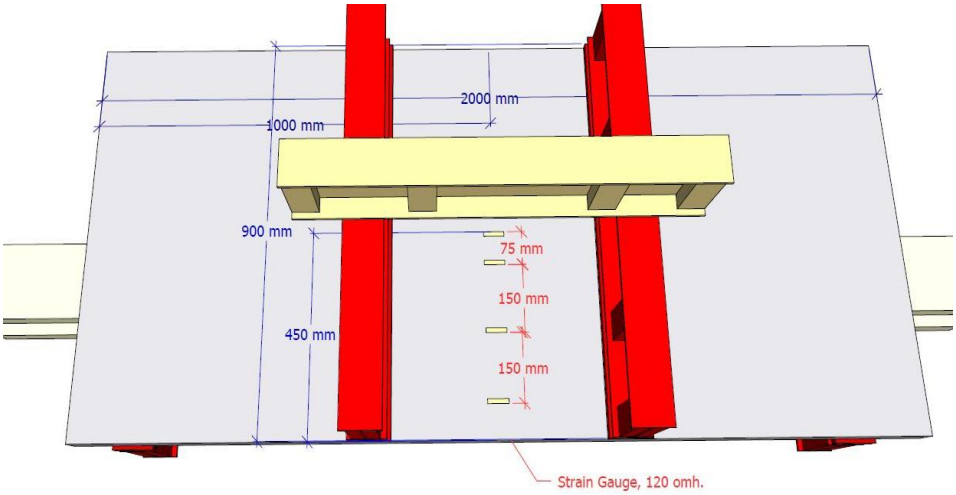

Figure (3-12) Distribution of strain gauges across width of the slab

- **Data logger:** A digital data logger with twelve channels had been connected to a laptop (dell precision M4800) supplied with a specific program set up in the LabVIEW 2020 to receive all the data. These data were saved as technical data management streaming (TDMS) files to be used later in various data management software like Excel or DIAdem.

- **Crack meter:** A micrometer optical type with an accuracy of 2×10^{-2} mm, as shown in Plate (3-14f) was used to measure crack width for all

slab specimens, and to make it simpler to observe and estimate the width of cracks, the slab surfaces were painted white.

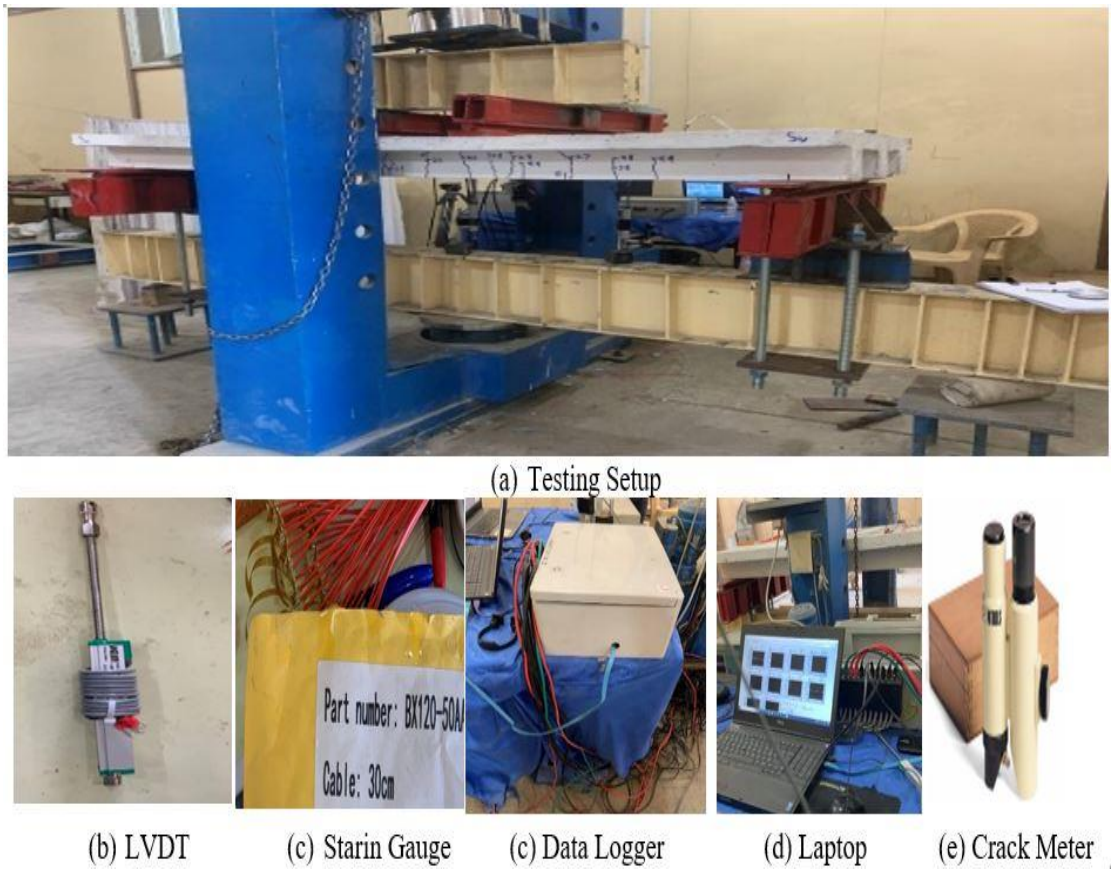

Plate (3-14) Instrumentations of static test

3.4.2 Instrumentations of Dynamic Test

- **Displacement:** In the dynamic loading test, displacement indicator was used to measure the displacement amplitude for the slab specimens subjected to harmonic loading (laser sensor (30mm)). The location of this indicator was at mid-span length, as shown in Plate (3-15). Laser sensor type was LK-081- KEYENCE, as shown in Plate (3-16a) and a description for this laser sensor is presented in (Appendix C). The reference distance between the slab and laser sensor was 80 mm. Some care was taken to set this sensor and secure it in the proper position to obtain accurate results.

- **Electric Motor:** A rotary motor of 1.5HP capacity and its mass of 22 kg. The eccentric (total mass and distance) of the motor was approximately 2.1kg and 24mm, respectively. A steel mass of 48 kg has been installed between the motor and the specimen. This mass was attached to be distributed on a projected area of (350 × 450) mm, as shown in Plate (3-16b).

- **Load Cell:** Five ultrasonic piezo transducers with 60W and 28 kHz capacity connected in series to find the average values were used to measure the adopted harmonic load after carrying out the calibration to transfer the values in (volt) to load in (kg), as illustrated in Plate (3-16c).

- **AC Driver:** This driver is used to regulate and control the operating frequency of the electric motor with the required step value for each test, as shown in Plate (3-16d)

- **Data Acquisition:** An advanced digital data acquisition for sound & vibration type (NI PXle -1062Q), with twenty-four channels, had been connected to a desktop computer and supplied with a specific program set up in the software (LabVIEW 2020), as shown in Plate (3-16e and f). All of the data on this device was received in LabVIEW 2020 and saved as a TDMS file for future use in data management software like DIAdem. A datasheet of this device is presented in (Appendix C).

- **Accelerometer:** Four accelerometers mounted on the top surface of the specimen and distributed at the center along the span of the specimen were used to measure the acceleration amplitude for the slabs under harmonic loading.

- **Microphone:** One microphone was used to record the sound which was induced by the operating of the motor, as shown in Plate (3-16h).

- **<u>Grounding System:</u>** As it is known any electrical device must be connected to the earth to release the excess electrons and protect the device. Therefore, copper rod was planted in the hole and connected from the top with steel wires, as shown in Plate (3-16i).

Plate (3-15) Experimental dynamic test setup

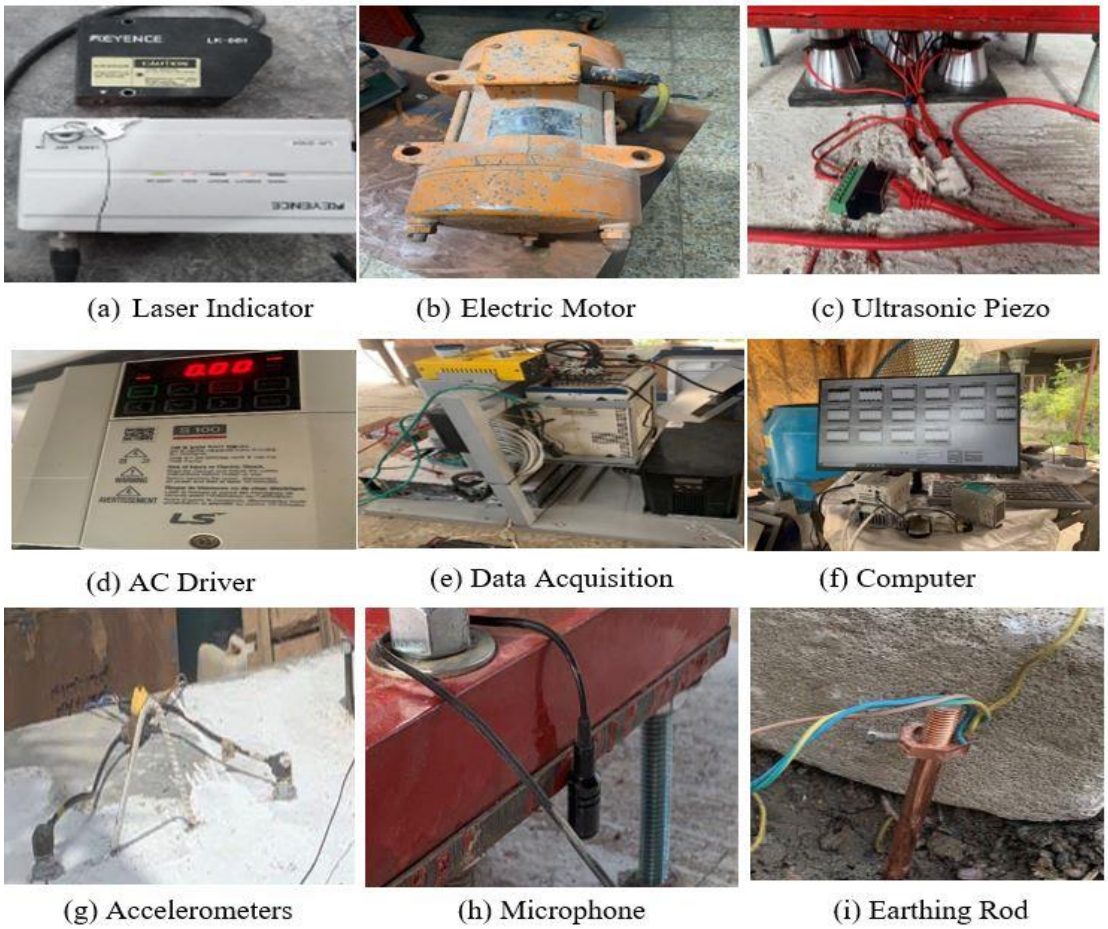

Plate (3-16) Instrumentations of dynamic test

3.5 Testing Procedure

In the static loading test, concrete slab specimens were tested till failure in the civil engineering department's structural laboratory at Babylon University, as simply supported (hinge-roller) one-way reinforced concrete slabs resting on a steel frame and subjected to a two-point loading system. Hinge support was designed to prevent horizontal movement and allows rotation. While the roller support was designed to for allowing both rotational and horizontal movements. Each one consists of a 20 mm thickness plate, and of 10 mm steel shaft that is welded with steel (I) section. This section supported with steel stiffener. In the beginning, the LVDT and strain gauges were set and checked by applying an initial load. Then, the load was returned to zero. After that, the initial reading of LVDT and strain gauges were reset to zero. At each specific loading increment, crack width was measured. The deflection and strain were recorded using a data logger. Furthermore, the magnitude of the first cracking load and its locations were recorded. Cracks development on each specimen were also traced and outlined by a marker.

Finally, a test was deemed complete when no additional rise in applied load was seen, along with an evident big deflection and extensive cracking. Figure (3-13) displays a schematic diagram for slab specimen under static load.

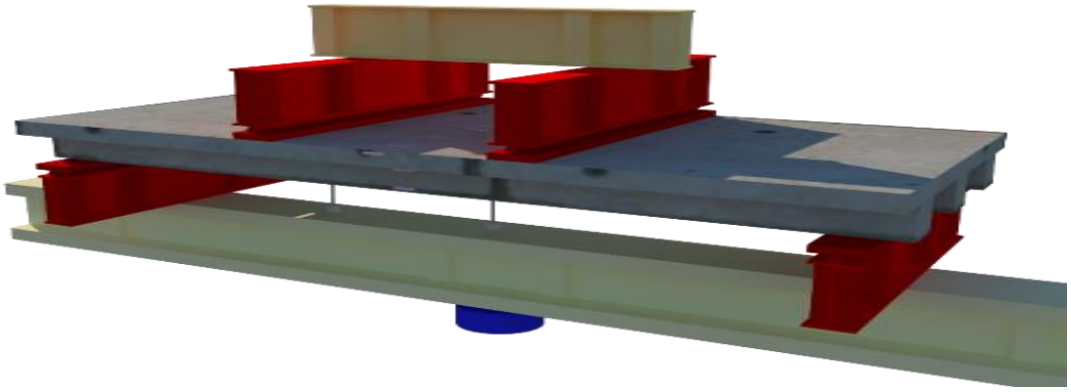

Figure (3-13) A schematic diagram of slab specimen under static test

In the dynamic loading test, concrete slab specimens were tested under different operating frequencies between (5-50) Hz, each step 5 Hz, as simply supported one-way reinforced concrete slabs resting on a fabricated steel frame and subjected to a harmonic loading system.

Load, displacement, acceleration, and sound were recorded using a data acquisition at each specific frequency increment. At each of these frequencies, the amplitude of displacement, acceleration, and sound level were found to stabilize approximately after 20 seconds; once it was stabilized, the readings were taken. Furthermore, cracks development on each specimen were also traced and outlined by a marker. Figure (3-14) shows a schematic diagram for slab specimen under dynamic load.

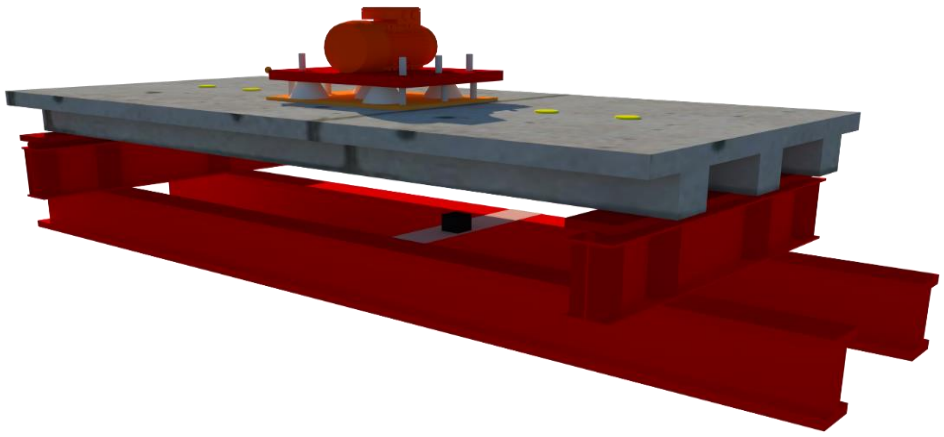

Figure (3-14) A schematic diagram of slab specimen under dynamic test

Chapter Four

Experimental Results and Discussion

Chapter Four: Experimental Results and Discussion

4.1 Introduction

This chapter discusses the outcomes of the experimental work which was presented in chapter three. At the beginning, the results of physical and mechanical properties of different types of concrete mixes are discussed. The results of the experimental static test of one–way reinforced concrete slabs specimens are evaluated and discussed. The findings of experimental dynamic testing are discussed in the final part of this chapter.

4.2 Mechanical and Physical Properties of Concrete Mixes

Several specimens were casted and tested from each concrete batch mix to find the mechanical and physical characteristics of the concrete, including compressive strength, indirect tensile strength (splitting tensile strength and modulus of rupture), ultrasonic pulse velocity, density, and thermal conductivity. For each of these mechanical characteristics, each value represents the average of a number of specimens.

4.2.1 Compressive Strength

The most important and relevant indicator for evaluating concrete is its compressive strength. It is also a significant feature of concrete. Table (4-1) gives the compressive strength test results for each kind of concrete utilized in this study. From the experimental test results, it was noticed that the cube and cylinder compressive strength increased in HSNWC by (56.78 and 70.59) % with respect to NSNWC, respectively. While in HSLWC, the cube and cylinder compressive strength increased by (69.71 and 81.12) % with respect to NSLWC, respectively. From these outcomes, it was found that the difference in the cube and cylinder compressive strength in LWAC was higher than in NWAC by 12.93%

and 10.53%, respectively. This behavior may be due to the effect of LWA (pumice stone), which is considered a pozzolanic material that was worked together with the silica fume and sugar molasses to improve cement paste strength.

Also, it is found that the failure of HSNWC appeared explosive behavior, while the replacement of gravel with pumice stone in HSLWC made the failure of specimen less explosive behavior. This behavior was due to HSNWC has higher compressive strength than HSLWC. Also, this replacement reduced the compressive strength (cube and cylinder) by about (23.61 and 27.24) %, for HSC and about (29.43 and 31.47) % for NSC, respectively. Thus, the effect of replacing gravel with pumice stone in HSC is smaller than in NSC. Furthermore, the addition of steel fibers with two volumetric ratios (0.25 and 0.5) % in the HSLWC mix gave an improvement in the (cube and cylinder) compressive strength of approximately (7.49 and 11.14) % and (13.63 and 16.35) %, respectively. This may belong to the fiber's exertion as confinement on the cement matrix.

Table (4-1): Results of compressive strength tests

Compressive Strength	NSNWC	NSLWC	HSNWC	HSLWC	F 0.25 HSLWC	F 0.50 HSLWC
f_{cu} (MPa)	43.5	30.7	68.2	52.1	56.0	59.2
f_c' (MPa)	34.0	23.3	58.0	42.2	46.9	49.1

4.2.2 Splitting Tensile Strength

The splitting tensile strength (f_t) of concrete is much lower than the compressive strength due to the ease of cracks in the tension zone. As shown in Table (4-2), the f_t of HSNWC increased by 38.24% with respect to NSNWC and f_t of HSLWC increased only by 34.78 % with respect to NSLWC. From these outcomes, it was found that the difference of f_t in NWAC was higher than in LWAC by 3.46%. This behavior

reflected the effect of LWA in this reduction. Moreover, f_t of HSLWC reduced by 34.04 % respected to HSNWC. While f_t of NSLWC reduced by about 32.35 % respected to NSNWC, thus the effect of replacement of gravel with pumice stone in HSC is more than in NSC. On the other hand, the addition of steel fibers with V_f equal to (0.25 and 0.5) % in HSLWC led to an increase in the f_t by (22.58 and 29.03) %, respectively. This improvement is due to the ability of steel fiber to restrict crack propagation.

The relation between the splitting tensile strength and cylinder compressive strength represents the brittleness ratio (BR) [94] which was computed for all concrete types in Table (4-2). From this ratio, it was found that using HSNWC instead of NSNWC led to an increase in the BR by 23.40%, while using HSLWC instead of NSLWC increased the BR by 34.35%. From these outcomes, it was found that the LWA was comparatively more brittle than NWA. On the other hand, the addition of steel fibers to HSLWC with (V_f = 0.25% and 0.5%) gave concrete mixes more ductile behavior by reducing the BR by 9.33% and 9.77%, respectively.

Table (4-2): Results of splitting tensile strength test

Splitting Tensile Strength	NSNWC	NSLWC	HSNWC	HSLWC	F 0.25 HSLWC	F 0.50 HSLWC
f_t (MPa)	3.4	2.3	4.7	3.1	3.8	4.0
(f_c'/f_t)	10.00	10.13	12.34	13.61	12.34	12.28

4.2.3 Flexural Tensile Strength (Modulus of Rupture)

The goal of the modulus of rupture (f_r) test is to determine the maximum load at which a concrete member in bending may crack owing to tension. It indicates the flexural tensile strength of concrete [95].

From outcomes presented in Table (4-3), it was found that using HSNWC instead of NSNWC led to increase the f_r by 47.37%, and using HSLWC instead of NSLWC led to increase the f_r by 40%. From these outcomes, it was noticed that the difference of f_r in NWAC was higher than in LWAC by 7.37%. This behavior reflected the effect of the presence of LWA in these mixes. Moreover, the presence of steel fibers in HSLWC led to increase the f_r by (17.14 and 28.57) % for (V_f = 0.25% and 0.5%), respectively. This may be because the hooked ends fiber was effective in bridging the cracks that appear in the first stage of cracking. The relationship between the flexural tensile strength and cylinder compressive strength for all concrete types is presented in Table (4-3), respectively. It was found that the ratio of (f_c'/f_r) increased by 15.75% when using HSNWC instead of NSNWC, also this ratio increased by 29.40% when using HSLWC instead of NSLWC. The addition of steel fibers in HSLWC led to decrease this ratio by (5.14% and 9.54%) for (V_f = 0.25% and 0.5%), respectively. It is important to note that the addition of steel fiber increases the flexural strength larger than the compressive strength in HSLWC.

Table (4-3): Results of modulus of rupture test

Modulus of Rupture	NSNWC	NSLWC	HSNWC	HSLWC	F 0.25 HSLWC	F 0.50 HSLWC
f_r (MPa)	3.8	2.5	5.6	3.5	4.1	4.5
$(f_c'lf_r)$	8.95	9.32	10.36	12.06	11.44	10.91

4.2.4 Ultrasonic Pulse Velocity (UPV)

The concept is to project the sound inside the material and measure the time to receive it. From the outcomes shown in Table (4-4), it was found that UPV increased by 25.99 % when using HSNWC instead of NSNWC, while it increased by 16.17 % when using HSLWC instead of NSLWC. From these results, it was found that the UPV in NWAC was

higher than in LWAC by 9.82 %. This behavior related to the effect of pores of LWA led to decrease the velocity of sound inside LWAC specimens. The addition of steel fibers led to increase UPV by 4.77% and 17.77%. This attitude might be because of the ability of steel fiber to minimize the bad effect of the voids and LWA on UPV. Moreover, according to Indian Standard (IS:13311-1: Part 1) [96] for classification of concrete quality as a function of UPV, it was found that (NSNWC, NSLWC, and HSLWC) have a good quality while (HSNWC, F0.25HSLWC, and F0.5HSLWC) have an excellent quality assessment.

Table (4-4): Results of ultrasonic velocity test

Ultrasonic Velocity	NSNWC	NSLWC	HSNWC	HSLWC	F 0.25 HSLWC	F 0.50 HSLWC
UPV (km/s)	4.355	3.823	5.487	4.441	4.653	5.230

4.2.5 Density

Oven dry (O.D) density for all six concrete types is presented in Table (4-5). The addition of LWA (pumice stone) instead of NWA (gravel) in all concrete mixes without steel fiber led to decrease the density by 16.69% and 19.31% for NSLWC and HSLWC with respect to NSNWC and HSNWC, respectively. This is due to the LWA having a lot of gaps or pores, and it forms the greatest ratio of concrete materials. On the other hand, the presence of steel fibers in concrete mixes led to increase the density of concrete by 0.98% for F0.25HSLWC and 1.54% for F0.50HSLWC, and this increment depends on the ratio of the volume fraction of fibers. The relation between strength and density appeared that using HSNWC instead of NSNWC led to increase the strength to density ratio by 63.95%, while using HSLWC instead of NSLWC led to the increase of this ratio by 79.34%. From these outcomes, it was found that the difference between replacing NWA with LWA in HSLWC is more

than NSLWC by 15.39%. Also, the addition of steel fibers in HSLWC had a significant effect in increasing the efficiency of strength to density ratio by 10.14 % for F0.25 HSLWC and 14.75% for F0.50HSLWC, respectively. It was worthy to mention that the fresh density for all types of concrete were ranged from (100 to 160) kg/m^3 higher than O.D density.

Table (4-5): Results of density test

Density	NSNWC	NSLWC	HSNWC	HSLWC	F 0.25 HSLWC	F 0.50 HSLWC
w_c (kg/m^3)	2313	1927	2408	1943	1962	1973
$(f'_c/w_c) \times 10^{-2}$	1.47	1.21	2.41	2.17	2.39	2.49

4.2.6 Thermal Conductivity (λ)

From the thermal conductivity test results, it could calculate another thermal properties of concrete, such as heat resistivity (r) and heat transfer rate (q). The equations (4-1) and (4-2) can be used to find the heat resistivity and the rate of heat transfer per hour, respectively [97]:

$r = t / \lambda$ …….(4-1)

$q = \lambda A\, dT/t$ ……..…(4-2)

Where:

r = heat resistivity (m^2.K/W).

q = heat transferred per unit time (W/ hour).

A = area of heat transfer (m^2).

λ = thermal conductivity (W/ (m.K)).

dT =temperature difference across the material (K).

t = thickness of material (m).

Using the value of λ from the experimental test and assuming that the temperature difference between day and night is 20ºC (293.15º K), the

area is (1×1) m^2 and the thickness is 15 cm, the r and q of each concrete type can be calculated as shown in Table (4-6). It was found that using HSNWC instead of NSNWC led to increase λ (i.e., decreasing the thermal insulation) by 23.92%, while using HSLWC instead of NSLWC led to increase λ by 14.57%. This revealed that using LWA instead of NWA for HSC decreased the thermal conductivity by 9.35%. Also, using HSLWC instead of HSNWC led to decrease λ by 43.55% due to the effect of LWA compared with NWA. Furthermore, it was found that the unclear effect of increasing the volume fraction of steel fibers on the λ may belong to the distribution of steel fibers in concrete mixes. Although there are slight increases in λ for fiber concrete by 9.88% for F0.5HSLWC over HSLWC, the increase is less than the effect of coarse aggregate type.

Table (4-6): Results of thermal properties

Thermal Properties	NSNWC	NSLWC	HSNWC	HSLWC	F 0.25 HSLWC	F 0.50 HSLWC
Thermal Conductivity (λ), (W/ (m.K)	1.158	0.707	1.435	0.810	0.795	0.890
Heat Resistivity (r), (m^2.K/W)	0.130	0.212	0.105	0.185	0.189	0.169
Heat Transferred Rate (q), (W/ hour)	2263	1382	2804	1583	1554	1739

4.2.7 Sound Insulation and Acoustic Impedance

One aim of this study is the physical property such as (sound insulation and acoustic impedance) of lightweight concrete. In this study, the sound insulation of concrete specimens was calculated according to a proposed empirical formula for transmission losses (TL) [98]. The ability to acoustic insulation of buildings, this insulation usually calculates at a frequency of 200 Hz then 1000 Hz.

$$TL=20 \log (f \times m) - 48 \quad \text{(4-3)}$$

Where:

TL= Transmission losses, dB.

f = frequency, 200 Hz.

m = mass per unit area, kg/m^2; take the values in the Table (4-5) and thickness= 0.15 m.

Acoustic Impedance (AI) for each concrete mixes that used in this study was calculated by equations (4-4) using the following equation [99]:

$AI = w_c \times UPV$ …… (4-4)

Where:

AI: Acoustic Impedance, (Rayl = kg/(m^2s)).

w_c: Density, kg /m^3.

VPV: Ultrasonic Pulse Velocity, m/s.

Table (4-7): Results of acoustic properties

Acoustic Properties	NSNWC	NSLWC	HSNWC	HSLWC	F 0.25 HSLWC	F 0.50 HSLWC
Acoustic Impedance (AI), $\times 10^6$ (Rayl)	10.1	7.4	13.2	8.6	9.1	10.3
Transmission Losses, (TL), (dB)	48.83	47.24	49.18	47.31	47.40	47.44

The results in Table (4-7) showed that in the NSLWC, the reduction in the AI and TL was (26.73 and 3.26) % with comparison to NSNWC, respectively. While in the HSLWC, the reduction was (34.85 and 3.80) % with comparison to HSNWC, respectively.

Moreover, the inclusion of steel fibers in HSLWC led to increase TL and AI, and this increment depends on the ratio of steel fibers. The AI

increased by (5.81and 19.77) % and TL increased by (0.19 and 0.27) % for F0.25HSLWC and for F0.50HSLWC, respectively, with reference HSLWC. The findings of TL showed that all types of concrete did not negatively affect sound insulation because all these values were over the lower limit of international codes of 40 dB [100].

4.2.8 Slump Test Results

The concrete slump test is performed to check the workability of fresh concrete. The effects of various kinds of aggregate, the addition of steel fiber, and molasse on slump values of concrete mixes are presented in Table (4-8). It can be seen that the effect of silica fume, superplasticizer, and sugar molasses is clear in the workability of HSNWC and HSLWC mixes as compared to NSNWC and NSLWC mixes, respectively, which were given higher slump values.

Also, it can be seen that the inclusion of steel fibers in HSLWC mixes reduced the slump values due to the formation of matrix–fiber network structure which results in an increase in the viscosity of concrete mixes and reduces the workability.

Table (4-8): Results of workability properties

Workability	NSNWC	NSLWC	HSNWC	HSLWC	F 0.25 HSLWC	F 0.50 HSLWC
Slump (mm)	50	42	127	110	94	87

4.3 Results of the Experimental Work of Slabs Specimens Under Static Loading

The following parts discuss the outcomes of the experimental study under the effect of static loading using characteristics including the load of the first crack, load-maximum crack width curves, crack pattern, failure mode, ultimate loading capacity, load-central deflection curves,

stiffness, ductility, and energy absorption for each group that depended in this study. Table (4-9) summarizes the cracking and deflection details of slabs under the effect of static load.

Table (4-9): Cracking and deflection details for slabs tested under static loading

Slab Symbol	Type of concrete	P_{cr} (kN)	W_{cr}* (mm)	P_y (kN)	δ_y (mm)	P_u (kN)	δ_u (mm)	μ	Mod of failure
S1	HSLWC	12.51	0.22	65.00	9.73	77.15	40.92	4.21	Flexure Failure
S2	HSNWC	22.50	0.11	76.62	8.40	93.74	49.50	5.89	
S3	NSLWC	10.02	0.24	61.51	11.61	72.36	43.00	3.70	
S4	NSNWC	13.00	0.17	72.00	14.26	76.46	37.00	2.59	
S5	F0.25HSLWC	15.02	0.20	72.50	10.00	90.73	44.86	4.49	
S6	F0.50HSLWC	16.82	0.15	77.50	10.00	96.48	48.00	4.80	
S7	HSLWC	11.54	0.25	27.51	5.14	48.13	33.13	6.45	
S8	HSLWC	15.91	0.18	101.30	9.80	118.8	29.98	3.06	
S9	HSLWC	12.86	0.13	67.50	9.72	77.45	41.96	4.32	
S10	HSLWC	13.00	0.10	65.11	10.54	76.79	48.26	4.58	
S11	HSLWC	14.50	0.21	69.67	9.57	83.58	46.29	4.84	
S12	HSLWC	16.78	0.17	73.29	10.22	88.70	49.85	4.88	
S13	HSLWC	9.51	0.12	30.24	17.52	33.49	42.62	2.43	
S14	HSLWC	8.00	0.14	10.50	5.36	18.37	27.84	5.20	
S15	HSLWC	11.00	0.10	56.01	17.27	60.10	31.79	1.84	

*Crack width at service load (0.65 P_u) [101].

4.3.1 Cracking Behavior

The performance of cracking of the all-tested slab specimens in the first group is evaluated and discussed in this section.

4.3.1.1 General Cracking Performance of Slab Specimens

This section summarizes the general cracking behavior. At first, the influence of static two-point loading on slab specimens indicated three distinct stages of deformation.

In the early stages of testing, before the first crack was begun, the deformations might be classed as elastic deformations. When the applied

load reached the first cracking load, which ranged from 0.134 to 0.435 of the ultimate loads, the first fracture occurred in the tension face of the tested slabs. The initial crack had a width not exceeding 0.02 mm. More flexural cracks appeared at the tension face of the tested slab specimens as the load raised, spreading horizontally from the mid-span to the support. The elastic-plastic stage is represented by this stage. The number of cracks grew, as did their width, and they traveled higher to the flange of one–way ribbed slab specimens and to the compression zone of one–way solid slab specimens. Finally, increasing the load magnitude caused the stiffness of the slab specimens to decrease (plastic stage), which was followed by failure. The slab specimens' failure of the tested under the effect of static two-point loading could be characterized as a flexural failure. Plate (4-1) displays the cracking outlines for slabs under the effects of static two-point loading. From this plate, one can be found that: With increasing of concrete strength, the width of the cracks decreased while the number of cracks increased. This behavior is due to the number of factors, including the increase in the modulus of elasticity of HSLWC slab S1 and HSNWC slab S2 in comparison with NSLWC slabs S3 and NSNWC S4, respectively, which belongs to the development of crushing failure across the aggregates and mortar rather than deboning or crushing through the mortar.

Using hooked end steel fibers in producing one-way ribbed slabs (S5 and S6) led to increase the number of cracks followed by a reduction in cracks width with an increase in the volume fraction of fiber in comparison with slab S1 without steel fibers at the same load level. This behavior is due to the bond between concrete components improving when steel fiber is added to the matrix.

Changing ρ from (0.28 to 0.16) % by using ϕ 6 mm in ribbed slab S7 led to decrease the number of cracks and an increase in the crack width of the slab at the same loading level. On the other hand, changing ρ from (0.28 to 0.44) % by using ϕ10 mm in ribbed slab S8 instead of ϕ8 mm in ribbed slab S1 led to increase the number of cracks and decrease in their width. This behavior belongs to the increase in the moment of inertia and therefore, the flexural rigidity of slabs will increase.

Changing the number of ribs with the same ratio of concrete volume, as presented in two–ribs in slab S9 and one–rib in slab S10, the effect of this changing on the outcomes of cracking was the number of cracks and its width nearly similar at the most load level, this may be belonging to the same volume of concrete and same steel reinforcement ratio.

The effect of the decreasing the spacing between ribs of one–way ribbed slab on the crack behavior by changing the width of ribs, which was 120 mm in slab S11 and 150 mm in slab S12, led to a large number of narrower cracks width. This behavior is due to the slabs' increased moment of inertia; hence, the flexural rigidity will increase.

Converting the type slab from ribbed slab (S1, S7, and S8) to solid slab (S13, S14, and S15) while maintaining the same concrete volume, the outcomes clarified that the ribbed slab of HSLWC gave better cracking behavior than solid slab, this behavior revert to the enhancement in the moment of inertia of ribbed slab at same concrete volume, hence; the flexural rigidity will increase.

The outcomes of the width of the maximum crack at the service load (about 65% of the ultimate load of each slab specimen) [101] as shown in Plate (4-1) were compared with the limitations of ACI 318-19 [18] that is

0.4 mm. The outcomes indicated that all slab specimens meet the limitation of the ACI code.

Plate (4-1) Cracks pattern for slabs under two-point loading

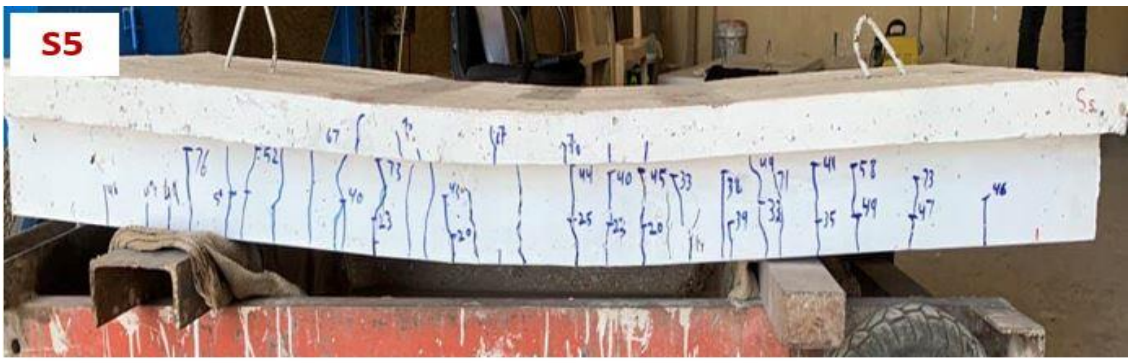

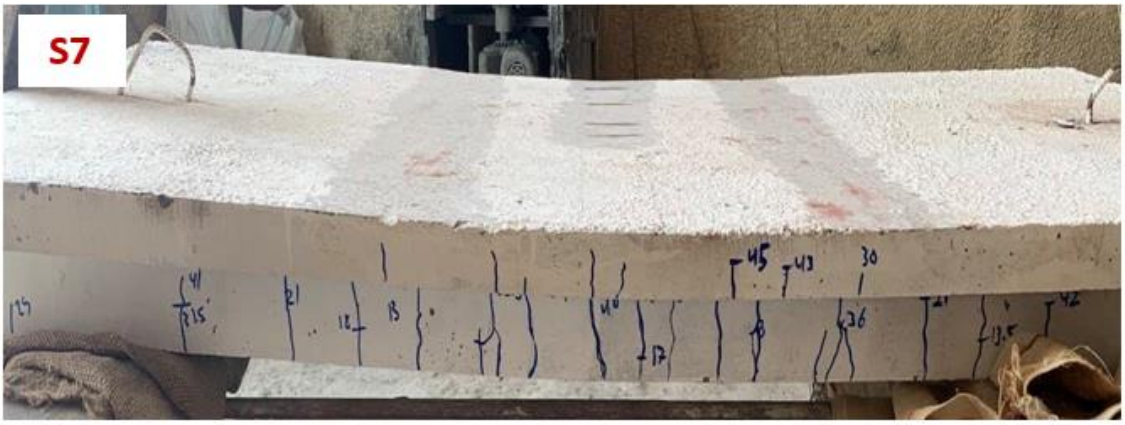

Plate (4-1) Continued

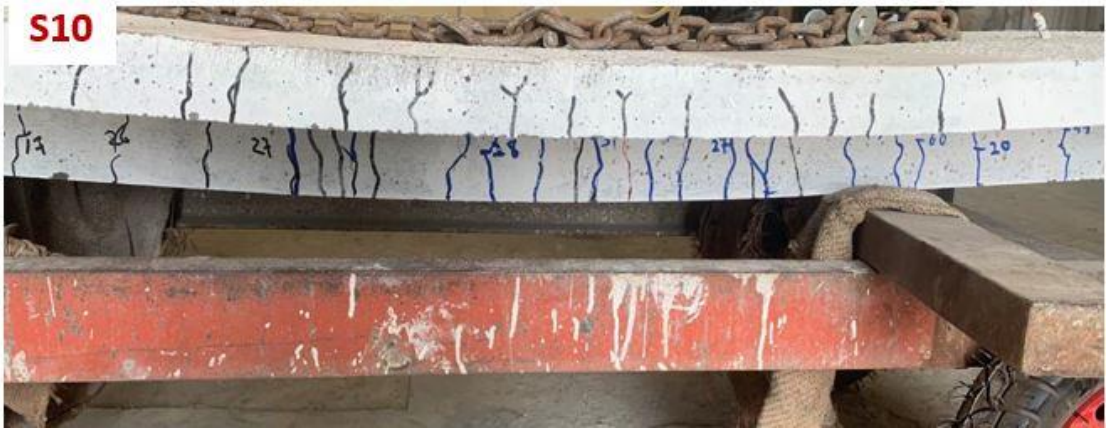

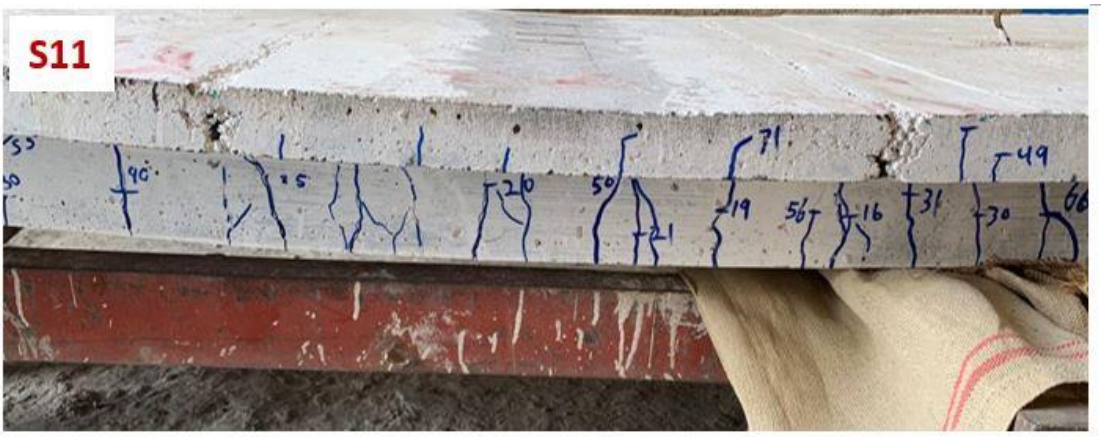

Plate (4-1) Continued

Plate (4-1) Continued

4.3.1.2 Load-Crack Width Curves for Slab Specimens

The tested slab specimen's maximum crack width was supervised throughout the test from the appearance of the first crack up to failure. The slab specimen's load-maximum crack width curves under the effect of two-point static loading were described in Figure (4-1) to Figure (4-6):

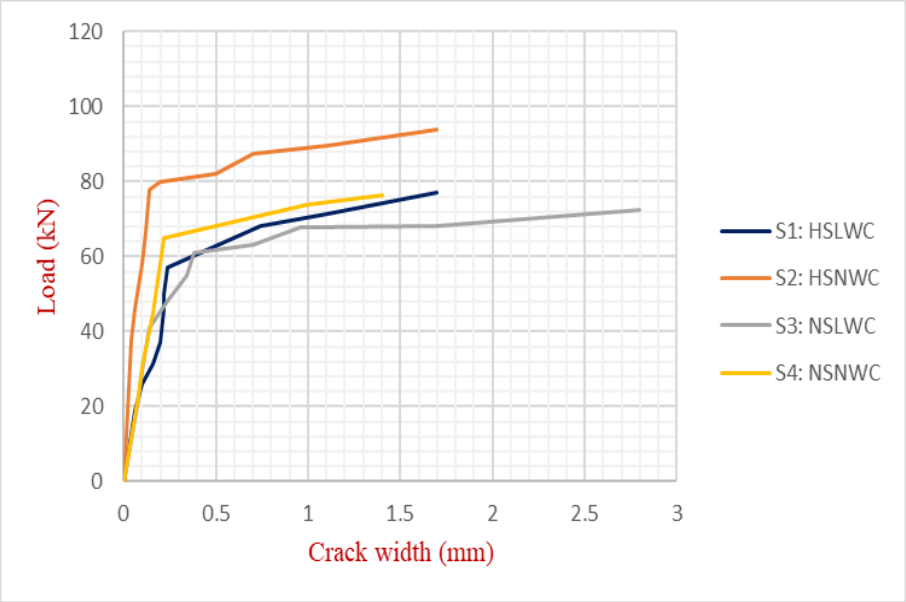

Figure (4-1) Load-crack width curves of G11

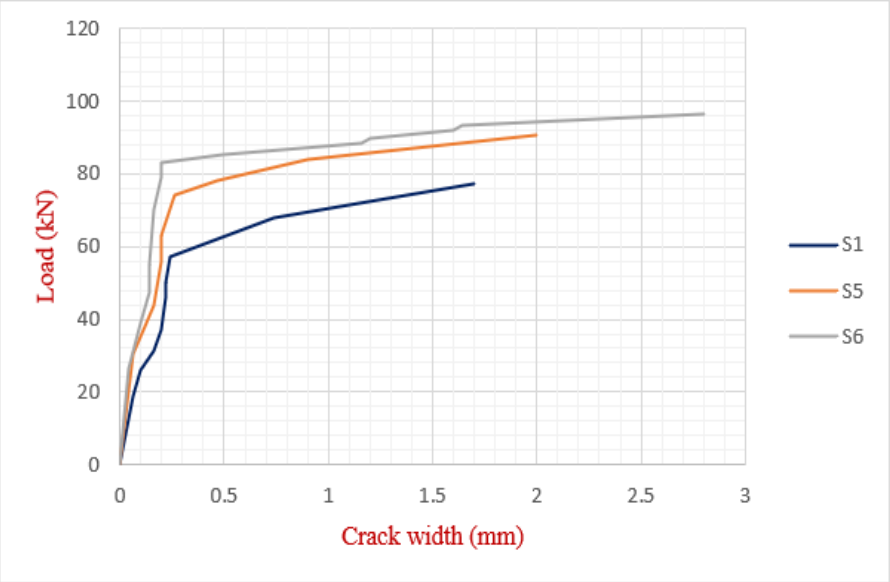

Figure (4-2) Load-crack width curves of G12

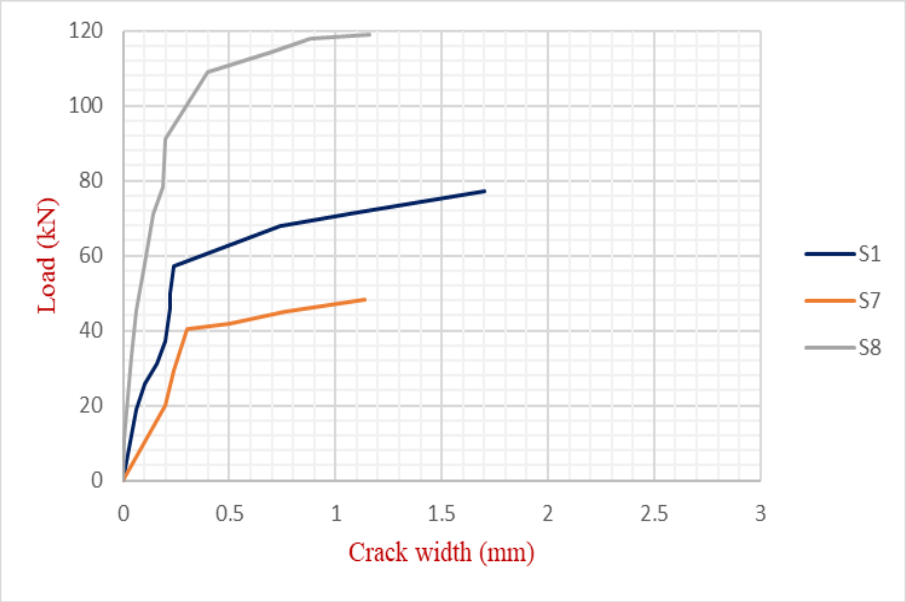

Figure (4-3) Load-crack width curves of G13

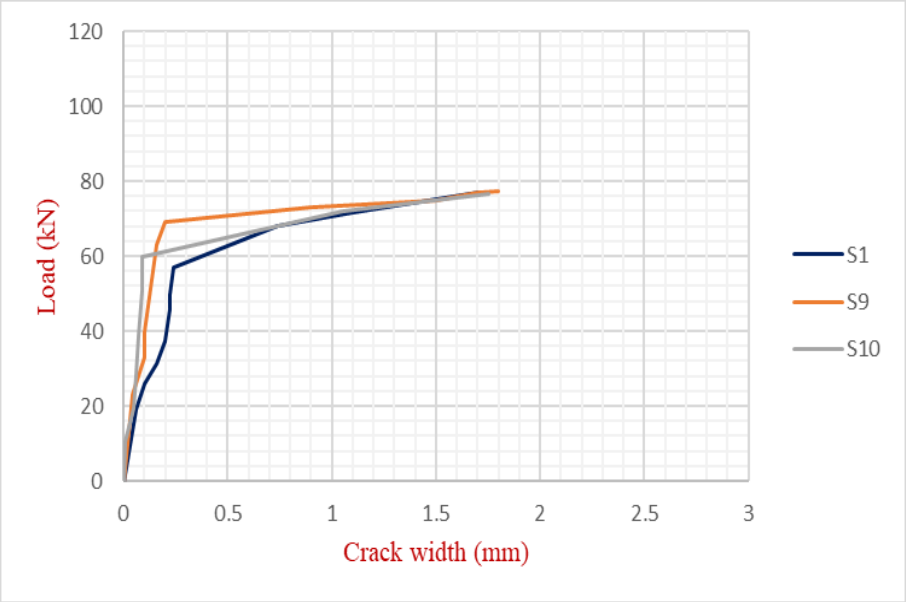

Figure (4-4) Load-crack width curves of G14

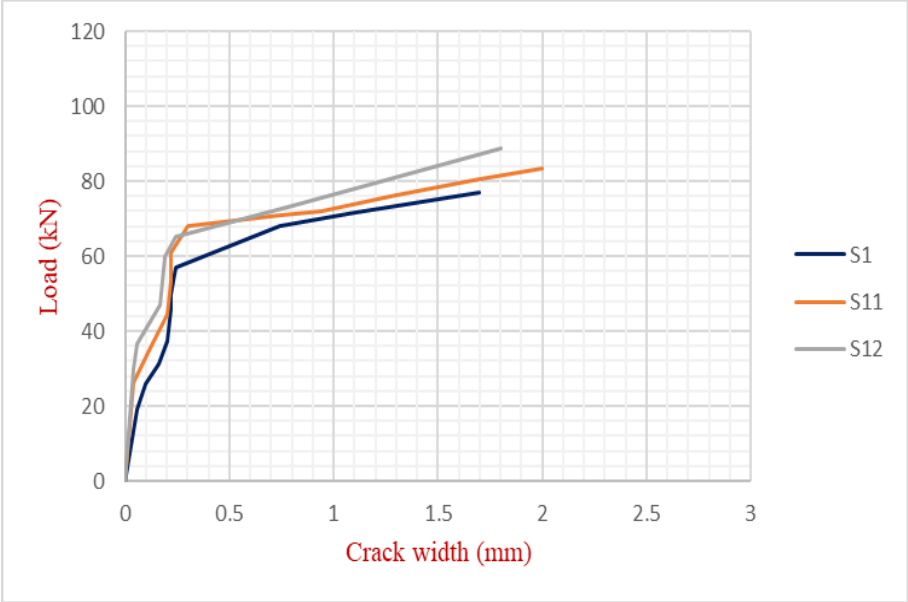

Figure (4-5) Load-crack width curves of G15

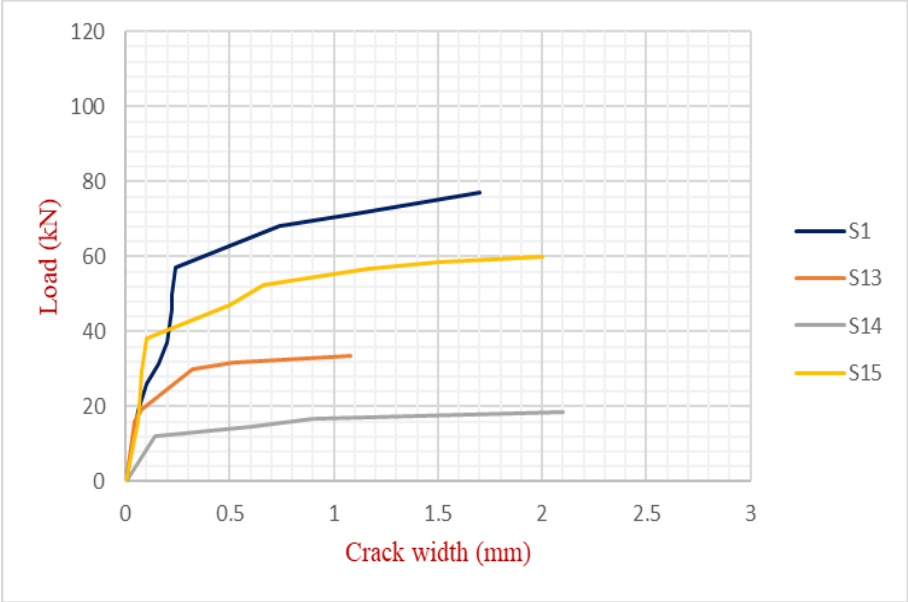

Figure (4-6) Load-crack width curves of G16

4.3.1.3 First Cracking Load

Load of the first crack in one–way slab specimens is evaluated and discussed in this section under the effect of two-point static loading as follow:

➢ **First Sub-Group (G11): Concrete Type**

The effect of concrete types (normal strength and high strength) concrete with NWA and LWA on the first crack load of one–way ribbed slabs will be discussed.

In one–way ribbed slab S1 was made from HSLWC, the first crack load increased by 24.85% in comparison to NSLWC ribbed Slab S3. In the same manner, using HSNWC in ribbed slab S2 instead of NSNWC in slab S4 improved the first crack capacity by 73.08 %, as shown in Figure (4-7). From the results, it was found that using HSC instead of NSC for both NWA and LWA gave a better improvement in the capacity of cracking loading because of the enhancement in the mechanical characteristics of the concrete, such as tensile strength and modulus of elasticity. Also, found that NWA gave a better improvement in first cracks more than LWA by 48.23 % because of the nature of aggerate and its mechanical properties.

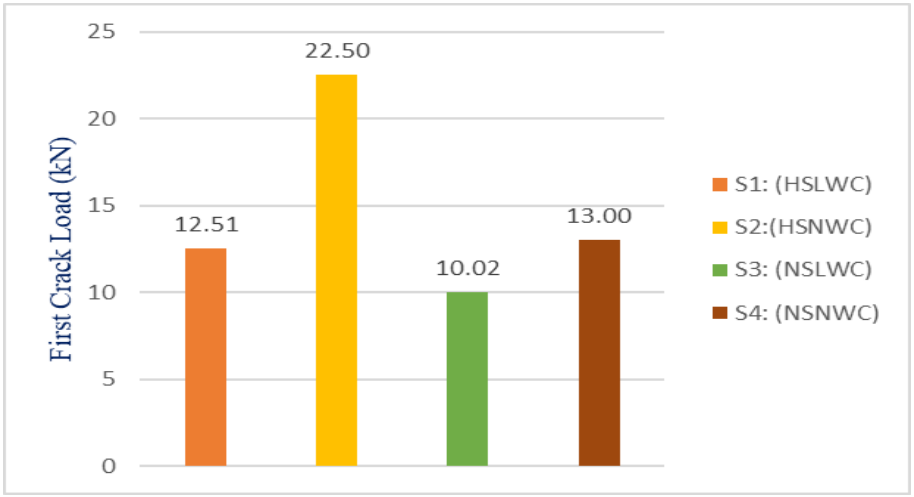

Figure (4-7) First crack load of G11

➢ **Second Sub-Group (G12): Inclusion of Steel Fiber**

It can be seen from Figure (4-8) that the inclusion of hooked end steel fibers in HSLWC ribbed slabs with two volume fractions of 0.25 % in

slab S5 and 0.50 % in slab S6 led to enhance the first crack load carrying capacity by 20.06 % and 34.45 % in comparison to S1, respectively. This behavior could be related to the fact that steel fibers improve the bond between concrete components, thereby arresting the growth of cracks.

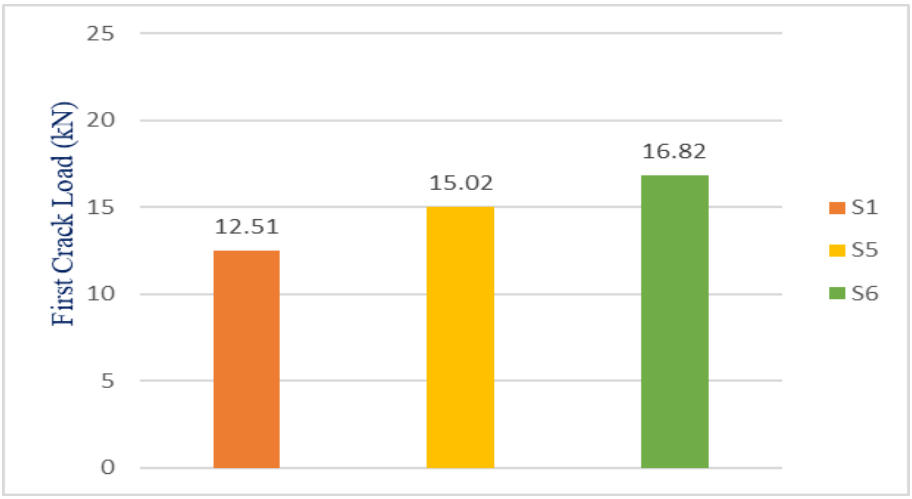

Figure (4-8) First crack load of G12

➢ **<u>Third Sub-Group (G13): Steel Reinforcement Ratio</u>**

Decreasing the reinforcement ratio of ribs by using ϕ 6 mm in slab S7 instead of ϕ 8 mm at the same number of bars in ribbed slab S1 displayed a reduction in the first crack load-carrying capacity of about 7.75%. While increasing the rib's main steel reinforcement ratio by using bar ϕ10 mm in slab S8 displayed an improvement in the first crack load-carrying capacity of about 27.18%. This behavior belongs to the effect of stiffness (i.e., the increase in the moment of inertia) of slab specimen. Figure (4-9) shows the effect of change ρ on cracking load.

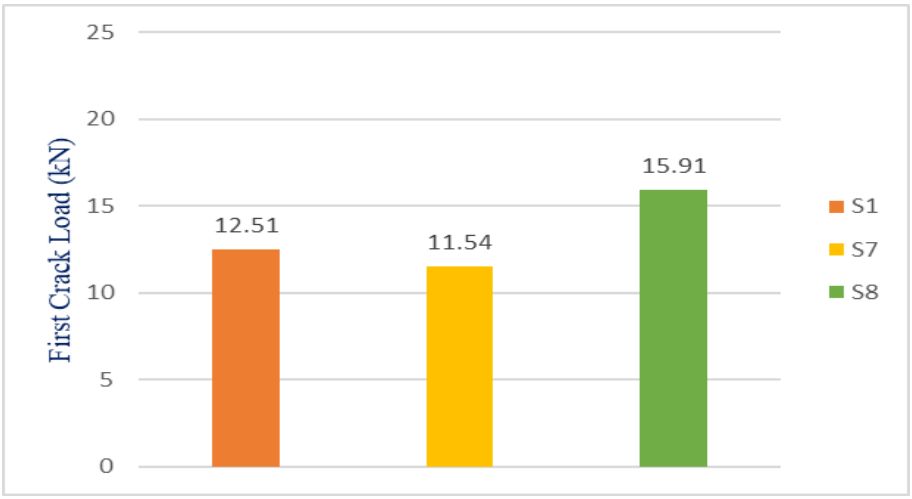

Figure (4-9) First crack load of G13

➢ **<u>Fourth Sub-Group (G14): Geometry of Section</u>**

At the same concrete volume which was used to produce the HSLWC one–way ribbed slabs, the effect of the geometry of section by changing the number of ribs on the first crack capacity is illustrated in Figure (4-10).

The comparison between reference slab S1 with three ribs and width of each rib equal to 100 mm and the slab with two–ribs S9 with the width of each – rib equal to 150 mm also, the slab with one–rib S10 with the width of rib equal to 300 mm. The strength at the first crack was increased slightly with the decrease in the number of ribs with the same characteristics of concrete as well as cross-section (cross-sectional area and second moment of area, the increment was 2.80% and 3.92% in comparison slab S1. The primary issue is very certainly related to the inability to distribute loads equally across the slab width. As a result, the normal stresses in the tensile zone would be concentrated on certain ribs. Nonetheless, this case is a good reveal difficulty to distribute loads on the width of larger space.

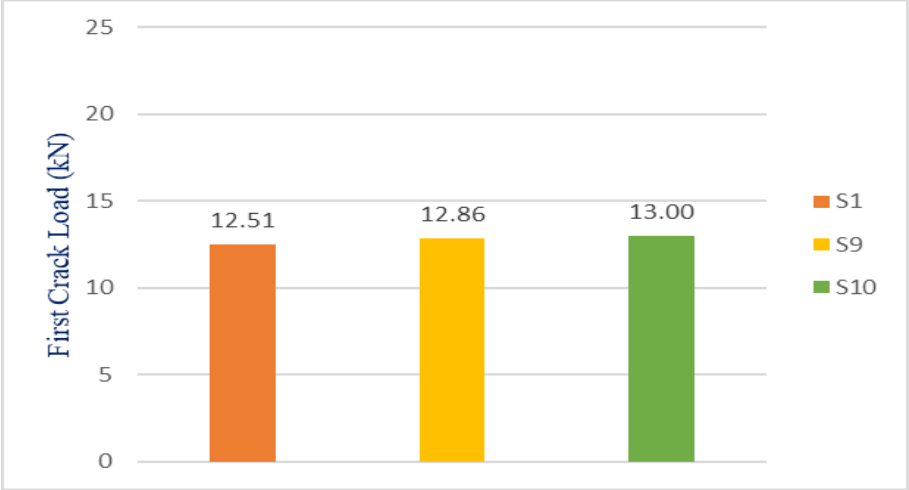

Figure (4-10) First crack load of G14

- **<u>Fifth Sub-Group (G15): Ribs Spacing</u>**

The effect of weight reduction on the production of HSLWC one–way ribbed slabs through changing the ribs spacing at the same number of ribs, gave a significant indication of the capacity of the first crack load of the slab. This behavior belonged to changing the stiffness of specimens through changing the moment of inertia. The reduction in ribs spacing from (200mm to 180mm) in slab S11 and to 150mm in slab S12 led to increase the first crack load by 15.91% and 34.13%, respectively, as shown in Figure (4-11).

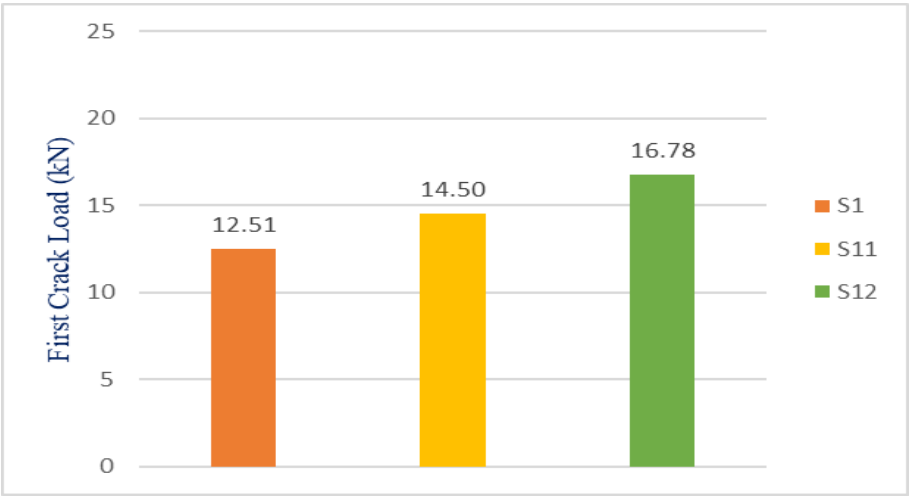

Figure (4-11) First crack load of G15

➢ **Sixth Sub-Group (G16): Slab Type**

Changing the slab type from solid slab S13 to ribbed type in S1 led to increase the first crack loading capacity by 31.55%. This is because a one-way ribbed slab has a larger moment of inertia than a one-way solid slab of the same concrete volume. From the Figure (4-12), it was found that the reduction in the ρ from 0.57% in slab S13 to 0.31% in slab S14 led to decrease the first crack load by 15.88%, while increasing the ρ to 0.90% in slab S15 led to increase the first crack by %15.67. The increase of ρ to 0.90% led to decrease the reduction in the first crack of slab S13 by 11.91% in comparison to S1.

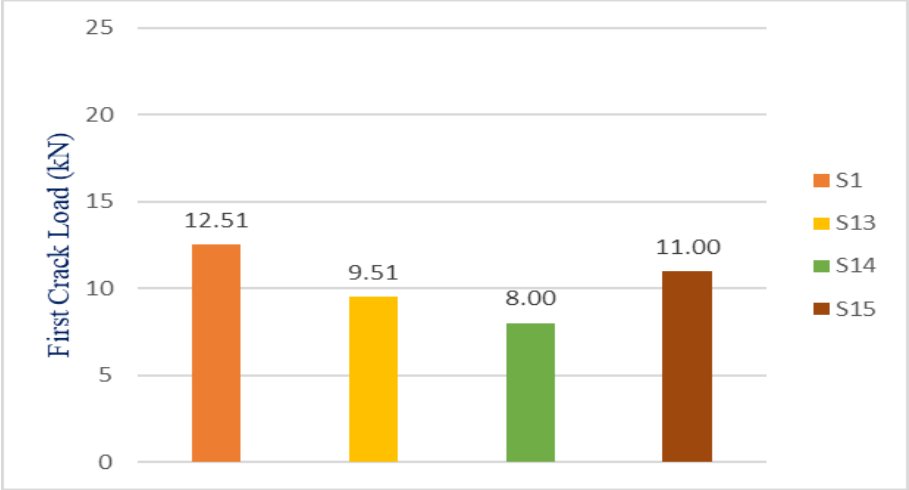

Figure (4-12) First crack load of G16

4.3.2 Deflection Behavior

The deflection at the middle point of each slab specimen was measured using the linear variable differential transducer (LVDT). The LVDT was placed at the mid-point of the span. Table (4-9) present the loads (P_{cr}, P_y, and P_u) and the corresponding midpoint of span deflections (δ_{cr}, δ_y, and δ_u) that correspond to each loading level, respectively.

4.3.2.1 Load-Deflection Curves

The results of this experimental work revealed that the deflection behavior for one–way slab specimens could be described as follows: at the early stage of loading, all slab specimens were in the pre-cracking stage, which presents the elastic state. In this stage, loading causes a linear increase in deflection. Because the strains in concrete and steel are relatively small, this behavior is to be expected. All the materials are in the elastic portion of their respective responses.

The second stage was the post-cracking stage (elastic-plastic stage). Cracking alters the slope of the load-deflection curve, resulting in a decrease in the effective moment of inertia. Following cracking, deflections continue to increase linearly with the load but with varying slopes until all tensile reinforcement yields. The third stage was the post–yielding stage (the plastic stage), which started after yielding the tensile reinforcement. In this stage, all the load-deflection relationships showed some variation in slope (a non-linear relationship). The neutral axis decreases dramatically, resulting in a quick rise in both curvature and deflection soon following the yielding up till the failure of the tested reinforced concrete specimen.

Each slab specimen demonstrated various post–yielding load-deflection behavior (as shown in Figure (4-13) to Figure (4-18)), depending on the concrete strength, types of aggregate, the geometry of section, amount of steel reinforcement, and slab type.

- **First Sub-Group (G11): Concrete Type**

Using HSLWC in one–way ribbed slabs S1 instead of NSLWC in slab S3 led to increase the ultimate load of 6.62% and decrease the deflection at the ultimate load by 4.84%.

On the other hand, using HSNWC in one–way ribbed slab S2 instead of NSNWC in slab S4 led to increase the ultimate load capacity by 22.60 % and increase the deflection at the ultimate load from 33.78%, as shown in Figure (4-13). Also, it is noted that the use of LWA makes the load-deflection curve more softening compared to NWA, due to the different modulus of elasticity for both concrete types.

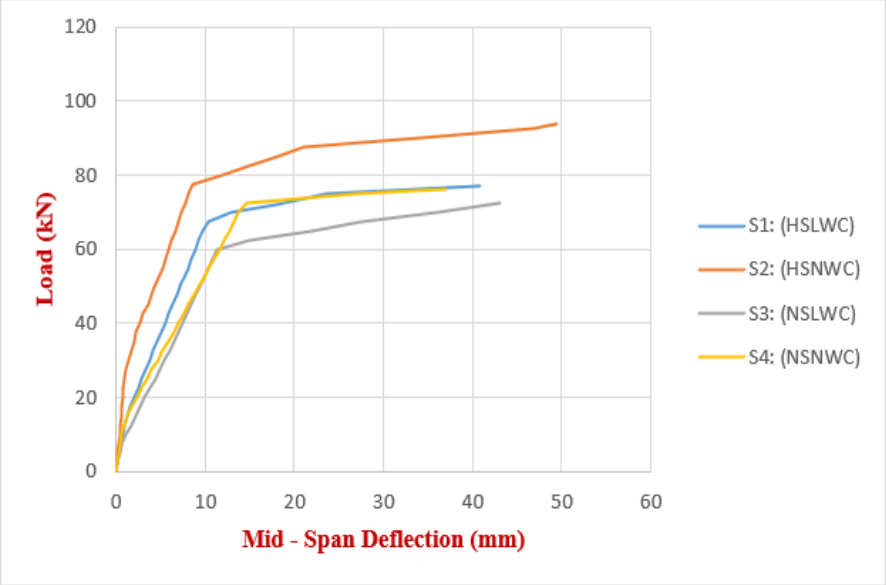

Figure (4-13) Load-deflection curves of G11

- **<u>Second Sub-Group (G12): Inclusion of Steel Fiber</u>**

Inclusion of hooked end steel fibers in HSLWC in one–way ribbed slab led to having higher values of ultimate load capacity, and their values are increased as fiber fraction increased in the concrete.

The results explained that adding steel fibers with 0.25% in slab S5 and 0.50 % in slab S6 led to increase the ultimate loading capacity by (17.60% and 25.06%) in comparison with slab without steel fiber S1, respectively. On the other hand, the strength improvement was more evident in slab S6, which led to recover the reduction in the ultimate loading capacity due to the using pumice stone instead of gravel in HSNWC. As shown in Figure (4-14), using steel fibers improved the

stiffness of slabs by decreasing the deflection at the same stage. This superior performance of fiber in HSLWC one–way ribbed slabs is due to the role of fibers in arresting the crack, which led to improving the stiffness and moment capacity of slabs.

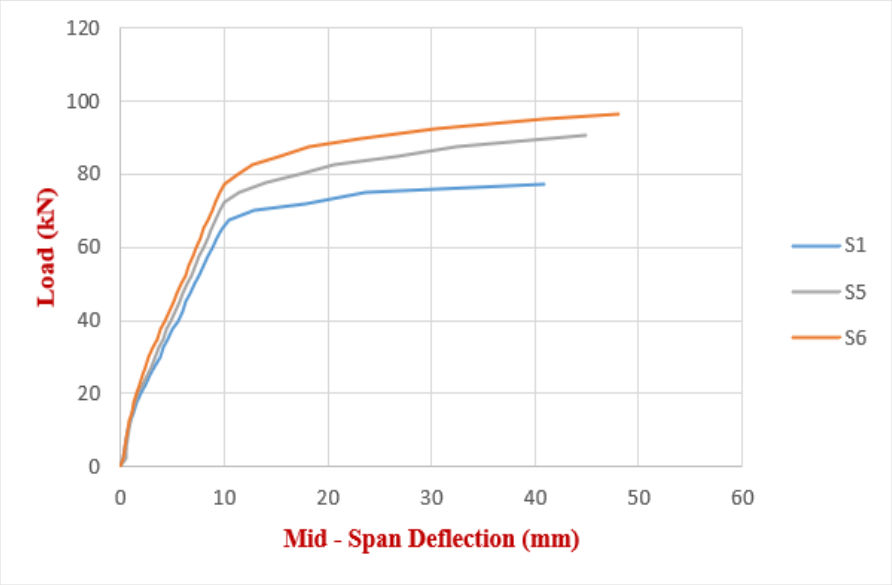

Figure (4-14) Load-deflection curves of G12

➢ **<u>Third Sub-Group (G13): Steel Reinforcement Ratio</u>**

Decreasing the ρ of slab S7 from (0.28 to 0.16) % led to decrease the load-carrying capacity by 37.62% and increase the deflection at the same stage of loading. While increasing the ρ in slab S8 from (0.28 to 0.44) % led to the recovery of the reduction in the load-carrying capacity due to the reduction in weight of HSLWC ribbed slabs as a result of using LWA (pumice stone) instead of gravel. The improvement in load-carrying capacity was 53.99 % over slab S1. This increment in ρ led to improve the moment of inertia of the slab. For this reason, the deflection was reduced at the same stage of loading, as shown in Figure (4-15).

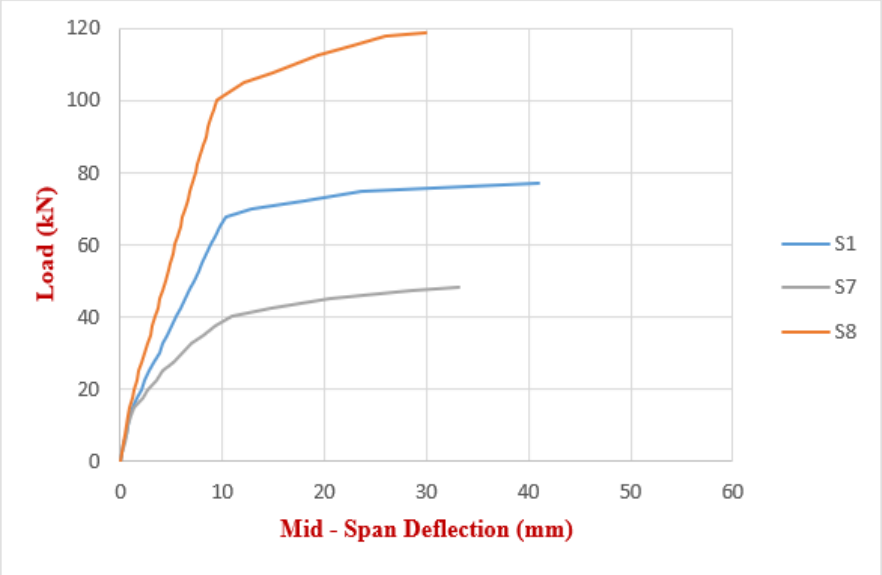

Figure (4-15) Load-deflection curves of G13

➢ **<u>Fourth Sub-Group (G14): Geometry of Section</u>**

Changing the geometry of section by changing the number of ribs led to a minor effect on the load-carrying capacity. This effect may be belonged to stress distribution on slabs (shear lag phenomena). For all the specimens in the sub-group G14 (S1, S9, and S10), the effective width of ribs is located within the whole width of the slab. The ultimate load carrying capacity for two–ribs was 77.45 kN, while one–rib was 76.79 kN. On the other hand, the one–way ribbed slab S10 gave the largest deflection (48.26 mm) more than two and three ribs, as shown in Figure (4-16) below.

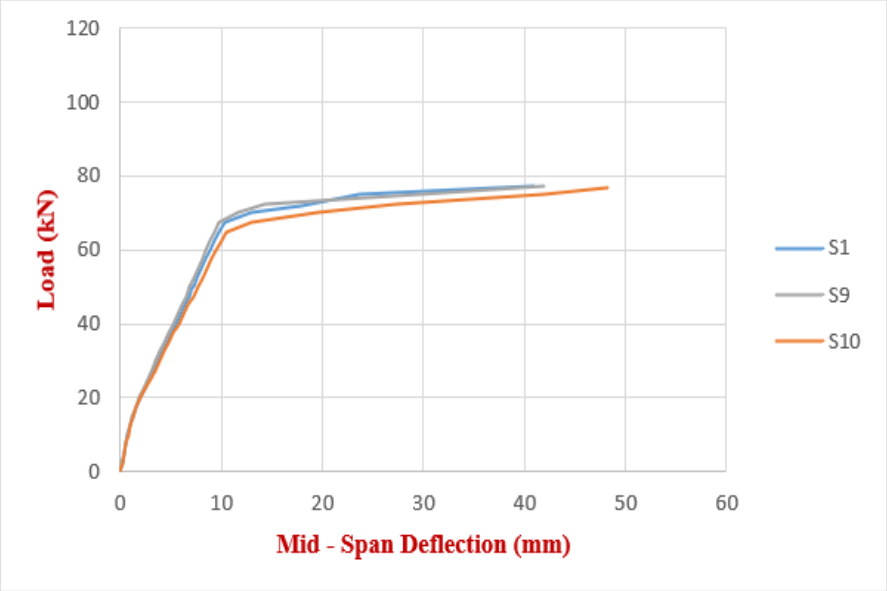

Figure (4-16) Load-deflection curves of G14

- **<u>Fifth Sub-Group (G15): Ribs Spacing</u>**

Decreasing the spacing between the ribs of the HSLWC one–way ribbed slab by increasing the width of ribs led to increase the ultimate load-carrying capacity by 8.33% and 14.97 % in slabs S11 and S12, respectively, over reference slab S1. This behavior is due to the formation of cracks in the tensile zone. Cracks developed more slowly in slabs S11 and S12 than in slab S1 due to an increase in the area of concrete that provides resistance to normal tensile stresses, This is agreed with result of the authors (Al-Azzwi and Al-Asdi, 2017) [102].

Furthermore, the results showed that lower deflection of one-way ribbed slab S12 was found through different loading stages in comparison with S11, as shown in Figure (4-17). This behavior is because of the larger cross-sectional area that led to decrease the moment of inertial and internal moment capacity.

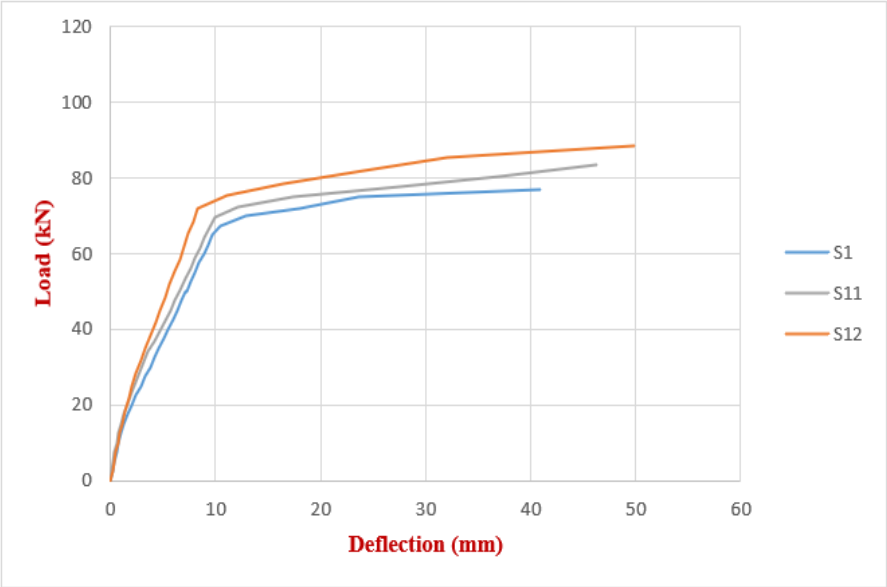

Figure (4-17) Load-deflection curves of G15

- **<u>Sixth Sub-Group (G16): Slab Type</u>**

Using one–way ribbed slab S1 instead one–way solid slab S13 with the same amount of concrete led to a positive impact on the ultimate capacity, which was increased by 130.37 %. On the other hand, the ratio of steel reinforcement decreases to 0.31% in slab S14 led to decrease the ultimate load capacity to 45.15 % in comparison to slab S13. Increasing the steel reinforcement ratio in the slab to 0.9% S15 led to improve the ultimate load capacity by 79.46% in comparison to S13 but remained less than the ultimate load capacity of S1.

On the other hand, the deflection of one–way solid slab increased in comparison to one–way ribbed slab. Also, the amount of steel reinforcement ratio played in changing the deflection of one–way solid slab specimens, as shown in Figure (4-18). This behavior is because of the reduction of the moment of inertia and internal moment capacity.

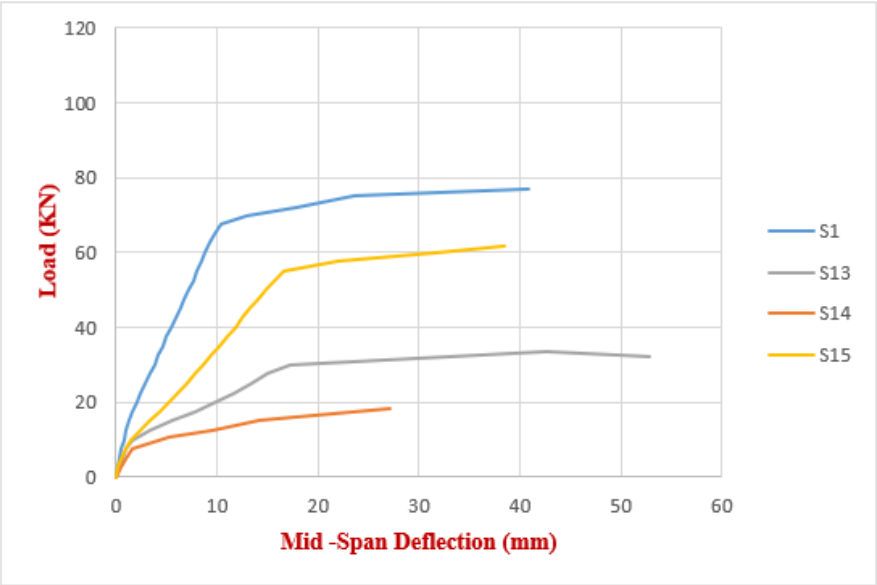

Figure (4-18) Load-deflection curves of G16

4.3.2.2 Stiffness

From the load-deflection curve of tested slab specimens, the stiffness (Ks), as shown in Figure (4-19) was calculated in this study at the service load stage [101].

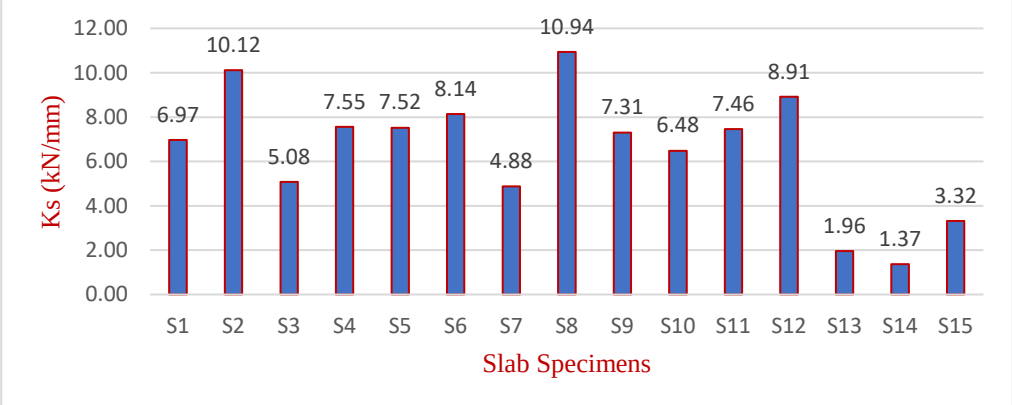

Figure (4-19) Stiffness of all tested slabs specimens

As illustrated in Figure (4-19), the results of sub-group G11 found that the stiffness of slab S1 increased by 37.20 % in comparison to slab S3, while the stiffness of slab S2 increased by 34.04 % in comparison to slab S4. In subgroup G12, the inclusion of steel fibers led to enhancement of the stiffness, and the degree of enhancement depends on the ratio of

volume fraction of steel fibers. The improvement of K_s was 7.89% and 16.79 % for S5 and S6, respectively, over slab S1. This behavior belongs to the enhancement of the modulus of elasticity of concrete when the compressive strength increases and the inclusion of steel fibers.

Also, the ribs steel reinforcement ratio in subgroup G13 had a clear influence on the stiffness. The K_s decreased by 29.99 % in slab S7, while K_s increased by 56.96% in slab S8 over slab S1. This behavior belongs to the effect of steel reinforcement amount on both strength capacity and the deflection.

The change of geometry of section at the same amount of concrete in sub-group G14 had a slight effect on the stiffness. The change in K_s did not exceed 7.03%. This behavior may belong to the similarity in mechanical properties of concrete and cross-sectional area.

The reduction in the ribs spacing (i.e., increment in concrete volume) of one–way ribbed slabs in sub-group G15 had a positive effect on the stiffness. This behavior belongs to the effect of the moment of inertia. The improvement of K_s was 7.03% and 27.83% for slabs S11 and S12 over slab S1, respectively.

Changing the slab type from one–way solid slab S13 at the same amount of concrete and reinforcement in sub-group G16 to one-way ribbed slab S1 led to increased stiffness by 255.6% due to an increment in the moment inertia. Furthermore, the steel reinforcement ratio has a clear effect on the K_s of solid slabs S14 and S15 by decreasing K_s in slab S14 by 30.10% and increasing the K_s in S15 by 69.39% over slab S13, respectively.

4.3.2.3 Ductility and Absorbed Energy

Ductility refers to a structural member's ability to endure substantial deformation after the yielding of tensile reinforcement [103]. A structural engineer must ensure sufficient strength when designing a flexural member and ensure that the member is ductile under overload conditions. In earthquake zones, individual structural members' and the structure's overall ductility becomes a crucial design factor.

Ductility (μ) for slab specimens was computed as the ratio between the deflection at the ultimate load (δ_u) to the deflection of the first yielding of the tensile reinforcement (δy) [103]. The change in slope of the curve between after the first crack forms and before the curve reaches its peak value indicates a yielding load [104]. The deflection at yielding load was calculated from the load-deflection curve.

Absorbed Energy (AE) is defined as the capacity of reinforced concrete members to absorb energy before showing a significant reduction in the load-carrying capacity[105]. AE presented the area under the load-deflection curve. Calculating the AE by using trapezoidal rule in Microsoft Excel.

This section discusses the AE and μ for reinforced concrete one-way slabs evaluated under two-point static loading. Table (4-9) presents the ultimate loads and mid-span deflections (yielding deflection (δ_y), and deflection at ultimate load (δ_u)).

- **<u>First Sub-Group (G11): Concrete Type</u>**

Using different types of concrete (HSLWC, HSNWC, NSLWC, and NSNWC) in production one–way ribbed slabs, causing different μ and AE behavior, as shown in Figure (4-20) and Figure (4-21). One-way

HSLWC slab S1 had improvement in the μ and AE equal to 13.78% and 7.35 %, respectively, as respected with NSLWC slab S3.

On the other hand, in this study, one-way HSNWC slab S2 had an improvement in the μ and AE equal to 127.41% and 76.34%, respectively, respected with NSNWC slab S4.

This behavior is due to the differences between the two types of aggregate (pumice stone and gravel) used in producing HSC and NSC mixes which affect the stiffness, ultimate load, and deflection of those slabs. The result of μ in HSC higher than NSC agree with the result of author (Tameemi, 2020) [106].

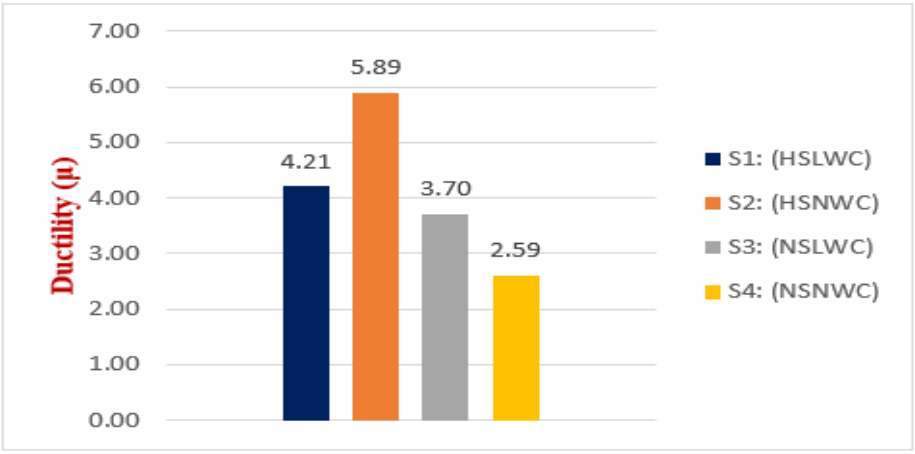

Figure (4-20) Ductility of G11

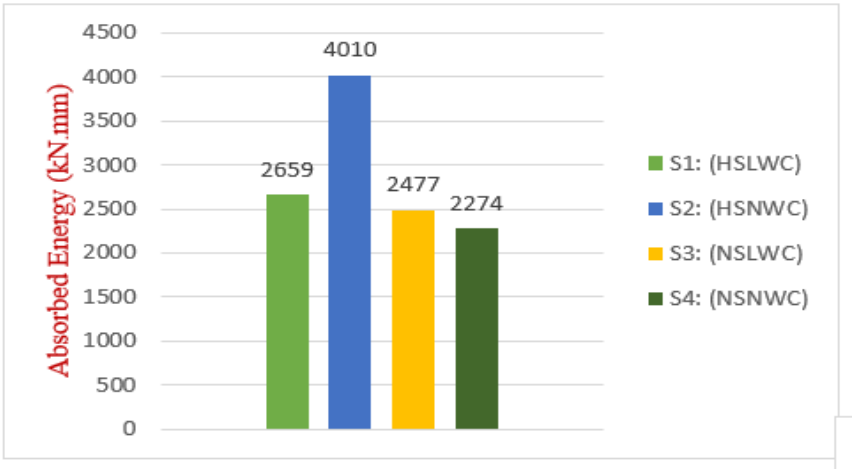

Figure (4-21) Absorbed energy of G11

➢ **Second Sub-Group (G12): Steel Fiber Inclusion**

The μ increased by 6.65% and 14.01% for slabs S5 and S6 over reference slab S1, as shown in Figure (4-22). This behavior is expected because the addition of the fibers causes a decrease in the deflection at the cracking load and increases deflection at the ultimate load. The AE of steel fiber- HSLWC one–way ribbed slabs, as shown in Figure (4-23), is more than that of the corresponding slabs without fibers. It increased by 25.72% and 46.07% for slabs S5 and S6 over reference slab S1.

This behavior may be explained by the fact that, in fiber-reinforced concrete slabs, crack propagation requires more energy because some or most of these cracks are bridged by randomly dispersed fibers that apply pinching stresses at the crack, slowing its propagation and extension.

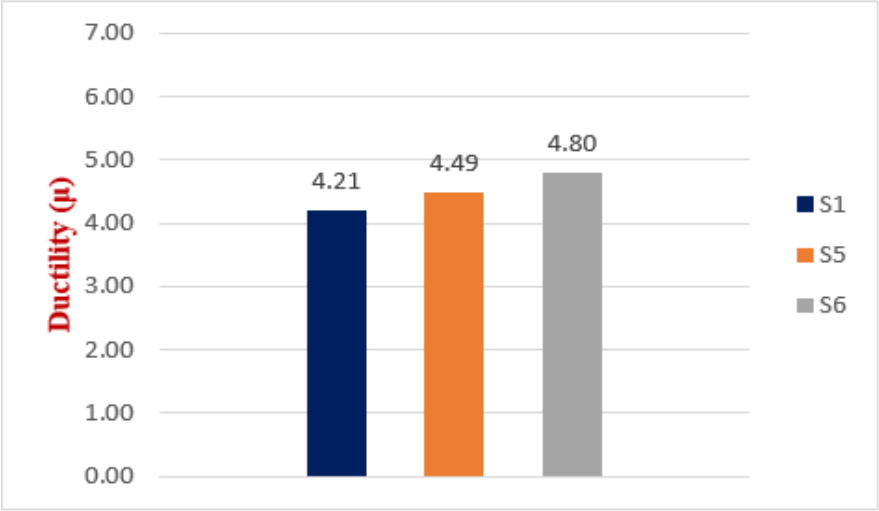

Figure (4-22) Ductility of G12

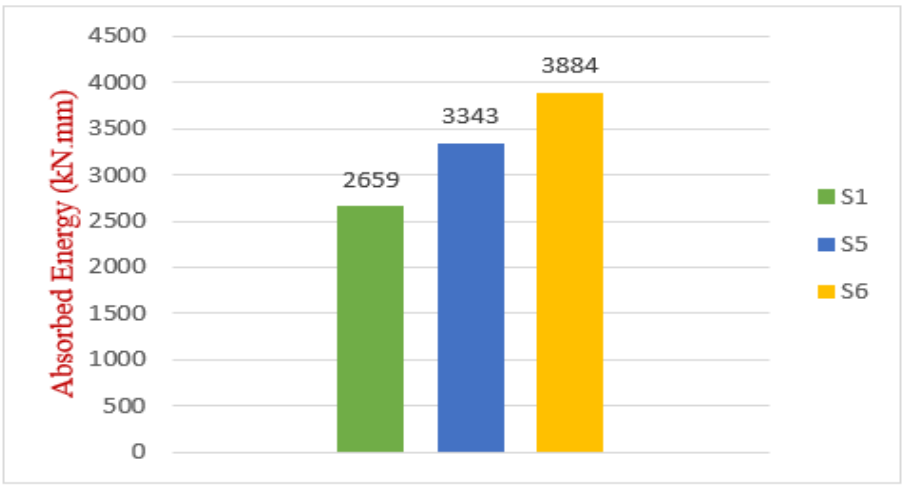

Figure (4-23) Absorbed energy of G12

➢ **<u>Third Sub-Group (G13): Steel Reinforcement Ratio</u>**

Decreasing the ρ of slab S7 by using 6 ϕ 6 mm in three ribs instead of 6 ϕ 8 mm in slab S1 led to increase the μ by 53.21 % in comparison to reference slab S1 and decrease the AE by 51.41 %, as shown in Figure (4-24) and Figure (4-25) below.

While increasing the ρ of slab S8 by using 6 ϕ 10 mm in three ribs instead of 6 ϕ 8 mm in slab S1 led to decrease the μ of slab S8 by 27.32% in comparison to reference slab S1 and increase the AE by 5.19%. This behavior occurs because increasing the reinforcement ratio results in an increase in strength, which makes the yielding load improve.

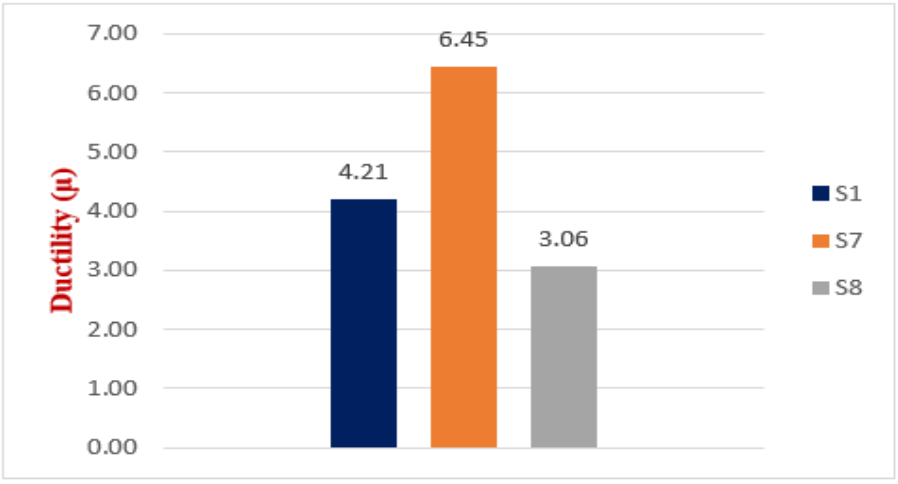

Figure (4-24) Ductility of G13

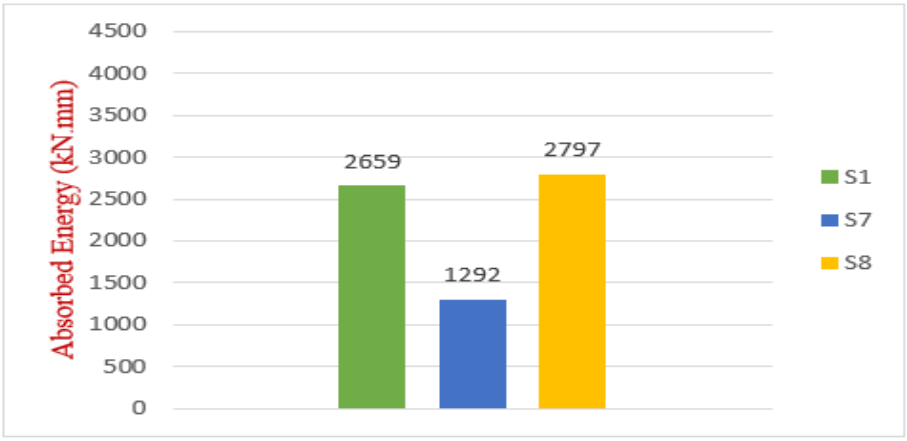

Figure (4-25) Absorbed energy of G13

➢ **<u>Fourth Sub-Group (G14): Geometry of Section</u>**

The outcomes of the effect of the geometry of section on μ and AE of one–way HSLWC ribbed slabs revealed that the one-rib slab S10 gave higher μ and AE from two–rib and three ribs in slabs S9 and S1, respectively, as shown in Figure (4-26) and Figure (4-27), respectively. The μ in slab S10 increased by 6.02 % and 8.79%. Also, the AE in slab S10 increased by 12.89 % and 16.96 % over slabs S9 and S1, respectively. This is due to the distribution of ribs and stresses in the specimens.

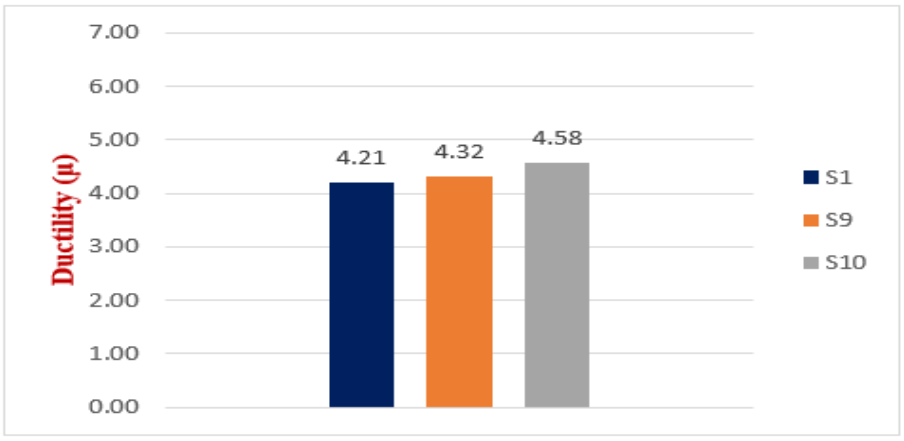

Figure (4-26) Ductility of G14

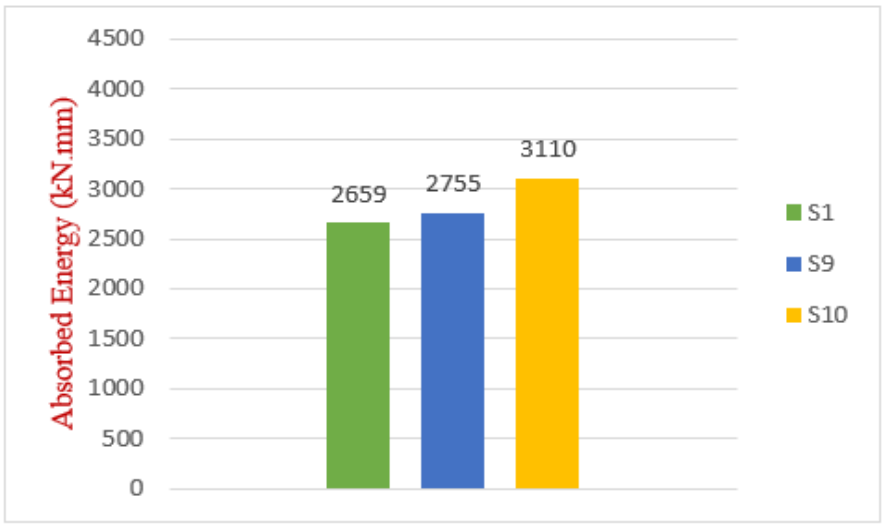

Figure (4-27) Absorbed energy of G14

➢ **<u>Fifth Sub-Group (G15): Ribs Spacing</u>**

Reducing the spacing between the ribs from 200mm to 180mm in slab S11 and 150mm in slab S12 led to increase the μ by 14.96 % and 15.91%, respectively, as shown in Figure (4-28). Moreover, AE increased by 21.51% and 42.05%, respectively, as shown in Figure (4-29). The increase in the cross-sectional area increased the deflection at the ultimate load and this contributed to this behavior.

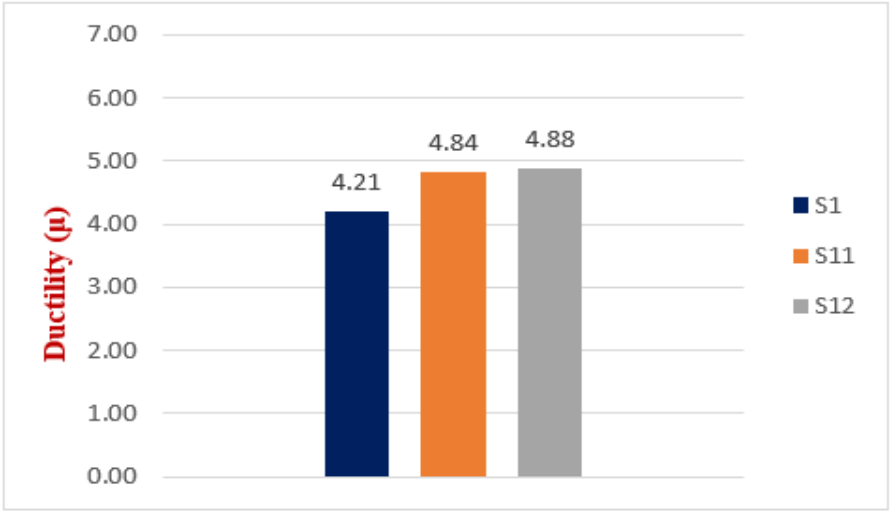

Figure (4-28) Ductility of G15

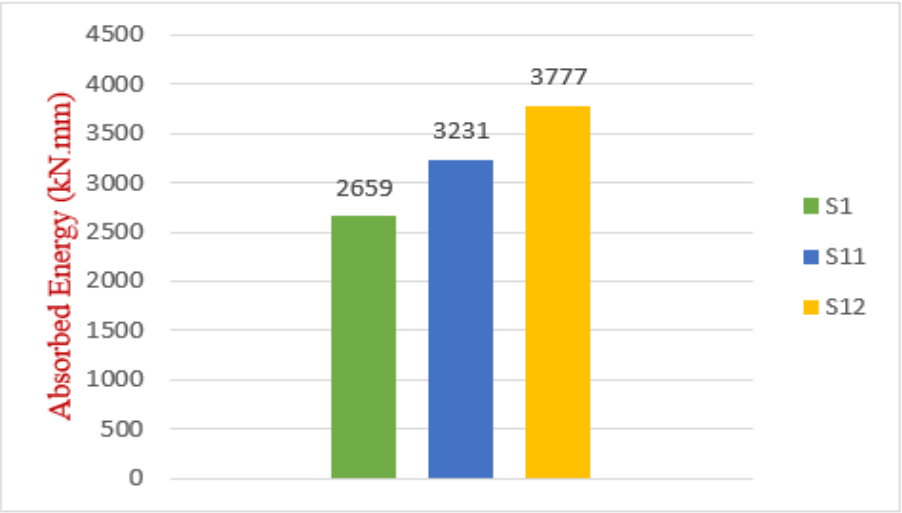

Figure (4-29) Absorbed energy of G15

- **<u>Sixth Sub-Group (G16): Slab Type</u>**

Changing the slab type from solid slab S13 to ribbed slab S1 led to an increment in μ and AE by 73.25 % and 85.81%, respectively. This behavior is because of the differences between the two types of slabs, including the moment of inertia and the ultimate and yielding loading capacity along with the corresponding deflection. Decreasing the ρ in the solid slab from (0.57 to 0.31) % in S14 led to increase the μ by 113.99% and decrease AE by 74.28%. Increasing the ρ in the solid slab from (0.57 to 0.9) % in S15 led to decrease the μ by 24.28% and increase AE by 39.69%.

For sufficient μ, particularly in the areas of seismic and moment redistribution, the μ of the 3 to 5 range is considered essential [47]; it appears that solid slabs (S13 and S15) would not meet this requirement. Thus, the ribbed slabs are more efficient for seismic considerations.

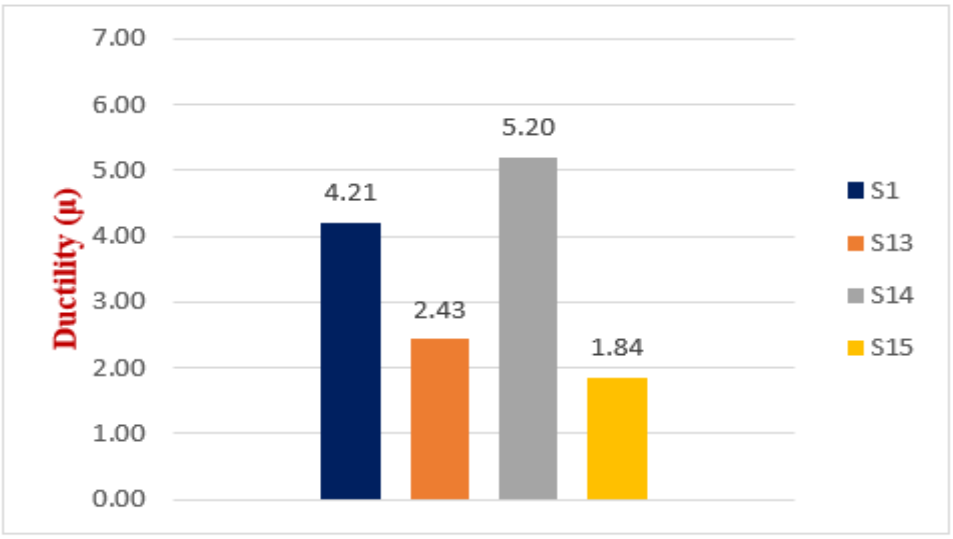

Figure (4-30) Ductility of G16

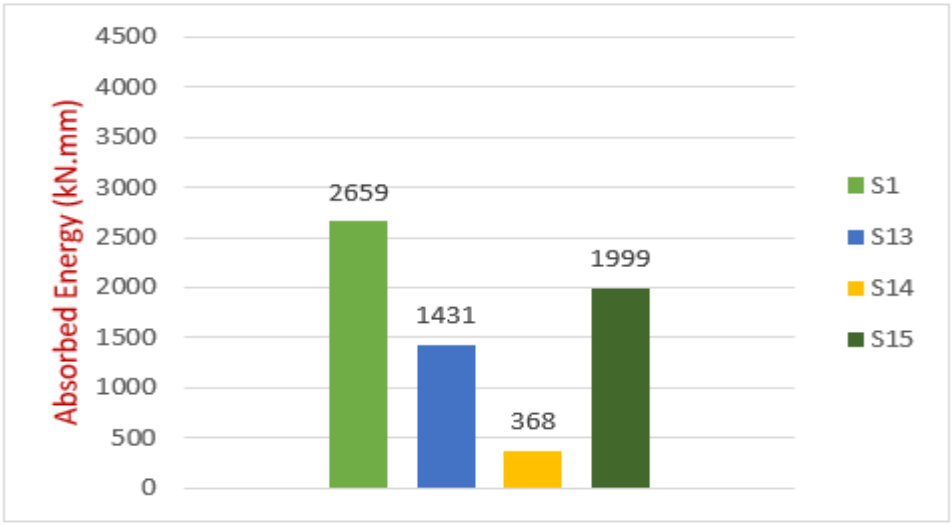

Figure (4-31) Absorbed energy of G16

4.3.3 Strain Behavior

The distribution of the strain on the top surface of slab specimens will be discussed in this section as follow:

4.3.3.1 Strain Distribution Across Width of Slab Specimens

The longitudinal strain distribution across slab width at mid-span of all slab specimen is measured to find the effect of variables that were

depended in this study on the effective width (shear lag) of slab specimens.

The traditional bending engineering theory assumes that the plane segments will remain flat before cracks, even after bending. The term shear lag describes the disparities between the theory of approximate engineering and real conduct, which results in both the increases of flange stresses adjacent to the web part in T-beams and reductions in flange component stresses outside of the web [107].

The effective width (b_o) may be defined in a number of different ways. This study depends on the equation (4-5) in the calculating of the b_o, which generally presents a function of the longitudinal strain at the slab's top surface; so, it may be derived by integration of the calculated longitudinal strain at the slab's top surface and divided by the highest value of strain.

$$b_o = \frac{\int_0^b \varepsilon_x . d_z}{(\varepsilon_x)_{max}} \quad \text{..... (4-5)}$$

Where b_o is the effective width of slab, mm, ε_x is a normal strain in a longitudinal direction, and $(\varepsilon_x)_{max}$ is maximum normal strain.

The outcomes of effective width were illustrated in Figure (4-32), which presented the strain at the service load level.

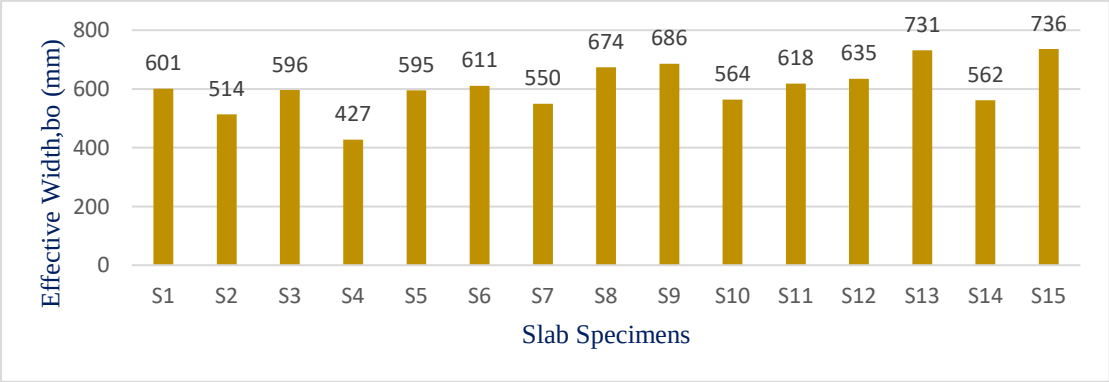

Figure (4-32) Effective width for all slab specimens

The effect of concrete compressive strength on the effective slab width at mid-span at service load is listed in Figure (4-32). From the obtained results, it is seen that when the cylinder compressive strength of LWC increased from (23.3 to 42.2) MPa, see Table (4-1) in slab S1 led to increase the b_o of the slab by 0.84%. While the increase in b_o for NWC slab S4 was 20.37% when the compressive strength increased from (34 to 58) MPa in slab S2. This yields from the increase in the stiffness of the slab due to concrete compressive strength increase.

From the outcomes of the influence of steel fibers on the b_o, it was found that the inclusion of steel fibers in HSLWC led to decrease b_o by 0.99 % when V_f increased from 0.00% to 0.25% in slab S5, while the b_o increased by 1.66 % when V_f equal to 0.50% in slab S6. This behavior may be to the amount and distribution of steel fibers in slabs.

The effect of ρ on b_o of slab revealed that the decrease of ρ from (0.28 to 0.16) % in slab S7 led to decrease of b_o by 8.49%. While increasing ρ from (0.28 to 0.44) % in Slab S8 led to increase the b_o by 12.15%. Increasing of ρ results in an increase in the compression block that leads to the largest area for flange longitudinal stresses.

When changing the number of ribs to investigate the effect of geometry of section on the b_o. It was found that using two ribs in slab S9 instead three ribs led to increase b_o by 14.14%. While using one–rib in slab S10 led to decrease the b_o by 6.16%. This behavior may have belonged to the distribution of ribs across the center of slab width.

Decreasing the spacing between the ribs from (200mm to 180mm and 150mm) in slabs S11 and S12 led to increase b_o by 2.83 % and 5.66 %, respectively.

Using ribbed slab S1 instead of solid slab S13 led to decrease the b_o by 17.78%. On the other hand, decreasing the ρ of solid slab S14 led to decrease the b_o by 6.49% and increasing ρ in solid slab S15 led to increase the b_o by 22.46 %, respectively, over ribbed slab S1. Strain distribution over the width for all slab specimens, as shown in Figure (4-33) to Figure (4-38).

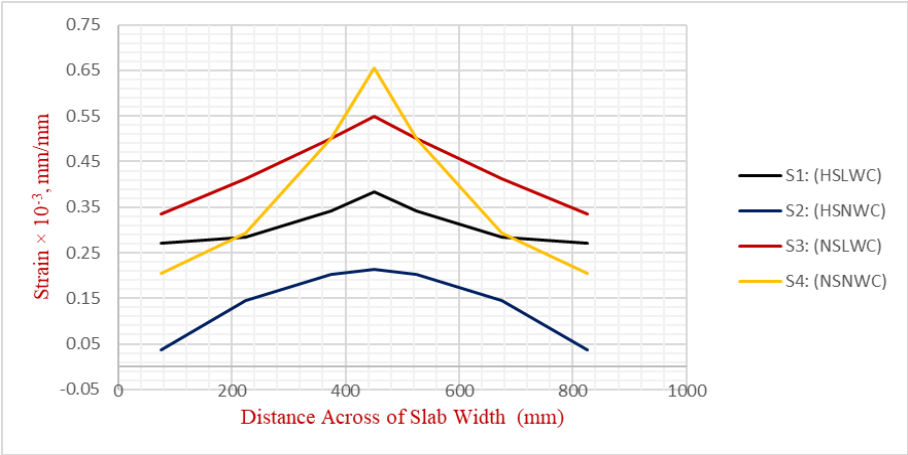

Figure (4-33) Strain distribution across width of slab for G11

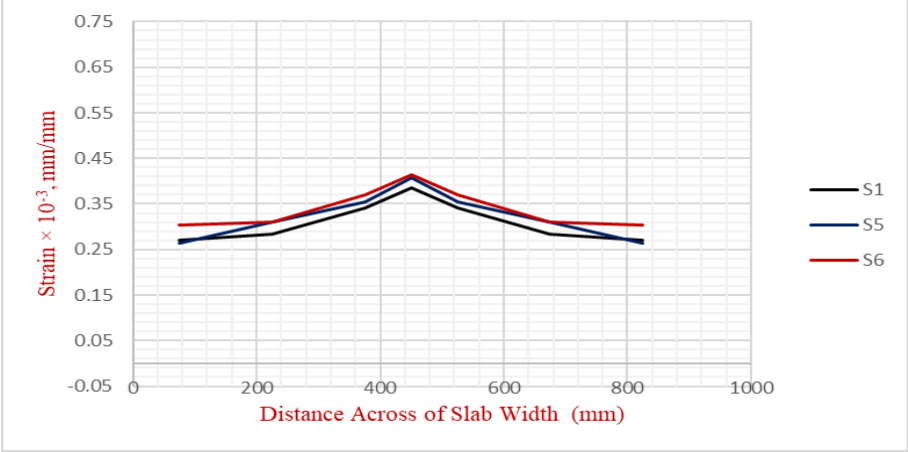

Figure (4-34) Strain distribution across width of slab for G12

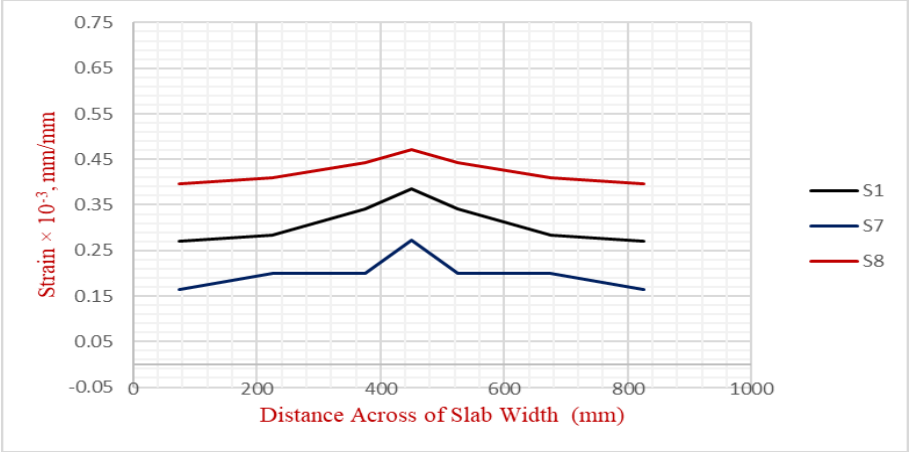

Figure (4-35) Strain distribution across width of slab for G13

Figure (4-36) Strain distribution across width of slab for G14

Figure (4-37) Strain distribution across width of slab for G15

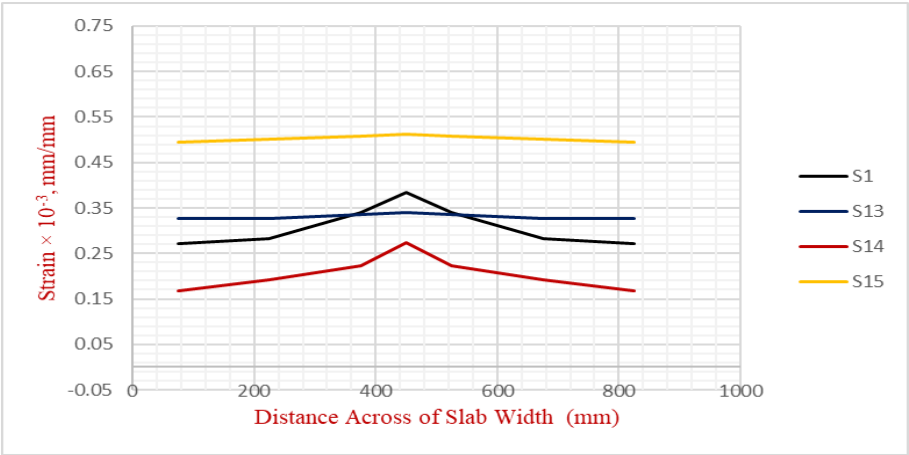

Figure (4-38) Strain distribution across width of slab for G16

4.3.4 Comparison between Experimental and Theoretical Results

The comparison between the experimental and the theoretical load's results are shown in Figure (4-39) .The theoretical loads were computed according to the ACI-318-19 [18] and ACI–544-4R [108], as shown in Appendix B, by using PTC Mathcad Prime 6.0 computer software. This comparison is very important to provide the designer with detailed information about the conservations taken out by ACI equations used in the design of slabs.

It was found that the load that was calculated by the equations of the ACI codes (P_{ACI}) for the slab S2 gave a value farther from the value of the experimental load (P_u), while P_{ACI} of the slab S14 gave the closest value to the P_u. On the other hand, taking the effect of steel fibers in the calculation of P_{ACI} for slabs (S5 and S6) gave fewer values of (P_{ACI} /P_u) than slab without fiber (S1). Generally, the average difference between the results of P_{ACI} and P_u was (-31.21) %.

This may be because the ultimate strength method adopted by the ACI code assumed a uniaxial state of stresses in a one-way slab and

neglected the influence of Poisson's ratio. In the case of beams, this coding assumption is nearly accurate, but it is not in the case of slabs. The situation is rather different [64]. The slab can resist more loads than that computed by the ACI code equations, and this is due to the small transverse stresses developed in the perpendicular axis. Another reason could be that the ACI code eliminates the effect of concrete at the tension zone and the friction between the steel plate of support and the bottom of concrete, which is attributed to increase the moment capacity of the slab. Also, ACI calculation depends on the yield stress of steel reinforcement, while in actuality, the slabs exceed the yield stress.

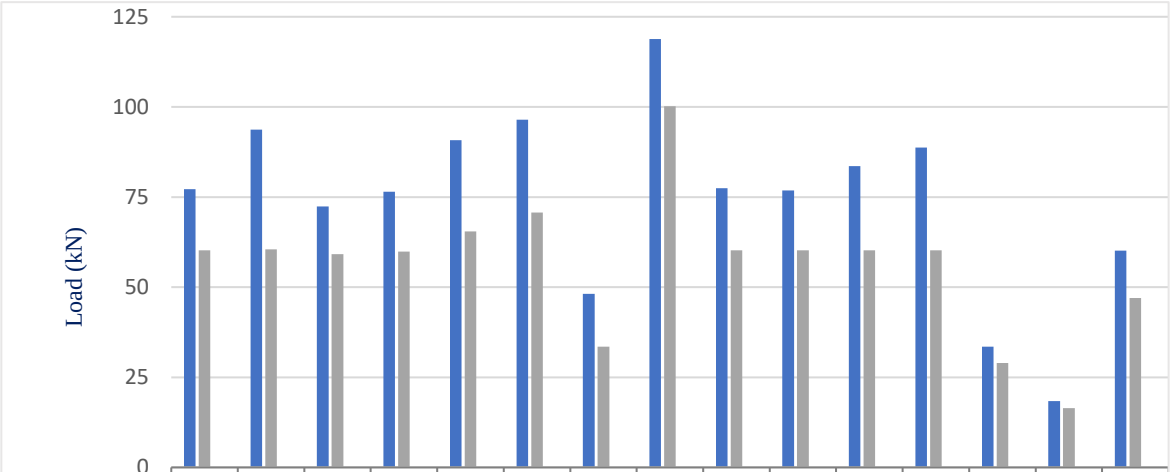

	S1	S2	S3	S4	S5	S6	S7	S8	S9	S10	S11	S12	S13	S14	S15
Pu (kN)	77.15	93.74	72.36	76.46	90.73	96.48	48.13	118.8	77.45	76.79	83.58	88.7	33.49	18.37	60.1
PACI (kN)	60.18	60.52	59.17	59.89	65.43	70.67	33.5	100.2	60.18	60.18	60.18	60.18	28.97	16.43	47.02
PACI/Pu	0.780	0.646	0.818	0.783	0.721	0.732	0.696	0.843	0.777	0.784	0.720	0.678	0.865	0.894	0.782

Figure (4-39) Comparison between experimental and theoretical load

4.3.5 Structural Efficiency Analysis of One–Way Slabs

The structural efficiency (SE) is defined by the strength/density ratio of the concrete used [15]. The ratio of ultimate load (P_u) to the weight of reinforced slab specimen (W_s) used in this study to calculate the SE. The values of the SE are shown schematically in Figure (4-40).

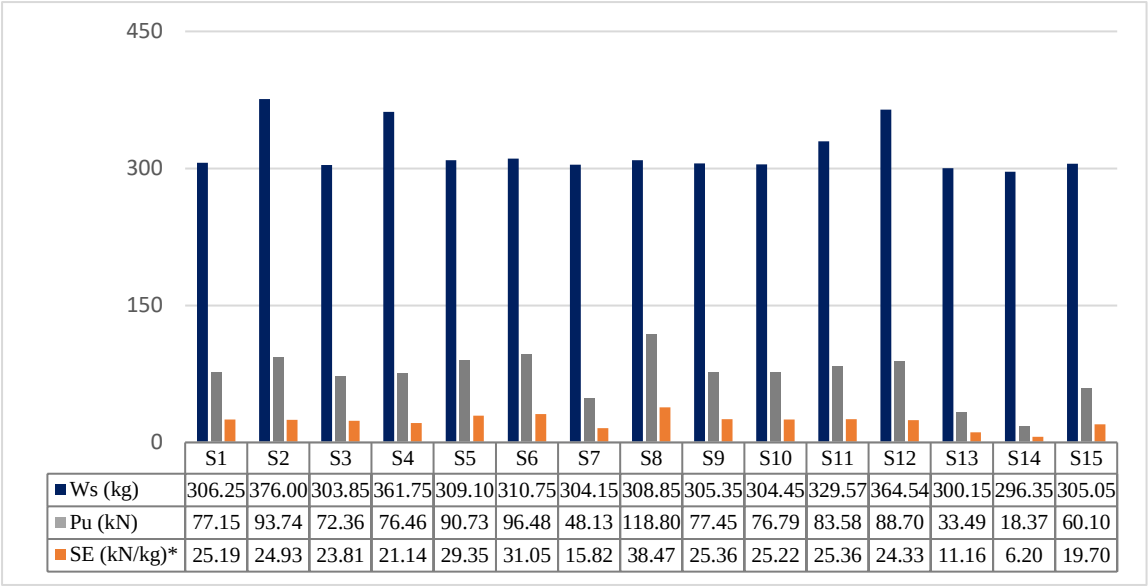

	S1	S2	S3	S4	S5	S6	S7	S8	S9	S10	S11	S12	S13	S14	S15
Ws (kg)	306.25	376.00	303.85	361.75	309.10	310.75	304.15	308.85	305.35	304.45	329.57	364.54	300.15	296.35	305.05
Pu (kN)	77.15	93.74	72.36	76.46	90.73	96.48	48.13	118.80	77.45	76.79	83.58	88.70	33.49	18.37	60.10
SE (kN/kg)*	25.19	24.93	23.81	21.14	29.35	31.05	15.82	38.47	25.36	25.22	25.36	24.33	11.16	6.20	19.70

*SE values multiplied by10^{-2}.

Figure (4-40) Structural efficiency for tested specimens

In subgroup G11, slab S1 with HSLWC gave the highest value of SE among other types of concrete slabs, which was increased by 1.04%, 5.80%, 19.16% over slabs S2, S3, and S4, respectively. This is due to the reduction of the weight of slab S1 in comparison to slab S2 and the increase of ultimate load of slab S1 in comparison to slab S3, while the reduction in weight and increase in ultimate load in comparison to slab S4.

In subgroup G12, slab S6 constructed from HSLWC with 0.5% steel fiber gave the highest value of SE, which was increased by 23.26% and 5.79% over slabs S1 and S5, respectively. This behavior belongs to the highest ultimate load for slab S6, and the increment in weight does not exceed 1.47% and 0.53% in comparison to S1 and S5, respectively.

In subgroup G13, slab S8 with the highest ρ (0.44) % gave the better SE, which was increased by 52.72% and 143.17% in comparison to ρ (0.28 and 0.16) % in slabs S1 and S7, respectively. This behavior reveals the improvement in the ultimate load capacity of S8 in comparison to the weight.

In Subgroup G14, the effect of section geometry with the same weight and nearly closed values in ultimate strength gave very close values of SE in slabs S1, S9, and S10.

In Subgroup G15, slab S11 with ribs spacing of 180mm gave the highest value of SE, which was increased by 0.67% and 4.23% in comparison to spacing of 200mm and 150mm in slabs S1 and S12, respectively.

In subgroup G16, converting the slab type from solid in slab S13 to ribbed slab S1 led to increase SE by 125.72%. Furthermore, increasing the steel reinforcement ratio from (0.57% to 0.9%) in slab S15 led to reduce the deficiency in SE of slab S13 to 33.90%.

4.3.6 Sustainability Analysis of One–Way Slabs

The “sustainable” refers to the ability to be maintained at a constant level with minimal long-term effect and less environmental impact [109].

Cement production accounts for around ten percent of total global CO_2 emissions. Because of the activities involved in the preparation of raw materials, concrete, which is the most widely used building material on the worldwide, has a substantial carbon footprint. Because ordinary Portland cement (OPC) is the primary binder material in concrete, it accounts for between (74 and 81) percent of the total CO_2 emissions. Because of the increased awareness of CO_2 emissions, alternative binder materials have been developed and/or used to reduce the reliance on OPC as the primary binder in concrete. Supplementary cementitious materials (SCMs), which include pozzolan materials, have been frequently employed to partially replace cement content. It is envisaged that the use of such SCMs will result in significant reductions in the overall embodied CO_2 emissions of concrete. This is a result of the fact that SCMs are often

manufacturing final products. In general, the energy required to create these SCMs is lower [110]. However, different materials will have different embodied CO_2 emissions. As for this current study, cement, silica fume as SCMs, steel fiber, LWA, NWA, water, SP, and amount of steel reinforcement were used as main materials to produce one-way slabs.

It was used to investigate the sustainability benefits of utilizing the dependent variables in this study for the carbon content being assessed. Table (4-10) shows the embodied carbon of materials based on a literature review. Equation (4-6) [111] was used to calculate the carbon embodied for each slab.

$$CO_{2e} = \sum_{i=1}^{r} W_i \times CO_{2i} \quad \text{..... (4-6)}$$

Where:

CO_{2e}: Total embodied CO_2 emission of each reinforced concrete slab, in $kgCO_2$.

W_i : Total amount in kg of material i to produce each slab.

r: Total raw material in each slab.

CO_{2i}: Equivalent CO_2 value of material i, $kgCO_2/kg$.

Table (4-10): Embodied carbon of material

Materials	Embodied Carbon ($kgCO_2/kg$)	References
Cement	0.930	Zhu, 2011[112]
Sand	0.0139	Turner and Collins, 2013[113]
Gravel	0.0408	
Pumice Stone	0.0028	Ameri et al.,2020 [114]
Silica Fume	0.024	Kumar et al.,2021 [111]
Water	0.000196	Yang et al., 2013 [115]
SP	0.60	Ameri et al., 2020 [114]
Sugar Molasses	0.00	Estimated
Steel Fiber	1.60	Kim et al., 2015 [116]
Steel Reinforcement	1.242	Ahmed, 2016 [117]

The value of embodied carbon for all slabs was illustrated in Figure (4-41).

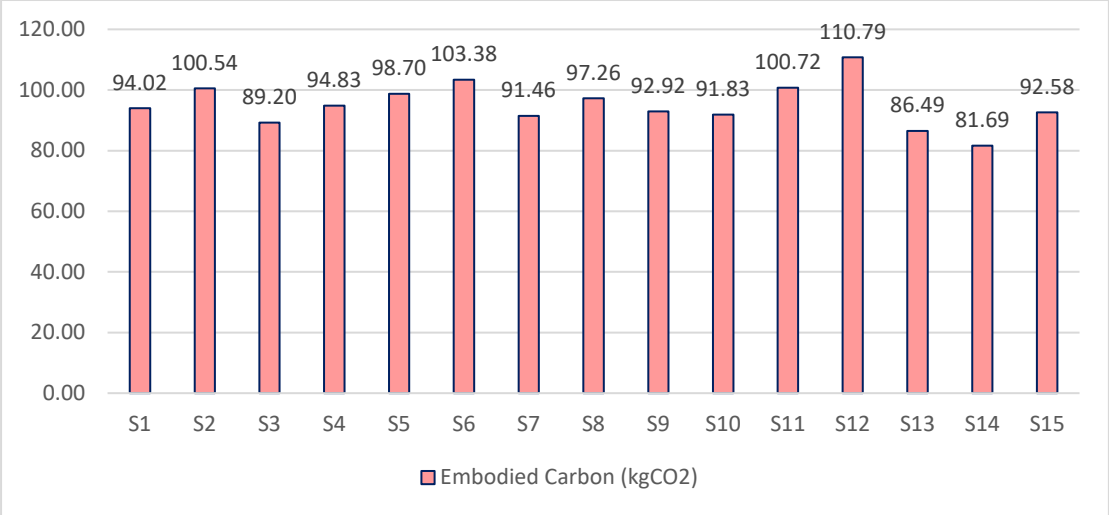

Figure (4-41) Embodied carbon emission for all slabs

From Figure (4-41), It was evident that:

Using HSNWC in slab S2 and NSNWC in slab S4 led to increase the carbon emission by 6.93% and 0.86%, respectively. While using NSLWC in slab S3 led to decrease in carbon emission by 5.13% in comparison to HSLWC in slab S1. This behavior is due to differences in the amount of materials involved in each type of concrete.

Using steel fibers in slabs S5 and S6 led to increase the carbon emission by 4.98% and 9.96% over slab S1, respectively. This behavior is because of amount of steel fiber.

Decreasing the steel reinforcement ratio from 0.28 to 0.16% in slab S7 led to reduce the carbon emission by 2.72%, while increasing the steel reinforcement ratio from 0.28% to 0.54% in slab S8 led to increase the carbon emission by 3.45%. This behavior is due to the difference in the amount of steel reinforcement to the same concrete volume.

Changing the number of ribs from 3-ribs to 2-ribs in slab S9 and to 1-rib in slab S10 led to decrease the carbon emission by 1.17% and 2.33%, respectively, due to decrease amount of shear reinforcement.

Reducing the ribs spacing from 200mm to 180mm in slab S11 and to 150mm in slab S12 led to increase the carbon emission by 7.13% and 17.84%, respectively, due to increase of concrete amount.

It is worthy to mention that reducing the ribs spacing in slab S1 to zero% (i.e., solid ratio 100%) led to increase the carbon emission by 64.37%. Converting slab type from ribbed slab S1 to solid slabs (S13, S14, and S15) led to decrease the carbon emission by 8.01%, 13.10, and 1.53%, respectively, due to omitting the temperature and shrinkage, also shear reinforcement.

The eco-strength efficiency of slab specimens can also be used to evaluate environmental impact. The eco-strength efficiency [110] can be defined as the amount of CO_2 emissions which are released to produce one unit of strength performance. It was calculated according to (P_u/CO_{2e}). From Figure (4-42), it was obvious that slab S8 gave a better performance while slab S14 gave the lowest performance.

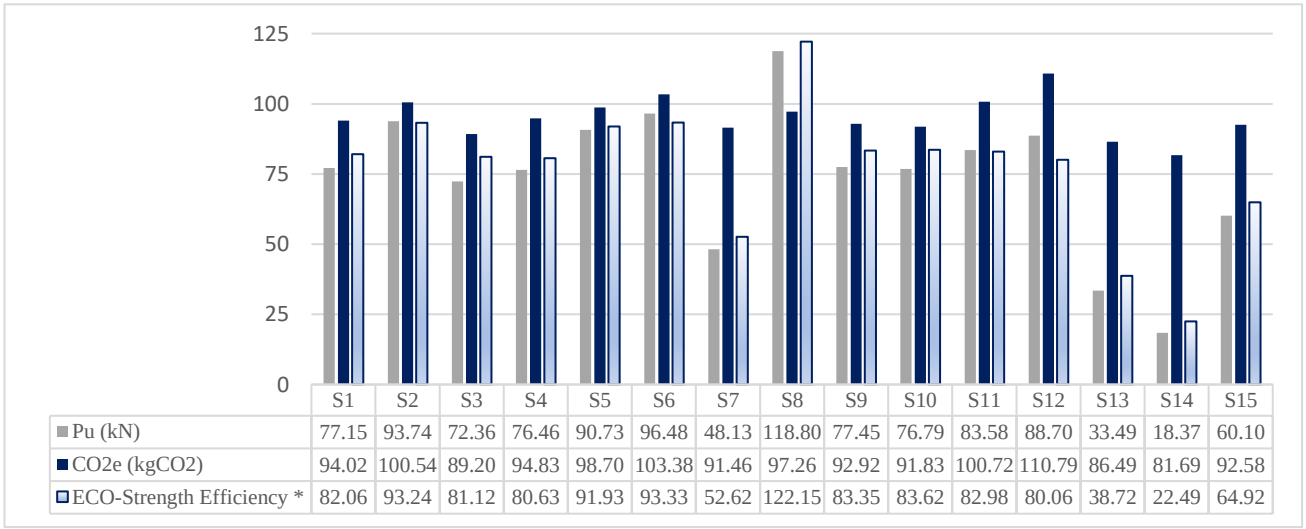

	S1	S2	S3	S4	S5	S6	S7	S8	S9	S10	S11	S12	S13	S14	S15
Pu (kN)	77.15	93.74	72.36	76.46	90.73	96.48	48.13	118.80	77.45	76.79	83.58	88.70	33.49	18.37	60.10
CO2e (kgCO2)	94.02	100.54	89.20	94.83	98.70	103.38	91.46	97.26	92.92	91.83	100.72	110.79	86.49	81.69	92.58
ECO-Strength Efficiency *	82.06	93.24	81.12	80.63	91.93	93.33	52.62	122.15	83.35	83.62	82.98	80.06	38.72	22.49	64.92

*SE values multiplied by10^{-2}.

Figure (4-42) Eco-strength efficiency of all slab specimens

4.4 Results of the Experimental Work of Slab Specimens Under Dynamic Loading

This section will discuss the second part of the experimental work, which was the dynamic behavior of tested slab specimens. As mentioned in chapter three, the harmonic loading of different frequencies was applied. Data were recorded from the laser indicator to measure the displacement amplitude and the microphone to measure the sound prssure level. Building up a computer program has been developed to modify the recorded data from the laser and microphone (remove the noise) to return the results to their original form, as shown in Figure (4-43).

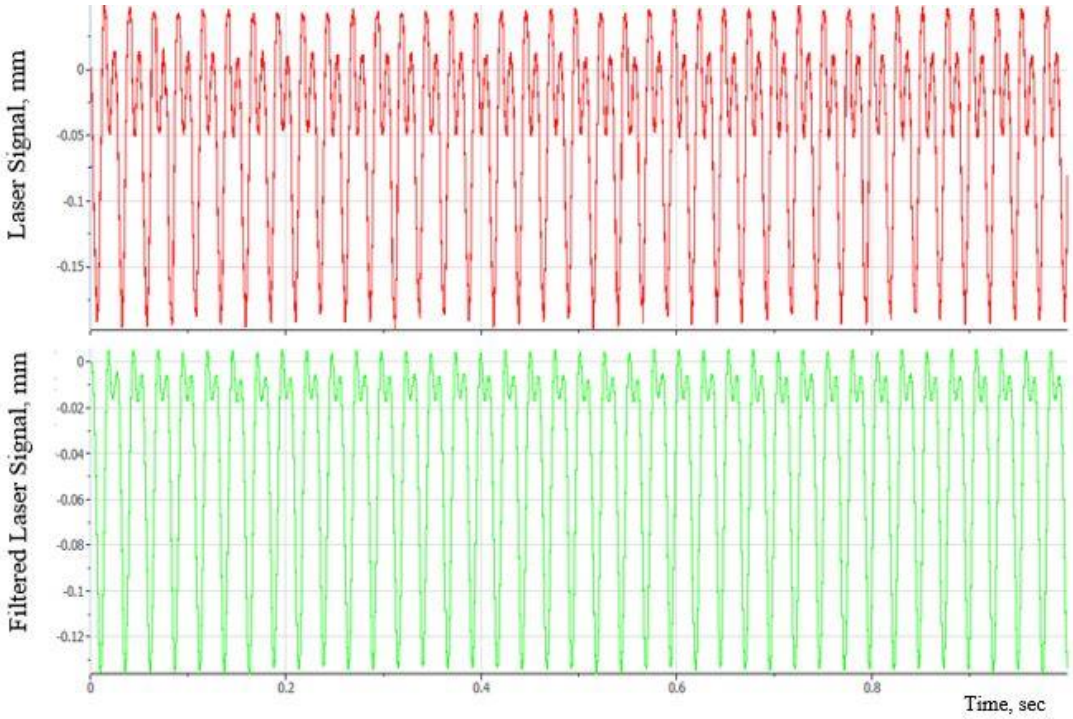

Figure (4-43) Noise removing from recorded dynamic data

4.4.1 Harmonic Load -Time History

In this investigation, the harmonic load was used as the dynamic load. In general, there are two parts to the mathematical formula for this load. The first indicates the harmonic load's amplitude ($2m_e e\ \omega_o^2$), while the second represents the sine wave ($\sin \omega_o$) term, Equation (4-7) [118].

$$P_d = 2\, m_e\, e\, \omega_o^2 \sin \omega_o t \quad \text{..... (4-7)}$$

Where:

P_d: dynamic force, N.

m_e: weight of the eccentric mass, kg.

e: eccentric distance between the center of mass and the center of rotation, m.

ω_o: operating frequency of machine, rad/sec.

A wide range of frequencies was applied on the slab specimens (0–50) Hz, step each 5 Hz, which was controlled throughout AC driver; to better understand the influence of this parameter on the response of both one–way solid and ribbed slabs. The recorded load time histories for the adopted load frequencies are shown in Figure (4-44).

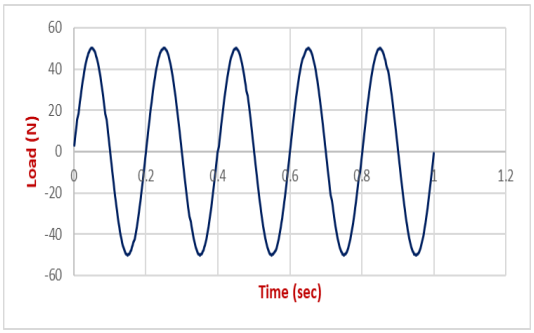

a- 5Hz

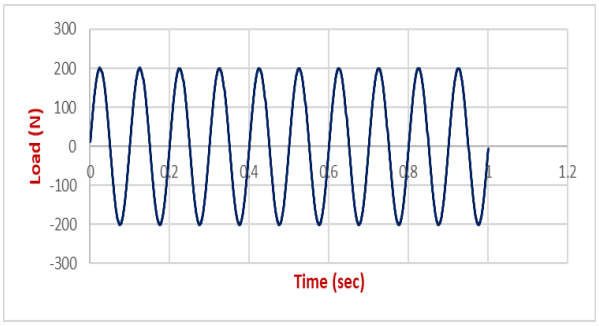

b- 10 Hz

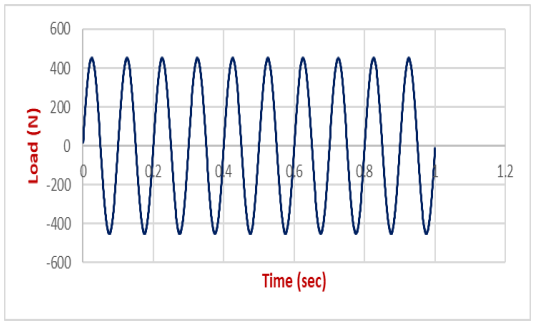

c- 15 Hz

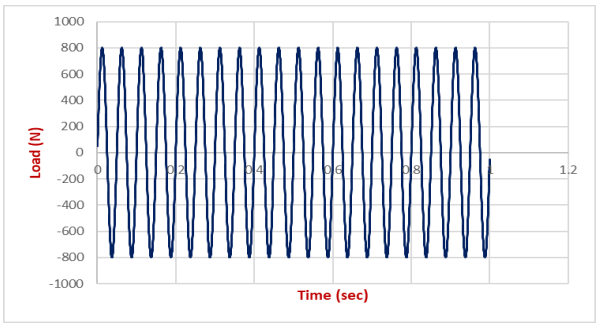

d- 20 Hz

Figure (4-44) Harmonic load- time history

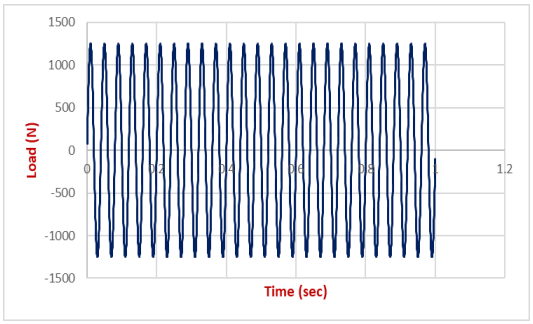

e- 25 Hz

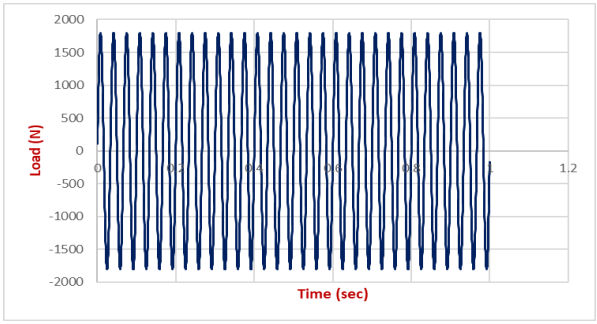

f- 30 Hz

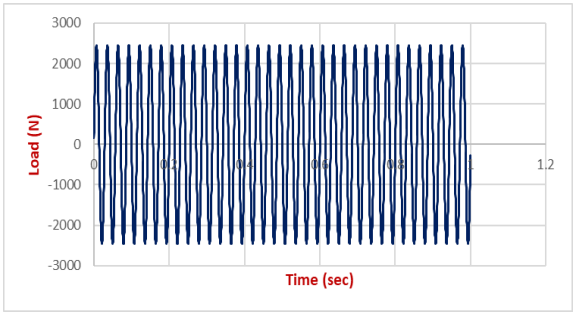

g- 35 Hz

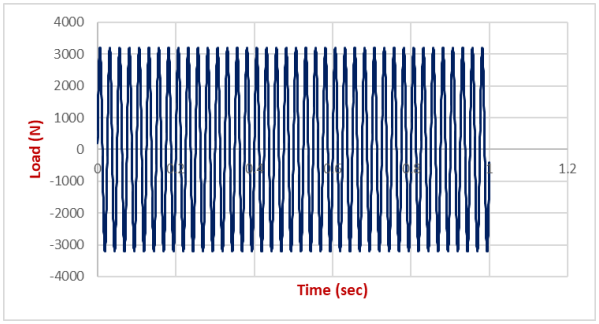

h- 40 Hz

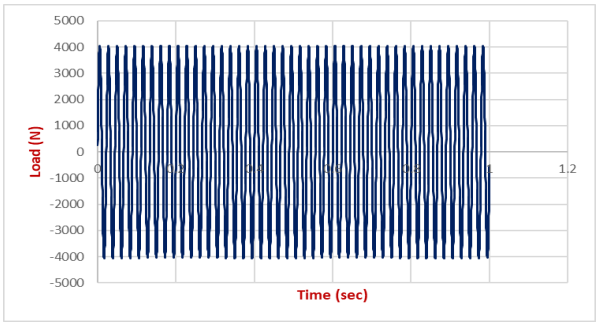

i- 45 Hz

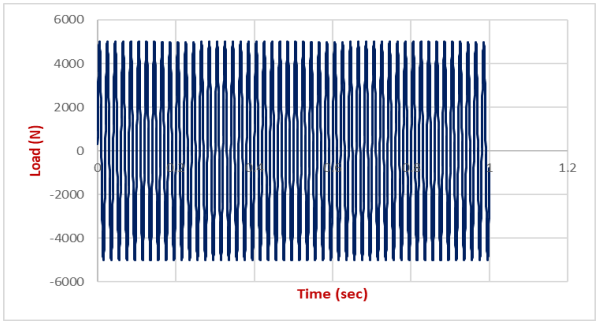

j- 50 Hz

Figure (4-44) Continued

4.4.2 Behavior of Displacement Amplitude

The displacement amplitude and displacement-time history as sine wave for all the adopted frequencies (0-50) Hz are shown in Figure (4-45) and Figure (4-46), respectively. The recorded displacement amplitude differed from one specimen to another, especially between the ribbed slabs and the solid ones, depending on the mass, stiffness, and damping characteristics of the specimen. From these figures, it was found that: Using of LWA (pumice stone) in HSLWC one–way ribbed slab specimen HS1 instead of NWA (gravel) in HSNWC in slab HS2 led to reduce the

displacement amplitude by about (0.55-30.11) % due to the nature of LWA, which has pores led to dissipate the vibration energy. On the other hand, using HSNWC in slab HS2 instead of NSNWS in HS3 led to increase the displacement amplitude of the slab by about (7.72-160.98) %. This could be due to the HSNWC's mass and it has denser composition and higher bonding strength between the aggregate and mortar, which results in the slab dissipating less energy.

The inclusion of steel fibers at a volume fraction equal to 0.25% led to improve displacement behavior of slab HS4 in comparison to a slab without steel fiber HS1 of about (0.81-34.19) %. This behavior is due to the stiffness improvement of the steel fiber HSLWC slab.

Changing the section geometry of one–way ribbed slab at the same volume of concrete by using one–rib in HS5 led to decrease the displacement amplitude in comparison to slab specimen HS1. The range of reduction in amplitude was (32.35-80.56) %. This behavior due to larger spacing between the rib led to the dissipation of the internal vibration.

Using HSLWC ribbed slab HS1 instead of HSLWC solid slab HS6 led to decrease the displacement amplitude by (8.42-60.44) % for all ranges of frequencies (5 to 50) Hz. This behavior belongs to the reduction in slab thickness of solid slab that reflects the stiffness of the slab.

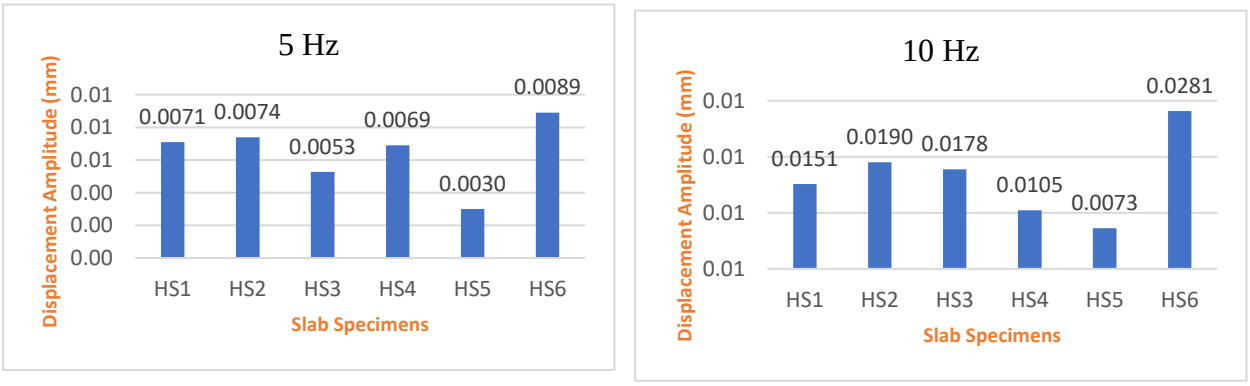

Figure (4-45) Amplitude displacement of tested slabs

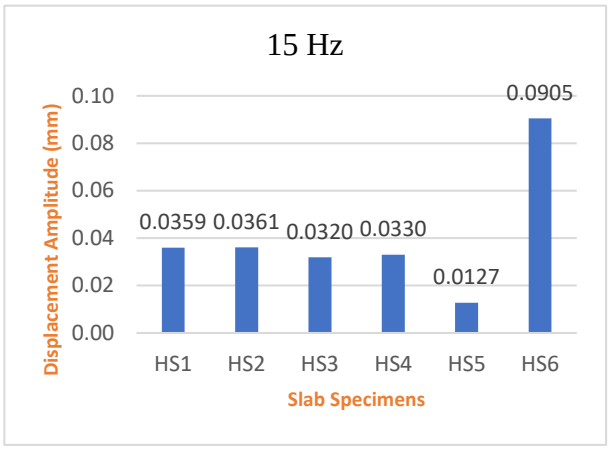

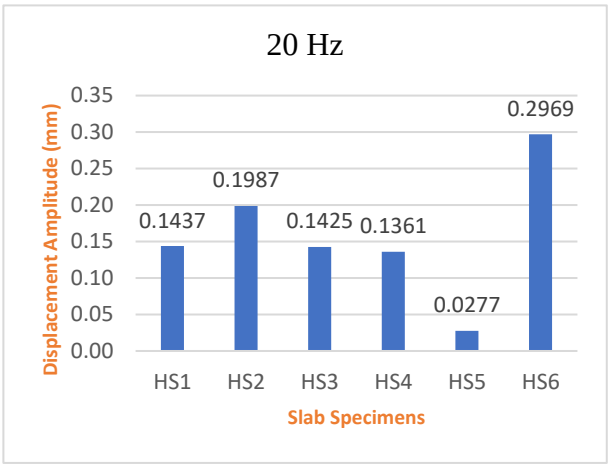

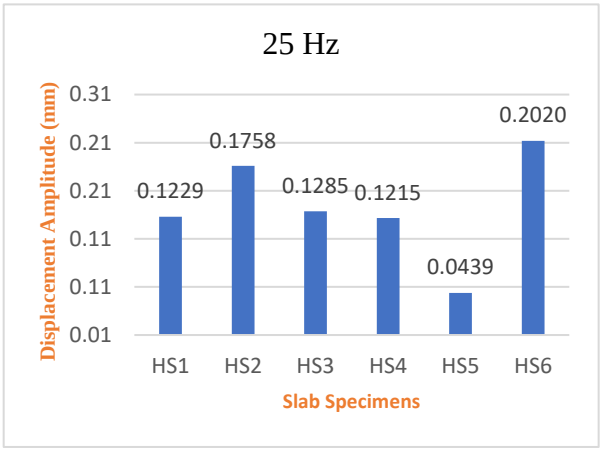

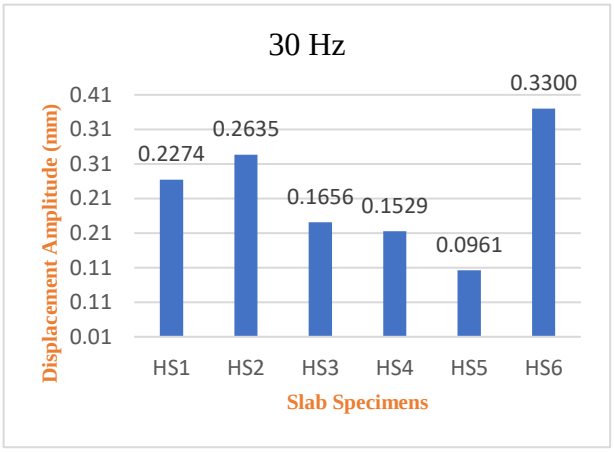

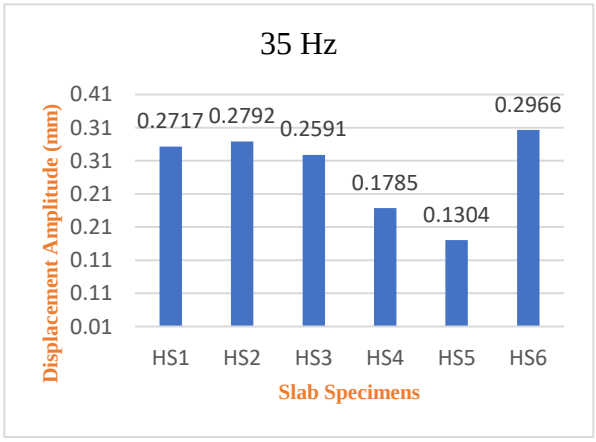

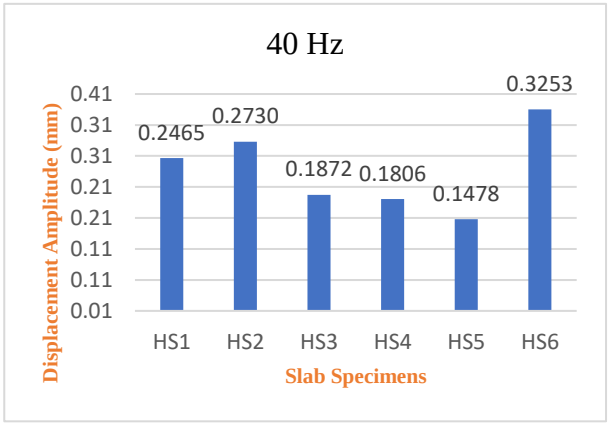

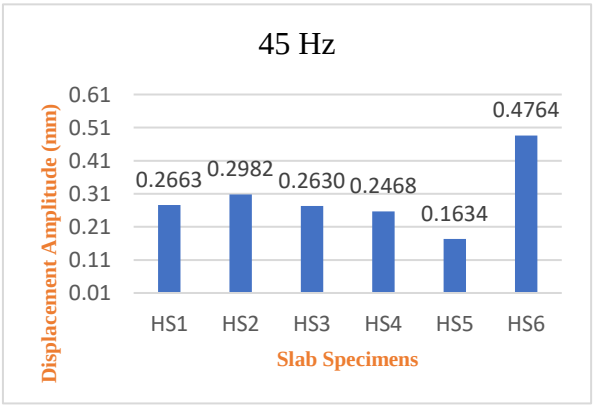

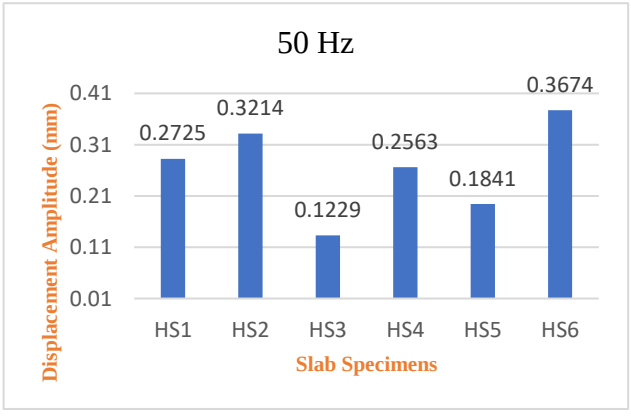

Figure (4-45) Continued

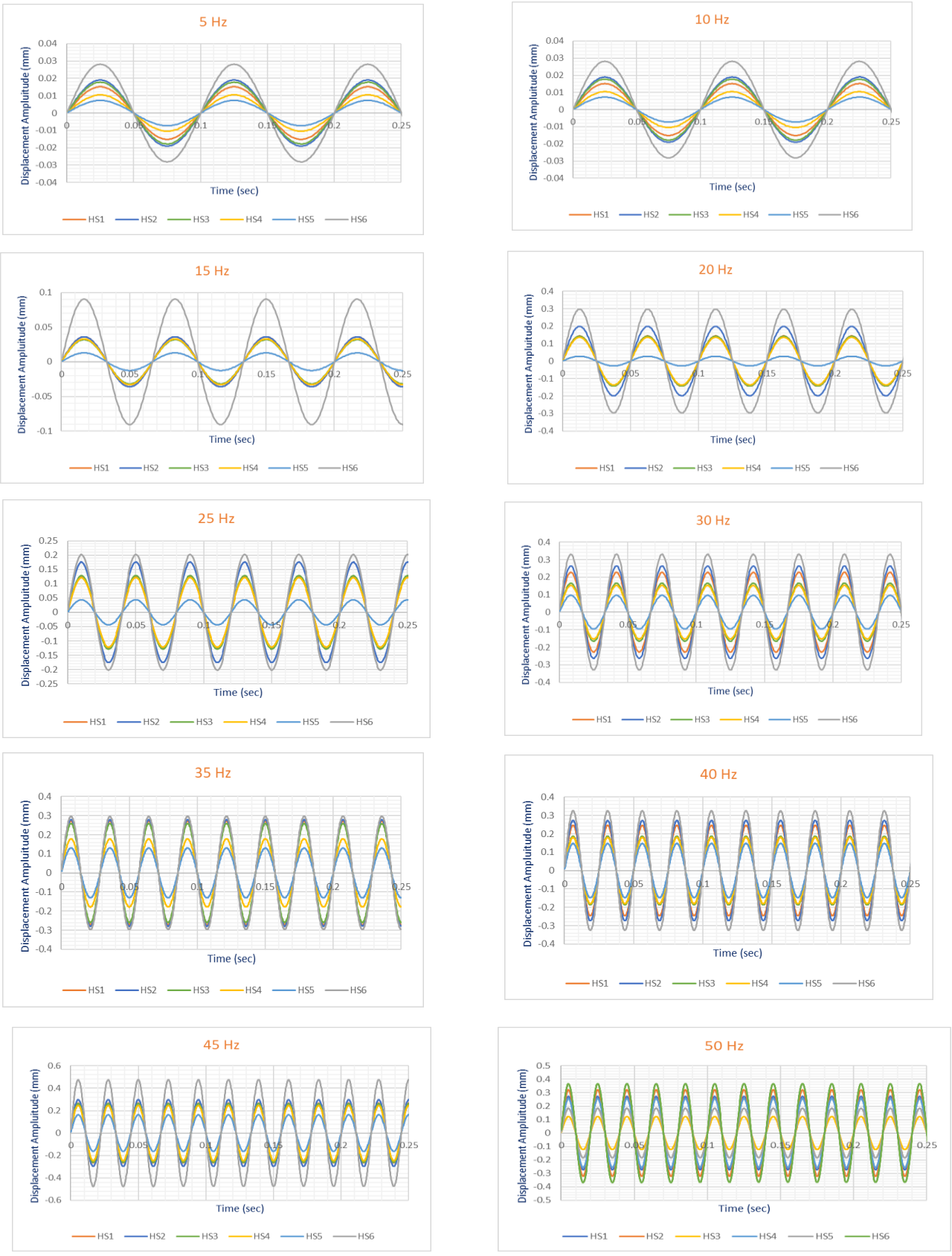

Figure (4-46) Displacement-time history for tested slabs under dynamic load

The hairline cracks were not initiated in one–way ribbed slab specimens with HSNWC and F0.25HSLWC, as shown in Plate (4-2). This may be because the small amount of the load applied.

Plate (4-2) Cracks pattern for slabs under harmonic loading

Plate (4-2) Continued

4.4.3 Sound level-Time History

This study included fixing sensitive microphone close to the point of contact between the electric motor and the surface of the slab specimen, On the other hand, a specialized software program for analysis of the sonic wave has been utilized to find sound pressure level. Sound level behavior for all tested slab specimens under dynamic load, also, the

sound levels–time history at highest operating frequency 50Hz were illustrated in Figure (4-47) and Figure (4-48). It can be seen that the one-rib in slab HS5 gave the lowest sound level while solid slab HS6 gave the highest sound–pressure level. The sound pressure increased by 2.77%, 0.70%, and 5.23% in slab HS2, HS4, and HS6 over slab HS1, respectively. Moreover, the sound pressure level decreased in HS3 and HS5 over slab HS1 by 2.91% and 8.24%, respectively.

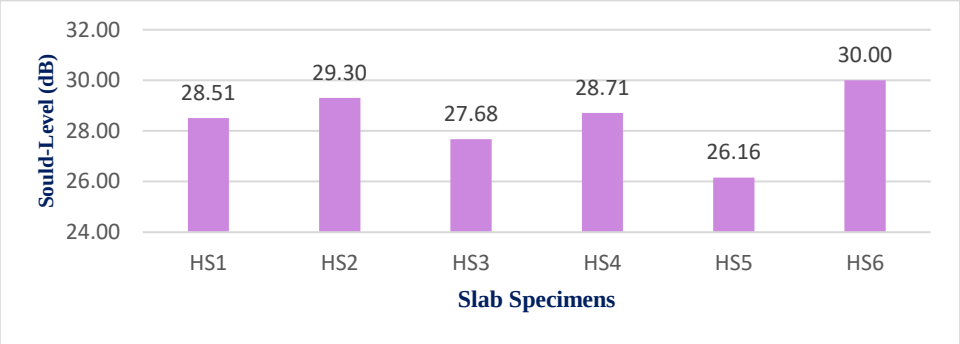

Figure (4-47) Sound level behavior for tested slab specimens

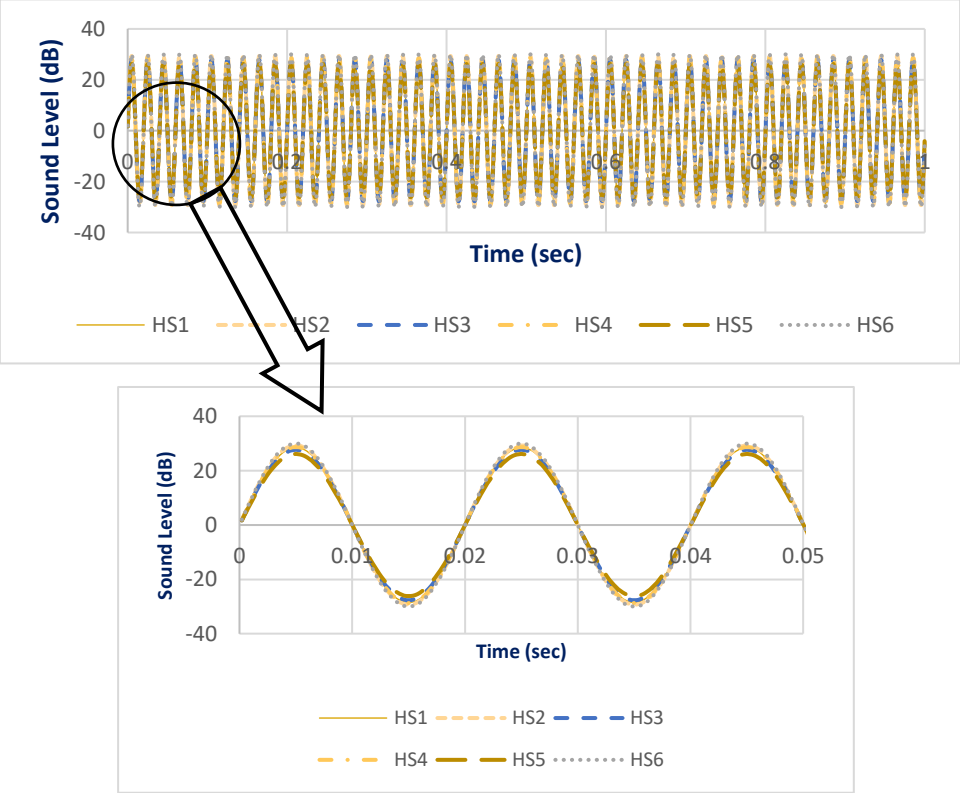

Figure (4-48) Sound level -time history for tested slab specimens

Chapter Five

Finite Element Analysis

Chapter Five: Finite Element Analysis

5.1 General

This chapter discusses the outcomes of numerical work. Also, the comparison is presented between the results of the experimental work and the results from the finite element analysis (FEA) method.

Six variables were considered, including the effects of concrete type, inclusion of steel fibers, steel reinforcement ratio, the geometry of section, ribs spacing, and slab type under static load. While, under dynamic load, all the above-mentioned variables were considered except the steel reinforcement ratio.

Abaqus/Standard 3D Experience R2019x, which is an advanced 3D finite element computer program was adopted to perform a nonlinear FEA to analyze the behavior of one-way ribbed and solid slabs that was conducted experimentally in the current study.

5.2 Modeling of Reinforced Concrete Slabs

This section presents detailed data about the simulation of the geometry as well as the boundary conditions of the supporting and loading conditions of the slab models that were tested.

5.2.1Parts and Assembly

Generally, seven parts were involved in modeling the one-way ribbed slabs. Those parts were concrete slab, reinforcement of the ribs, mesh square steel reinforcement of flange, reinforcement of stirrups, and bearing plates for the load and support. While modeling of solid slabs involved five parts. Those parts were concrete slab, bottom reinforcement in the long direction, bottom reinforcement in the short direction, and bearing plates for the load and support.

Each one of those parts was firstly drawn, and then different parts were assembled and merged to produce the modeling slab specimens. Figure (5-1) shows the modeling of the ribbed and solid slabs that tested under the effects of two-point loading. Moreover, the details of modeling the steel reinforcement are presented in Figure (5-2). The numerical model was meshed by choosing the suitable number of elements (53335) according to the convergence study. The ABAQUS/Standard default solution parameters are intended to give a reasonable optimal solution of complicated problems including multiple nonlinearities, as well as an efficient solution of simpler nonlinear instances.

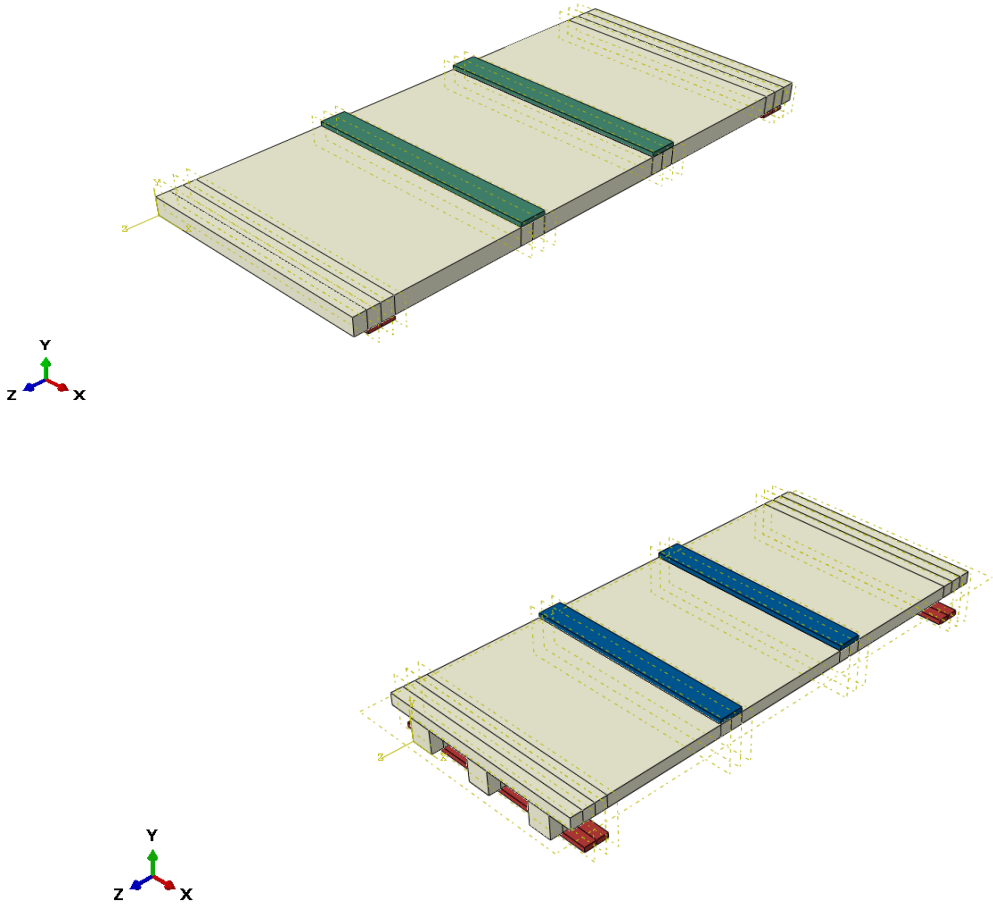

(a) One-way ribbed slab

(b) One-way solid slab

Figure (5-1) Modeling of slabs under two-point loading

Solid brick elements were used in meshing the ribbed concrete slabs, solid concrete slabs, and steel plates in order to achieve a proper stress distribution in a 3D finite element analysis. The ABAQUS program includes a variety of solid brick elements for meshing.

Linear hexahedral elements (C3D8)[119], [120] that is an 8-node linear brick were selected for meshing ribbed slabs, solid slabs, and steel plates. Also, a two-node linear 3D truss (T3D2) [119], [120]was adopted for meshing steel rebar for ribs reinforcement, shear reinforcement, the square mesh of flange reinforcement, and both longitudinal and transverse reinforcement bars of solid slabs.

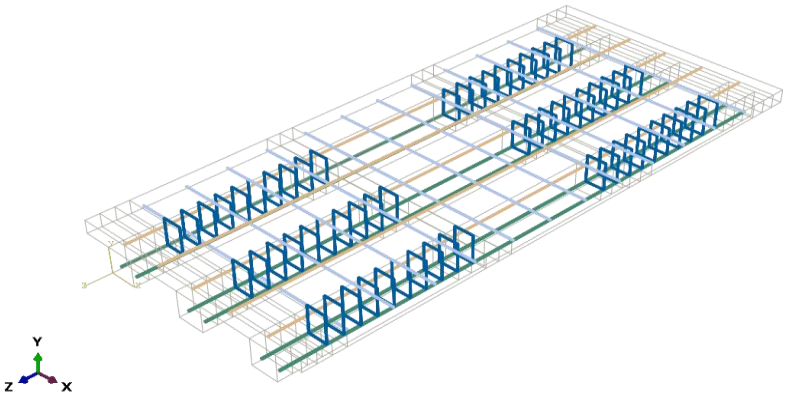

(a) One-way ribbed slab

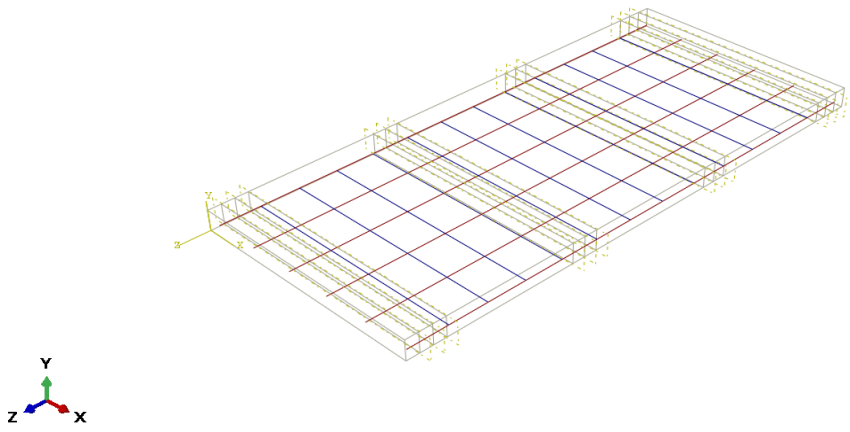

(b) One-way solid slab

Figure (5-2) Details of modeling steel reinforcement

5.2.2 Convergence Study

In order to determine the best mesh density (i.e., number of elements), selecting a suitable mesh size is an important step in finite element modeling. One-way slab models were subjected to a convergence analysis in order to obtain an appropriate mesh size by dividing one-way slab models into an appropriate number of elements. When the reduction in mesh size (increment in the number of elements) has no effect on the results, the results have reached a suitable convergence.

The convergence study was performed for one-way slab models by evaluating the effects of reducing the number of elements from (9393 to 162548) on the ultimate loading capacity. As could be noticed in Figure (5-3) and Figure (5-4), an increasing number of the elements from 53335 to 162548 led to negligible effects on the load-carrying capacity and deflection. In addition, selecting a number of an element equal to 53335 was adopted in this study because it led to more compatible ultimate load in comparison with the experimental outcomes.

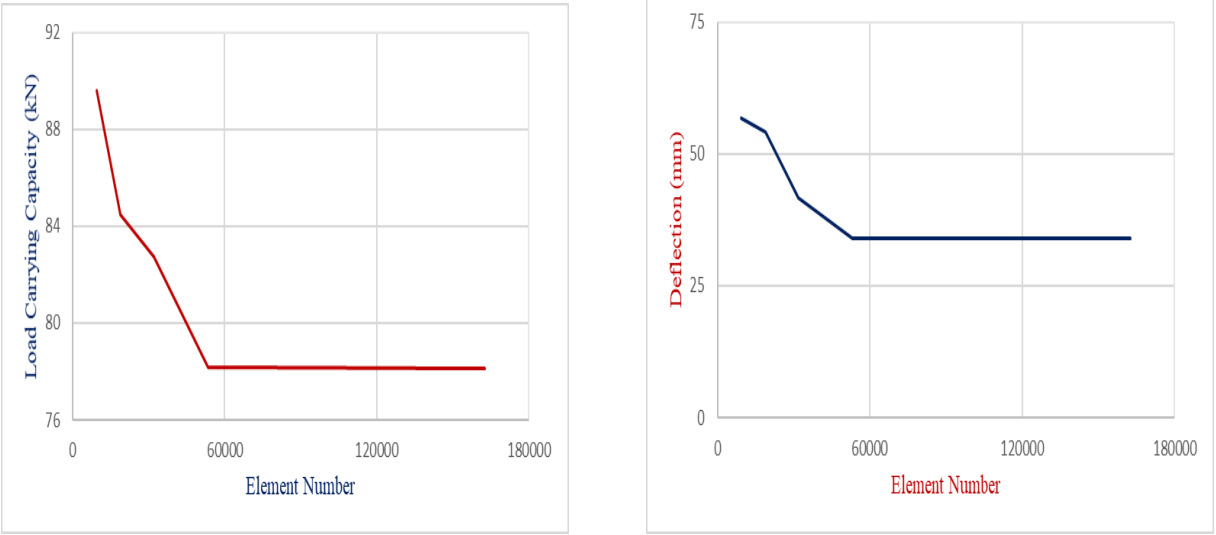

(a) Load convergence **(b)** Deflection convergence

Figure (5-3) The convergence study

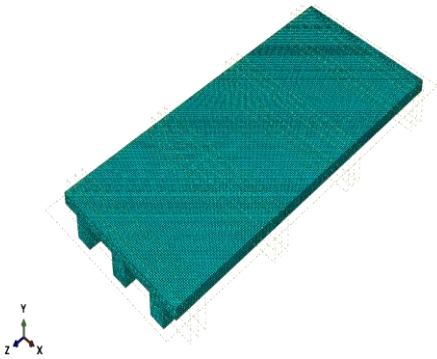

(a) Elements number (162548)

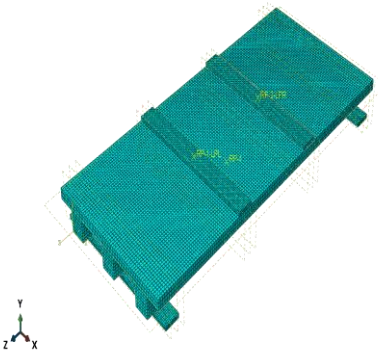

(b) Elements number (53335)

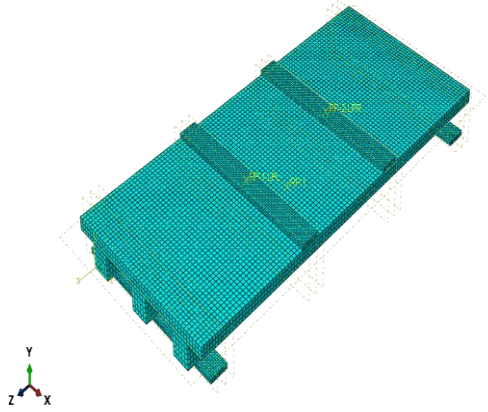

(c) Elements number (31924)

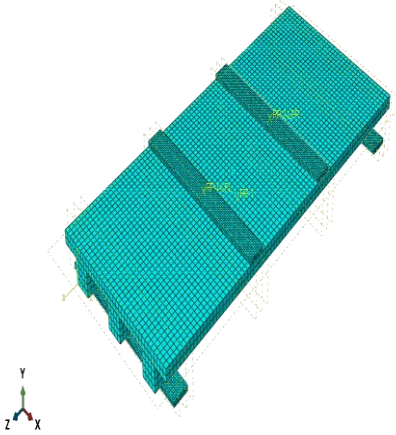

(d) Elements number (18906)

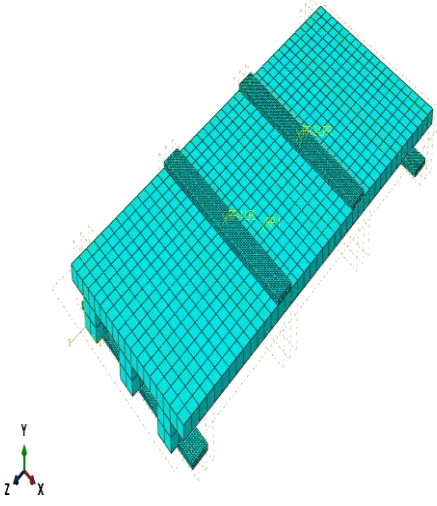

(e) Elements number (9393)

Figure (5-4) Finite element mesh density

5.2.3 Modeling of Materials

The material specifications data in the ABAQUS program are input in stages based on the material's behavior, with the first stage being elasticity and the second being plasticity. In this study, the elastic stage Poisson ratio and the material's elasticity modulus are used. ABAQUS presents many plasticity models based on the material behavior following the elastic stage. As explained in the following paragraphs, the concrete damaged plasticity model is employed for concrete and plastic for reinforced bars in this study. To imitate the plates used at supports or loading points, just an elastic stage is used.

5.2.3.1 Modeling of Concrete

ABAQUS provides three models (smeared cracking, brittle cracking, and concrete damaged plasticity (CDP))[121] to represent concrete material under low confining pressures following the elastic stage. In this study, CDP is used as a material model for HSLWC, HSNWC, NSLWC, NSNWC, and Fibers HSLWC. Since it can be found in ABAQUS/Standard and ABAQUS/Explicit and is suited for evaluating the response of all concrete structures and other quasi-brittle materials under static, cyclic, and dynamic load.

Compressive crushing and tensile cracking are the two failure mechanisms assumed by the CDP model. This model also accounts for material stiffness loss and the influence of stiffness recovery under cyclic load. Damage plasticity is used to identify concrete phenomena in compression and tension using the CDP model.

- **Compression Behavior**

Figure (5-5b) depicts the compressive behavior of concrete under uniaxial compressive load. The stress-strain relationship in this figure can

be divided into three stages: the first is a linear-elastic relationship up to yield stress (σ_{co}), the second is stress hardening until the ultimate compressive stress value (σ_{cu}), and the third stage is strain hardening. The damage parameters d_t (at tension) and d_c (at compression), These functions of strains in the plastic stage and temperature are used in the CDP model to account for degradation in concrete stiffness at elastic. These variables shift from 0 to 1, with 0 denoting an undamaged material and 1 denoting that it has been damaged. The flowing equations were used to calculate the damage parameters [122]:

$$d_t = 1 - \frac{\sigma_t}{\sigma_{tu}} \quad \text{(5-1)}$$

$$d_c = 1 - \frac{\sigma_c}{\sigma_{cu}} \quad \text{(5-2)}$$

Figure (5-5b) demonstrates a standard stress-strain relation of uniaxial concrete compression in the finite element model.

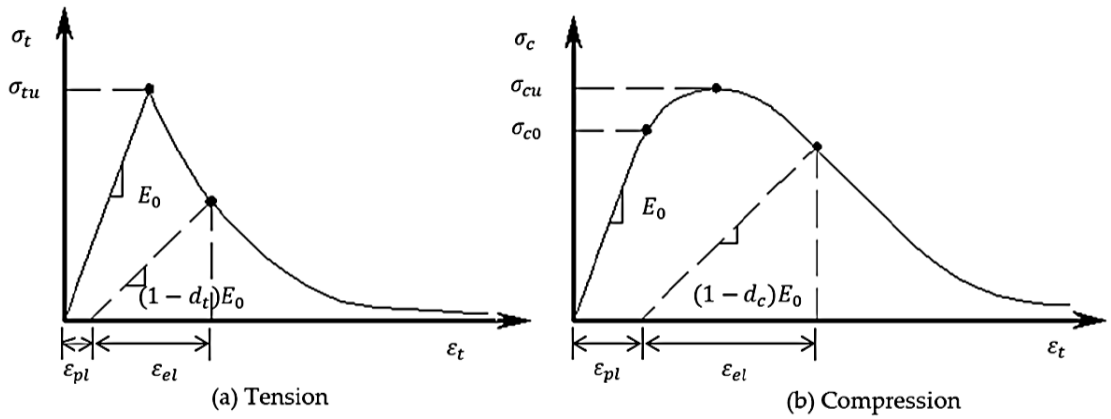

Figure (5-5) Concrete response to uniaxial loading based on manual of the ABAQUS theory [119]

In the current study, the concrete in compression was modeled with Hognestad parabola [123]. Under uniaxial compressive loading, the expected stress-strain relationship behavior of the concrete can be split into three domains. The linear-elastic branch is represented by the first one. The stress level is σ_{co} when the linear branch comes to an end

that was taken here as $\sigma_{co} = 0.4f_c'$ for HSC and $\sigma_{co} = 0.3f_c'$ for NSC. The second part discusses the rising branch of the uniaxial stress-strain relationship when compression loading is applied to the peak load at the corresponding strain level $\varepsilon_o = \frac{2f_c'}{E_c}$. Table (5-1) shows the values of E_c, for all concrete that used in this study which was calculated using Equation (5-4) for HSNWC [3], Equation (5-5) for LWC [18], Equation (5-6) for NSNWC [18], and Equation (5-7) [124] for fiber concrete. The final segment of this stress-strain curve, beginning with the peak stress and ending with the strain $\varepsilon_c < 0.01$ that is referred to as the post-peak part. The assumed compressive stress-strain curve's equation is given in Equation (5-3). Figure (5-6) represents the compressive stress-strain curves for all concrete.

$$\sigma_c = f_c' \left[2\left(\frac{\varepsilon_c}{\varepsilon_o}\right) - \left(\frac{\varepsilon_c}{\varepsilon_o}\right)^2\right] \quad \text{.....(5-3)}$$

$$E_c = 3320\sqrt{f_c'} + 6900 \quad \text{.....(5-4)}$$

$$E_c = 0.043\, w_c^{1.5}\sqrt{f_c'} \quad \text{.....(5-5)}$$

$$E_c = 4700\sqrt{f_c'} \quad \text{.....(5-6)}$$

$$E_c = E_f V_f + \left(1 - V_f\right)E_m \quad \text{.....(5-7)}$$

Where:

f_c' is concrete cylinder compressive strength, taken from Table (4-1).

w_c is the density of concrete, taken from Table (4-5).

V_f is the volume fraction ratio of fiber, %.

E_f is the elastic modulus of fiber equal to 200000MPa.

E_m is modulus elasticity of HSLWC equal to 23924 MPa.

Table (5-1): Calculated values of E_c

Elasticity Modulus	NSNWC	NSLWC	HSNWC	HSLWC	F0.25 HSLWC	F0.50 HSLWC
E_c (MPa)	27405	17558	32184	23924	24364	24804

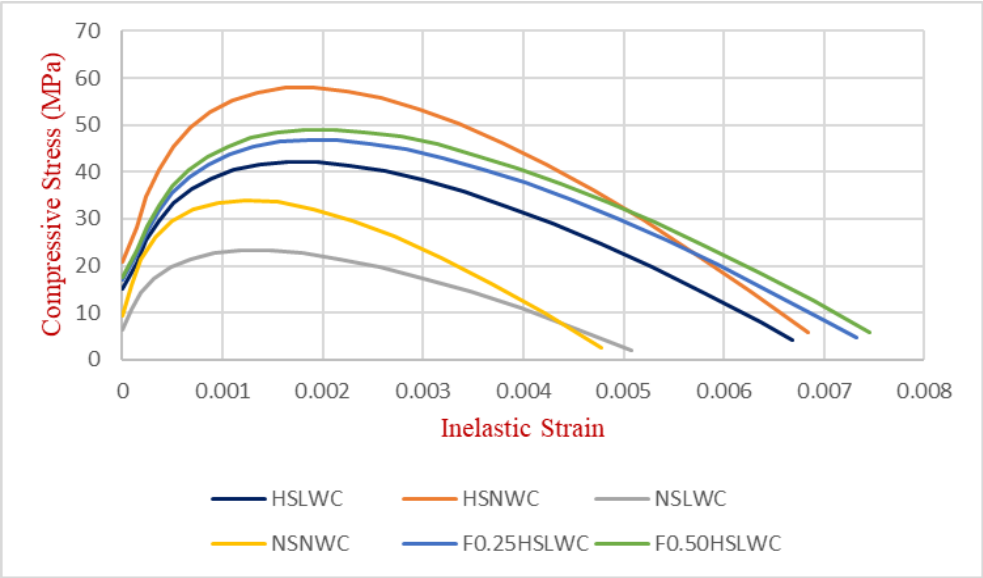

Figure (5-6) Compressive stress-inelastic strain curves

Damage parameter in terms of the compression (d_c) of concrete damaged plasticity model was introduced for all concrete types according to Figure (5-7), the values of d_c were calculated according to Equation (5-2).

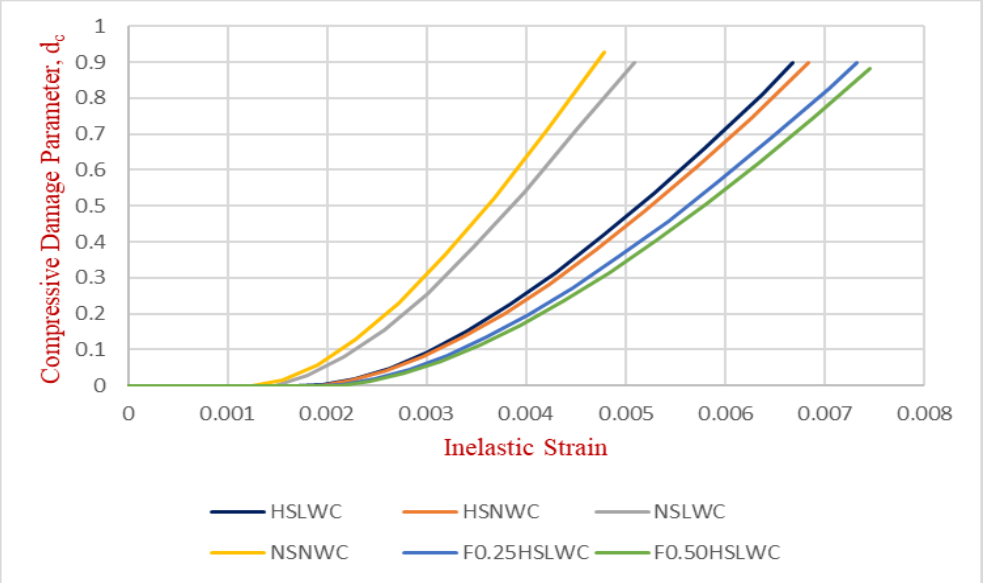

Figure (5-7) Compressive damage parameter-strain relationship for all concrete types

- **Tensile Behavior**

The stress-strain relation, the stress-displacement relation, and the fracture energy (G_f) [120] approaches are all included in ABAQUS for defining tension softening behavior.

In the present study, the stress-strain relationship of concrete in tension was modeled by using a relation that suggested by Wang and Hsu [125] and modified by Kmiecik and Kaminski [126], consisting of two parts. The first one, the curve linearly increases up to the point of cracking failure (f_{cr}), is taken from Table (4-2). Afterward, the second part is the curve gradually descends and follows a parabola shape. This behavior is expressed as follows:

$$\varepsilon_{cr} = f_{cr}/E_c \quad \text{.....(5-8)}$$

$$f_t = E_c.\varepsilon_t \quad \text{for} \quad \varepsilon_{t<}\varepsilon_{cr} \text{ .....(5-9)}$$

$$f_t = f_{cr}(\frac{\varepsilon_{cr}}{\varepsilon_t})^n \quad \text{for } \varepsilon_t > \varepsilon_{cr} \text{ ..... (5-10)}$$

Where:

n: Rate of weakening, this study calibrated the n values at (0.6 for non-fiber concrete and 0.4 for fiber HSLWC). Figure (5-8) shows the theoretical stress-strain behavior for concrete in tension.

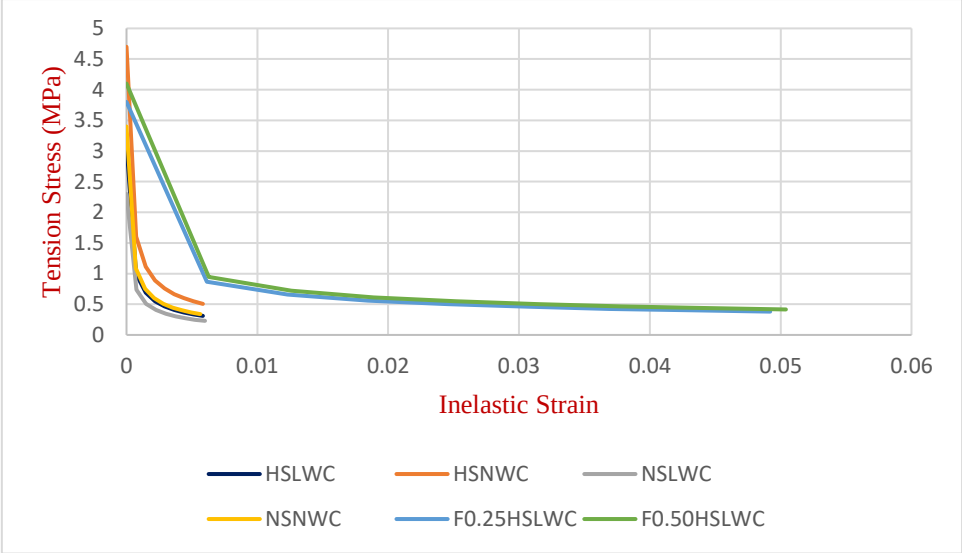

Figure (5-8) Tension stress-inelastic strain curves

Damage parameter in terms of tension (d_t) of concrete damaged plasticity model was introduced for all concrete types according to Figure (5-9), the values of d_t were calculated according to Equation (5-1).

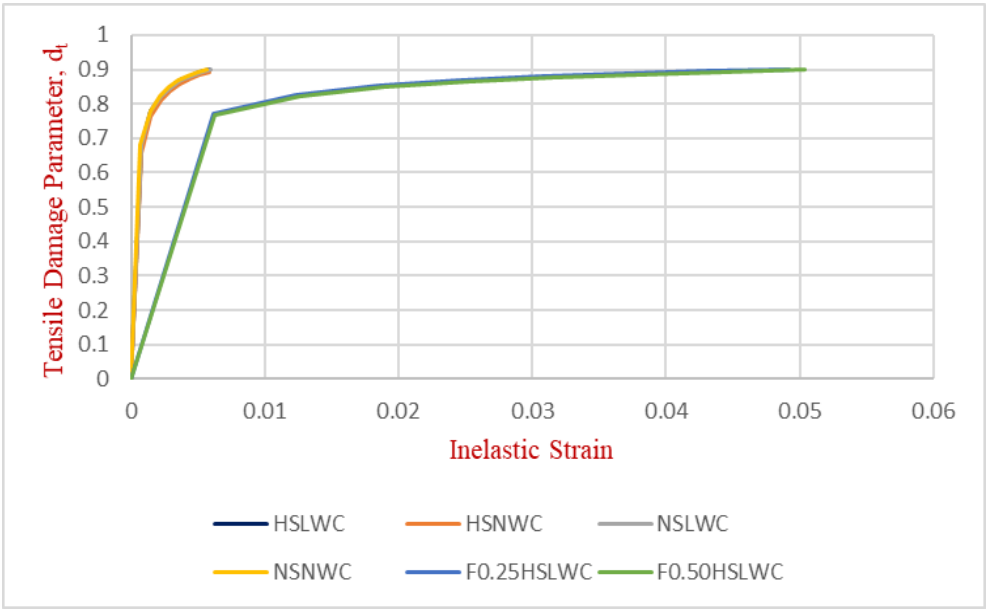

Figure (5-9) Tension damage parameter-strain relationship for all concrete types

- **Plasticity Parameters**

In ABAQUS, the following plasticity parameters are necessary for the CDP model:

1- Dilation angle (ψ) is one of the ABAQUS parameters that must be set, defined as the inclination angle of the potential plastic function. The allowed value of ψ varies from 0º to 56º in ABAQUS [126]. This study calibrated the ψ that was equal to (34º for HSLWC, 40 º for (HSNWC and fiber HSLWC), 25º for NSLWC, and 28º for NSNWC) throughout many trials.

2- ($\frac{\sigma_{bo}}{\sigma_{co}}$) is the ratio of (the initial uniaxial compressive to the initial biaxial compressive) of yield stress [125]. This study determined this ratio to be equal to 1.16.

3- The eccentricity of flow potential (ϵ), This study found the suitable value of ϵ was equal to 0.1 (default value) [127].

4- A viscosity parameter that defines the visco-plastic regularization, 0, is the default value[127], 10^{-6}, a viscosity parameter was depended on in this study.

5- (K_c) is utilized to characterize the multi-axial concrete behavior. It represents the ratio between the second stress invariant of the tensile meridian and the compressive meridian. The values of K_c ranges between (0.5-1), in this study the value of K_c was equal to 0.667 (default value) [125].

5.2.3.2 Modeling of Steel Reinforcement bars

Elastic and plastic behavior characteristics must be entered to describe steel bars. The Poisson ratio (ν) and young's modulus of steel bar (E_s) for the elastic stage were calculated using usual values (0.3) and

200000 MPa, respectively. The yield and ultimate stresses, as well as the accompanying strains from the experimental test, were utilized to model the plastic properties (bilinear behavior) of the steel bar.

5.2.3.3 Supporting plates and loading plates

Only the elastic stage is utilized to define the behavior of supporting and loading plates. The input parameters needed for steel plates included of E_s (200 GPa) and ν (0.3).

5.2.4 Interaction

Following the step of assembly, parts including concrete slab, steel reinforcement, and steel bearing plates were interacted together using different constraints types based on the experimental observations to produce a successive composite system. In this study, embedded region constrain was used between the steel reinforcement and the surrounding concrete model, as shown in Figure (5-10a). Furthermore, a tie constraint was chosen to connect the concrete slab and the bearing steel plates (loading and support plates), as shown in Figure (5-10b).

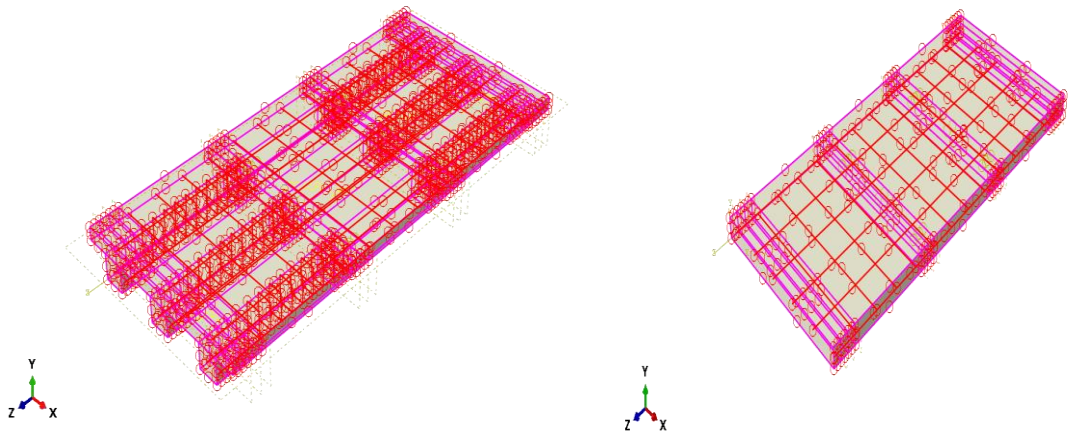

(a) Embedded region constraint for ribbed and solid slabs

Figure (5-10) Constraints types adopted in this study

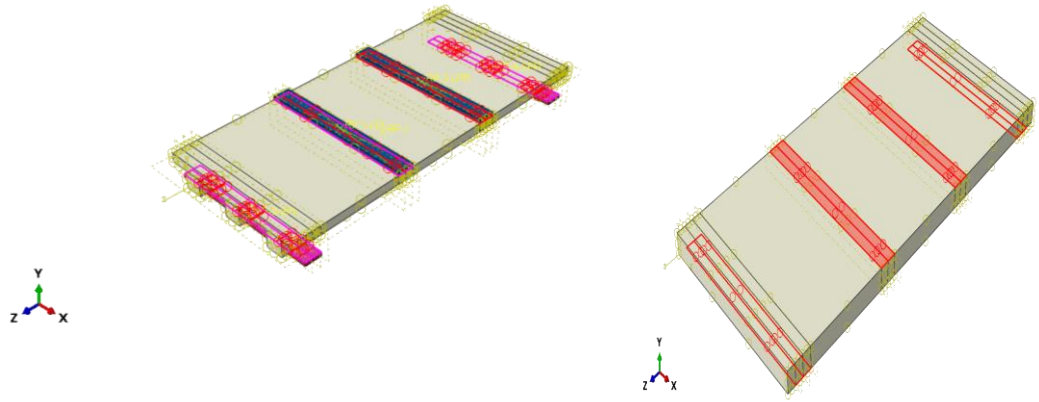

(b) Tie constraint of loading and support plates for ribbed and solid slabs

Figure (5-10) Continued

5.2.5 Boundary Condition

Boundary conditions were carefully defined to simulate the setup of the experimental program. Simply supported conditions were assigned at the bottom surface of the steel plates that were attached to the bottom of the external surface of the concrete slab using tie constrain.

The boundary condition was created as a roller and a hinge end, as presented in Figure (5-11). Rotation is free at the steel base plate for both ends, but movements along the x, y, and z-axis are restrained for right-end hinge support. However, the left-end roller support is only restrained in the x and y-axis, thus free to move in the z-direction. The hinge and roller support were placed at a distance of 100 mm from the slab's edges to simulate the finite element model behavior closest to the experimental results.

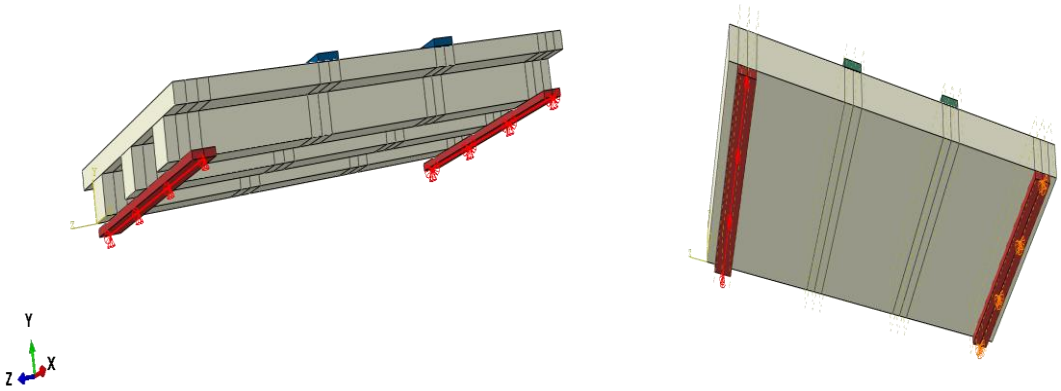

(a) One-way ribbed slab **(b)** One-way solid slab

Figure (5-11) Details of boundary conditions of supports

5.2.6 Loading

This study considered two types of load; the first is a static load (two-point loading). The load is applied as the uniform concentrated load applied on the reference points which is located at the center of both loading plates. These points transfer the loads uniformly on the loading plate through tie coupling constrain surface, as shown in Figure (5-12a). On the other hand, the second is a dynamic load (harmonic load), which is represented in ABAQUS, applied on the mid surface of the slab to simulate the experimental conditions of load application, as shown in Figure (5-12b).

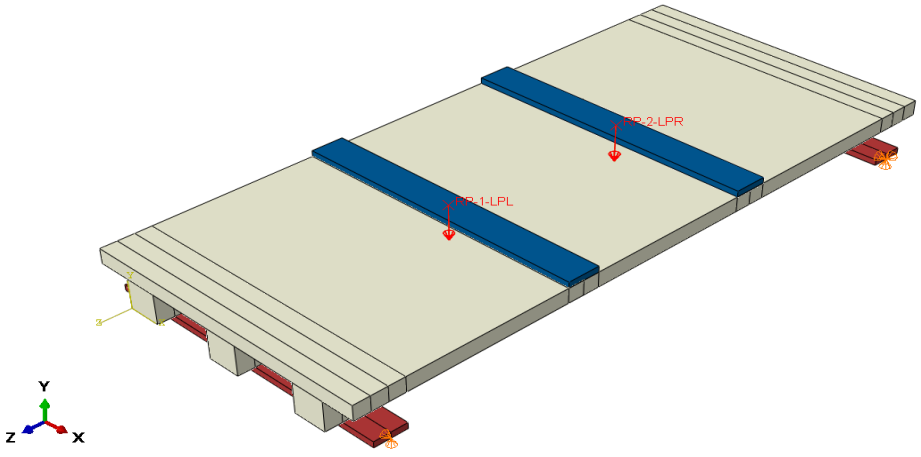

(a) Static load (two-point load)

Figure (5-12) The applied load on the specimens

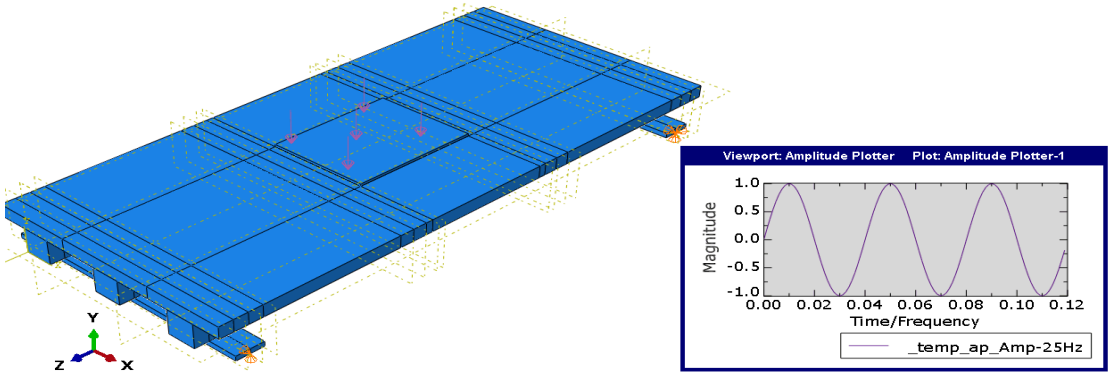

(b) Dynamic load (harmonic load)

Figure (5-12) Continued

5.2.7 Type of Analysis

The general static step analysis was selected to apply two-point loading to analyze the static effect. In contrast, the implicit step analysis was selected to apply harmonic loading to analyze the dynamic effect.

5.3 Comparison Study Between the Results of the Experimental and FEM Analysis Under Static Load

This section offers a comparative study between the outcomes of the experimental investigation and the results of nonlinear FEM analysis. The nonlinear FEA method was conducted for all slab models by considering the types of concrete (HSLWC, HSNWC, NSLWC, and NSNWC), steel reinforcement ratios, the inclusion of steel fiber, characteristics of different geometry of sections, ribs spacing, and types of the one-way slab.

The structural behavior of one-way slab models that achieved from the nonlinear FEA method showed comparable agreement with the structural performance obtained from the experimental program. The comparison study includes the ultimate load level, the deflection at the ultimate load, and the load-deflection curves.

5.3.1 Ultimate Load and Deflection Under Static Load

The comparison between the outcomes of the FEA method and the results of the experimental study showed an acceptable agreement regarding the ultimate loading capacity and the corresponding deflection slabs under static load (two-point loading). As illustrated in Table (5-2), the ultimate load that was conducted from the FEA method was higher than the experimental data by about 0.03% to 21.01% in specimens (S3, S4, S8, S9, S10, S13, and S14). While it is lower the experimental data by about 0.10% to 9.49% in specimens (S1, S2, S5, S6, S7, S11, S12, and S15).

Conversely, the deflection at the ultimate load from the numerical study was lower than that of the experimental study by about 1.38% to 14.52%, except for specimens (S2, S6, S7, S8, S11, S12, S13, and S15) that had a higher value by about 1.93% to 11.67%.

Table (5-2): Experimental and numerical results for tested slabs

Slab Symbol	P_u Exp (kN)	P_u FEM (kN)	$\frac{P_u\ FEM}{P_u\ Exp}$	δ_u Exp (mm)	δ_u FEM (mm)	$\frac{\delta_u FEM}{\delta_u Exp}$
S1	77.15	77.07	0.999	40.92	34.98	0.85
S2	93.74	84.84	0.91	49.5	53.57	1.08
S3	72.36	74.88	1.03	43.00	40.83	0.95
S4	76.46	79.04	1.03	37.00	35.02	0.95
S5	90.72	85.82	0.95	44.86	41.48	0.92
S6	96.48	88.87	0.92	48.00	49.74	1.04
S7	48.13	44.10	0.92	33.13	35.21	1.06
S8	118.71	118.74	1.0003	29.98	30.56	1.02
S9	77.45	77.90	1.01	41.96	41.38	0.99
S10	76.79	78.72	1.03	48.26	46.01	0.95
S11	83.58	80.92	0.97	46.29	49.93	1.08
S12	88.71	82.9	0.93	49.85	53.67	1.08
S13	33.49	35.79	1.07	42.62	46.84	1.10
S14	18.37	22.23	1.21	27.15	23.52	0.87
S15	61.62	56.24	0.91	38.57	43.07	1.12

5.3.2 Load-Deflection Curves

For comparison, the mid-span deflection for all slab models was measured and plotted vs. the corresponding load in both experimental and numerical studies.

The outcomes of this study showed that most of the slab specimens that were analyzed by the finite element method (FEM) had stiffer behavior in comparison with the experimental response in the pre-cracking portion of the load-deflection curve. In addition, almost FEM shows stiffer behavior compared to some experimental responses in the post-cracking portion of the load-deflection curve, as presented in the following load-deflection curves.

This behavior could be due to different reasons, including the following:

- Microcracks in the concrete are caused by drying shrinkage and handling. While the FEA method by ABAQUS does not account for micro-crack effects, this would reduce the stiffness of the real specimen.
- Concrete was assumed to be a homogeneous material by the FEA method by ABAQUS, but it is actually a heterogeneous material.
- The inability to test the actual stress-strain curve of concrete has affected the stiffness of specimens in numerical modeling.
- The FEA method by ABAQUS assumed a full bond between the steel reinforcement bars and the concrete, while this modeling in reality is imperfect behavior. This idealization may also contribute to the spurious initial higher stiffness in the numerical model.

According to the previous reasons, we can consider that there is a reasonable agreement between the experimental test and the FE analysis.

Figure (5-13) to Figure (5-27) represents a comparison study between the load-deflection curves that were conducted using the FEA method and the experimental work for slab models.

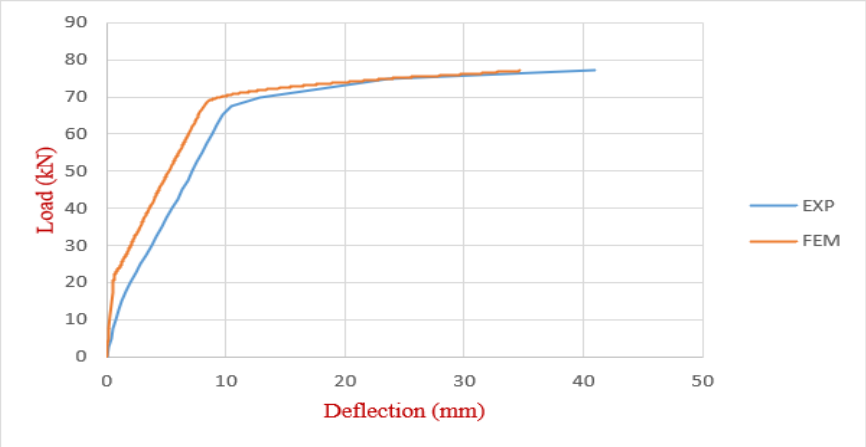

(a) Load – deflection curve for S1

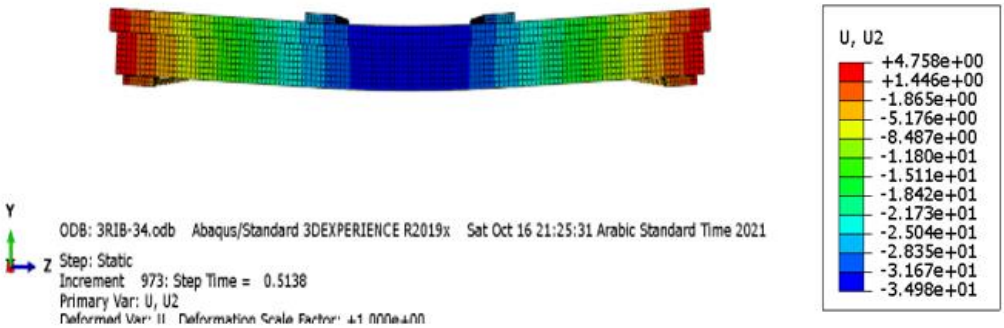

(b) Deflection shape for S1

Figure (5-13) Experimental vs. FEM deflection behavior for S1

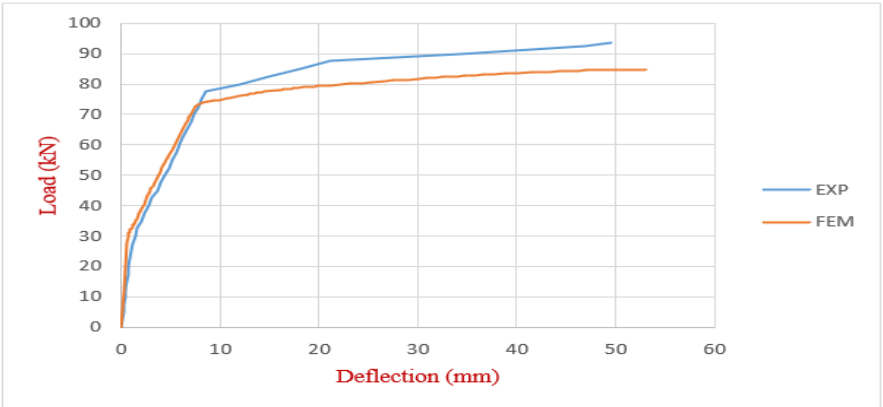

(a) Load – deflection curve for S2

Figure (5-14) Experimental vs. FEM deflection behavior for S2

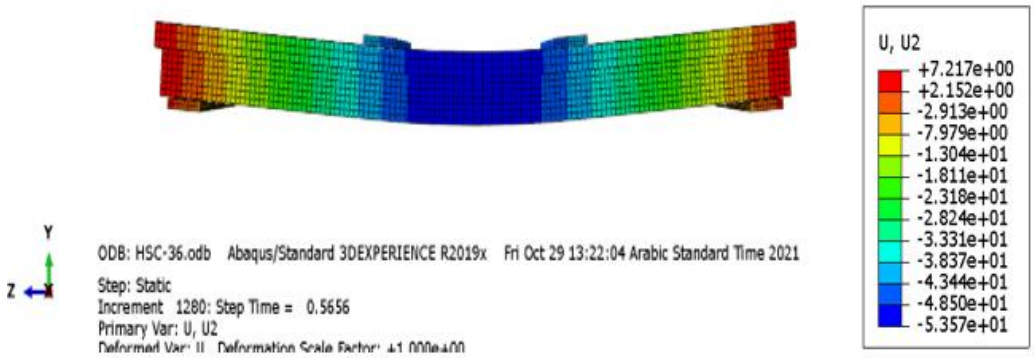

(b) Deflection shape for S2

Figure (5-14) Continued

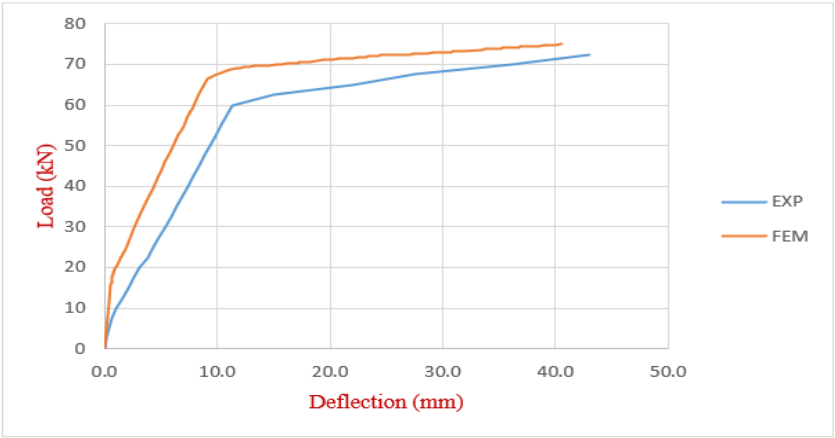

(a) Load – deflection curve for S3

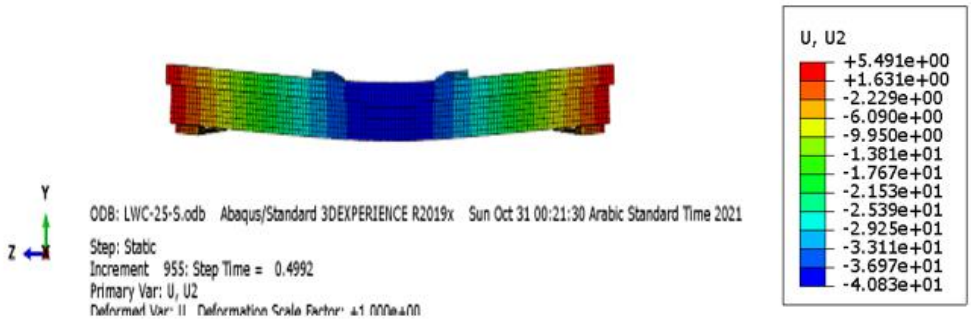

(b) Deflection shape for S3

Figure (5-15) Experimental vs. FEM deflection behavior for S3

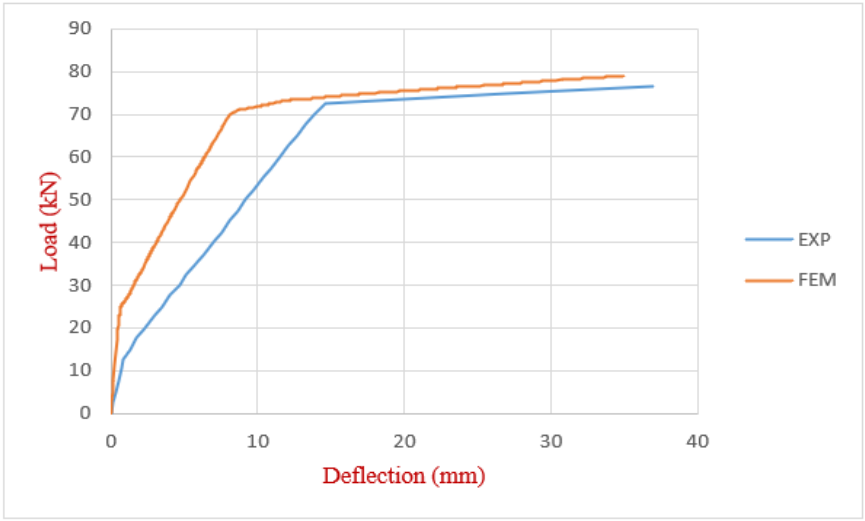

(a) Load – deflection curve for S4

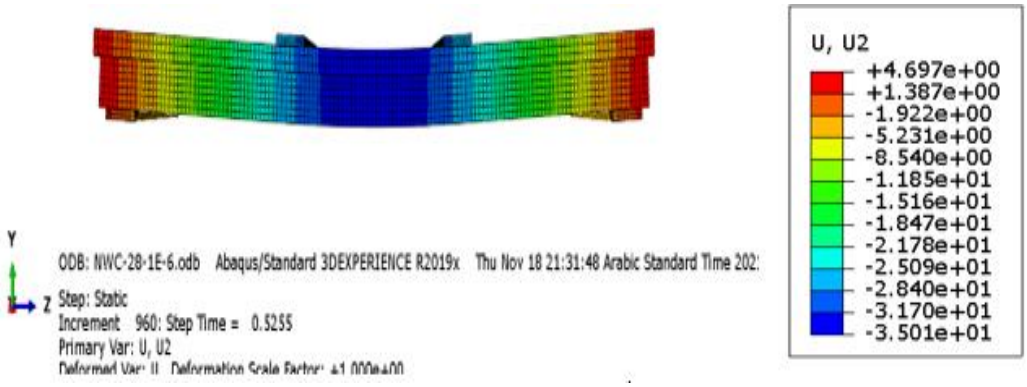

(b) Deflection shape for S4

Figure (5-16) Experimental vs. FEM deflection behavior for S4

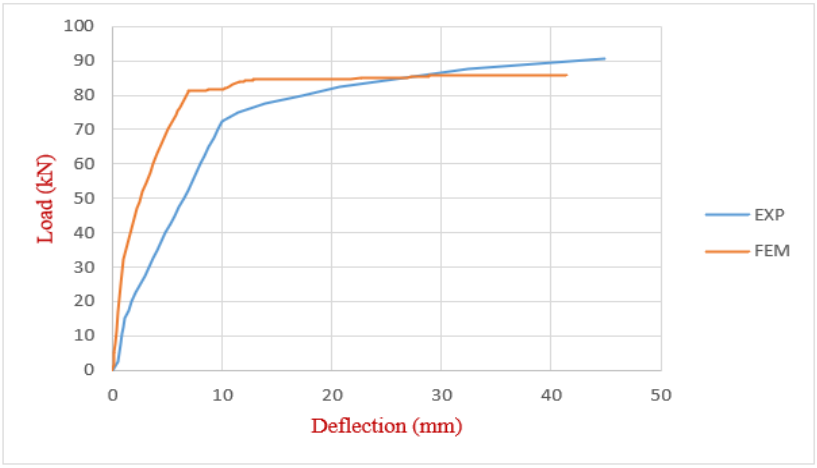

(a) Load – deflection curve for S5

Figure (5-17) Experimental vs. FEM deflection behavior for S5

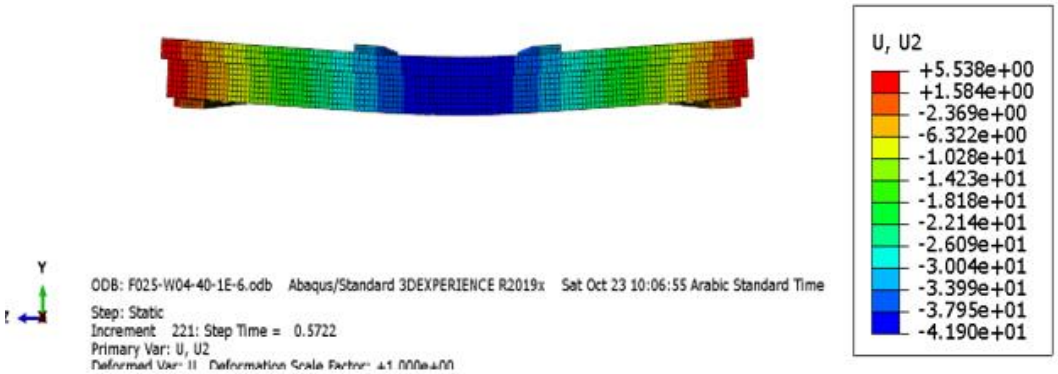

(b) Deflection shape for S5

Figure (5-17) Continued

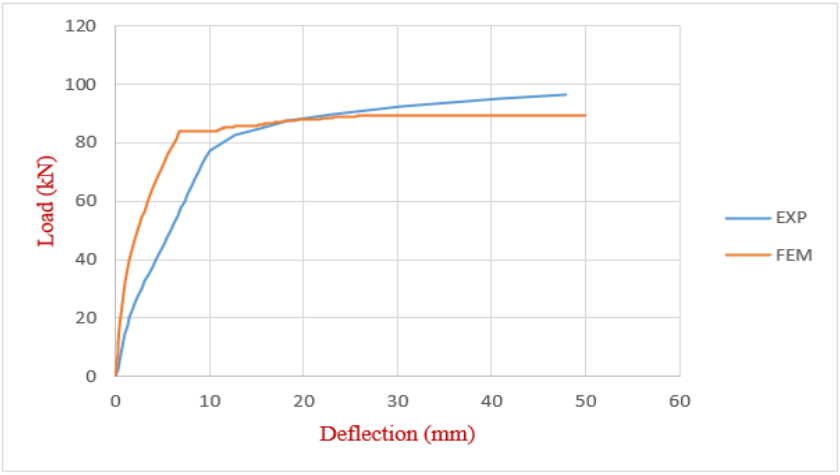

(a) Load – deflection curve for S6

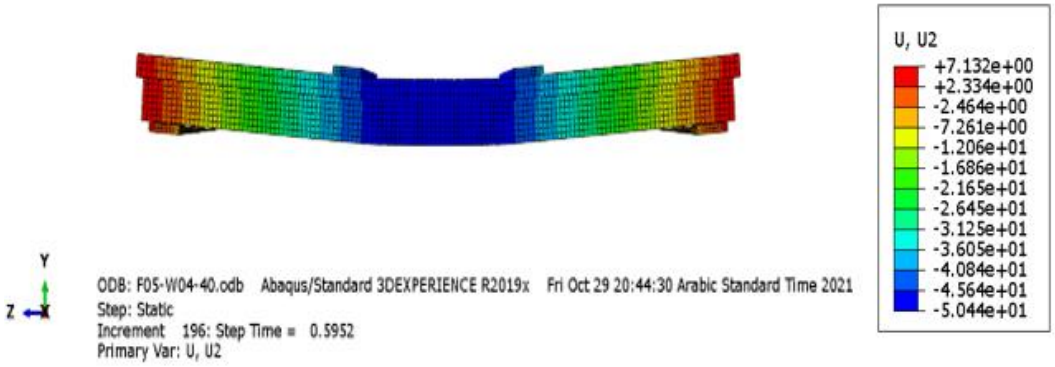

(b) Deflection shape for S6

Figure (5-18) Experimental vs. FEM deflection behavior for S6

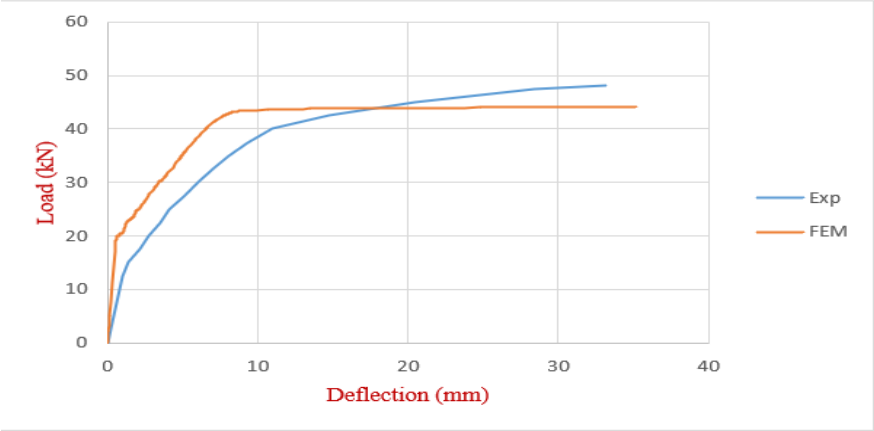

(a) Load – deflection curve for S7

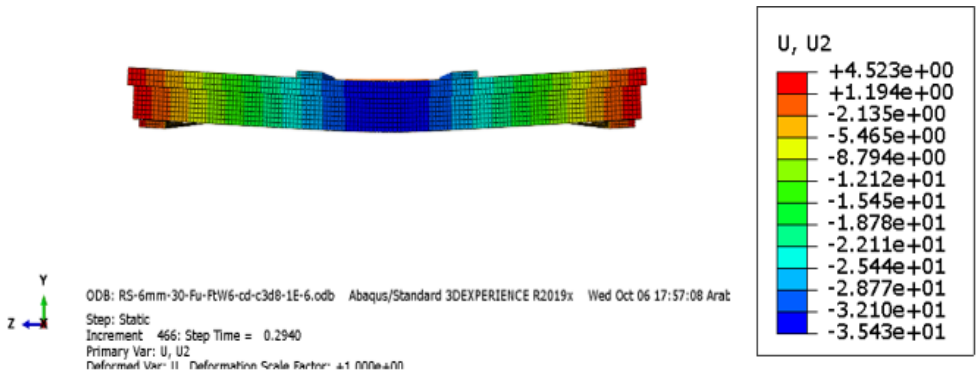

(b) Deflection shape for S7

Figure (5-19) Experimental vs. FEM deflection behavior for S7

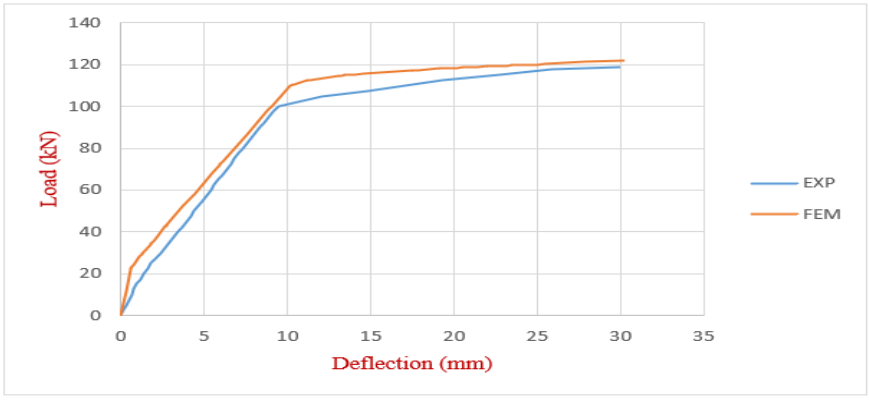

(a) Load – deflection curve for S8

Figure (5-20) Experimental vs. FEM deflection behavior for S8

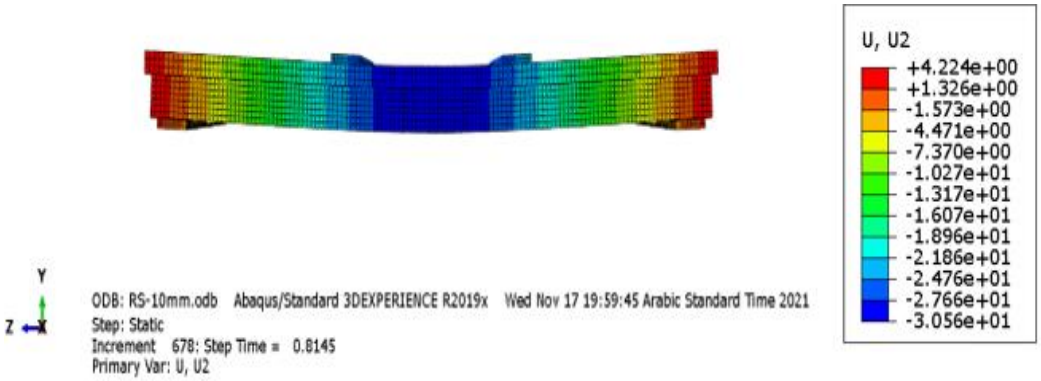

(b) Deflection shape for S8

Figure (5-20) Continued

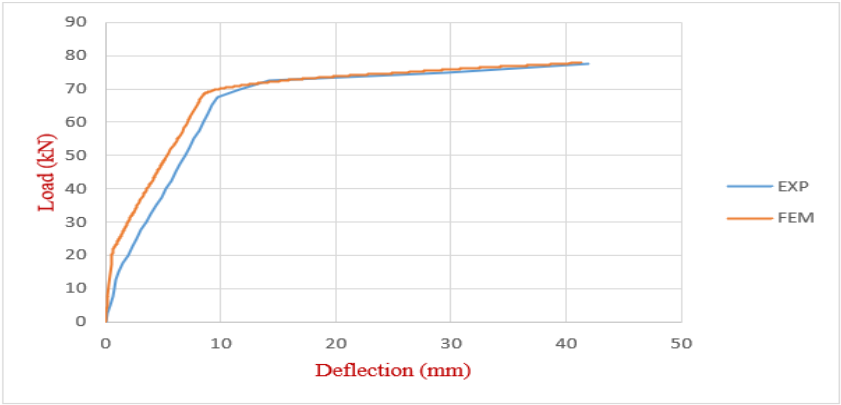

(a) Load – deflection curve for S9

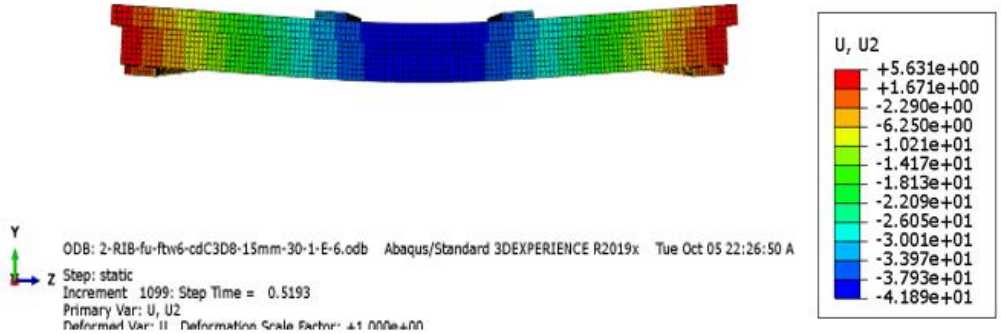

(b) Deflection shape for S9

Figure (5-21) Experimental vs. FEM deflection behavior for S9

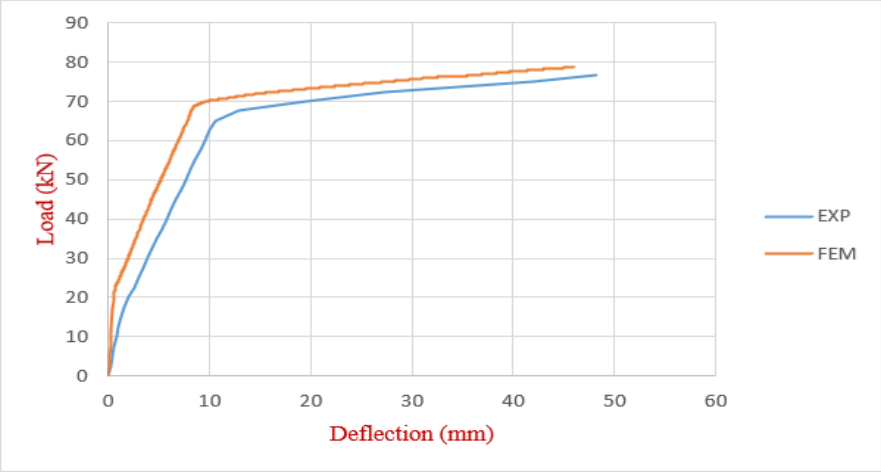

(a) Load – deflection curve for S10

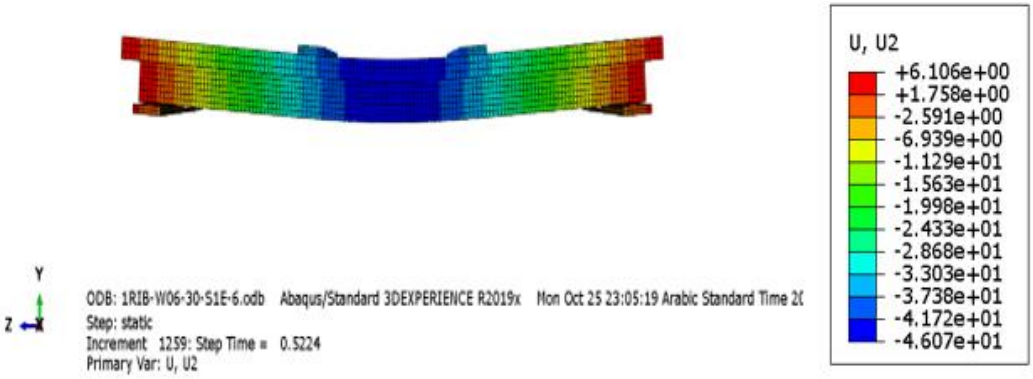

(b) Deflection shape for S10

Figure (5-22) Experimental vs. FEM deflection behavior for S10

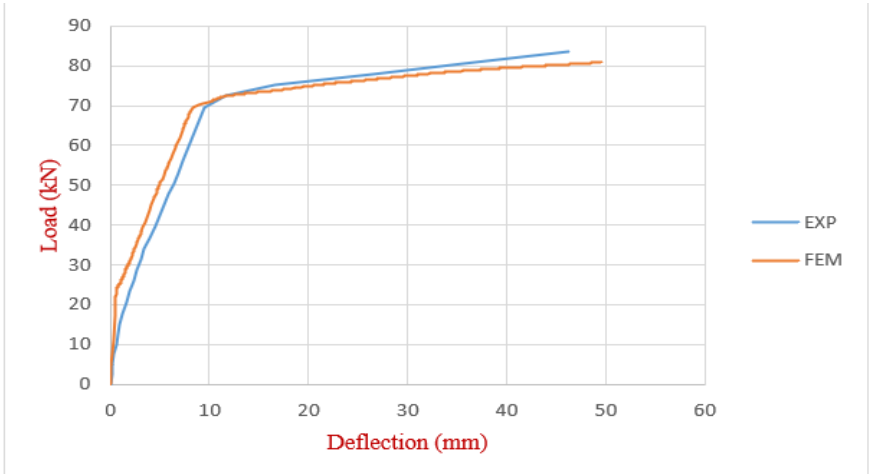

(a) Load – deflection curve for S11

Figure (5-23) Experimental vs. FEM deflection behavior for S11

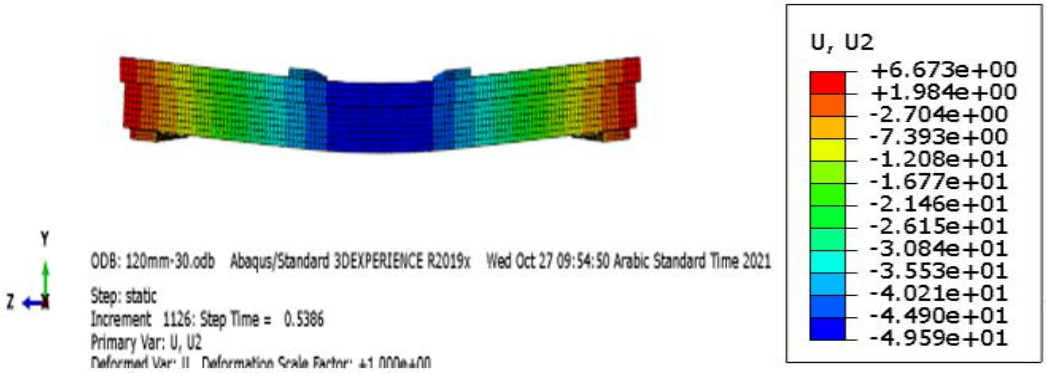

(b) Deflection shape for S11

Figure (5-23) Continued

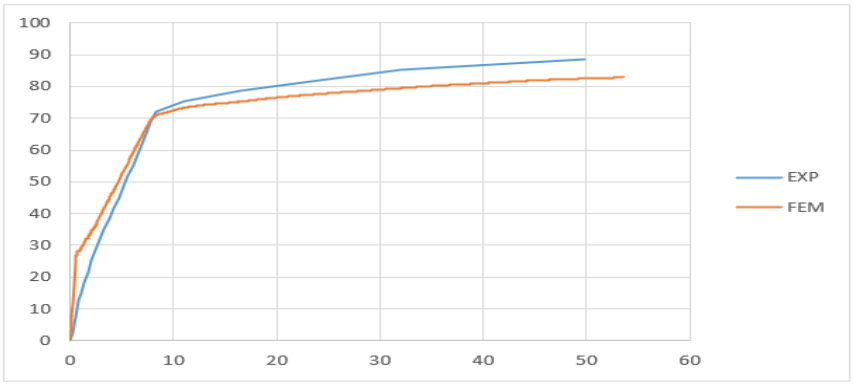

(a) Load – deflection curve for S12

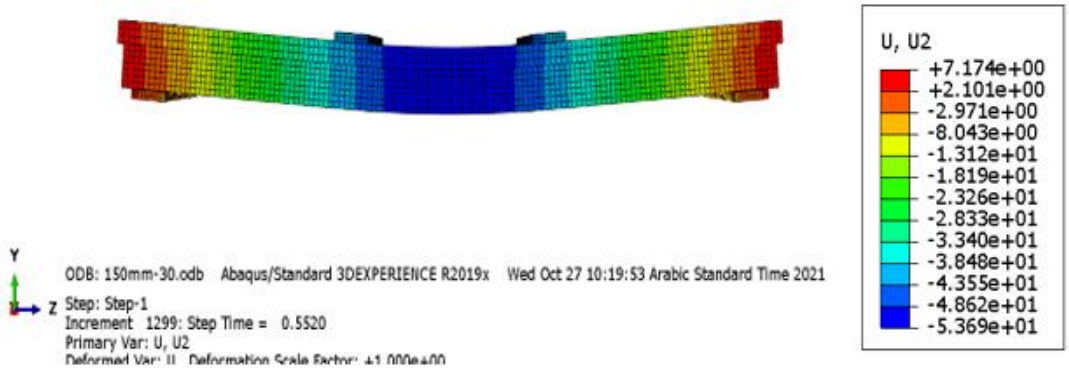

(b) Deflection shape for S12

Figure (5-24) Experimental vs. FEM deflection behavior for S12

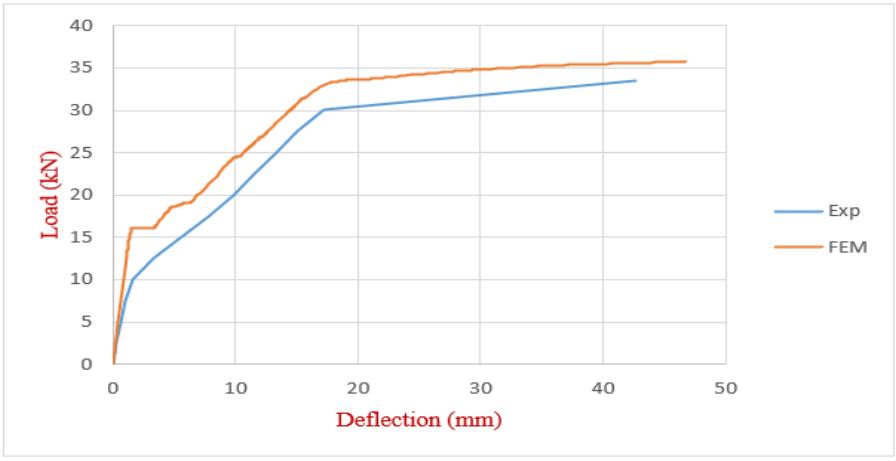

(a) Load – deflection curve for S13

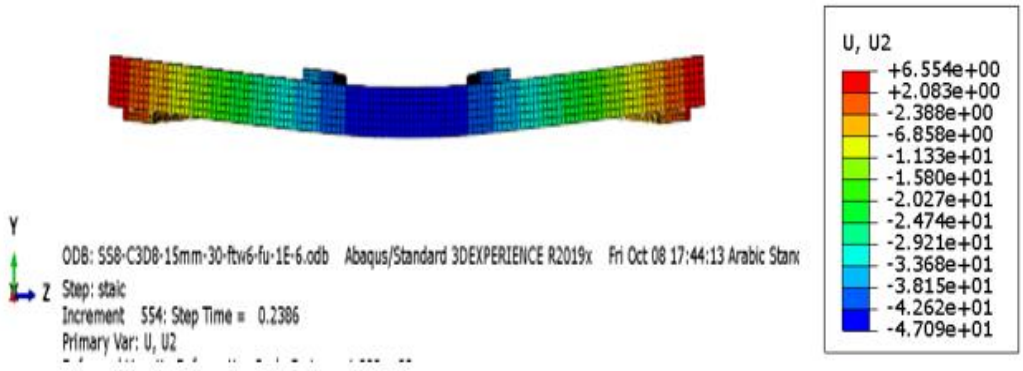

(b) Deflection shape for S13

Figure (5-25) Experimental vs. FEM deflection behavior for S13

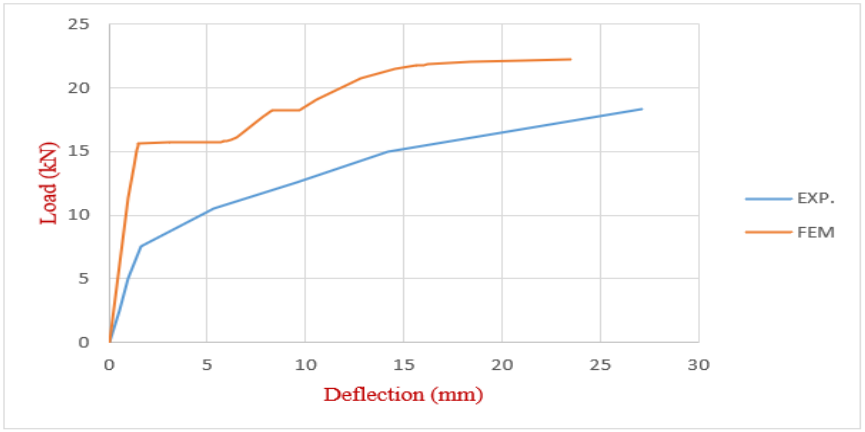

(a) Load – deflection curve for S14

Figure (5-26) Experimental vs. FEM deflection behavior for S14

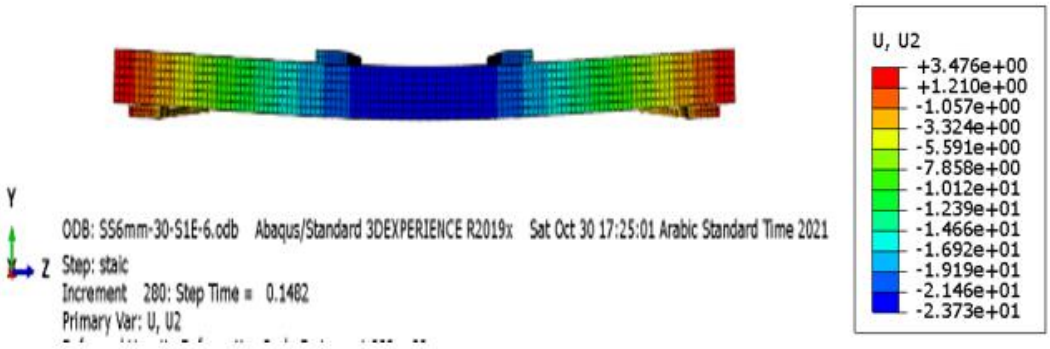

(b) Deflection shape for S14

Figure (5-26) Continued

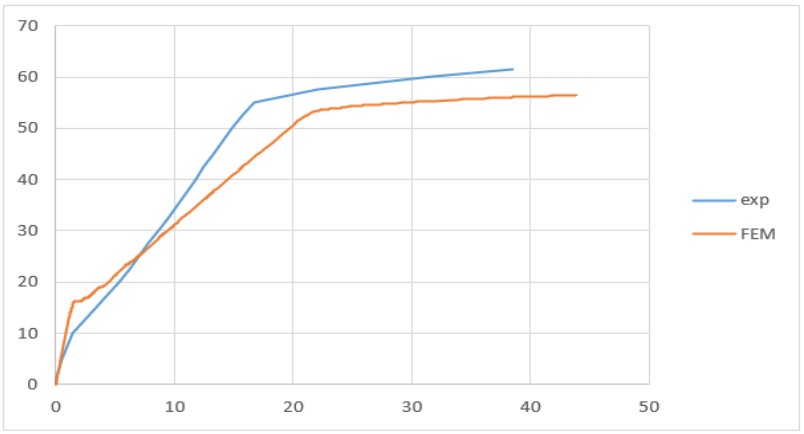

(a) Load – deflection curve for S15

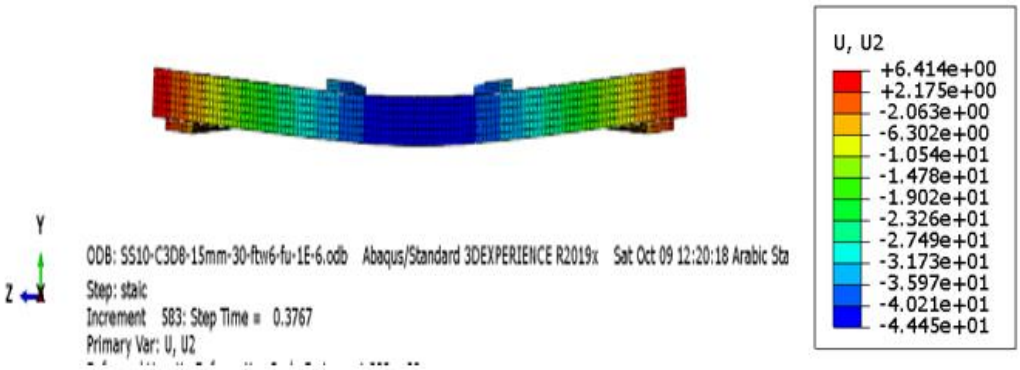

(b) Deflection shape for S15

Figure (5-27) Experimental vs. FEM deflection behavior for S15

5.3.3 Distribution of Von Mises stress at reinforcement bars

Von Mises stresses for the reinforcement bars at the ultimate load, which were obtained numerically by ABAQUS, were presented in Figure (5-28) to Figure (5-42). it's clear that stress for the steel main reinforcement bars in the maximum moment's zones is reached to the maximum value stresses.

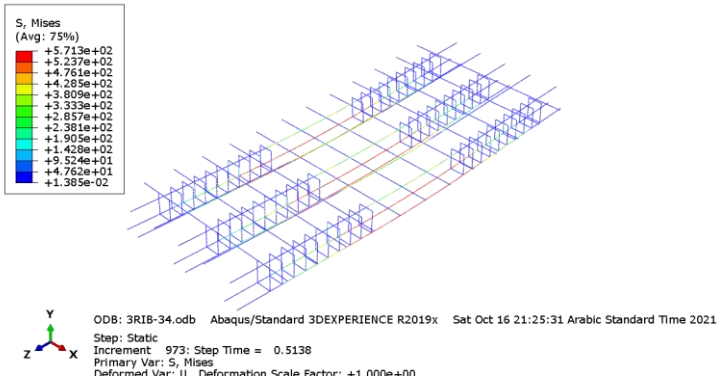

Figure (5-28) Reinforcement bars stresses of slab S1

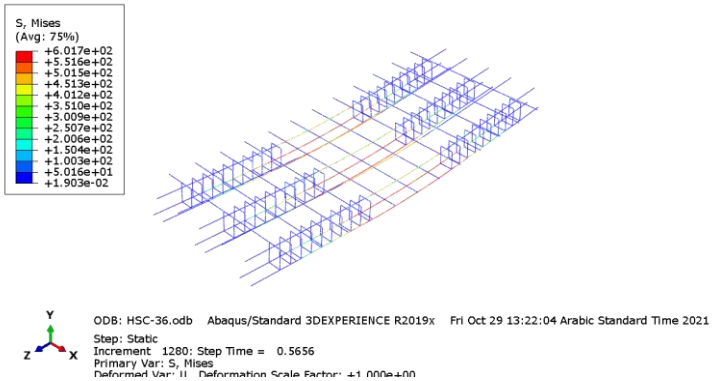

Figure (5-29) Reinforcement bars stresses of slab S2

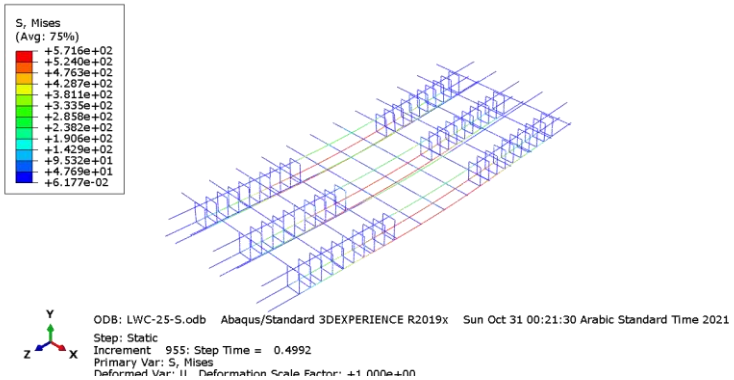

Figure (5-30) Reinforcement bars stresses of slab S3

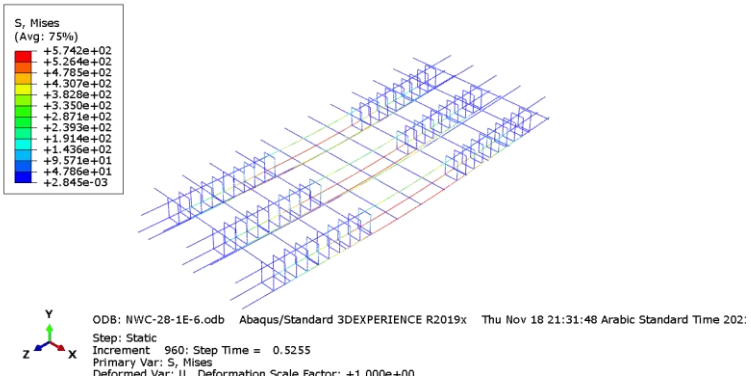

Figure (5-31) Reinforcement bars stresses of slab S4

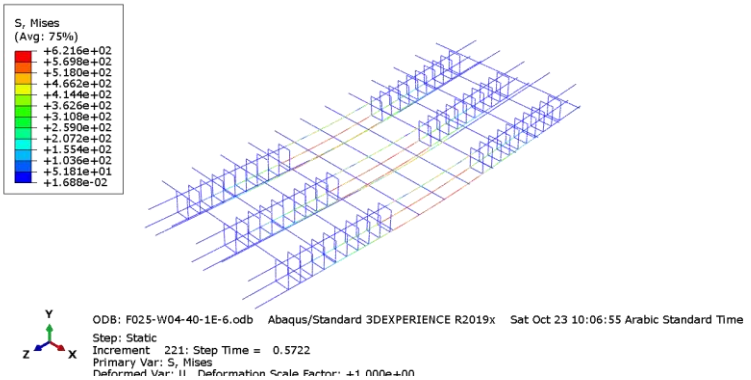

Figure (5-32) Reinforcement bars stresses of slab S5

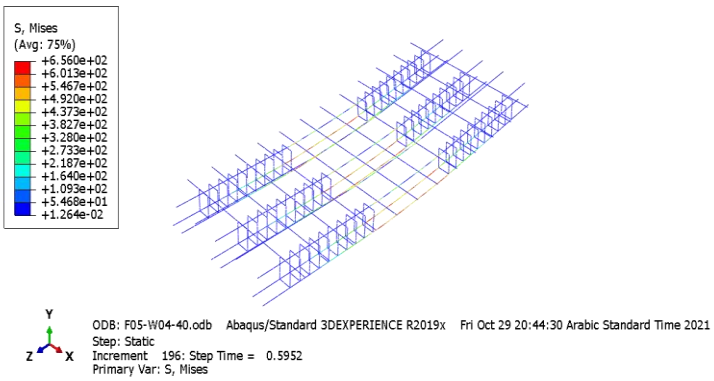

Figure (5-33) Reinforcement bars stresses of slab S6

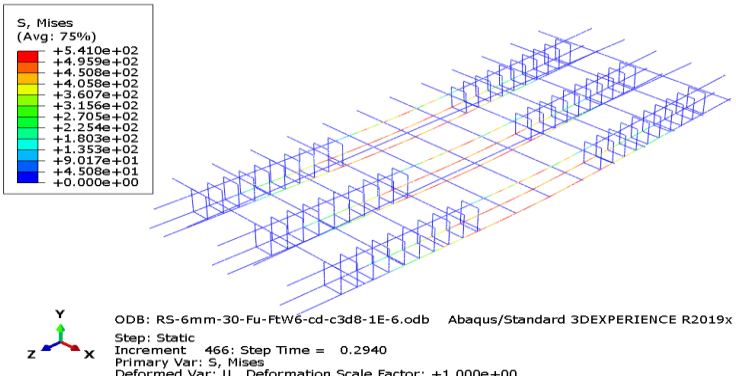

Figure (5-34) Reinforcement bars stresses of slab S7

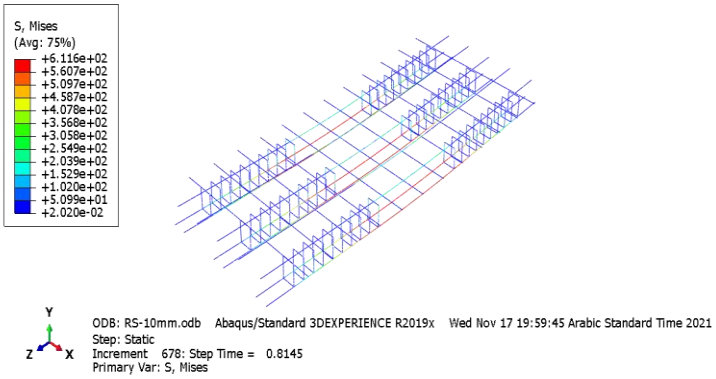

Figure (5-35) Reinforcement bars stresses of slab S8

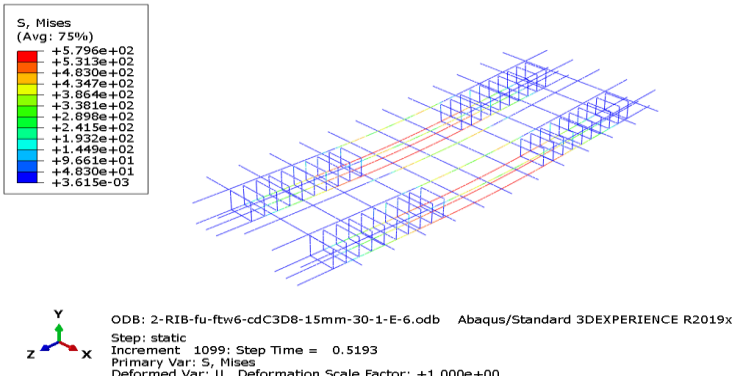

Figure (5-36) Reinforcement bars stresses of slab S9

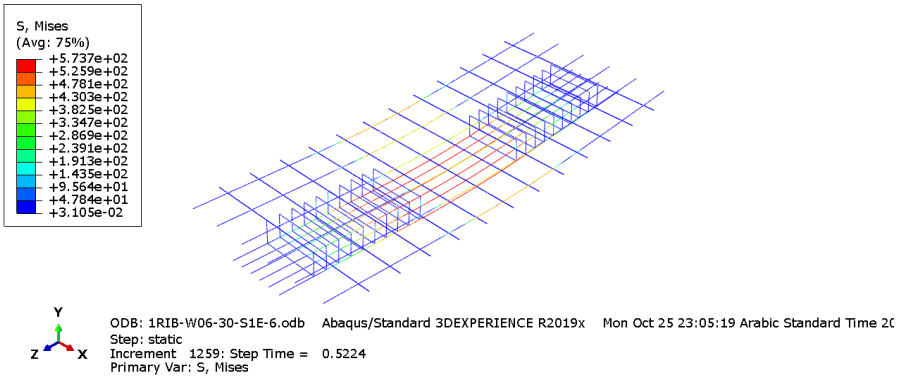

Figure (5-37) Reinforcement bars stresses of slab S10

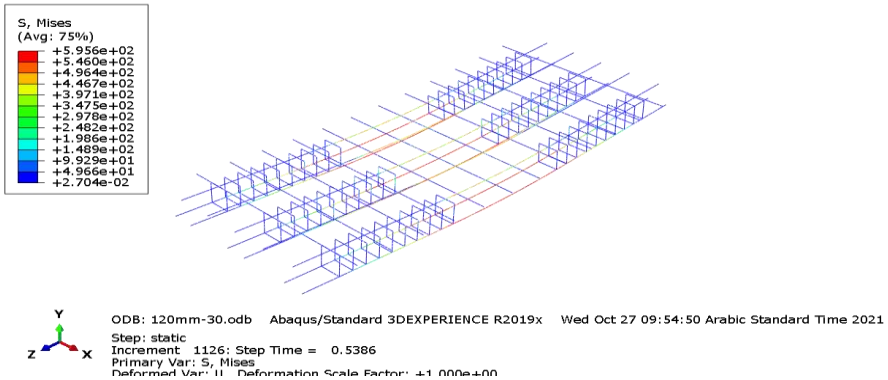

Figure (5-38) Reinforcement bars stresses of slab S11

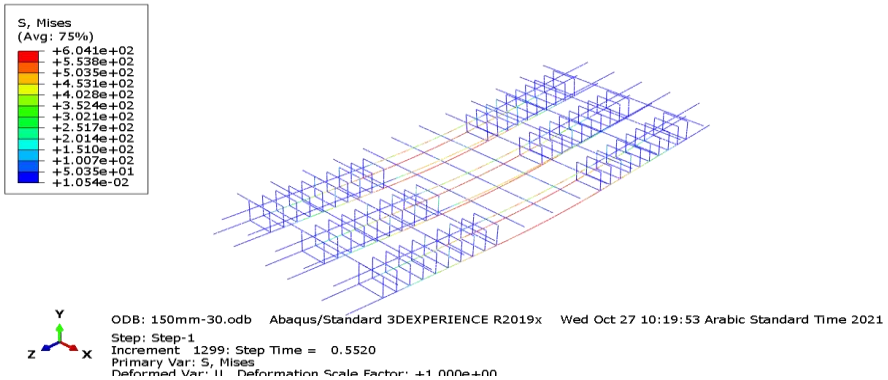

Figure (5-39) Reinforcement bars stresses of slab S12

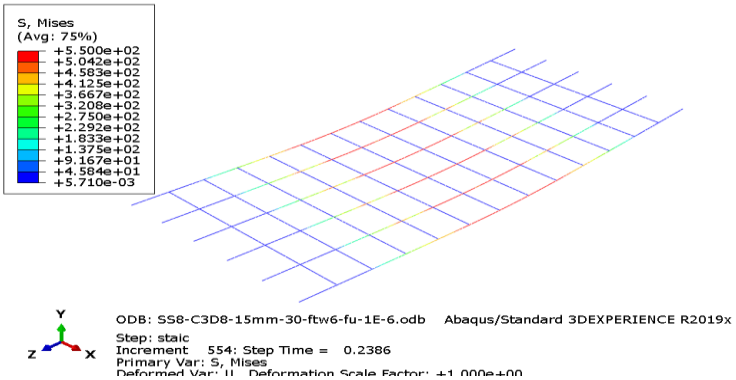

Figure (5-40) Reinforcement bars stresses of slab S13

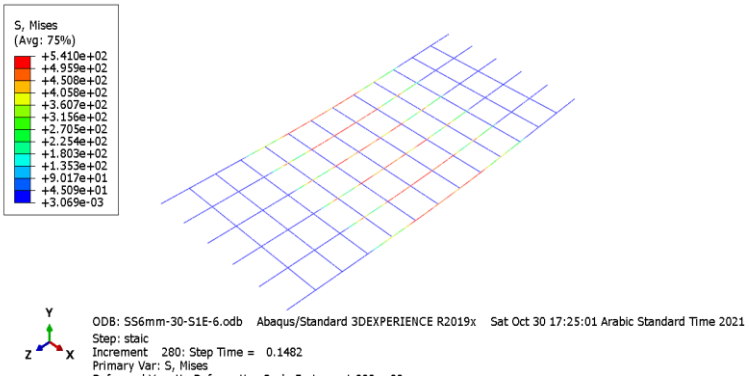

Figure (5-41) Reinforcement bars stresses of slab S14

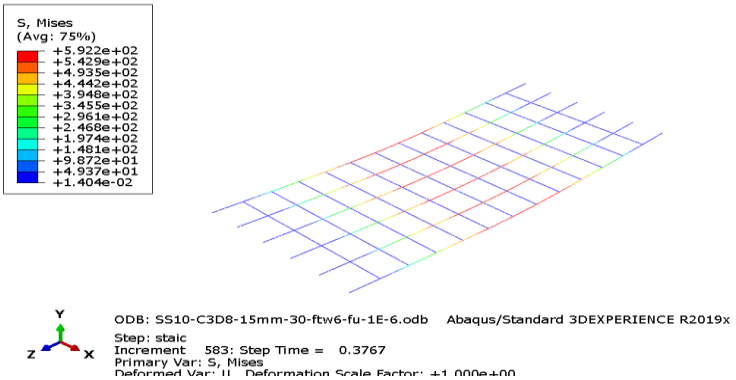

Figure (5-42) Reinforcement bars stresses of slab S15

5.3.4 Crack Patterns

At each step of subjected load, the pattern of cracks was reported by the program of ABAQUS. As an example, Figure (5-43) shows the pattern of the cracks at ultimate load for the S1 model.

The clear agreement between the numerical and theoretical results may be noticed by comparing them to crack patterns discovered during the experimental study.

(a) Experimental cracks pattern

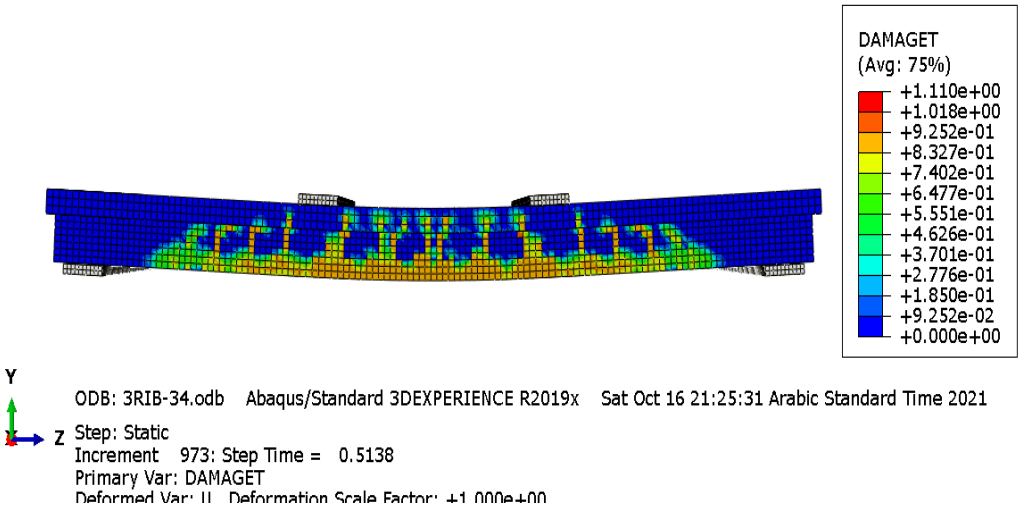

(b) ABAQUS cracks pattern

Figure (5-43) Crack patterns at failure for S1

5.4 Comparison Study between the Results of the Experimental and FEM Analysis Under Dynamic Load

In the case of the dynamic load effect and for verification sakes of the finite element model, a comparison between the experimental and the numerical results were considered for a maximum operating frequency of 50 Hz was numerically evaluated since these frequencies were validated successfully and there was no need to repeat it throughout this subsection to save time and effort without demonstrating an important subject.

The numerical model can be evaluated by comparing the maximum amplitude response, as shown in Table (5-3). The finite element model has a stiffer behavior in models (HS1 and HS4) when compared to the experimental results. The maximum difference of displacement amplitude equal to 30 percent for the specimen HS5, as shown in Figure (5-44).

Table (5-3): Comparison between experimental and numerical results for tested slabs

Specimens	Displacement Amplitude (mm) at 50 Hz		
	Exp.	Num.	$\frac{Num.}{Exp.}$
HS1	0.272	0.224	0.82
HS2	0.321	0.343	1.07
HS3	0.123	0.153	1.24
HS4	0.256	0.232	0.91
HS5	0.184	0.240	1.30
HS6	0.367	0.399	1.09

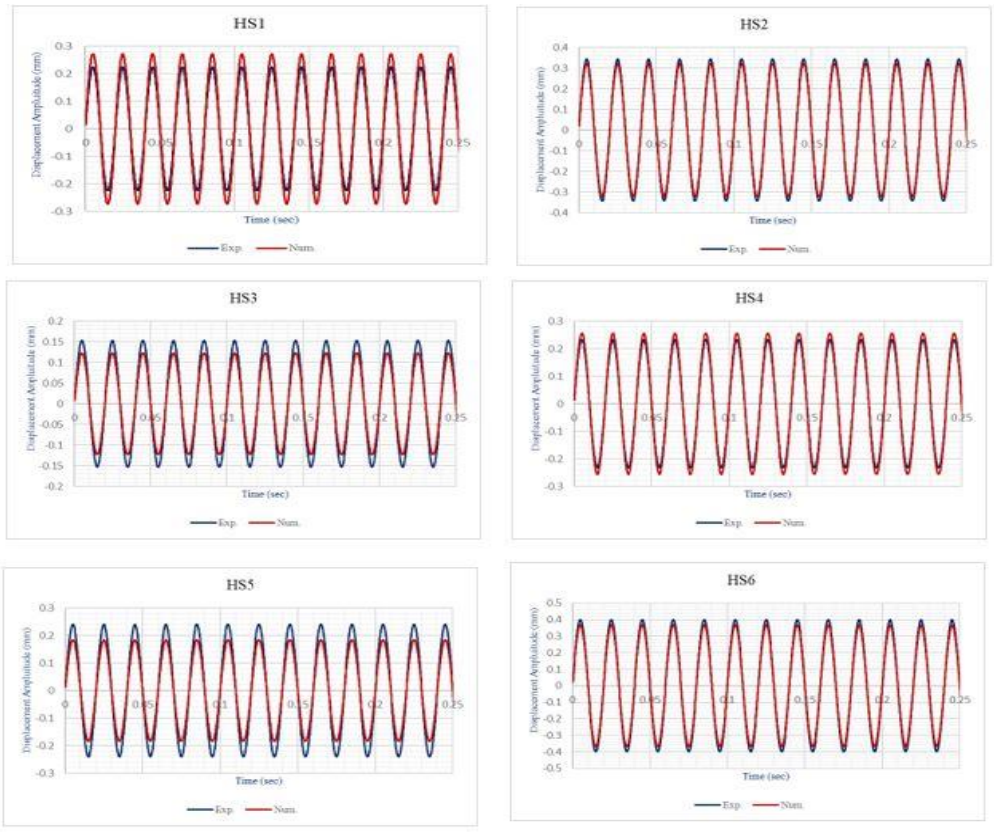

Figure (5-44) Experimental vs. numerical displacement-time history for tested slabs at 50Hz

5.5 Parametric Studies

In this study, some important aspects were investigated using an ABAQUS numerical model to see how they affected the behavior of one-way slabs under dynamic load. Parameters considered are:

- Natural frequency and vibration modes for simply and fixed support conditions.
- Increasing the operating frequency from (60 to 80) Hz which was applied on the simply supported ribbed and solid slabs.
- Changing the supports boundary condition of ribbed and solid slabs from simply support to fixed support at the operating frequency of 60 Hz.
- Changing the spacing between ribs for one-way HSLWC ribbed slab.

5.5.1 Natural Frequency and Vibration Modes

ABAQUS / 2019 provides the option to select a model solution free of external influences. Any structure's natural frequencies can be extracted using this technique. The Block Lanczos Method was selected as an engine solver. In order to achieve a robust design, the natural frequency is a crucial parameter to be considered.

Three modes were selected to be extracted. However, only lower modes have a significant effect, and, in some cases, only the fundamental mode (the first mode) is important. The obtained natural frequencies for three modes shapes for the slab specimens are listed in Table (5-4).

Table (5-4): Natural frequencies of all tested slabs under dynamic loading

Specimens	Natural Frequencies (Hz)					
	Simply Support Mode			Fixed Support Mode		
	1st	2nd	3rd	1st	2nd	3rd
HS1	69.51	146.97	222.36	131.04	159.53	235.69
HS2	71.88	152.05	229.72	135.60	165.57	243.48
HS3	68.07	143.92	217.65	128.32	156.44	230.64
HS4	69.77	147.52	223.16	131.53	160.17	236.54
HS5	66.78	151.74	199.43	120.19	152.07	205.38
HS6	40.14	136.94	152.53	76.84	140.60	153.58

Using HSNWC instead of HSLWC led to increase the numerical fundamental natural frequency of HS2 by 3.41% due to an increase in the stiffness of simply supported slab.

Using NWNSC in ribbed slab HS3 instead of HSLWC led to decrease the numerical natural frequency of 2.07% due to an increase in the weight of simply supported ribbed slab.

The inclusion of steel fiber with (V_f = 0.25%) in HSLWC slab HS4 led to increase the numerical natural frequency of by 0.37% due to an increase in the stiffness of the slab.

One-rib slab HS5 gave a reduction in numerical fundamental natural frequency by 3.93% in comparison to 3-ribs slab HS1.

Converting the solid slab HS6 to ribbed slab HS1 led to increase the numerical natural frequency by 73.17% due to an increase in the stiffness of the ribbed slab.

While using fixed supported instead of simply supported led to increase the numerical fundamental natural frequency by 88.52%, 88.65%,

88.51%, 88.52%, 79.98%, and 91.43% in slabs (HS1, HS2, HS3, HS4, HS5, and HS6), respectively.

The deformation shapes of three modes of frequencies of ribbed slab HS1 are shown in Figure (5-45) as an example of the deformation shapes under free dynamic response.

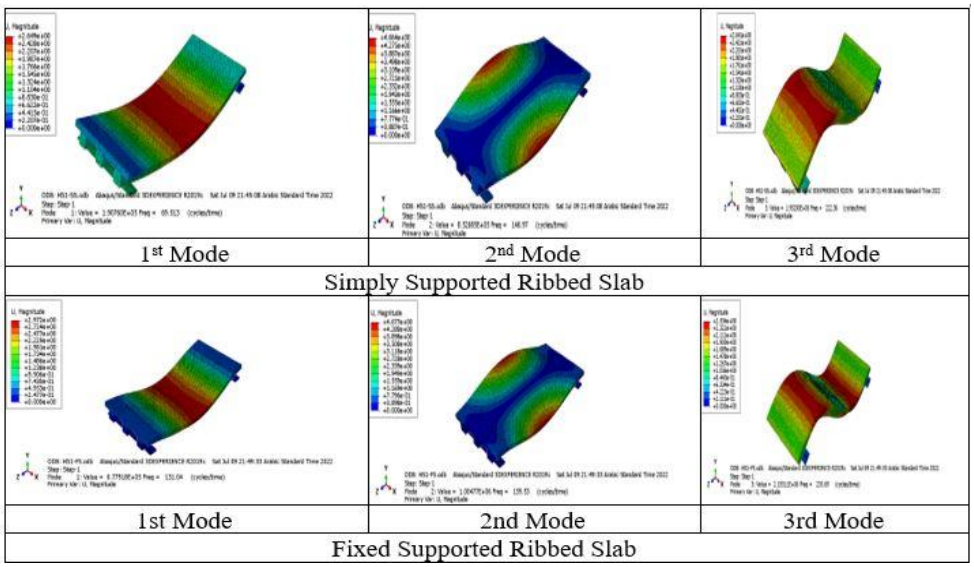

Figure (5-45) Mode shapes of one-way ribbed slab

On the other hand, the theoretical calculations of natural frequency for the tested simply supported slabs are tabulated in Table (5-5), these calculations were done in PTC Mathcad Prime 6.0 software, as shown in Appendix B. Comparison between the numerical and theoretical results of 1st mode natural frequency in Table (5-5) for ribbed slabs gave good convergence with a maximum difference of (+3.8) %, while for solid slab gave (+5.5) %.

Table (5-5): Theoretical and numerical results of natural frequency

Specimens	**HS1**	**HS2**	**HS3**	**HS4**	**HS5**	**HS6**
Theo. natural frequency (Hz)	66.95	70.08	66.51	67.25	67.15	38.03
Num. natural frequency (Hz)	69.51	71.88	68.07	69.77	66.78	40.14
Num./ Theo.	1.038	1.026	1.023	1.037	0.994	1.055

5.5.2 Increasing the Operating Frequency

The displacement amplitude of (HSLWC, HSNWC, and NSLWC) one-way ribbed slabs and HSLWC one-way solid slab at operating frequencies beyond the 50 Hz were investigated numerically, as shown in Figure (5-46). From this figure, one found that the HSLWC solid slab HS6 gave higher displacement amplitude by 94.36%, 118.58%, and 156.67% in comparison to HSLWC ribbed slab HS1 at frequencies 60Hz, 70Hz, and 80Hz, respectively. This behavior is due to the sectional properties of HS1 being better than HS6. On the other hand, using HSNWC instead of HSLWC and NSLWC instead of HSLWC increased the displacement amplitude by about (44.51%, 40.71%, and 36.11%), and (25.08%, 30.05%, and 34.17%) at frequencies 60Hz, 70Hz, and 80Hz, respectively. These outcomes revealed that HSLWC ribbed slab gave better performance under dynamic load among the HSNWC, NSLWC ribbed slabs and HSLWC solid slab.

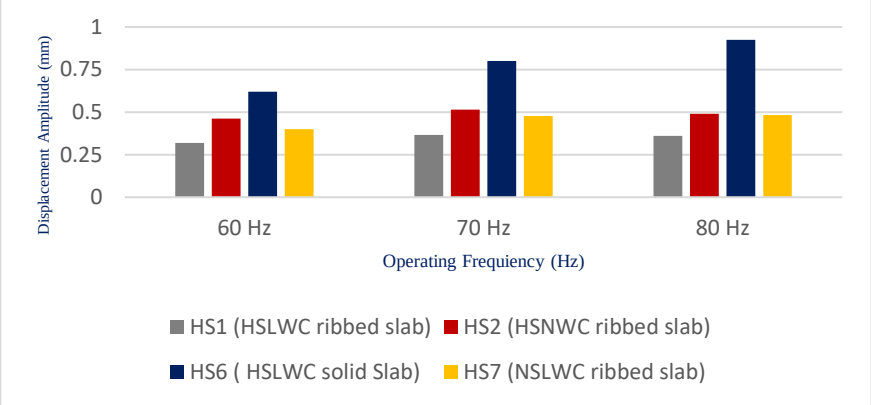

Figure (5-46) Displacement amplitude of one-way slabs at frequencies 60 Hz to 80 Hz

5.5.3 Changing the Boundary Condition of the Supports

The displacement amplitudes comparison between simply and fixed supported of three ribs one-way (HSLWC, HSNWC, and NSLWC) ribbed and solid slabs at the operating frequency of 60 Hz were

investigated, as shown in Figure (5-47). The simply supported condition of (HSLWC, HSNWC, and NSLWC) ribbed and solid one-way slabs gave higher displacement amplitude by 49.33%, 150.54%, 110%, and 100% than fixed supported, respectively.

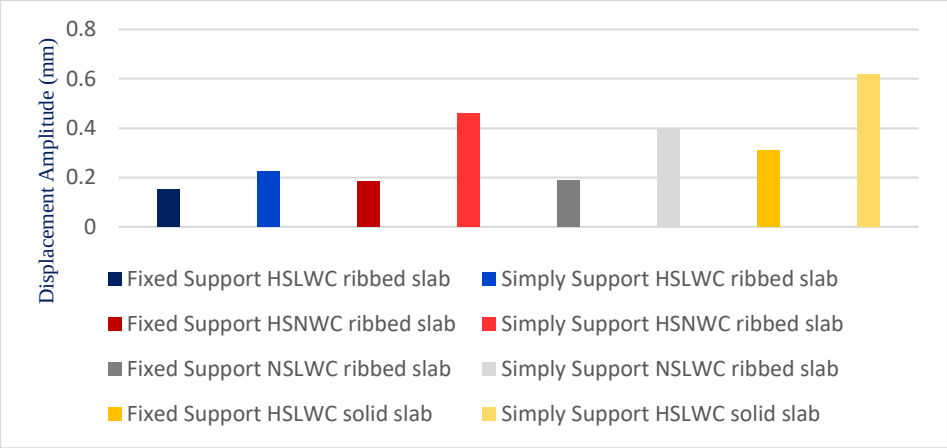

Figure (5-47) Effect of support boundary condition on displacement amplitude of one-way Slabs

5.5.4 Changing the Ribs Spacing

Changing the spacing between ribs of the one-way ribbed slab from 200mm to 150mm by increasing the width of the rib from 100mm to 150mm led to increase the displacement amplitude by 4.91% at 60Hz, as shown in Figure (5-48). This behavior may be belonged to decrease the spacing between the ribs led to decrease the dispersion of vibration effect.

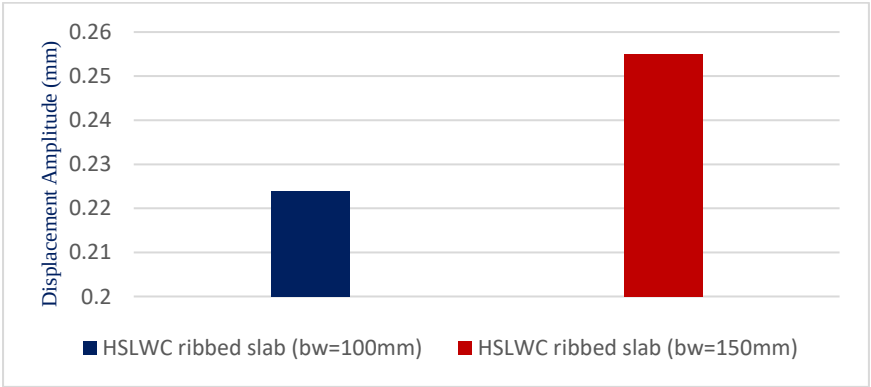

Figure (5-48) Effect of ribs spacing on vibration amplitude of one-way HSLWC ribbed slab

Chapter Six

Conclusions and Recommendations for Future Studies

Chapter Six: Conclusions and Recommendations for Future Studies

6.1 Conclusions

Following conclusions are drawn based on the results

1- HSLWC can be produced with an average cylinder compressive strength of about 42.2 MPa and an average dry density of 1943 kg/m^3 by using volcanic aggregate (pumice stone) as coarse aggregate, sand, Portland cement, silica fume, superplasticizer, and by-product material (sugar molasses).

2- Inclusion of steel fibers in HSLWC mix with (V_f = 0.25%) led to increase the cube and cylinder compressive strength by (7.49 and 11.14) %, respectively, while the enhancement in compressive strength with (V_f = 0.50%) was (13.63 and 16.35) %. The maximum strength to density ratio was achieved with the inclusion of (V_f = 0.5%) of steel fibers in HSLWC mix.

3- Using HSNWC instead of NSNWC led to increase the brittleness ratio by 23.40%, while using HSLWC instead of NSLWC led to increase the BR by 34.35%, so the LWA made the concrete less ductile by 10.95%.

4- Inclusion of steel fibers with two volume fractions (0.25% and 0.5%) led to recover the ductile deficiency by using HSLWC instead of NSLWC by 12.54% and 13.13%, respectively.

5- Using LWA for both HSC and NSC instead of NWA led to increase the thermal insulation by reducing conductivity by 43.55% and 38.95%, respectively. Moreover, the cost of heating and cooling loads decreases with increasing the heat resistivity (r).

6- Using NWA in HSC and NSC gave sound insulation acceptable.

7- Using HSLWC instead of NSLWC in the production of a one-way ribbed slab led to increase the ultimate load by 6.62% and decreased the maximum crack width by 39.28%. On the other hand, using HSLWC instead of NSNWC with a density reduction equal to 16% led to increase the ultimate load and maximum crack width by 0.9% and 21.43%, respectively.

8- Using HSLWC ribbed slab instead of HSNWC ribbed led to decrease the weight and ultimate load capacity by 19% and 17.70%, respectively. This behavior led to increase the structural efficiency (SE) of the HSLWC slab. On the other hand, using 0.25% of steel fibers in HSLWC ribbed slab led to recover of about 14.49% of strength reduction, which also led to increase the SE by 16.51%.

9- Using steel reinforcement ratio (ρ = 0.44%) and 0.50% of steel fibers led to recover the strength reduction due to decreasing of spacing between ribs, also led to an additional improvement in ultimate load capacity.

10- In this study, using the higher ratio of steel reinforcement (ρ = 0.44%) in the HSLWC ribbed slab led to decrease the ductility by 27.32%, while using steel fibers led to enhance the ductility of HSLWC ribbed slabs by 6.64% and 14.01% for (0.25 and 0.50) %, respectively. In terms of safety considerations, these findings led to the fact that adding steel fibers with specific ratios in HSLWC ribbed slabs gave a good performance in recovering the reduction in strength from increasing steel reinforcement ratio.

11- In this study, spacing between ribs equal to 180 mm improved SE over the spacings of 200 mm and 150 mm, respectively, so that the width of rib (b_w), equal to 120 mm, was considered the suitable width of rib.

12-Using a ribbed slab instead of a solid slab led to increase the ultimate load capacity by 130.37% and decrease the deflection by 3.99%. On the other hand, increasing the steel reinforcement ratio in solid slabs from 0.57% to 0.90% led to recover of 34.49% of strength reduction.

13-Changing the diameter of steel reinforcement in the solid slab from 8 mm to 6 mm (i.e., reduction in steel reinforcement ratio of about 45.61%) gave a reduction in strength by 45.15%, while changing this diameter from 8 mm to 6 mm (i.e., reduction in steel reinforcement ratio of about 42.86%) in the ribbed slab gave a reduction only of 37.62%.

14-In terms of sustainability impact, HSLWC ribbed slabs with fewer ribs number at the same concrete volume gave a better performance in reduction of vibration, CO_2 emission, and cost of shear reinforcement.

15- Ribbed slab with one rib under static load gave the largest deflection, while under dynamic load gave less displacement amplitude in comparison to three ribs one-way HSLWC ribbed slab.

16- Using the same width of each rib which is equal to 150 mm in a ribbed slab with 2-ribs instead of 3-ribs, gave more advantages related to structural efficiency and eco-strength efficiency by 4.23% and 4.12%, respectively.

17-The expression of ACI for the moment capacity of HSLWC becomes less conservative than HSNWC and fibers HSLWC ribbed slabs. In contrast, the expression of ACI becomes more conservative as the steel ratio decreases.

18-Using HSLWC, NSNWC, and F0.25HSLWC in the production of a one-way ribbed slab led to decrease the displacement amplitude of harmonic loading more than using HSNWC.

19-Using 1-rib instead of 3-ribs HSLWC ribbed slab, while using 3-ribs HSLWC ribbed slab instead of the solid slab at the same HSLWC

volume gave a better performance in displacement amplitude under the effect of dynamic (harmonic) load.

20-Using HSLWC in the production ribbed slab reduced the sound level more than HSNWC by 2.70 %. On the other hand, Using HSLWC ribbed slab instead of HSLWC solid slab reduced sound level by 4.70%.

21-Finite element analysis of static models by ABAQUS/2019 was capable of simulating the structural behavior of one-way slabs (ribbed and solid) under static load with a variation of not more than 15% for deflection, while under dynamic load, the difference of displacement amplitude did not exceed 30%.

22-Using HSLWC instead of HSNWC in ribbed slab reduced the fundamental natural frequency, while using fibers in HSLWC increased its fundamental natural frequency.

23-Changing the support condition of HSLWC one-way slabs from simply to fixed support increased their fundamental frequency and decreased the displacement amplitude.

6.2 Recommendations for Future Studies

1- Investigating the structural behavior of high strength-lightweight reinforced concrete continuous one-way ribbed slabs.

2- Studying the effect of dynamic impact load on the behavior of high strength- lightweight concrete one-way ribbed slabs.

3- Studying the effect of fire on the structural behavior of high strength-lightweight reinforced concrete one-way ribbed slabs.

4- Investigating the structural behavior of strength-lightweight reinforced concrete one-way ribbed slabs that are strengthened and repaired using different strength techniques such as (carbon fiber reinforced polymer

sheets, steel plate, and slurry infiltrated fiber concrete (SIFCON) laminate sheets).

5- Studying the effect of other types of concrete, such as (high-strength rubberized concrete, SIFCON, and reactive powder concrete) on the behavior of one-way ribbed slabs under different loading conditions.

References

References

[1] M. Singh and B. Saini, Analytical and Experimental Study of Voided Slab, Vol. 21 LNCE. Springer International Publishing, 2019.

[2] N. H. M. Fodzi and M. H. M. Hashim, "Structural Effect of Using Steel Fiber Reinforcement on the Punching Shear of Self-Compacting Fiber Reinforced Concrete (SCFRC) Ribbed Slabs," Materials Science Forum, Vol. 972, pp. 99–104, 2019.

[3] ACI 363R-10, "Report on High-Strength Concrete," American Concrete Institute, 2010.

[4] M. A. Rashid and M. A. Mansur, "Considerations in producing high strength concrete," Journal of Civil Engineering (IEB), Vol. 37, No. 1, pp. 53–63, 2009.

[5] J. Newman and B. S. Choo, Advanced Concrete Technology 3: processes, First edit. Great Britain: Butterworth-Heinemann, 2003.

[6] S. Chandra and L. Berntsson, Lightweight Aggregate Concrete, First Edit. William Andrew, 2002.

[7] A. M. Neville, Properties of Concrete, Fourth Edi. London: Wiley, 1996.

[8] R. K. Saini, A. Godara, A. Maheswari, and M. A. Kumar, "Experimental Study on Light Weight Concrete with Pumice Stone as a Partial Replacement of Coarse Aggregate," Universal Review, Vol. 7, No. V, pp. 48–55, 2018.

[9] BS EN1992-1-1, Eurocode 2: Design of concrete structures - Part 1-1 : General rules and rules for buildings. London,UK: British Standards Institution, 2004.

[10] ENV 1992-1-4, Eurocode 2: Design of concrete structures - Part 1-4: General rules - Lightweight aggregate concrete with closed structure. 1994.

[11] UNI 7548.1, Lightweight concrete by expanded clay or shale. Definitions and classification. Italy.

[12] PN-91/B-06263, Lightweight Aggregate Concrete. Poland, 1991.

[13] NS 3473, Design of Concrete Structure. Norway, 1992.

[14] DIN 1045-1, Concrete, reinforced and prestressed concrete structures - Part 1: Design and construction. Germany, 2008.

[15] ACI 213R-14, "Guide for structural lightweight concrete," American Concrete Institute, 2014.

[16] "Chapter 8:Design of One-Way Slabs." https://pdf4pro.com/view/8-chapter-8-design-of-one-way-slabs-618aa3.html.

[17] BS 8110:1997, Structural Use of Concrete, Part 1-Code of Practice for Design and Construction. London, UK: British Standards Institution, 1997.

[18] ACI 318-19, "Building Code Requirments for Structural Concrete." American Concrete Institute, 2019.

[19] A. Paul, "Ribbed or Waffle Slab System–Advantages & Disadvantages," 2014. https://civildigital.com/ribbed-waffle-slab-system-advantages-disadvantages/.

[20] S. Rajasekaran, Structural dynamics of earthquake engineering: theory and application using MATHEMATICA and MATLAB. Elsevier, 2009.

[21] I. T. AL-Rubayie, "Using local materials to produce lightweight

paving units for Baghdad Municipality projects," M.Sc. Thesis, University of Technology, Iraq, 2007.

[22] M. A. M. Abdeen and H. Hodhod, "Experimental Investigation and Development of Artificial Neural Network Model for the Properties of Locally Produced Light Weight Aggregate Concrete," Engineering, Vol. 02, No. 06, pp. 408–419, 2010, doi: 10.4236/eng.2010.26054.

[23] N. A.-M. Al-Bayati, K. F. Sarsam, and I. A. S. Al-Shaarbaf, "Compressive Strength of Lightweight Porcelanite Aggregate Concrete -New Formulas," Eng. &Tech. Journal, Vol. 31, No. 10, pp. 1897–1913, 2013.

[24] M. J. H. Al-Aridhee, "Some Properties of Lightweight Concrete Containing Attapulgite," MSc. Thesis, University of Technology, Iraq, 2014.

[25] A. N. Abbas and H. H. Abdulzahra, "Studying the Properties of Lightweight Concrete Using Construction Materials Waste," Journal of Environmental Science and Engineering A, Vol. 4, No. 6, pp. 295–302, 2015, doi: 10.17265/2162-5298/2015.06.004.

[26] M. M. Jomaa'h and E. K. Algubory, "Effect of Lightweight Coarse Aggregate From Claystone and Thermostne on Physical and Mechanical Properties of Concrete," Diyala Journal of Engineering Sciences, Vol. 10, No. 1, pp. 1–17, 2017.

[27] W. I. Khalil, H. K. Ahmed, and Z. M. A. Hussein, "Properties of Sustainable High Performance Lightweight Aggregate Concrete Reinforced With Fibers," Diyala Journal of Engineering Sciences, Vol. 10, No. 3, pp. 1–13, 2017, doi: 10.24237/djes.2017.10301.

[28] F. H. N. Al-mamoori, M. H. N. Al-mamoori, and W. N. Najim, “Production of Structural Light-Weight Aggregate Concrete Using Different Types of Iraqi Local Crushed Materials As Coarse Aggregate,” Journal of University of Babylon, Engineering Sciences, Vol. 26, No. 1, pp. 362–375, 2018.

[29] S. M. Hama, S. M. Hama, and M. H. Mhana, “Improving Strengths of Porcelanite Aggregate Concrete by Adding Chopped Carbon Fibers,” Al-Nahrain Journal for Engineering Sciences (NJES), Vol. 21, No. 1, pp. 161–165, 2018.

[30] M. M. Jomaa’h, B. T. Kamil, and O. S. Baghabra, “Mechanical and Structural Properties of a Lightweight Concrete with Different Types of Recycling Coarse Aggregate,” Tikrit Journal of Engineering Sciences, Vol. 26, No. 1, pp. 33–40, 2019, doi: 10.25130/tjes.26.1.05.

[31] X. Jin and Z. Li, “Effects of Mineral Admixture on Properties of Young Concrete,” Journal of Materials in Civil Engineering, Vol. 15, No. 5, pp. 435–442, 2003, doi: 10.1061/(ASCE)0899-1561(2003)15:5(435).

[32] M. Mazloom, A. A. Ramezanianpour, and J. J. Brooks, “Effect of Silica Fume on Mechanical Properties of High-Strength Concrete,” Cement and Concrete Composites, Vol. 26, No. 4, pp. 347–357, 2004, doi: 10.1016/S0958-9465(03)00017-9.

[33] J. M. Justice et al., “Comparison of Two Metakaolins and a Silica Fume Used as Supplementary Cementitious Materials,” SP-228, ACI, Farmington Hills, Mich, pp. 213–236, 2005.

[34] A. R. Hariharan, A. S. Santhi, and G. M. Ganesh, “Study on Strength Development of High Strength Concrete Containing

Alccofine and Fly-Ash," International Journal of Engineering Science and Technology (IJEST), Vol. 3, No. 4, pp. 2955–2961, 2011.

[35] H. K. Ahmed and O. A. Abd, "Mechanical Properties of High Strength Concrete Containing Different Cementitious Materials," Eng. &Tech.Journal, Vol. 34, No. 1, part A, pp. 96–110, 2016.

[36] F. H. N. Al-Mamoori and A. H. N. Al-Mamoori, "Reduce the Influence of Horizontal and Vertical Cold Joints on the Behavior of High Strength Concrete Beam Casting in Hot Weather by Using Sugar Molasses," International Journal of Engineering & Technology, Vol. 7, No. 4.19, pp. 794–800, 2018, doi: 10.14419/ijet.v7i4.19.27999.

[37] F. O. Slate, A. H. Nilson, and M. Salvador, "Mechanical Properties of High - Strength Lightweight Concrete," Journal proceedings, Vol. 83, No. 4, pp. 606–613, 1986.

[38] M. H. Zhang and O. E. Gjorv, "Mechanical Properties of High-Strength Lightweight Concrete," ACI Materials Journal, Vol. 88, No. 3, pp. 240–247, 1991.

[39] A. Mor, "Steel-concrete bond in high-strength lightweight concrete," ACI Materials Journal, Vol. 89, No. 1, pp. 76–82, 1992, doi: 10.14359/1248.

[40] H. Al-Khaiat and M. N. Haque, "Effect of Initial Curing on Early Strength and Physical Properties of a Lightweight Concrete," Cement and Concrete Research, Vol. 28, No. 6, pp. 859–866, 1998.

[41] J. A. Rossignolo, M. V. C. Agnesini, and J. A. Morais, "Properties of high-performance LWAC for precast structures with Brazilian

lightweight aggregates," Cement and Concrete Composites, Vol. 25, No. 1, pp. 77–82, 2003, doi: 10.1016/S0958-9465(01)00046-4.

[42] H. Katkhuda, B. Hanayneh, and N. Shatarat, "Influence of Silica Fume on High Strength Lightweight Concrete," World Academy of Science, Engineering and Technology, Vol. 3, No. 10, pp. 407–414, 2009.

[43] H. M. Al-baghdadi, "Using Local Materials Wastes For Development Of High Strength Lightweight Concrete," Journal of Babylon University/Pure and Applied Sciences, Vol. 19, No. 1, pp. 226–239, 2011.

[44] F. Sajedi and P. Shafigh, "High-Strength Lightweight Concrete Using Leca, Silica Fume, and Limestone," Arabian Journal for Science and Engineering, Vol. 37, No. 7, pp. 1885–1893, 2012, doi: 10.1007/s13369-012-0285-3.

[45] N. M. Fawzi, K. I. Aziz, and S. M. Hama, "Effect of Metakaolin on Properties of Lightweight Porcelinate Aggregate Concrete," Journal of Engineering, Vol. 19, No. 4, pp. 439–452, 2013.

[46] H. Wei, Y. Liu, T. Wu, and X. Liu, "Effect of Aggregate Size on Strength Characteristics of High Strength Lightweight Concrete," Materials, Vol. 13, No. 6, 2020, doi: 10.3390/ma13061314.

[47] S. H. Ahmed and R. Barker, "Flexural Behavior of Reinforced High-Strength Lightweight Concrete Beams," ACI Structural Journal, Vol. 88, No. 1, pp. 69–77, 1991.

[48] S. H. Ahmed and J. Batts, "Flexural Behavior of Doubly Reinforced High-Strength Lightweight Concrete Beams with Web Reinforcement," ACI Structural Journal, Vol. 88, No. 3, pp. 351–

358, 1991.

[49] S. H. Ahmed, Y. Xie, and T. Yu, “Shear Ductility of Reinforced Lightweight Concrete Beams of Normal Strength and High strength Concrete,” Cement and Concrete Composites, Vol. 17, No. 2, pp. 147–159, 1995.

[50] ACI 318-89, “Building Code Requirements for Reinforced Concrete and Commentary.” American Concrete Institute, 1989.

[51] L. H. Sin, W. T. Huan, M. R. Islam, and M. A. Mansur, “Reinforced Lightweight Concrete Beams in Flexure,” ACI Structural Journal, Vol. 1, No. 108, pp. 3–12, 2011.

[52] R. N. F. Carmo, H. Costa, T. Simões, C. Lourenço, and D. Andrade, “Influence of Both Concrete Strength and Transverse Confinement on Bending Behavior of Reinforced LWAC Beams,” Engineering Structures, Vol. 48, pp. 329–341, 2013, doi: 10.1016/j.engstruct.2012.09.030.

[53] F. Altun and T. Haktanir, “Flexural Behavior of Composite Reinforced Concrete Elements,” Journal of Materials in Civil Engineering, Vol. 13, No. 4, pp. 255–259, 2001.

[54] M. Adil and O. A. Abdulrazzaq, “Flexural Behavior of Composite Reinforced Concrete Slabs,” Iraqi Journal of Civil Engineering, Vol. 11, No. 2, pp. 55–65, 2017.

[55] M. M. Jomaa’h, S. Ahmed, and H. M. Algburi, “Flexural Behavior of Reinforced Concrete One-Way Slabs with Different Ratios of Lightweight Coarse Aggregate,” Tikrit Journal of Engineering Sciences, Vol. 25, No. 4, pp. 36–44, 2018, doi: 10.25130/tjes.25.4.07.

[56] A. H. Adheem, L. S. Rasheed, and I. M. Ali, “Flexural Behavior of Lightweight Aggregate Concrete One-Way Slabs,” International Journal of Civil Engineering and Technology (IJCIET), Vol. 9, No. 13, pp. 277–289, 2018.

[57] J. S. Babu and J. Rex, “Experimental Investigation on Lightweight Concrete Slabs,” International Journal of Recent Technology and Engineering, Vol. 7, No. 5, pp. 502–506, 2019.

[58] W. M. Souza, T. R. G. Caetano, M. P. Ferreira, and D. R. C. Oliveira, “Shear Strength of Reinforced Concrete One-Way Ribbed Slabs,” Ibracon Structures and Material Journal, Vol. 7, No. 4, pp. 648–684, 2014.

[59] A. A. Al-Azzwi and A. J. AL-Asdi, “Nonlinear Behavior of One Way Reinforced Concrete Hollow Block Slabs,” ARPN Journal of Engineering and Applied Sciences, Vol. 12, No. 5, pp. 1679–1691, 2017.

[60] F. A. Rahman, A. A. Bakar, M. H. M. Hashim, and H. Ahmed, “Flexural Performance of Steel Fiber Reinforced Concrete (SFRC) Ribbed Slab with Various Topping Thicknesses,” Proceedings of the 3rd International Conference on Construction and Building Engineering (ICONBUILD), 2017, doi: 10.1063/1.5011493.

[61] H. Ahmad, M. H. M. Hashim, A. A. Bakar, S. H. Hamzah, and F. A. Rahman, “Flexural Strength and Behaviour of SFRSCC Ribbed Slab Under Four Point Bending,” in AIP Conference Proceedings, 2017, Vol. 1903, doi: 10.1063/1.5011494.

[62] T. A. Abdulkareem and A. A. Alfeehan, “Effect of the Rib Depth to the Overall Beam Depth Ratio in the Lightweight One-Way Ribbed Slabs,” International Journal of Engineering & Technology, Vol. 7,

No. 4.20, pp. 438–442, 2018.

[63] M. A. Farouk, “The Effect Of Cross Ribs and Rigidity Of Middle supports On The non-linear Behavior Of Ribbed Slabs,” American Journal of Engineering Research (AJER), Vol. 7, No. 1, pp. 65–77, 2018.

[64] A. O. Khaleel, “Behavior of Light Weight Aggregate Concrete Slabs with Styropor Blocks,” MSc. Thesis, Al-Nahrain University, Iraq, 2018.

[65] N. H. M. Fodzi, M. H. Mohd Hashim, and M. S. Mhd Radzi, “Testing Setup to Examine Punching Shear Strength in Self-Compacting Fibre Reinforced Concrete (SCFRC) Ribbed Slabs,” IOP Conference Series: Materials Science and Engineering, Vol. 615, 2019, doi: 10.1088/1757-899X/615/1/012095.

[66] N. H. M. Fodzi and M. H. M. Hashim, “Numerical Analysis of Punching Shear Failure of Self-Compacting Fiber Reinforced Concrete (SCFRC) Ribbed Slabs,” Materials Science Forum, Vol. 972, 2019.

[67] M. Al-Nasra et al., “Investigating the Effect of Ribs Spacing on the One Way Reinforced Concrete Ribbed Slab Strength,” Journal of Engineering and Applied Sciences, Vol. 14, No. 15, pp. 5138–5142, 2019.

[68] K. Buka-Vaivade, J. Sliseris, D. Serdjuks, G. Sahmenko, and L. Pakrastins, “Numerical Comparison of HPFRC and HPC Ribbed Slabs,” IOP Conference Series: Materials Science and Engineering, Vol. 660, No. 1, 2019, doi: 10.1088/1757-899X/660/1/012054.

[69] S. S. Abdulhussein and A. A. Alfeehan, “Experimental Study of

Depth Variation in Flanged Ribbed Lightweight Concrete Slabs," Journal of Engineering and Sustainable Development, Vol. 24, No. Special, pp. 359–364, 2020, doi: 10.31272/jeasd.conf.1.38.

[70] Z. Yanling, L. Bei, L. Huan, L. Yunsheng, and Z. Yue, "Experimental research on the dynamic responses of the steel-concrete composite beams under the harmonic forces," Procedia Engineering, Vol. 199, pp. 2997–3002, 2017, doi: 10.1016/j.proeng.2017.09.392.

[71] A. S. Mahdi and S. D. Mohammed, "Experimental and Numerical Analysis of Bubbles Distribution Influence in BubbleDeck Slab under Harmonic Load Effect," Engineering, Technology & Applied Science Research, Vol. 11, No. 1, pp. 6645–6649, 2021, doi: 10.48084/etasr.3963.

[72] Z. H. Dakhela and S. D. Mohammed, "Response of composite steel-concrete cellular beams of different concrete deck types under harmonic loads," Journal of the Mechanical Behavior of Materials, Vol. 31, No. 1, pp. 127–134, 2022, doi: 10.1515/jmbm-2022-0014.

[73] EN 197-1, "Cement - Part 1: Composition, Specifications and Conformity Criteria for Common Cements." British Standard Institution BSI, p. 50, 2011.

[74] Iraqi Specification Standard No.5/2019, "Portland Cement," Central Organization for Standardization and Quality Control, Baghdad, 2019.

[75] Iraqi Specification Standard No.45/1984, "Aggregate of Natural Sources Using in Concrete and Building," Central Organization for Standardization and Quality Control, Baghdad, 1984.

[76] ASTM C330/C330M-17a, “Standard Specification for Lightweight Aggregates for Structural Concrete,” American Society for Testing and Materials, 2017.

[77] ASTM C1240-15, “Standard Specification for Silica Fume Used in Cementitious Mixtures.” American Society for Testing and Materials, p. 7, 2015.

[78] ASTM C494/C494M-19, “Standard Specification for Chemical Admixtures for Concrete,” American Society for Testing and Materials, 2019.

[79] ASTM A496, “Standard Specification for Steel Wire, Deformed, for Concrete Reinforcement.” American Society for Testing and Materials, 2017.

[80] ASTM A615/A615M-16, “Standard Specification for Deformed and Plain Carbon-Steel Bars for Concrete Reinforcement.” American Society for Testing and Materials, p. 8, 2016.

[81] ACI 211.2-98 (Reapproved 2004), “Standard Practice for Selecting Proportions for Structural Lightweight Concrete,” American Concrete Institute, 1998.

[82] ASTM C143/C143M-15, “Standard Test Method for Slump of Hydraulic-Cement Concrete.” American Society for Testing and Materials, p. 4, 2015.

[83] ASTM C567/C567M-19, “Standard Test Method for Determining Density of Structural Lightweight Concrete,” American Society for Testing and Materials, 2019.

[84] ASTM C642-13, “Standard Test Method for Density, Absorption, and Voids in Hardened Concrete,” American Society for Testing

and Materials, West Conshohocken, PA, 2013.

[85] ASTM C39/C39M−15a, “Standard Test Method for Compressive Strength of Cylindrical Concrete Specimens,” American Society for Testing and Materials, 2015.

[86] BS 1881-Part 116, “Method for Determination of Compressive Strength of Concrete Cubes.” British Standards Institute, London, 2000.

[87] ASTM C496/C496M−17, “Standard Test Method for Splitting Tensile Strength of Cylindrical Concrete Specimens,” American Society for Testing and Materials, 2017.

[88] ASTM C78/C78M−18, “Standard Test Method for Flexural Strength of Concrete (Using Simple Beam with Third-Point Loading).” American Society for Testing and Materials, 2018.

[89] ASTM C597-16, “Standard Test Method for Pulse Velocity Through Concrete,” American Society for Testing and Materials, 2016.

[90] ASTM C1113/C1113M−09 (Reapproved 2013), “Standard Test Method for Thermal Conductivity of Refractories by Hot Wire (Platinum Resistance Thermometer Technique),” American Society for Testing and Materials, 2013.

[91] Quick Thermal Conductivity Meter (QTM-500), “Operation Manual.” .

[92] ASTM F710−19, “Standard Practice for Preparing Concrete Floors to Receive Resilient Flooring.” American Society for Testing and Materials, p. 8, 2019.

[93] V. Kumar, “Protection of Steel Reinforcement for Concrete: A

Review," Corrosion Reviews. pp. 317–358, 1998, doi: 10.1515/CORRREV.1998.16.4.317.

[94] M. M. Kadhum, "Studying of Some Mechanical Properties of Reactive Powder Concrete Using Local Materials," Engineering Journal, Vol. 21, No. 7, pp. 113–135, 2015.

[95] M. K. Maroliya and C. D. Modhera, "A Comparative Study of Reactive Powder Concrete Containing Steel Fibers and Recron 3S Fibers," Journal of Engineering Research and Studies, Vol. I, No. I, pp. 83–89, 2010.

[96] IS 13311-1, "Non-destructive testing of concrete methods of test. part 1." Bureau of Indian Standards, 1992.

[97] P. Sukontasukkul, "Use of Crumb Rubber to Improve Thermal and Sound Properties of Pre-Cast Concrete Panel," Construction and Building Materials, Vol. 23, No. 2, pp. 1084–1092, 2009, doi: 10.1016/j.conbuildmat.2008.05.021.

[98] Y. K. Yousif, "A Proposed New Formula to Determine the Sound Insulation of Concrete Walls," Anbar Journal of Engineering Sciences, Vol. 2, No. 2, pp. 117–128, 2009.

[99] H. K. Ahmed, W. A. Abbas, and D. M. Abdul-Razzaq, "Effect of Plastic Fibers on Properties of Foamed Concrete," Engineering & Technology Journal, Vol. 31, Part A, No. 7, pp. 1313–1330, 2013.

[100] N. M. Fawzi, "Properties of Lightweight Concrete with A View to Thermal Insulation and Acoustic Impedance." M.Sc. Thesis, University of Baghdad, Iraq, 1997.

[101] S. R. Jeffrey, Prestrectives in Civil Engineering. ASCE Publications, 2003.

[102] A. A. Al-Azzawi and A. J. Al-Asdi, “Behavior of one way reinforced concrete slabs with styropor blocks,” Advances in Concrete Construction, Vol. 5, No. 5, pp. 451–468, 2017, doi: 10.12989/acc.2017.5.5.451.

[103] M. J. N. Priestly and R. Park, “Strength and Ductility of Concrete Bridge Columns Under Seismic Loading,” ACI Structural Journal, Vol. 84, No. 1, pp. 61–76, 1987.

[104] Akmaluddin, Pathurahman, Suparjo, and Z. Gazalba, “Flexural Behavior of Steel Reinforced Lightweight Concrete Slab with Bamboo Permanent Formworks,” Procedia Engineering, Vol. 125, pp. 865–872, 2015, doi: 10.1016/j.proeng.2015.11.054.

[105] S. Alasadi, P. Shafigh, and Z. Ibrahim, “Experimental Study on the Flexural Behavior of Over Reinforced Concrete Beams Bolted with Compression Steel Plate: Part I,” Applied Sciences, Vol. 10, No. 3, 2020, doi: 10.3390/app10030822.

[106] W. A. Tameemi, “Behavior of Two-Way Hollow Core High Strength Self-Compacting Reinforced Concrete Slabs Under Repeated Loading,” Ph.D. Dissertation, Babylon University, Iraq, 2020.

[107] M. H. M. Al-Sherrawi and G. A. Fadhil, “Effect of Stiffeners on Shear Lag in Steel Box Girders,” Al-Khwarizmi Engineering Journal, Vol. 8, No. 2, pp. 63–76, 2012.

[108] ACI 544.4R-18, “Guide to Design with Fiber-Reinforced Concrete.” ACI Concrete Institute, p. 37, 2018.

[109] P. Glavič and R. Lukman, “Review of sustainability terms and their definitions,” Journal of Cleaner Production, Vol. 15, No. 18, pp.

1875–1885, 2007, doi: 10.1016/j.jclepro.2006.12.006.

[110] R. Kumar, N. Shafiq, A. Kumar, and A. A. Jhatial, “Investigating Embodied Carbon, Mechanical Properties, and Durability of High-Performance Concrete Using Ternary and Quaternary Blends of Metakaolin, Nano-Silica, and Fly Ash,” Environmental Science and Pollution Research, Vol. 28, No. 35, 2021, doi: 10.1007/s11356-021-13918-2.

[111] A. Kumar, N. Bheel, I. Ahmed, S. H. Rizvi, R. Kumar, and A. A. Jhatial, “Effect of Silica Fume and Fly Ash As Cementitious Material on Hardened Properties and Embodied Carbon of Roller Compacted Concrete,” Environmental Science and Pollution Research, Vol. 29, No. 1, pp. 1210–22, 2021, doi: 10.1007/s11356-021-15734-0.

[112] Q. Zhu, “CO_2 Abatement in the Cement Industry.” IEA Clean Coal Centre, 2011.

[113] L. K. Turner and F. G. Collins, “Carbon Dioxide Equivalent (CO_2-e) Emissions : A Comparison Between Geopolymer and OPC Cement Concrete,” Construction and Building Materials, Vol. 43, pp. 125–130, 2013, doi: 10.1016/j.conbuildmat.2013.01.023.

[114] F. Ameri, S. A. Zareei, and B. Behforouz, “Zero-Cement VS. Cementitious Mortars: An Experimental Comparative Study on Engineering and Environmental Properties,” Journal of Building Engineering, Vol. 32, 2020, doi: 10.1016/j.jobe.2020.101620.

[115] K.-H. Yang, J.-K. Song, and K.-I. Song, “Assessment of CO_2 Reduction of Alkali-Activated Concrete,” Journal of Cleaner Production, Vol. 39, pp. 265–272, 2013, doi: 10.1016/j.jclepro.2012.08.001.

[116] S.-W. Kim, S.-J. Jang, D.-H. Kang, K.-L. Ahn, and H.-D. Yun, “Mechanical Properties and Eco-Efficiency of Steel Fiber Reinforced Alkali-Activated Slag Concrete,” Materials, Vol. 8, No. 11, pp. 7309–7321, 2015, doi: 10.3390/ma8115383.

[117] Q. W. Ahmed, “Punching Shear Behavior of Lightweight Fiber Reinforced Concrete Slabs,” Diyala Journal of Engineering Sciences, Vol. 9, No. 01, pp. 55–66, 2016.

[118] B. M. Das and G. V. Ramana, Principles of Soil Dynamics, Second Edi. USA: Stamford, CT 06902, 2011.

[119] ABAQUS Version 6.13, “Analysis User‟s Manual,” 2013.

[120] K. Hibbitt, B. I. Karlsson, and E. P. Sorenson, ABAQUS/Standard theory manual. Sorenson Inc, 2016.

[121] C. A. Issa and R. A. Izadifard, “Numerical simulation of the experimental behavior of RC beams at elevated temperatures,” Advanced Modeling and Simulation in Engineering Sciences, Vol. 8, No. 1, pp. 1–17, 2021, doi: 10.1186/s40323-021-00198-1.

[122] T. Yu, J. G. Teng, Y. L. Wong, and S. L. Dong, “Finite element modeling of confined concrete-II: Plastic-damage model,” Engineering Structures, Vol. 32, No. 3, pp. 680–691, 2010, doi: 10.1016/j.engstruct.2009.11.013.

[123] A. S. Genikomsou and M. A. Polak, “Finite Element Analysis of Punching Shear of Concrete Slabs Using Damaged Plasticity Model in ABAQUS,” Engineering Structures, Vol. 98, pp. 38–48, 2015, doi: 10.1016/j.engstruct.2015.04.016.

[124] L. M. Al-Shather, A. A. Ali, and H. M. Abed, “The Shear Behavior of Reinforced Concrete I–Beams With Polypropylene Fibers,” Al-

Nahrain Journal for Engineering Sciences (NJES), Vol. 20, No. 5, pp. 1040–1046, 2017.

[125] T. Wang and T. T. C. Hsu, “Nonlinear Finite Element Analysis of Concrete Structures Using New Constitutive Models,” Computers and Structures, Vol. 79, No. 32, pp. 2781–2791, 2001, doi: 10.1016/S0045-7949(01)00157-2.

[126] P. Kmiecik and M. Kamiński, “Modelling of Reinforced Concrete Structures and Composite Structures with Concrete Strength Degradation Taken Into Consideration,” Archives of Civil and Mechanical Engineering, Vol. XI, No. 3, pp. 623–636, 2011, doi: 10.1016/s1644-9665(12)60105-8.

[127] L. Chen and B. A. Graybeal, “Modeling Structural Performance of Ultrahigh Performance Concrete I-Girders,” Journal of Bridge Engineering, Vol. 17, No. 5, pp. 754–764, 2012, doi: 10.1061/(asce)be.1943-5592.0000305.

Appendix A

Summary of Materials Properties

Appendix A: Summary of Materials Properties

A.1 Cement Properties

Table (A-1): Cement's chemical and physical test results

Chemical properties			
Oxide Composition	**Oxide content %**	**Limit of IQS No.5/1984**	**Limit of (EN 197-1:2011)**
SiO_2	19.64	----	----
Al_2O_3	5.50	----	----
Fe_2O_3	4.32	----	----
CaO	61.51	----	----
MgO	1.50	≤ 5%	----
SO_3	2.20	≤ 2.5%	4%
Loss on Ignition	3.5	≤ 4.0%	----
Insoluble Residue	1.26	≤ 1.5%	5% Max
L.S. F	0.92	1.02-0.66	----
The main components			
C3S	48.01	----	
C2S	19.33	----	
C3A	8.27	----	
C4AF	13.15	----	
Physical Properties			
Property	**Test Result**	**Limit of (EN 197-1:2011)**	
Specific Gravity	3.15	----	
Fineness (Blaine) cm^2/gm	314	----	
Setting time, (hour: min) Initial Final	 0:90 3:13	 ≥ 60 min ----	
Soundness (Autoclave method) %	0.61	≤ 10mm	
Compressive Strength at: 2 Days (MPa) 7 Days (MPa)	 21 25.79	 ≥ 20.00 ≥ 23.00	

*According to the testing certification.

A.2 Aggregate Properties

Table (A-2): Grading and properties of fine aggregate

Sieve size (mm)	Passing%	I.Q.S.45:1984 Limits Zone (2)
10	100	100
4.75	98	90-100
2.36	89	75-100
1.18	75	55-90
0.60	46	35-59
0.30	10	8-30
0.15	1	0-10
Physical and Chemical Properties		
Property	**Test Result**	**I.Q.S.45:1984 Limits**
Fineness modulus	2.81	----
Specific Gravity	2.60	----
Absorption %	2	----
Sulphate content (SO_3) %	0.21*	5%≤

*According to the testing certification.

Table (A-3): Grading and properties of coarse aggregate (gravel)

Sieve size (mm)	% Passing	I.Q.S.45:1984 Limits
14	100	100
10	98	85-100
5	14	0-25
2.36	4	0-5
Physical and Chemical Properties		
Properties	**Test Result**	**I.Q.S.45:1984 Limits**
Loose Density (kg/m^3)	1570	----
Specific Gravity	2.65	----
Sulphate content (SO_3) (%)	0.03*	≤ 1.0%
Absorption (%)	0.6	----

*According to the testing certification.

Table (A-4): Grading and properties of coarse aggregate (Pumice Stone)

Sieve size (mm)	% Passing	ASTM C330 Limits
12.5	100	100
9.5	99	80-100
4.75	24	5-40
2.36	2	0-20
1.18	1	0-10
Chemical and Physical Properties		
Properties	**Test Result**	**ASTM C330 Limits**
Loose Density (kg/m^3)	708	Max. 880
Absorption (%)	22	----

A.3 Sugar Molasses

Table (A-5): Chemical analysis of Sugar Molasses [36]

Test	Test Result
Brix	83
pH	5.37
Ash	9.4%
Reducing Sugar (R. S)	12.1%
Total Reducing Sugar (TR. S)	71.2%
Sucrose	59.1%

A.4 Steel Fiber

Table (A-6): Physical characteristics of steel fibers

Property	Test Result
Density	7800 kg/m^3
Tensile Strength	1100 MPa
Form	Hooked End
Length	35 mm
Diameter	0.5 mm
Aspect Ratio	70

*According to the certification of the manufacturer.

A.5 Silica Fume

The Manufacture Company Catalogue of Silica Fume MegaAdd Ms(D).

Construction Chemicals

CON MIX

MegaAdd MS(D)

Densified Microsilica

DESCRIPTION

MegaAdd MS(D) is a very fine pozzolanic, ready to use high performance mineral additive for use in concrete. It acts physically to optimize particle packing of the concrete or mortar mixture and chemically as a highly reactive pozzolan.
MegaAdd MS(D) in contact with water, goes into solution within an hour. The silica in solution forms an amorphous silica rich, calcium poor gel on the surface of the silica fume particles and agglomerates. After time the silica rich calcium poor coating dissolves and the agglomerates of silica fume react with free lime ($CaOH_2$) to form calcium silicate hydrates (CSH). This is the pozzolanic reaction in cementitious system.

STANDARDS

ASTM C1240

USES

MegaAdd MS(D) can be used in a variety of applications such as concrete, grouts, mortars, fibre cement products, refractory, oil/gas well cements, ceramics, elastomer, polymer applications and all cement related products.

ADVANTAGES

- High to ultra high strength
- High resistance to chlorides and sulfates
- Protection against corrosion
- Increased durability, longer service life for structures
- Enhanced rheology, control of mixture segregation and bleed
- Greater resistance to chemicals

TYPICAL PROPERTIES at 25°C

PROPERTY	TEST METHOD	VALUE
State	Amorphous	Sub-micron powder
Colour	-	Grey to medium grey powder
Specific Gravity	-	2.10 to 2.40
Bulk Density	-	500 to 700 kg/m³
Chemical Requirements		
Silicon Dioxide (SiO_2)	-	Minimum 85%
Moisture Content (H_2O)	-	Maximum 3%
Loss on Ignition (LOI)	-	Maximum 6%
Physical Requirements		
Specifi Surface Area	-	Minimum 15 m²/g
Pozzolanic Activity Index, 7 days	-	Maximum 105% of control
Over size particles retained on 45 micron sieve	-	Maximum 10%

COMPATIBILITY

MegaAdd MS(D) is suitable for use with all types of cement and cementitious materials.
With Admixtures :
MegaAdd MS(D) is compatible to use with all types of water reducing plasticisers / superplasticisers and polycarboxylate based superplasticiser.

DOSAGE

The normal dosage of **MegaAdd MS(D)** is 5 - 8% by weight of cement, but it can be used upto 10%. Site trials should be carried out to establish the optimum dosage for the mix to be used as the dosage varies depending on application.

MegaAdd MS(D)

BATCHING	Batch **MegaAdd MS(D)** into the concrete mixer and mix thoroughly with the other mixture ingredients, adopting a procedure that ensures full dispersion of the product.	
PACK SIZE	600 Kgs and 1200 Kgs Jumbo bags	
GENERAL INFORMATION	**Shelf Life**	12 months from date of manufacture when stored under warehouse conditions in original unopened packing. Extreme temperature / humidity may reduce shelf life.
	Cleaning	Clean all equipments and tools with water immediately after use.
HEALTH and SAFETY	**PPE's**	Gloves, goggles and suitable mask must be worn.
	Precautions	Contact with skin, eyes, etc. must be avoided.
	Hazard	Regarded as non-hazardous for transportation.
	Disposal	Do not reuse bags. To be disposed off as per local rules and regulations.
	Additional Information	Refer MSDS. (Available on request.)
TECHNICAL SERVICE	**CONMIX Technical Services** are available on request for onsite support to assist in the correct use of its products.	

MSASA
Construction Solutions for Africa

CAPE TOWN
Tel: +27 (0)87 231 0253
Unit 5 | M5 Freeway Park
Upper Camp Rd | Maitland | 7405
Cape Town | South Africa

JOHANNESBURG
Tel: +27 (0)82 785 8529
64 Maple Street | Pomona
Kempton Park | Johannesburg | 1619
South Africa

Email: info@msasa.co.za | www.msasa.co.za

Manufacturer:
CONMIX LTD.
P.O. Box 5556, Sharjah
United Arab Emirates
Tel: +971 6 5314155
Fax: +971 6 5314332
Email: conmix@conmix.com

Sales Office:
Tel: +971 6 5883422
Fax: +971 6 5881442
www.conmix.com

A.6 Sika ®ViscoCrete ®– 5930L IQ

The Manufacture Company Catalogue of Sika® ViscoCrete® 5930-L IQ

PRODUCT DATA SHEET

Sika® ViscoCrete®-5930 L IQ

HIGH RANGE WATER REDUCING ADMIXTURE

DESCRIPTION

Sika® ViscoCrete®-5930 L IQ is a High range water reducing and super plasticizing admixture for Concrete & Mortar utilizing Sika's 'ViscoCrete®' polycarboxylate polymer technology (3rd Generation) .

USES

Sika® ViscoCrete®-5930 L IQ is mainly used for the following applications:
1- Concrete Containing GGBS , Micro Silica , Fly ash , ... Etc.
2- Production of Ready Mixed Concrete, High performance Concrete .
3- Impermeable & dense Concrete with smooth surface , Water tight mix design proportion must be considered.
4- Production of Self-compacting Concrete (SCC) , SCC mix design proportion must be considered.
5- Production of complex & fine elements such as Slabs , Foundations , Walls , Beams & Columns even through congested reinforcement .

CHARACTERISTICS / ADVANTAGES

Sika® ViscoCrete®-5930 L IQ is a powerful superplasticizer which acts through several different mechanisms including surface adsorption and sterically effects separating the cementitious binder particles. The following advantages properties are achieved:
1- High water reduction, resulting in high density, high strength and reduced permeability
2- Superior plasticizing effect, resulting in improved flow, placing and compaction characteristics
3- Reduced shrinkage during curing and reduced creep when hardened .
4- Chloride Free thus; no corrosion effect on steel.
5- Reduced rate of carbonation of the Concrete .
6- NO need for vibration , thus NO noise pollution .
7- Suitable for Winter conditions .

APPROVALS / CERTIFICATES

Sika® ViscoCrete®-5930 L IQ meets the requirements of ASTM C-494 Types F.

PRODUCT INFORMATION

Composition	Aqueous solution of modified polycarboxylates
Packaging	Bulk Deliveries 1000 Kgs IBC 20 kg Pail
Appearance / Colour	Brownish liquid
Shelf life	12 months from date of production if stored properly in undamaged un-opened, original sealed packaging.
Storage conditions	In dry conditions at temperatures between +5°C and +35°C. Protect from direct sunlight. It requires recirculation when held in storage for extended periods.
Specific gravity	1.085 ± (0.01) g/cm3
pH-Value	4 - 6
Total chloride ion content	Nil

TECHNICAL INFORMATION

Concreting guidance	The standard rules of good concreting practice, concerning production and placing, are to be followed. Laboratory trials shall be carried out before concreting on site, especially when using a new mix design or producing new concrete components. Fresh concrete must be cured properly and curing applied as early as possible.

APPLICATION INFORMATION

Recommended dosage	Recommended dosage for concrete: 1- For plastic Concrete (0.2 - 0.8 %) by weight of Binder (200 - 800 gm) for 100 kg cement . 2- For Flow & Self Compacting Concrete (0.8 - 1.8 %) by weight of Binder (800 - 1800 gm) for 100 kg cement . 3- Optimum dosage should be determined by site trials. When adjusting the consistency , high water reduction property of the ad-mixture must be taken in consideration , excessive water addition must be prevented .
Compatibility	Sika® ViscoCrete®-5930 L IQ can be used in conjunction with : 1- SikaFiber® 2- Sika®PlastoCrete-N 3- Sika®Antifreeze 4- SikaRapid® 5- SikaRetarder® All admixtures must be added separately. Trials are always recommended before combining products . For additional information, please contact Sika technical personnel.
Dispensing	Sika® ViscoCrete®-5930 L IQ is added to the gauging water or added with it into the concrete mixer. To take advantage of the high water reduction, a wet mixing time, which is depending on the mixing conditions and mixer performance, of at least 2 mins. per cubic meter after the admixture addi-tion is recommended. Sika® ViscoCrete®-5930 L IQ shall not be added to dry cement.
Restrictions	Over dosage effect An over dosage of Sika® ViscoCrete®-5930 L IQ with water excess will cause the following : 1- Increase of air entrainment . 2- Bleeding or Segregation .

BASIS OF PRODUCT DATA

All technical data stated in this Product Data Sheet are based on laboratory tests. Actual measured data may vary due to circumstances beyond our control.

IMPORTANT CONSIDERATIONS

When using Sika® ViscoCrete®-5930 L IQ the following points should be taken in consideration :
1- A suitable mix design has to be taken into account and local material sources shall be trialed.
2- Do not use with naphthalene based admixtures.

ECOLOGY, HEALTH AND SAFETY

For information and advice on the safe handling, storage and disposal of chemical products, users shall refer to the most recent Safety Data Sheet (SDS) containing physical, ecological, toxicological and other safety-related data.

APPLICATION INSTRUCTIONS

Application Method / Tools :
The standard rules of good concreting practice , concerning production as well as placing are to be followed , refer to relevant standards . Fresh Concrete must be cured properly .
Cleaning of tools :
Clean all tools & application equipment with water immediately after use .
Hardened / Cured material can only be mechanically removed .

LOCAL RESTRICTIONS

Please note that as a result of specific local regulations the declared data for this product may vary from country to country. Please consult the local Product Data Sheet for the exact product data.

LEGAL NOTES

The information, and, in particular, the recommendations relating to the application and end-use of Sika products, are given in good faith based on Sika's current knowledge and experience of the products when properly stored, handled and applied under normal conditions in accordance with Sika's recommendations. In practice, the differences in materials, substrates and actual site conditions are such that no warranty in respect of merchantability or of fitness for a particular purpose, nor any liability arising out of any legal relationship whatsoever, can be inferred either from this information, or from any written recommendations, or from any other advice offered. The user of the product must test the product's suitability for the intended application and purpose. Sika reserves the right to change the properties of its products. The proprietary rights of third parties must be observed. All orders are accepted subject to our current terms of sale and delivery. Users must always refer to the most recent issue of the local Product Data Sheet for the product concerned, copies of which will be supplied on request.

Sika Iraq (Sika Trading L.L.C.)
Erbil / Baghdad / Basra
Tel: +96 477 303 74451
info@iq.sika.com
irq.sika.com

Appendix B

Theoretical Calculations

Appendix B: Theoretical Calculations

One-Way Ribbed Slab

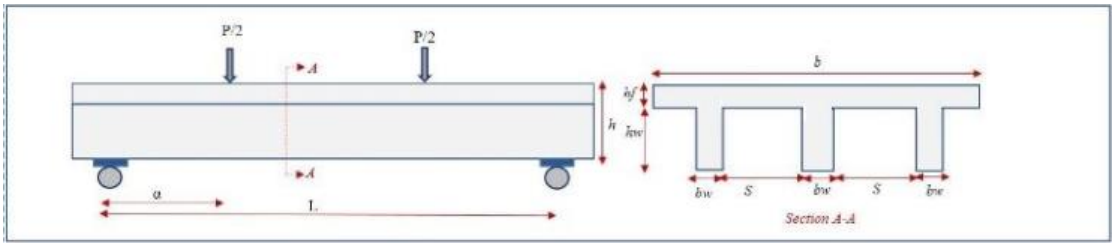

Figure (B-1) Geometry of Ribbed Slab

Input Data

Compressive Strength	$f'_c := 42.2\ MPa$	Width of Slab	$b := 900\ mm$
Depth of Rib	$h_w := 100\ mm$	Width of Rib	$b_w := 100\ mm$
Density of Concrete	$\gamma_c := 19.43\ \frac{kN}{m^3}$	Effective Span	$L := 1800\ mm$
Unit Weight of Concrete	$w_c := 1943\ \frac{kg}{m^3}$	Overall Depth	$h := 150\ mm$
Number of Ribs	$n_{rib} := 3$	Thickness of Slab	$h_f := 50\ mm$
Slab Length	$L_t := 2000\ mm$	Shear Span	$\alpha := 600\ mm$
Max. Conc. Strain at Comp. Fiber	$\varepsilon_{cu} := 0.003$	Volume Fraction of Steel Fiber	$V_f := 0\%$
Bond Efficiency of fiber	$F_{be} := 0$	Aspect Ratio of Steel Fibers	$\Lambda := 0\ \frac{mm}{mm}$
Modulus of Elasticity	$E_c := 23924\ MPa$	Modulus of Rupture	$f_r := 3.5\ MPa$

Diameter of Reinforcement Bar of Rib	$d_{brib} := 8\ mm$
Diameter of Stirrups Reinforcement Bar	$d_s := 6\ mm$
Diameter of shrinkage Reinforcement	$d_{shr.} := 6\ mm$
Yield Stress of Reinforcement Bar of Ribs	$f_y := 509\ MPa$
Yield Stress of Stirrups Reinforcement Bar	$f_{ys} := 495\ MPa$
Yield Stress of Shrinkage Reinforcement Bar	$f_{ysh} := 495\ MPa$
Elastic Modulus of Steel Reinforcement Bar	$E_s := 200000\ MPa$
Number of Main Reinforcement Bar / Rib	$n_b := 2$
Clear Concrete Cover	$C_c := 20\ mm$
Tensile Stress of Steel Fibers	$f_f := 0\ MPa$

Output Data

"β_1" Calculation

$$\beta_1 := \begin{cases} 0.85 & \text{if } 17\ MPa \le f'_c \le 28\ MPa \\ 0.65 & \text{else if } f'_c \ge 55\ MPa \\ \left(0.85 - \left(\left(\frac{f'_c - 28\ MPa}{7\ MPa}\right) \cdot 0.05\right)\right) & \text{else} \end{cases}$$

$\beta_1 = 0.75$

Calculation of Compression Block Depth

$$A_{s1} := \frac{\pi}{4} \cdot (d_{brib})^2 \cdot n_b \cdot n_{rib}$$

$A_{s1} = 301.59\ mm^2$

$$d_t := h - C_c - d_s - 0.5 \cdot d_{brib}$$

$d_t = 120\ mm$

$$\sigma_t := 0.772\ MPa \cdot \Lambda \cdot V_f \cdot F_{be}$$

$\sigma_t = 0\ MPa$

$$\varepsilon_f := \frac{f_f}{200000\ MPa}$$

$$a := \frac{A_{s1} \cdot f_y}{0.85 \cdot f'_c \cdot b}$$

$a = 4.76\ mm$

$$e := (\varepsilon_f + 0.003)\left(\frac{a}{\beta_1 \cdot 0.003}\right)$$

$e = 6.35\ mm$

Calculation of Loads

Self-Weight Load on Slab $W_{dslab} := (h_f \cdot \gamma_c)$

$W_{dslab} = 0.97\ kPa$

Self-Weight Load on Rib $W_{drib} := (b \cdot h_f \cdot \gamma_c + b_w \cdot n_{rib} \cdot h_w \cdot \gamma_c)$

$W_{drib} = 1.46\ \frac{kN}{m}$

$$W_{total} := W_{drib} \cdot L_t$$

$W_{total} = 2.91\ kN$

Calculation of Modification Factor λ

$$\lambda := \begin{cases} 0.75 & \text{if } w_c \le 1600 \ \frac{kg}{m^3} \\ \frac{0.0075}{16} \ \frac{m^3}{kg} \cdot w_c & \text{else if } 1600 \ \frac{kg}{m^3} < w_c \le 2160 \ \frac{kg}{m^3} \\ 1.0 & \text{else} \end{cases}$$

$\lambda = 0.91$

Calculation of Shear and Moment Capacity

Calculation Ultimate Load Capacity

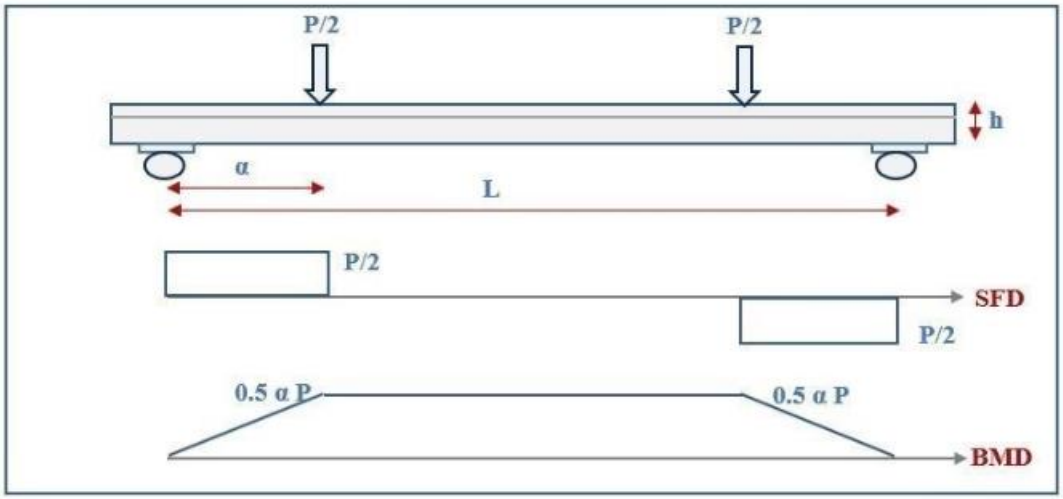

Figure (B-2) Moment and Shear Diagram

Flexural Capacity

$$M_n := A_{s1} \cdot f_y \cdot \left(d_t - \frac{a}{2}\right) + \sigma_t \cdot b \cdot (h - e) \cdot \left(\frac{h}{2} + \frac{e}{2} - \frac{a}{2}\right)$$

$M_n = 18.06 \ kN \cdot m$

$Mext. := M_n$

$Mext. = 18.06 \ kN \cdot m$

$P_n := M_n \cdot \frac{2}{\alpha}$

$P_n = 60.19 \ kN$

Shear Capacity

$$V_c := 0.17 \cdot \lambda \cdot \sqrt{\frac{f'_c}{MPa}} \cdot MPa \cdot b_w \cdot d_t \cdot n_{rib} \cdot 1.1 \qquad V_c = 39.83\ kN$$

$$A_v := 2 \cdot \frac{\pi}{4} \cdot (d_s)^2 \qquad A_v = 56.55\ mm^2$$

$$S_{str.} := 60\ mm$$

$$V_s := A_v \cdot f_{ys} \cdot \frac{d_t}{S_{str.}} \cdot n_{rib} \qquad V_s = 167.95\ kN$$

$$V_n := V_c + V_s \qquad P_{ns} := 2 \cdot V_n \qquad P_{ns} = 415.56\ kN$$

Calculation of Cracking Moment

$$y_t := \frac{b \cdot h_f \cdot (0.5 \cdot h_f) + (b_w \cdot h_w \cdot (0.5 \cdot h_w + h_f)) \cdot n_{rib}}{(b \cdot h_f) + (b_w \cdot (h - h_f) \cdot n_{rib})} \qquad y_t = 55\ mm$$

$$y_b := h - y_t \qquad y_b = 95\ mm$$

$$I_g := \begin{cases} \dfrac{b \cdot y_t^{\,3}}{3} + \dfrac{(b - (b_w \cdot n_{rib})) \cdot (h_f - y_t)^3}{3} + \dfrac{(b - (b_w \cdot n_{rib})) \cdot (y_b)^3}{3} & \text{if } y_t \le h_f \\ \dfrac{b \cdot y_t^{\,3}}{3} + \dfrac{b_w \cdot n_{rib} \cdot y_b^{\,3}}{3} - \dfrac{(b - (b_w \cdot n_{rib})) \cdot (y_t - h_f)^3}{3} & \text{else} \end{cases} \qquad I_g = (1.3563 \cdot 10^8)\ mm^4$$

$$M_{cr} := \frac{f_r \cdot I_g}{y_b} \qquad M_{cr} = 5\ kN \cdot m$$

$$P_{cr} := \left(M_{cr} - \frac{W_{drib} \cdot L^2}{8}\right) \cdot \frac{2}{\alpha} \qquad P_{cr} = 14.69\ kN$$

Calculation of Natural Frequency

$$M := 306.25\ kg$$

$$\aleph := \pi$$ For simply support equal to π and to 4.73 for fixed support

$$f_n := \frac{\aleph^2}{2\ \pi} \cdot \sqrt{\frac{E_c \cdot I_g}{M \cdot L^3}} \qquad f_n = 66.95\ Hz$$

One-Way Solid Slab

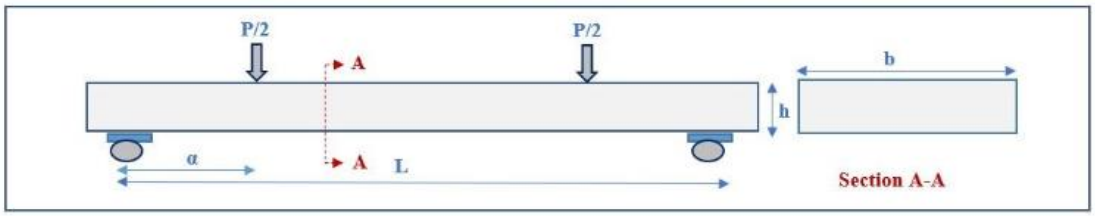

Figure (B-3) Geometry of Solid Slab

Input Data

Compressive Strength	$f'_c := 42.2\ MPa$	Width of Slab	$b := 900\ mm$
Density of Concrete	$\gamma_c := 19.43\ \frac{kN}{m^3}$	Effective Span	$L := 1800\ mm$
Unit Weight of Concrete	$w_c := 1943\ \frac{kg}{m^3}$	Thickness of Slab	$h := 83\ mm$
Slab Length	$L_t := 2000\ mm$	Shear Span	$\alpha := 600\ mm$
Max. Conc. Strain at Comp. Fiber	$\varepsilon_{cu} := 0.003$	Modulus of Rupture	$f_r := 3.5\ MPa$
Modulus of Elasticity	$E_c := 23924\ MPa$		

Diameter of Main Reinforcement Bar	$d_b := 8\ mm$
Yield Stress of Main Reinforcement	$f_y := 509\ MPa$
Elastic Modulus of Steel Reinforcement Bar	$E_s := 200000\ MPa$
Number of Main Reinforcement Bar	$n_b := 6$
Clear Concrete Cover	$C_c := 20\ mm$

Output Data

"β_1" Calculation

$$\beta_1 := \begin{cases} 0.85 & \text{if } 17\ MPa \le f'_c \le 28\ MPa \\ 0.65 & \text{else if } f'_c \ge 55\ MPa \\ \left(0.85 - \left(\left(\frac{f'_c - 28\ MPa}{7\ MPa}\right) \cdot 0.05\right)\right) & \text{else} \end{cases}$$

$\beta_1 = 0.75$

Calculation of Compression Block Depth

$$A_{s1} := \frac{\pi}{4} \cdot (d_b)^2 \cdot n_b$$

$A_{s1} = 301.59\ mm^2$

$$d_t := h - C_c - 0.5 \cdot d_b$$

$d_t = 59\ mm$

$$a := \frac{A_{s1} \cdot f_y}{0.85 \cdot f'_c \cdot b}$$

$a = 4.76\ mm$

Calculation of Loads

Self-Weight Load on Slab $W_{dslab} := (h \cdot \gamma_c \cdot b)$

$W_{dslab} = 1.45\ \frac{kN}{m}$

Calculation of Modification Factor λ

$$\lambda := \begin{cases} 0.75 & \text{if } w_c \le 1600\ \frac{kg}{m^3} \\ \frac{0.0075}{16}\ \frac{m^3}{kg} \cdot w_c & \text{else if } 1600\ \frac{kg}{m^3} < w_c \le 2160\ \frac{kg}{m^3} \\ 1.0 & \text{else} \end{cases}$$

$\lambda = 0.91$

Calculation of Shear and Moment Capacity

Calculation Ultimate Load Capacity

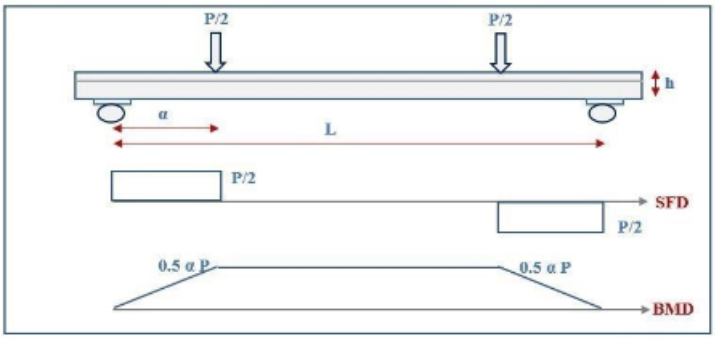

Figure (B-4) Moment and Shear Diagram

Flexure Capacity

$M_n := A_{s1} \cdot f_y \cdot \left(d_t - \frac{a}{2}\right)$ $M_n = 8.69\ kN \cdot m$

$Mext. := M_n$ $P_n := M_n \cdot \frac{2}{\alpha}$ $P_n = 28.97\ kN$

Shear Capacity

$V_c := 0.17 \cdot \lambda \cdot \sqrt{\frac{f'_c}{MPa}} \cdot MPa \cdot b \cdot d_t$ $V_c = 53.41\ kN$

$V_n := V_c$ $V_n = 53.41\ kN$

$P_{ns} := 2 \cdot V_n$ $P_{ns} = 106.82\ kN$

Calculation of Cracking Moment

$y_t := \frac{h}{2}$ $y_b := h - y_t$ $y_b = 41.5\ mm$

$I_g := \frac{b \cdot h^3}{12}$ $I_g = \left(4.29 \cdot 10^7\right)\ mm^4$

$M_{cr} := \frac{f_r \cdot I_g}{y_b}$ $P_{cr} := \left(M_{cr} - \frac{W_{dslab} \cdot L^2}{8}\right) \cdot \frac{2}{\alpha}$ $P_{cr} = 10.1\ kN$

Calculation of Natural Frequency

$M := 300.15\ kg$ $\aleph := \pi$ For simply support equal to π and to 4.73 for fixed support

$f_n := \frac{\aleph^2}{2\ \pi} \cdot \sqrt{\frac{E_c \cdot I_g}{M \cdot L^3}}$ $f_n = 38.03\ Hz$

Appendix C

Devices Specifications

Appendix C: Device Specifications

C.1 Data Acquisition System Type NI

Chassis Description

Figures 1-1 and 1-2 show the key features of the NI PXIe-1062Q chassis front and back panels. Figure 1-1 shows the front view of the NI PXIe-1062Q. Figure 1-2 shows the rear view of the NI PXIe-1062Q.

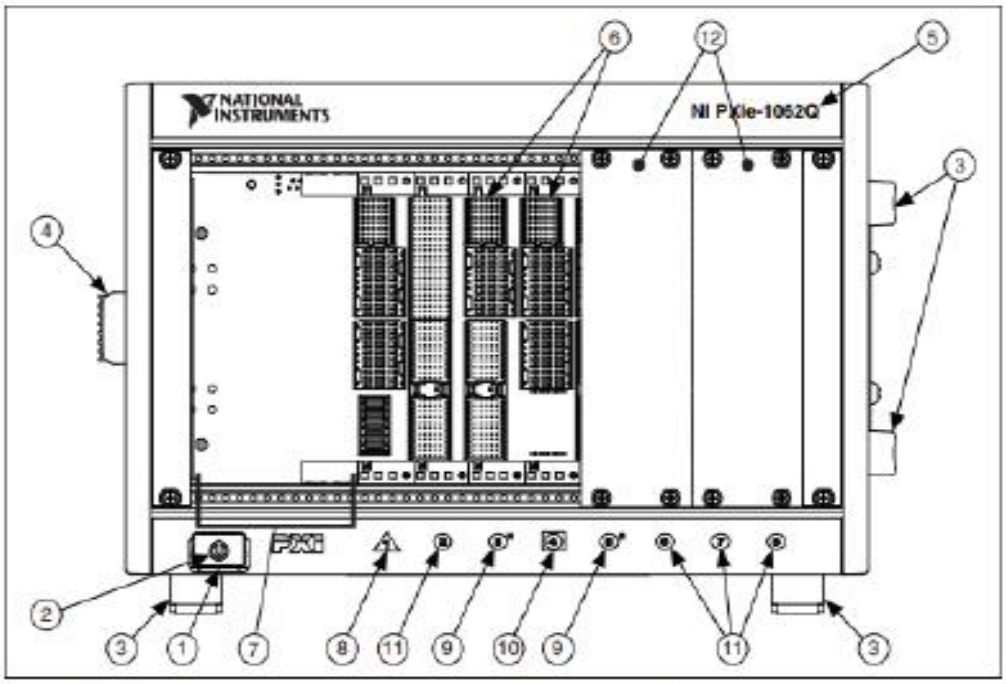

1 Power Inhibit Switch
2 Power Inhibit Switch LED
3 Removable Foot
4 Chassis Carry Handle
5 Chassis Model Name
6 Backplane Connectors
7 System Controller Expansion Slots
8 PXI Express System Controller Slot
9 PXI Express Hybrid Peripheral Slots
10 PXI Express System Timing Slot
11 PXI Peripheral Slot
12 PXI Filler Panels

Figure 1-1. Front View of the NI PXIe-1062Q Chassis

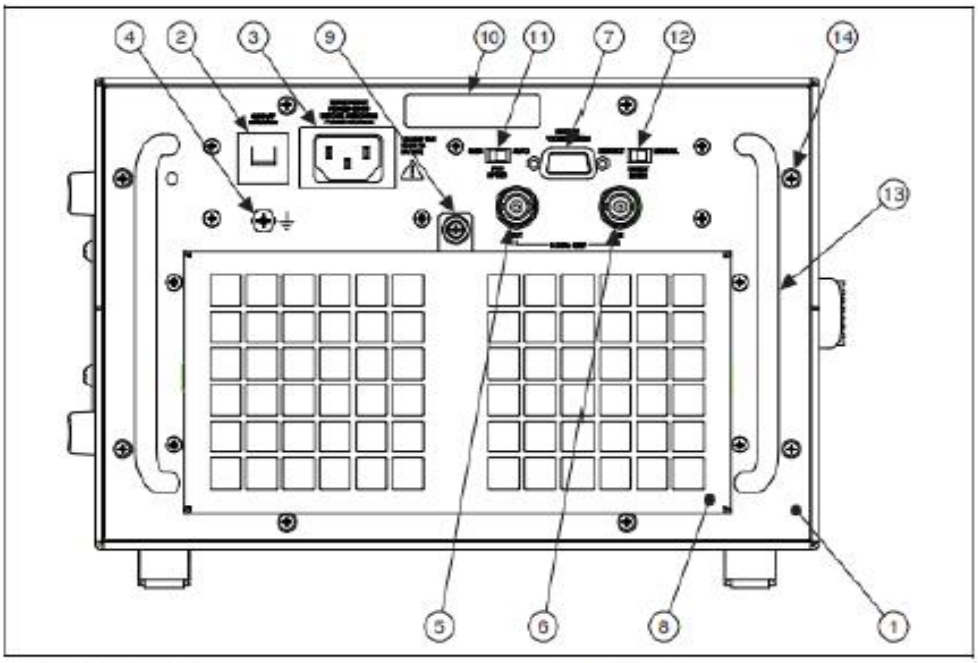

1	Power Supply Shuttle	8	Air Filter Retainer
2	Push-Reset Circuit Breaker	9	Air Filter Retainer Screw
3	Universal AC Input	10	Power Supply Shuttle ID Label
4	Chassis Ground Screw	11	Fan Speed Selector Switch
5	10 MHz REF OUT BNC	12	Inhibit Mode Selector Switch
6	10 MHz REF IN BNC	13	Power Supply Shuttle Handle (2x)
7	Remote Inhibit and Voltage Monitoring Connector	14	Power Supply Shuttle Mounting Screws (8x)

Figure 1-2. Rear View of the NI PXIe-1062Q Chassis

Specifications

AC Input

Input voltage range..... 100 to 240 VAC

Operating voltage range[1]..... 90 to 264 VAC

Input frequency..... 50/60 Hz

Operating frequency range[1]..... 47 to 63 Hz

Input current rating..... 8 A

Over-current protection..... 10 A circuit breaker

Line regulation

- 3.3 V..... <±0.2%
- 5 V..... <±0.1%
- ±12 V..... <±0.1%

C.2 Laser Displacement Sensor

SPECIFICATIONS

Model		Sensor head	LK-031	LK-081	LK-501/LK-503	
		Controller	LK-2001	LK-2101	LK-2501/LK-2503	
Measurement mode			—	—	Long-range	High-precision
Reference distance			30 mm	80 mm	500 mm	350 mm
Measuring range			±5 mm	±15 mm	±250 mm	±100 mm
Light source			Visible red semiconductor laser			
	Maximum output		0.95 mW		LK-501: 15 mW, LK-503: 0.95 mW	
	Pulse duration	FDA	3 to 482 µs	3 to 994 µs	3 to 994 µs	
		IEC	3 to 482 µs	3 to 994 µs	3 to 994 µs	
		DIN EN 60825-1 07.1994	3 to 482 µs	3 to 994 µs	3 to 994 µs	
	Wavelength		670 nm		690 nm	
	Class	FDA	Class II		Class IIIb (LK-501), Class II (LK-503)	
		IEC	Class 2		Class 3b (LK-501), Class 2 (LK-503)	
		DIN EN 60825-1 07.1994	Klasse 2		Klasse 3b (LK-501), Klasse 2 (LK-503)	
Spot diameter			Approx. 30 µm (at reference distance)	Approx. 70 µm (at reference distance)	Approx. 0.3 mm dia. (at reference distance)	Approx. 0.7 mm dia. (at reference distance)
Linearity			±0.1% of F.S. [1]			
Resolution			1 µm [2]	3 µm [2]	50 µm [2]	10 µm [2]
Analog output		Voltage	±5 V (1 mm/V)	±5 V (3 mm/V)	±5 V (50 µm/mV)	±10 V (10 µm/mV) [3]
		Impedance	100 Ω			
		Current	4 to 20 mA (350 Ω max.) [3, 4]			
Alarm output			NPN open-collector 100 mA (40 V) max. (N.C.) Residual voltage 1 V max. [3]			
Sampling cycle			512 µs	1024 µs		
Other functions			AUTO ZERO, Alarm hold, GAIN selection, Response speed selection, Span/Shift adjustment			
Power supply			24 VDC ±10% Ripple (p-p): 10 % max.			
Current consumption			400 mA max.			
Temperature fluctuation		Sensor head	0.01% of F.S./°C		0.02% of F.S./°C	
		Controller	0.01% of F.S./°C			
Enclosure rating			IP-67			
Ambient light			Incandescent or fluorescent lamp: 10,000 lux max. [5]			
Ambient temperature		Sensor head	0 to 50 °C (32 to 122 °F), No freezing			
		Controller	0 to 50 °C (32 to 122 °F), No freezing			
Relative humidity			35 to 85%, No condensation			
Vibration			10 to 55 Hz, 1.5 mm double amplitude in X, Y, and Z directions, 2 hours respectively			
Material		Sensor head	Aluminum die-cast			
		Controller	Polycarbonate			
Weight (including cable)		Sensor head	Approx. 260 g	Approx. 385 g	Approx. 700 g	
		Controller	Approx. 515 g			

1. Linearity was obtained using KEYENCE's standard target (white ceramic block gauge).
2. Resolution was obtained using KEYENCE's analog sensor controller (RD 60) with the number of averaging measurements set to 64.
   Note: The ripple of the analog output may be 1 mV or more due to common mode noise when observed with an oscilloscope or high-speed A/D conversion board.
3. When measurement is impossible, 12 V (31.2 mA) is output.
4. The analog current output is 4 to 20 mA over the measurement range with an analog voltage output of ±5 V.
5. 5,000 lux max. with LK-503/2503.

الخلاصة

تتضمن الدراسة الحالية تحرياً عملياً وعددياً لسلوك البلاطات المضلعة ذات الاتجاة الواحد والمصنوعة من الخرسانة المسلحة عالية المقاومة خفيفة الوزن.

يتكون البرنامج العملي من فحص أحدى وعشرون عينة من البلاطات الخرسانة المسلحة أحادية الأتجاه. تم تقسيم هذه العينات إلى مجموعتين حسب نوع التحميل. تم إختبار خمسة عشر عينة تحت تاثير الحمل الستاتيكي (حمل من نقطتين)، وتم اختبار العينات المتبقية تحت تأثير الحمل الديناميكي (الحمل التوافقي). تم تقسيم البلاطات في المجموعة الأولى التي تم اختبارها تحت الحمل الستاتيكي إلى ستة مجموعات فرعية وفقًا لـ: نوع الخرسانة؛ خرسانة عالية المقاومة خفيفة الوزن (HSLWC)، خرسانة عالية المقاومة إعتيادية الوزن (HSNWC)، خرسانة عادية المقاومة خفيفة الوزن (NSLWC)، أو خرسانة عادية المقاومة إعتيادية الوزن (NSNWC)، النسبة الحجمية للألياف الفولاذية، نسب حديد تسليح الأضلاع، تغيير المقطع الهندسي (عدد الاضلاع) عند نفس حجم الخرسانة عالية المقاومة خفيفة الوزن، المسافة بين الأضلاع، نوع البلاطة؛ بلاطة مضلعة أو مصمتة بنفس حجم الخرسانة عالية المقاومة خفيفة الوزن تقريبا، ونسب حديد تسليح مختلفة. في حين تم تقسيم المجموعة الثانية التي تم اختبارها تحت الحمل الديناميكي إلى أربع مجموعات فرعية وفقاً لـ نوع الخرسانة، النسبة الحجمية الألياف الفولاذية، تغيير المقطع الهندسي، نوع البلاطة. كما تم فحص المكعبات، الأسطوانات، والموشورات لكل خلطة لتحديد الخصائص الفيزيائية والميكانيكية للانواع المختلفة للخرسانة التي تم أعتمادها في هذة الدراسة.

بناءً على نتائج الفحص العملي، وجد بالأمكان انتاج خرسانة عالية المقاومة خفيفة الوزن باستخدام حجر الخفاف مع إستخدام المواد المضافة (دبس السكر، الملدنات الفائقة، ، وأبخرة السيليكا) بمتوسط مقاومة إنضغاط للأسطوانة تبلغ حوالي ٤٢,٢ ميكا باسكال، ومتوسط الكثافة الجافة ١٩٤٣ كجم / م ٣، وذات موصلية حرارية تبلغ حوالي ٠,٨١ واط / (متر كلفن)، بينما كانت متوسط مقاومة إنضغاط الأسطوانة والكثافة الجافة والتوصيل الحراري هي ٥٨ ميكا باسكال، ٢٤٠٨ كجم / م٣، و ١,٤٣٥ واط / (متر كلفن)، على التوالي للخرسانة عالية المقاومة إعتيادية الوزن. ووجد أن عينة البلاطة ذات الخرسانة عالية المقاومة خفيفة الوزن تمتلك أقل؛ وزن إجمالي، سعة تحميل قصوى، وهطول بمقدار ١٩٪ ١٧,٧٠٪ و ١٧,٣٣٪ على التوالي، بالمقارنة مع عينة البلاطة الخرسانية عالية المقاومة إعتيادية الوزن التي تم اختبارها تحت الحمل الستاتيكي. نتيجة لذلك، تفوقت الكفاءة الهيكلية لبلاطه HSLWC على بلاطات، HSNWC ، NSLWC، و NSNWC بحوالي ١,٠٤٪، ٥,٨٠٪، و ١٩,١٦٪ على التوالي.

علاوة على ذلك، أدى تقليل المسافة بين الأضلاع من ٢٠٠ ملم إلى ١٨٠ ملم و ١٥٠ملم إلى زيادة الحمل النهائي بنسبة ٨,٣٣٪ و ١٧,٩٧٪ على التوالي. علاوة على ذلك، فإن استخدام البلاطة المضلعة بدلاً من البلاطة المصمتة ذات الخرسانة عالية المقاومة خفيفة الوزن زاد من الحمل النهائي و الكفاءة الهيكلية بنسبة ١٣٠,٣٧٪ و ١٢٥,٧٢٪ على التوالي، بينما انخفض الهطول بنسبة ٣,٩٩٪.

من ناحية أخرى، فإن تغيير عدد الأضلاع عند نفس حجم الخرسانة لا يعطي فرقًا كبيرًا في قدرة القوة ولكنه يعطي فائدة اقتصادية من خلال تقليل تكلفة تصنيع حديد تسليح القص.

على أي حال، وجد أن إضافة الالياف الفولاذية بنسبة ٠,٥٪ واستخدام نسبة ٠,٤٤٪ من حديد التسليح في البلاطات المضلعة HSLWC أدى إلى التغلب على انخفاض المقاومة بسبب استخدام HSLWC بدلاً من HSNWC.

أظهرت النتائج العملية لعينات البلاطات تحت تأثير الحمل الديناميكي أن استخدام البلاطة HSLWC ذات ثلاثة أضلاع تقلل من متوسط سعة الإزاحة عند ترددات تتراوح من ٥ إلى ٥٠ هرتز بنسبة ١٣,٤٤٪ و ٣٥,١٠٪ مقارنة مع البلاطات ذات HSNWC والمصمتة، على التوالي. على العكس من ذلك، أدى إستخدام البلاطة HSLWC ذات الضلع الواحد والبلاطة التي تحتوي على نسبة ٠,٢٥٪ من الالياف الفولاذية إلى تقليل متوسط سعة الإزاحة بنسبة ٥٤,٠٣٪ و ١٥,٥٤٪،على التوالي، مقارنة بالبلاطة ذات الخرسانة عالية المقاومة خفيفة الوزن والخالية من الالياف والمكونة من ثلاثة أضلاع .

أخيراً، أظهرت المقارنة بين نتائج تحليل العناصر المحدودة التي تم إجراؤها باستخدام ABAQUS/2019 ونتائج العملي توافقا معقولاً، حيث كان الفرق الاقصى للحمل النهائي والهطول حوالي ٢١,٠١٪ و ١٤,٥٢٪ على التوالي لجميع العينات التي تحت تأثير الحمل الستاتيكي. وفي الوقت نفسه، يبلغ أقصى فرق في سعة الإزاحة حوالي ٣٠ ٪ لجميع العينات التي تحت تأثير الحمل الديناميكي. تضمنت الدراسة أيضاَ دراسة متغيرات أخرى عددياً مثل إيجاد التردد الطبيعي وأنماط الإهتزاز و دراسة تأثير كل من زيادة تردد التشغيل، حالة الإسناد و التباعد بين الأضلاع على سلوك البلاطات ذات الاتجاه الواحد تحت الحمل الديناميكي.

جمهورية العراق
وزارة التعليم العالي والبحث العلمي
جامعة بابل
كلية الهندسة
قسم الهندسة المدنية

سلوك الخرسانة المسلحة عالية المقاومة خفيفة الوزن للبلاطات المضلعة ذات الاتجاه الواحد

أطروحة

مقدمة إلى كلية الهندسة في جامعة بابل

كجزء من متطلبات نيل درجة الدكتوراه فلسفة في الهندسة /الهندسة المدنية /إنشاءات

من قبل

تمارا عامر محمد عبد الأمير

اشراف

أ.د. حيدر محمد كاظم خضير

١٤٤٣ هـ

٢٠٢٢ م